THE AUSTENITE → FERRITE TRANSFORMATION IN TUNGSTEN STEELS AND SOME OTHER TERNARY STEELS

By

SUNIL KISHORE SAHAY

Darwin College, Cambridge

A dissertation submitted for the degree of
Doctor of Philosophy
at the University of Cambridge, September 1986

PREFACE

This dissertation is submitted for the degree of Doctor of Philosophy in the University of Cambridge. The research described was performed during the period from October 1983 to September 1986 in the Department of Metallurgy and Materials Science, University of Cambridge.

Except where acknowledgment and reference to previous work has been made, this work is, to my best knowledge, original and has been carried out without collaboration. Neither this dissertation, nor any one substantially similar to it has been or is being submitted for a degree, diploma or other qualification at any other University. This dissertation consists of less than 60,000 words. The research was carried out under the supervision of Prof. R.W.K. Honeycombe R.F.S. (1983-84) and Dr. H.K.D.H. Bhadeshia (1984-86).

Sunil Kishore Sahay

Sunil Kishore Sahay

September 1986

ACKNOWLEDGEMENTS

I would like to express my sincere gratitude to Professor R.W.K. Honeycombe (1983-84) and Professor D. Hull (1984-86) for laboratory facilities and for their encouragement and advice throughout the course of this work. I am also grateful to my friends and colleagues in the Department of Metallurgy and Materials Science, in particular, J.L. Steiner, G. Hillier, D. Burry, Y. Sato, R. Paulo, B. Soylü, J.R. Yang, M. Strangwood, A. Sugden and S. Atamert.

Acknowledgement is also made to the Assistant staff of the laboratory, in particular, J. Leader, for his aid in alloy preparation and B. Barber for photography.

I greatly acknowledge my wife Anjali for her moral support in all possible ways during the entire period of my research. I also express my gratitude to my parents for their constant encouragement in the time of need. My son Abhisek needs special appreciation.

The research has been financially supported through Cambridge Commonwealth Trust Award, ORS and an award from Darwin College.

Thanks is also due to Miss Lesley Parks for her careful typing.

CONTENTS

ABSTRACT

The present work is concerned with "The Austenite→Ferrite transformation in tungsten steels and some other ternary steels". Emphasis is given to the understanding of the fundamental factors influencing nucleation and growth phenomena during the diffusional decomposition of austenite. Precipitation at the advancing γ/α interface (i.e. interphase precipitation) has also been studied.

It is found that the $\gamma \rightarrow \alpha$ transformation proceeds by the nucleation of α i.e. allotriomorphic ferrite) at the prior-austenite grain boundaries, followed by its growth. Hence the kinetics of the $\gamma \rightarrow \alpha$ transformation depend on the ease with which the α is nucleated at the austenite grain-boundaries as well as its ability to grow. In order to enhance hardenability, it is essential to impede both the nucleation of ferrite and its subsequent growth.

Using a Fe-W-C alloy, an attempt has been made to suppress the grain boundary nucleation of α by first partially covering these boundaries with copious precipitation of tungsten carbide. The presence of such precipitation at the prior austenite grain-boundaries was found to lead to a drastic drop in the nucleation rate of α, at low undercoolings in spite of the fact that carbide formation removes carbon from solid solution. However, at high undercoolings, the reverse phenomenon was observed. It is concluded that at low undercoolings, nucleation kinetics depend more on the number of available active sites; the prior formation of tungsten carbides reduces the number of sites and hence causes a drop in nucleation frequency. On the other hand, at high undercoolings, driving force dominates the nucleation kinetics (i.e. since carbon is precipitated at the prior austenite grain-boundaries as carbide, it causes an overall increase in the driving force for transformation) and so leads to an increased nucleation rate. The growth kinetics of allotriomorphic ferrite (α) in Fe-C-X alloys (where X is Cr or Ni) have been studied. Parabolic rate constants for thickening kinetics of α have been determined as a function of isothermal transformation temperature and compared with calculated values based on a para-equilibrium model for one-dimensional growth. A good agreement was noticed for a Ni-containing steel. But in the case of a Cr-steel, the agreement was rather poor. The sources of discrepancies were examined in the light of available experimental observations. It was concluded that factors such as presence of planar facets, pinning of the γ/α interface by

carbides, solute drag-like effect and stereological effects are responsible for the discrepancies in our results.

Another part of the research is concerned with the study of interphase-precipitation during the $\gamma \rightarrow \alpha$ transformation. Interphase-precipitation has been studied in Fe-Si-W-C alloys and compared with alloys of similar composition but without silicon. It was observed that silicon has strong tendency to induce interphase-precipitation at high temperatures. High proportions of low energy facets (i.e. semi-coherent interface) containing ledges of variable height were noticed in silicon-containing steels transformed at high temperatures (i.e. low undercoolings). It is suggested that silicon tends to favour the development of low energy facets which move by ledge mechanism. At the same time silicon is believed to decrease the solid-solubility of carbides in ferrite. These factors probably combine to enhance interphase precipitation.

Finally, the effect of a small addition of titanium on the $\gamma \rightarrow \alpha$ transformation in Fe-5W-0.23C(wt.%) alloy has been investigated. Like Nb, titanium showed a tendency to retard $\gamma \rightarrow \alpha$ transformation. Titanium forms carbides both at the prior austenite grain-boundaries and within the grains. Formation of TiC at the austenite grain-boundaries impedes nucleation while the growth is hindered by the pinning action of TiC which are present within the austenite grains.

CHAPTER I

General Introduction

The austenite (γ) → ferrite (α) transformation in alloy steels is a topic of vital concern to metallurgists. Considerable attention has been given in recent years to elucidate the mechanisms which govern the nucleation and growth of the α during the diffusional decomposition of the austenite.

The present dissertation is an attempt to understand and explore the various aspects of the diffusional decomposition of the austenite. Attention has been focused on both the nucleation and growth processes and on the role of carbide particles in influencing these aspects.

The project initially started with work on four alloy systems and was extended to include other systems. Tungsten was selected as the main substitutional alloying element. It forms coarse tungsten carbides which can easily be detected using optical microscopy. Two of the four initial alloys also contained silicon. Silicon was added to suppress the pearlite reaction. Silicon is also believed to decrease the solid-solubility of carbides in ferrite. This aspect may be utilized to enhance interphase-precipitation during the transformation. In addition, it extends the α phase-field. So the temperature range for the study of interphase-precipitation can be expanded. In one of the tungsten steels (Fe-5.9W-0.21C (wt%)), a small amount of titanium (0.14% wt) was also added to examine its effect on the transformation kinetics. For studies of growth kinetics, Fe-C-X (where X is Cr or Ni) systems were selected. Nickel was selected primarily because it does not form its own carbide. So the effects of carbide precipitation on growth kinetics could in principle be eliminated, allowing an appropriate test for the theory for growth. In another alloy Cr was added. The addition of Cr helps us to understand any deviation of the experimental results from growth theory due to carbide precipitation or other effects such as solute-drag.

The dissertation has been set out as follows:

Chapter II is mainly devoted to the experimental techniques. Techniques such as alloy preparation and fabrication, heat-treatment, nickel plating, optical microscopy, transmission electron microscopy, scanning electron microscopy Quantimet and dilatometry are briefly discussed. Chapter III reviews the current understanding in the area of diffusional decomposition of austenite. It contains a literature review on the morphological

development of α and carbide precipitation during the transformation. Chapter IV highlights the microstructural features which develop during the γ → α transformation in a Fe-5.5W-2.03Si-0.37C (wt%) alloy. An alloy with similar composition but without silicon has also been studied to compare transformation characteristics. Many differences are reported between Fe-W-Si-C and Fe-W-C alloys and explanations are offered for these variations. Chapter V deals with the γ → α transformation in Fe-5W-0.23C (wt%). Special attention has been paid to the mechanism of the carbide precipitation, which occurred during the latter stages of growth. The effects of small addition of titanium on the kinetics of the γ → α transformation in this particular alloy have been examined. Chapter VI is concerned with the γ → α transformation in Fe-5W-2.3Si-0.15C (wt%) alloy. The nature of carbide precipitation has been observed and discussed in detail. The effects of carbide pre-precipitation on the kinetics of the γ → α transformation are reported in Chapter VII. An attempt has been made to establish the fact that the pre-precipitation of carbides at the austenite grain-boundaries can be employed to retard the γ → α transformation at low supersaturation. Studies on growth kinetics of α in a Fe-3.05Cr-0.11C (wt%) also are reported in the Chapter VIII. Similarly Chapter IX is concerned with growth kinetics of α in a Fe-3.28Ni-0.11 C (wt%) alloy. Finally, conclusions and suggestions for future work are presented in Chapter X.

CHAPTER II

LITERATURE REVIEW

2.1 INTRODUCTION

Study of the Austenite→Ferrite transformation in alloy steels is important partly because of the technological importance of the transformation and also because of the rich variety of structures and related properties accessible through variations in heat treatment. This transformation can be utilized as a direct route for strengthening alloy steels by fine dispersions of alloy carbides. These dispersions occur by repeated nucleation of carbides at the γ/α interface during the transformation and the reaction is therefore termed "interphase precipitation". Microstructures developed by interphase-precipitation are sensitive to both transformation temperature and alloy composition. Microstructurally, this mode of precipitation appears in planar, curved and irregular dispersions of alloy carbides. Planar or banded structures predominate when the interface is semi-coherent in the majority of cases. (Semi-coherent interfaces are regarded as low energy facets which move by a ledge mechanism. The band spacing depends upon the ledge height and may vary in the range of 5 to 50nm. Temperature and composition are the two main variables which decide the band spacing. Interphase precipitation is not only confined to low energy facets but it can also occur on the mobile high energy incoherent interfaces, leading to curved and irregular dispersion of alloy carbides.A bowing mechanism operates to form irregular dispersions of alloy carbides while quasi-ledge mechanism is responsible for curved dispersion of alloy carbides. The bowing mechanism predominates when the precipitate spacing is more than the minimum critical value, whereas a quasi-ledge mechanism operates when it is less than the critical value.

Though the mechanism of interphase precipitation has undergone considerable development in the recent past, many difficulties still persist, particularly with respect to the mechanism responsible for banded alloy carbide dispersions in isothermally transformed steels. Several recent reviews explore the ledge mechanism but none of them fully explain the factors that govern the ledge mechanism.

2.2 The $\gamma \rightarrow \alpha$ reaction

Depending upon the alloy composition and transformation temperature, austenite can decompose into proeutectoid ferrite, proeutectoid cementite, pearlite and bainite. Among those reactions, the proeutectoid ferrite reaction is the most important one. This is the first transformation product to occur over wide ranges of temperature and composition in most steels produced in large quantities. The kinetics of this reaction directly determine the hardenability of these steels and play a major role in establishing the mechanical properties. The proeutectoid ferrite reaction is also simplest from the viewpoint of ascertaining the effects of alloying elements upon the fundamental quantities determining the kinetics of a diffusional transformation, namely the rates of nucleation and the rates of growth.

The morphologies of proeutectoid ferrite can be complex and strongly temperature-dependent. The effects of alloying elements on the morphologies of ferrite have been deemed to be of least importance[1], although the kinetics are greatly altered by the presence of alloying elements. However, no correlation has ever been reported in literature concerning the effects of alloying elements on the morphologies of ferrite but the intuitive feeling is that it follows the general trends of Dube's morphological classification. This classification was further extended in detail by Aaronson.[2,3] Dube observed that the various shapes which ferrite crystals develop in plain carbon steels as the γ/α transformation temperature is lowered, can be classified into a few distinctive and well-defined morphologies. The following are the components of the Dube system in its present form:

1. Grain boundary allotriomorphs (Figure 1.1a): Crystals which nucleate at grain-boundaries in the matrix phase and grow preferentially and more or less smoothly along these boundaries. The morphology of a grain-boundary allotriomorphs does not reflect its internal crystallographic symmetry. These allotriomorphs start nucleating at the highest temperatures, i.e. just below Ae_3, and during the growth stage have a semi-coherent interface with one abutting austenite grain and an incoherent interface with the other adjacent abutting grain. As the transformation temperature is lowered, these crystals develop facets on at least one side but often on both sides of the boundary.

2. Widmanstätten side plate (Figure 1.1b): These plates nucleate at the γ-boundary but grow along well-defined matrix planes. They grow either directly from the boundaries (Primary side plates) or grow on pre-existing ferrite allotriomorphs (Secondary side plates).

3. Widmanstätten sawteeth (Figure 1.1c): They develop from the austenitic grain-boundaries and possess a triangular cross section in the plane of polish. Primary sawteeth grow directly from the matrix grain-boundaries whereas the secondary sawteeth develop from grain-boundary allotriomorphs.

4. Idiomorphs are equiaxed in shape and usually prefer to form within the interior of austenite grains (Figure 1.1d), but occasional evidence of grain-boundary idiomorphs has also been reported in literature.[4,5]

5. Intragranular Widmanstätten plates: These plates form within the grain and are similar to those growing from grain-boundaries (Figure 1.1e).

6. Massive structure: Such structure develops due to impingement of crystals of other morphologies (Figure 1.1f).

Although similar comprehensive reviews have never been reported concerning alloy steels, it is quite probable that this generalisation with some modifications may be applicable to these complex alloy systems.

Grain-boundary allotriomorphs are the dominant morphology which develops over wide ranges of composition and temperature in plain carbon steels. Nucleation of allotriomorphs takes place at high angle grain boundaries. Toney and Aaronson[4] using Fe-Si alloy, Hawbolt and Brown[6] and Clark[7] in Al-Ag alloy came to similar conclusions after examining the nature of the grain-boundaries at which allotriomorphs first nucleate. It is believed[8] that the formation of allotriomorphs takes place by the formation of a coherent plate-shaped nucleus at a high angle grain-boundary (Figure 1.2a). Grain-boundaries are more energetically favourable sites for the nucleation of allotriomorphs compared with interior of the grains, especially at the highest transformation temperatures where the driving force is rather low. The surface energy barrier to nucleation is minimized by elimination of grain-boundary area by precipitate matrix interface. Moreover, a coherent plate-shaped nucleus may be expected

whenever the precipitate and the matrix differ in volume and represent a compromise in the minimization of strain and surface energies.[9] Growth of the particle normal to the habit plane occurs due to enhanced diffusion along the grain-boundary (Figure 1.2a). The combination of transformation and growth along the boundary results in a loss of the strict precipitate habit and thus an allotriomorph with a disordered boundary is thought to develop from the initial nucleus. An alternate mechanism[10] for the development of allotriomorphs is shown in Figure 1.2b. Here the grain-boundary is believed to reorientate itself parallel to the habit plane of the nucleus. The driving force for this reorientation is the minimization of the interfacial energy of the particle. Again diffusion along the grain-boundary is invoked to produce non-crystallographic growth and subsequent loss of good matching between the precipitate and the matrix lattice.

With increasing supersaturation, secondary side plates develop from only one side of a grain-boundary allotriomorph. Widmanstätten plates are refined (i.e. length to width ratio increases) and growth occurs from both sides of allotriomorphs as the transformation temperature is lowered further. The source for the generation of secondary side-plates is believed to be the presence of protuberences which develop due to differences in the rates of migration of the interphase-boundaries. A second school of thought concerning the nucleation of secondary side-plates is due to Townsend and Kirkaldy[10] who postulated that ferrites nucleate at austenite grain-boundaries on $\{111\}_\gamma$ planes tangent to the boundaries (Figure 1.3a). A rational orientation relationship (K-S orientation relationship[11]) is proposed with respect to the grain in which nucleation occurs. This results in one low energy interface, the other being generally irrational. As the precipitate grows in dimensions, it loses its coherency (Figure 1.3b) and develops perturbation on the γ/α interfaces (Figure 1.3c) due to anisotropic surface tension. Widmanstätten plates ultimately develop due to anisotropic growth rate of the γ/α interface (Figures 1.3d,e).

Primary side-plates develop directly from the small-angle austenite grain-boundary[12] or near coincidence site boundaries. Plate-shaped nucleus is considered to form at or near dislocations in the boundary in order to minimize the effect of volume strain energy accompanying the transformation. The coherent regions between dislocations do not provide diffusion short circuit. The interfacial energy nor the mobility is available to convert the nucleus into

allotriomorphs. The broad faces of the nucleus thus remain immobile and the crystallographic shape is maintained during growth.

Plate-shaped nuclei grow through the action of the point effect of diffusion at the edge of growing plate, the concentration gradient about the edges are much steeper than the broad faces of the plates.[13] The crystallographic relationships which determine the orientation and habit plane of the nucleus are considered to be unimportant during the growth.[8] The shape and the habit plane of the nucleus are simply reproduced by the geometry of the diffusion of solute toward or away from the nucleus. However, a point effect alone cannot account for the evolution of side-plates almost invariably parallel to only one of four habit planes from such a crystal. It is speculated[8] that the anisotropic nature of the strain fields of the dislocations in the boundary produces an unequal distortion of the four $\{111\}_{\gamma}$ habit planes. As a result of this the atomic configuration on one of these equivalent habit planes is thought to best match with that of the precipitate, with a reduction of the surface energy for nucleation. This preferential reduction in interfacial energy is thought to result in the observed unique precipitate habit.

Nabarro attempted to analyse in detail the influence of volume strain energy on precipitate morphology in a series of excellent reviews.[14,15,16] According to his analysis, the plate-shaped morphology results from minimization of volume strain energy accompanying a transformation. However, the crystallographic nature of the plate morphology in transformations in which the lattice structures of the matrix and precipitate are different does not appear to be so explicable on this basis. The crystallography of the broad faces of Widmanstätten plates points strongly to interfacial energy and structure, rather than strain energy as the fundamental factors in the formation of plates. C.S. Smith[17] proposed a general theory of morphology in terms of interfacial structures and their migration characteristics. According to his hypothesis, the ferrite nuclei would have one coherent or semi-coherent interface with the austenite and thus normally a random or incoherent interface with the adjacent austenite grain. The normal orientation relationship between austenite and ferrite is represented by the Kurdjumov-Sachs relationship which applies to Widmanstätten ferrite and indeed probably in many cases to ferrite with an equiaxed appearance; viz

partially transformed specimens of a vanadium steel to show that precipitates formed in sheets parallel to the γ/α interface. They also made a detailed crystallographic analysis associated with these carbide formations. They observed that VC obeyed a Baker-Nutting[29] orientation relationship with the ferrite:

$$\{100\}_{\alpha} // \{100\}_{VC}$$

$$\langle 011\rangle_{\alpha} // \langle 010\rangle_{VC}$$

Since VC is crystallographically related to the ferrite, they came to the conclusion that these carbides nucleated at the γ/α interface and grew in the ferrite. They also noticed that only one variant of this orientation relationship was found within any precipitate colony. This was attributed to the restricting effects of the phase boundary on the precipitation reaction, forcing the precipitate to adopt the habit plane close to that of the boundary. This common mode of precipitation has been observed in many isothermally transformed alloy steels containing Ti[30], Mo[31], Nb[32], Cr[33], Cu[34], Au[35], etc. and termed as "interphase precipitation".

While there is general agreement that the sheets of precipitate form on the interphase interface, the exact mechanism for the movement of this interface during the precipitation reaction remained unexplained until 1974.[36] Heikkinen [38,39] proposed that an interface bowing mechanism may operate (Figure 1.4) in V-steel. The alloy carbide (VC) initially exerts a pinning action on the interface but as it grows the austenite ahead of the interface is depleted of carbon and thereby reduces the stability of the austenite. Under these circumstances, the interface would easily bow between precipitate particles. Having crossed the precipitate, it will straighten due to the surface tension and the process would continue. However, this mechanism could explain the observation of curved sheets of interphase precipitation but cannot be applied to explain the formation of planar arrays of interphase precipitation. Campbell and Honeycombe[36] proposed a ledge mechanism responsible for planar arrays precipitated in chromium steels. Frequent observations[37,35,36] of ledges on planar interfaces, strongly implies that these interfaces are of the partially coherent type which are related by a Kurdjumov-Sachs orientation relationship and displaced by the migration of ledges. The planar array of

precipitates nucleates at regular intervals on low energy interfaces and not on the energetically more favourable ledges during transformation. This is because the high mobility of the ledge prohibits nucleation and this has been confirmed by Aaronson et al.[23]

Curved as well as irregular dispersions of alloy carbides have sometimes been observed in association with planar arrays of precipitates. Those two types of carbide dispersion are associated with mobile incoherent γ/α interfaces Figure 1.5 is a schematic diagram illustrating the essential features of the bowing mechanism[40] which operate when the spacing between the precipitate is greater than the critical value. The critical value of precipitate spacing can be obtained using the relationship

$$a_{cri} = \frac{2\delta V}{\Delta G}$$

where a_{cri} = ½ spacing of precipitates along the row

ΔG = the free energy change per mole of γ transformed

V = the molar volume of austenite

δ = the surface energy/unit area

When the precipitate spacing is below this critical value, a quasi-ledge mechanism operates[41] to form curved arrays of precipitates (Figure 1.6).

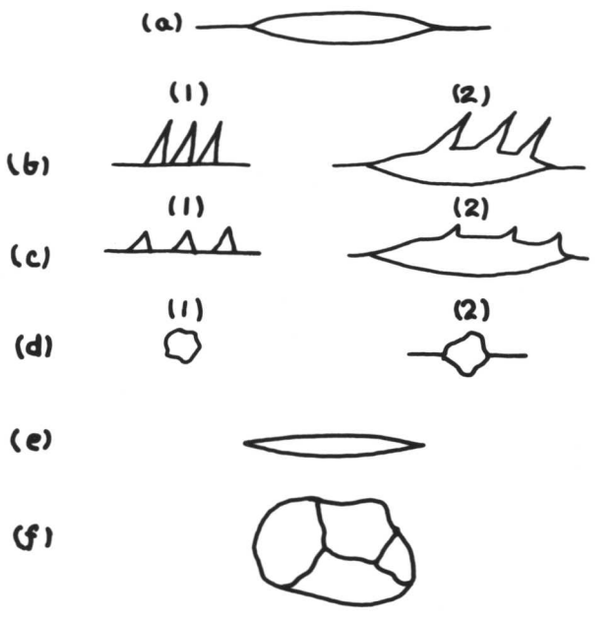

Fig. 1.1: (a) Grain-boundary allotriomorph

(b) Widmanstätten side plate

(c) Widmanstätten sawteeth

(d) Idiomorphs

(e) Intragranular Widmanstätten plates

(f) Massive structure

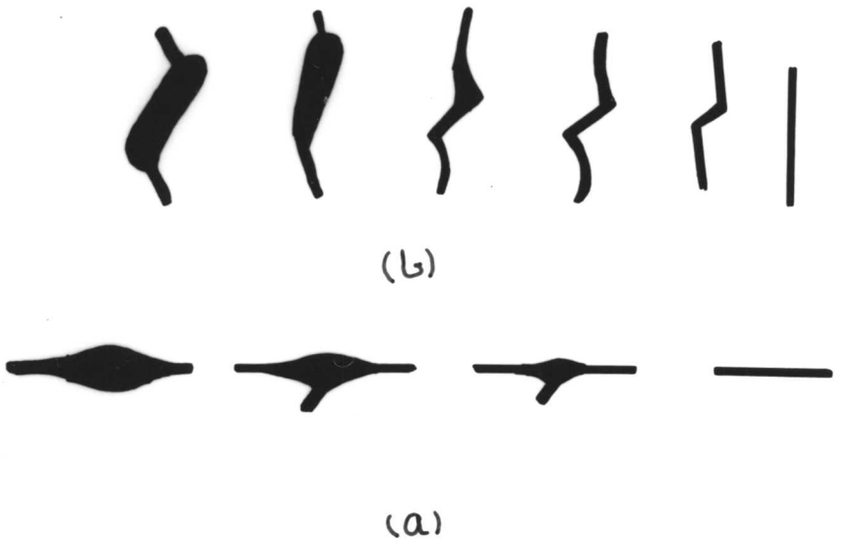

Fig. 1.2: Formation of grain-boundary allotriomorphs

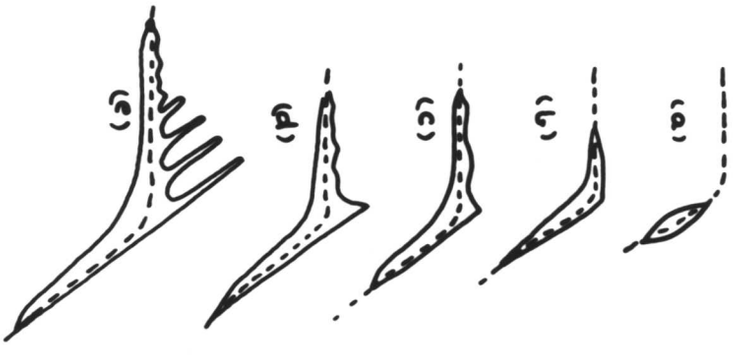

Fig. 1.3: Profile for developing Widmanstätten ferrite

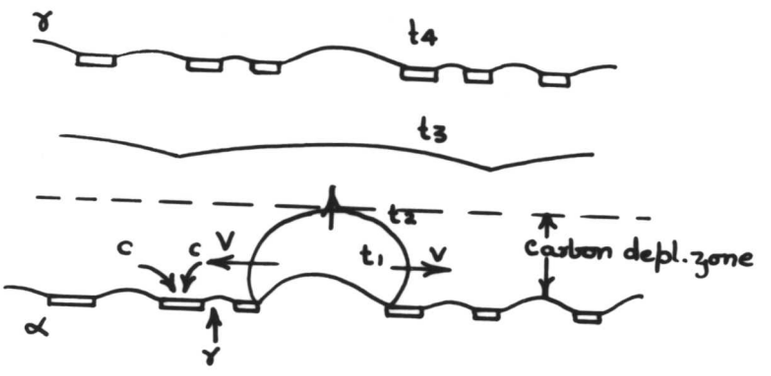

Fig : schematic model for the mechanism of interphase precipitation, proposed by Heikkinen

---

Fig. 1.4: Schematic model for the mechanism of interphase precipitation, proposed by Heikkinen.[38,39]

Where C = Carbon atom

V = Solute atom (i.e. vanadium)

t_i = Surface tension/area

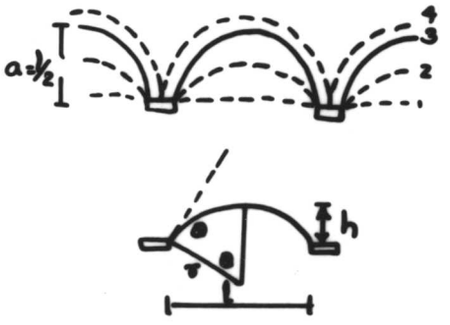

Fig: Schematic diagram of geometry of model used to calculate free energy balance associated with migration of interphase boundary by bowing mechanism.

Fig. 1.5: Schematic diagram of geometry of model used to calculate free-energy balance associated with migration of interphase boundary by bowing mechanism.[40]

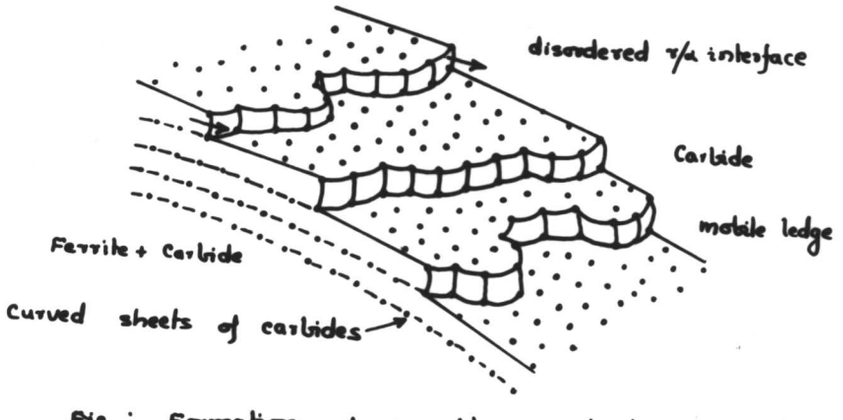

Fig: Formation of non planar sheets of precipitate by a "quasi-ledge" mechanism

Fig. 1.6: Schematic diagram showing quasi-ledge mechanism.[41]

In the third and final step of heat-treatment, the austenitized specimens were subjected to isothermal transformation in the temperature range of 850° to 700°C, followed by water quenching. The time of transformation varied from 0 to 500 minutes. After austenitizing, the silica tube was smashed and the specimen was immediately introduced in the fluidised bed furnace for isothermal transformation. It was felt essential to break the silica tubing before the commencement of isothermal transformation and to bring the specimen to transformation temperature as quickly as possible. The fluidising effect was produced by introducing air through the bottom of the bed. The flow rate of the air in the outer chamber was maintained at 250 cm^3/sec while in the inner chamber it was 84 cm^3/sec. An uniform temperature was maintained in the fluidised bed under these flow conditions. Al_2O_3 powder was used as fluidising medium for the outer chamber while Zr_2O_3 powder was used in the inner chamber. The temperature variation in all cases was maintained within the limit of ±2°C. Hand gloves and tongs were used while handling the specimens during heat-treatment.

The heat-treatment given to Fe-C-X alloys for optical metallograpy consisted of two stages. During the first stage, the specimens were austenitized at 1250°C for one hour and fifteen minutes. The long holding time at high austenitizing temperature was selected to ensure that the grain-boundaries are essentially perpendicular to the intended plane of polish. The specimens were in the form of small strips having a thickness of 5 mm. Prior to heat-treatment, more specimens were encapsulated in silica tubing containing argon gas at a partial pressure of 120 mm Hg.

In the second stage of heat-treatment, the austenitized specimens were subjected to isothermal transformation in the fluidized bed, followed by quenching in iced-brine solutions. The temperature of isothermal transformation varied from 750 to 600°C depending upon the type of alloy used. Similarly the time of transformation varied in the range 0 to 180 minutes or even higher in some cases. The silica-tube containing the specimen was broken quickly before introducing it into the fluidised bed for isothermal treatment.

The heat-treatment given to each alloy for TEM examination followed the same steps as mentioned above except that the austenitizing temperature was reduced to 900°C for 15 minutes. The low austenitizing temperature was selected to obtain a smaller grain size. The smaller grain size helps in locating the grain boundaries more easily during transmission electron microscopy.

3.4 Optical Microscopy

For optical metallography the heat-treated specimens were mounted on non-conducting bakelite and prepared by standard techniques. Care was taken during initial grinding to remove sufficient material to avoid any error caused by nucleation of the transformation product at the free surface.

After final polishing, the specimen was thoroughly cleaned and washed in methanol. 2% nital was used as an etchant in each case. Photography was carried out using an Olympus microscope.

A Quantimet 720 image analysing computer was used to determine the percentage of transformation in each specimen. The Quantimet 720 is attached with a Reichart optical microscope/epidiascope and Videcon/plumbicon television scanner which transfers the image analogue to a computer system. The image is composed of up to 705x896 picture points or pixels and discriminates between phases on a "grey level" basis. The areal fraction of a phase detected by means of grey level is D/N, where D is the number of detected picture points and N is the number of picture points in the "live frame". The machine scans the image with 720 lines at the rate of 7560 lines/sec which is much less than ordinary television camera scanners (i.e. 15650 lines/sec). This scan speed gives a better signal to noise ratio with improved resolution. Additionally, these scans are digitally controlled so that every pixel is of equal length and precisely positioned. The scanners used are plumbicon and videcon. The sensitivity variation of these scanners never exceeds more than 6% over half-million points. This sensitivity variation can be further reduced by "shade correction" by viewing a blank field for 30 seconds. The electrical noise levels are very low; it departs from the true value by one-and-half percent for 500 pixels. The noise variation can further be reduced by a factor of four by taking at least 16 scans of each field. The resolution of the Quantimet is limited by its ability to generate enough contrast from small features. The modulus transfer function $\{M(\lambda)\}$ which is a ratio of the output modulus to the input modulus exhibits a clear loss of resolution on very small feature. However, the videcon seems better than the plumbicon for very small features, and that is why in the present investigation the videcon scanner was preferred over plumbicon. Moreover, the videcon scanner has a constant low noise level than the plumbicon. The noise level in the plumbicon scanner increases as the light levels decrease down, and becomes troublesome. The dark

current or leakage of the Videcon system is higher and becomes troublesome at low light levels. The gamma value which refers to the ability of the electron/photon conversion process varies from 0.3 to 1 for Videcon and 0.9 - 1 for Plumbicon. This is adjusted by varying the illumination and light-sensitivity. In order to achieve high sensitivity at low light levels and to distinguish features of closely similar light intensity, it is essential to precisely adjust the resolution, shading, noise, absolute light sensitivity, dark current and gamma-value. However, at reasonable light levels, the Plumbicon can distinguish two features which differ slightly in their brightness. The Videcon on the other hand can distinguish features which slightly differ in their darkness. But if the features have high contrast, then both scanners will work efficiently. In general, Videcon has a broader dynamic range and should be preferred at distinguishing many different grey levels, while the Plumbicon is better at distinguishing pale features in a narrow contrast range, i.e. the microstructures showing high contrast levels should not be used on Plumbicon. To improve accuracy and stability, the signal from the scanner is passed to the control processor where an internally generated graticule is superimposed on the image for both measurement and calibration. There is also a provision to avoid the edge error by correctly setting the guard region.

The guard region is an area between the two limiting frames. The outer frame is called the live frame. The use of single frame may result in edge error when features are intercepted by frame and are sampled more than once in successive measurements. When the guard region is set correctly to a size which is larger than the largest features measured, the edge error vanishes.

Each feature of the image has an anti-coincidence point associated with it; the anti-coincidence point is a terminating point at the end of each feature (which also identifies a memory containing information about the feature). If the guard region is larger than the largest feature, then the feature which intersects the blank frame has an ACP inside the live frame. Consequently, if ACP lies in the live frame then all the feature must lie in the blank frame and will be correctly detected. Hence, all size and edge errors vanish.

The magnification of the imaging system is usually adjusted so that the smallest particle to be sized has an image at least one pixel in size. However, this is not always possible, because the largest particle may then cut down the size of the live frame to an unacceptably small level, since the size of the live frame equals 896 x 705.

The errors associated with point counting (i.e. D/N) can be assessed on a statistical basis. The relative error which is also called the coefficient of variance is given by σ_{v_f}/V_f where σ_{v_f} is the standard deviation and V_f is the volume fraction of the α-phase. The square of the relative error is known as the proportional variance (i.e.$(\sigma_{v_f}/V_\alpha)^2$) Hilliard and Cahn[2] derived an expression to determine the total proportional variance associated with a real analysis as follows:

$$(\sigma_{v_f}/V_f)^2 = \frac{1}{N_\alpha} \cdot \left| 1 + (\sigma_\alpha/a_\alpha)^2 \right|$$

where D = Number of the detected points/area.

N = Total number of points/area.

N_α = Number of α-phase particles measured.

σ_α = Standard deviation of the area of individual α-phase particles.

a_α = Mean area of the individual α-phase particle.

The above equation denotes that the proportional variance depends on the number of α-phase particles with respect to the size of the area examined and the variation in the size of the α-phase particles within the area examined.

However, in case of two-dimensional random point counting (i.e. D/N), the above expression has been modified to obtain the proportional variance. i.e. for point counting, the proportional variance is given by

$$(\sigma_{v_f}/V_f)^2 = \frac{1}{N_\alpha} \cdot \left| 1 + (\sigma_\alpha/a_\alpha)^2 \right| + \frac{1}{P_\alpha}(1-V_f)$$

where P_α = The number of intersections of the grid (i.e. number of detected picture points) falling in the α-phase.

3.5 Transmission Electron Microscopy

A Philips EM400 TEM was used for the examination of thin foils. A single tilt specimen stage was generally used but some times double tilt was used to obtain diffraction pattern from carbide by controlled tilting. The foils were examined at 120 kV. A magnetic correction was employed to improve resolution and to obtain a sharp image.

1.5 Preparation of thin foil: Discs of 0.25 mm thickness were cut from 3.2 mm diameter rod with the help of an oil-cooled carborundum slitting wheel. The discs were then thinned down to 0.05 mm by abrasion on wet 600 grade silicon

carbide paper. This thinning of the specimen was considered essential to reduce its magnetic mass, thereby minimizing magnetic aberrations in the electron microscope. The discs were jet polished with a "Twin Jet Electropolisher" (Fisschione). 5% perchloric acid plus 25% glycerol in ethanol was used as electrolyte. Optimum polishing conditions varied between alloys and heat-treatments but good results were obtained at an applied voltage between 40 to 50V and at a temperature of $15^{o}C$. After electropolishing, the thin foils were carefully cleaned in methanol and then dried. The foils were immediately examined after jet polishing to minimize the possibility of oxidation and contamination.

3.6 Isothermal Dilatometry

Isothermal transformation studies were done on a high speed dilatometer, namely "Dilatronic III" manufactured by Theta Industries Inc. of Post Washington, New York. Specimens having length of 20 mm and a diameter of 3.2 mm with internal diameter of 1.5 mm were used in this present study of isothermal transformation by Theta dilatometer. This particular dimension was selected to achieve rapid quenching. This hollow rod-shaped specimen was placed inside the silica tube (25 mm long and 4 mm diameter). It was then supported between two hollow silica-push rods and surrounded by radio-frequency induction coil. Radio-frequency induction coil is used to heat the specimen to the desired temperature at a controlled rate. Rapid quenching was achieved by flushing helium gas through the specimen. A vacuum of the order of 10^{-4} torr was created in the heating chamber before starting the experiment to protect the specimen from oxidation and decarburizing. The change in length of the specimen was transmitted to the transducer via a push rod and magnified to 100X 100 times. Both the change in length and temperature were monitored on a chart recorder which moved with a pre-set speed. Using the computer program developed by Yang and Bhadeshia,[3] the instantaneous change in length as a function of time at each isothermal temperature was recorded on a computer disc. These data were then transferred to the mainframe computer. Using the "Camplot" program on main frame, it became easy to plot the curve between the relative length change versus time. While recording the data on the computer disc, a correction was applied for the magnification. An automatic temperature control device was used to quench the specimen from its solution treatment temperature ($1200^{0}C$) to

the pre-set transformation temperature. By carefully setting the valve trigger, it was possible to avoid temperature overshoot by cutting off the quench gas at a pre-set temperature above the isothermal transformation temperature.

3.7 Microanalysis on a SEM

The scanning electron microscope with microanalysis facilities serves as a powerful technique to characterise the microstructural features of the specimen. The area to be examined is irradiated with a finely focused electron beam, which may be static or may sweep in a raster across the surface of the specimen. When the electron beam hits the surface, it emits radiation such as secondary electrons, backscattered electrons, Auger electrons, characteristic X-rays and photons of various energies. These radiations serve as signals to examine many characteristics of the samples (e.g. composition, surface topography etc.). For microanalysis on a SEM, the primary radiation of interest are the characteristic X-rays, emitted as a result of the electron bombardment. These characteristic X-rays are analysed to give both qualitative and quantitative compositional information from regions of a specimen as small as a few micrometers in diameter. Moreover, the detailed microcompositional information can be directly correlated with optical metallography.

For microanalysis, one needs to measure the energy and intensity distribution of the X-ray signal generated by a focused electron beam and to convert these data into a useful form for qualitative and quantitative analysis. This can be achieved in two ways:

(a) Wavelength-Dispersive Spectrometer (WDS)

In this method, a small portion of the X-ray signal generated from the specimen passes out of the electron optical and impinges on an analysing crystal. The incoming X-rays are diffracted by the analysing crystals provided the Bragg law is satisfied (i.e. $n\lambda = 2d \sin \phi$.)

The diffracted X-rays are detected by a proportional counter and then they are amplified, converted to a standard pulse size by a single-channel analyser (SCA) and finally, counted with a scaler or displayed as a rate meter output on a strip chart recorder. Standard tables are used to identify the element from crystal spectrometer readings.

(b) Energy-Dispersive X-ray Spectrometer (EDS)

In this method, the X-ray signal from the samples passes through a thin beryllium window into a cooled lithium-drifted silicon detector. The incoming X-rays are absorbed by the detectors which in turn ejects photo-electrons. These photo-electrons give up most of their energy to the formation of electron-hole pairs. The electron-hole pairs are swept away by the applied bias to form a charge pulse by a charge-sensitive pre-amplifier. The signal is finally passed to a multi-channel analyser (MCA) after amplified by main amplifier. MCA sorts out the pulses by voltage. The contents of the MCA memory are transmitted to a computer for further processing such as peak identification or quantification.

All the microanalysis experiments have been done on the ISI scanning electron microscope. This is capable of doing both quantitative and qualitative microanalysis of the specimen. It works on the principle of EDS. There is a suite of programs available which permits the calibration and routine quantitative electron microprobe analysis of polished bulk specimen to be carried out. One such set of programs is ZAF-4/FLS. This program is stored on a diskette and operates on 1K spectra using 10, 20 or 40 eV/channel calibration. It can handle all radiations within the selected range. All overlapping peaks including K, L or M series are deconvolved using standard profiles. In cases where both K and L or L and M lines from one element exist within the spectron, both are deconvolved but only one is used in the ZAF correction procedure.

For quantitative analysis of the specimens using the program ZAF-4/FLS, the relative X-ray intensity ratio between the elements of interest in the specimen (I_{sp}) and the same elements in the standard (I_{st}) are measured. Both specimen and the standard (i.e. cobalt and copper) are examined under identical experimental conditions. The measured intensity ratio is commonly called K_i. The K_i value is then further corrected to take into account the effects such as (1) atomic-number effect expressed by the factor Z_i (2) absorption of X-rays within the specimen, A_i, (3) fluorescence effects F_i. The weight fractions of the element (C_i) of interest is obtained by using the relation

$$C_i = Z_i A_i F_i K_i$$

Table 1.1

Alloy Composition

wt% W	wt% C	wt% Si	wt% Ti	wt% Fe
5.5	0.37	2.03	0.0	Balance
5.8	0.4	0.0	0.0	Balance
5.0	0.15	2.3	0.0	Balance
5.0	0.23	0.0	0.0	Balance
5.8	0.5	0.0	0.0	Balance
5.9	0.21	0.0	0.14	Balance

Table 1.2

Alloy Composition

wt% Cr	wt% Ni	wt% C	Fe
3.05	0.0	0.11	Balance
0.0	3.28	0.11	Balance

CHAPTER IV

The Austenite→Ferrite transformation in Fe-5.5W-2.03Si-0.37C (wt%) and Fe-5.8W-0.4C(wt.%) alloys

4.1 INTRODUCTION

This chapter is concerned with the study of the $\gamma \rightarrow \alpha$ transformation in tungsten steels of composition Fe-5.5W-2.03Si-0.37C (wt.%) and Fe-5.8W-0.4C(wt.%). This transformation has been utilised for the fundamental investigation of interphase precipitation in many alloy steels. In recent years, it has become increasingly clear that interface precipitation represents the common mode of precipitation of alloy carbide in steels containing carbide formers like V, Ti, Nb, Cr, Mo, etc. Non-carbide forming elements such as Cu and Au have also precipitated by the interphase precipitation mechanism. In this structure, the ferrite contains closely spaced parallel bands or sheets of fine alloy carbide precipitates. The sheet spacing is sensitive to temperature and composition, and varies in the range of 5 to 50 nm. The planar array of precipitates nucleates at regular intervals on low energy interfaces during the transformation and hence delineates the path of the γ/α interface. These low energy interfaces are displaced by the migration of ledges which are taken to have a "disordered" structure. In all studies to date, the precipitation has been found to be limited to the low energy interface facets in preference to the ledges. According to classical nucleation theory, the ledges should be the favoured sites for nucleation to occur relative to the low energy facets. The most convincing and yet very powerful argument in support of this interesting reversal of nucleation behaviour is given by Honeycombe in his excellent review[1] on "Transformation from Austenite in Alloy Steels". These ledges move during transformation and hence provide the least opportunity for nucleation to occur there. Consequently nucleation takes place on the low energy, less mobile interfaces. This hypothesis was further confirmed by Aaronson et al.[2] Their theory indicates that carbide nuclei will be overrun before their development is complete when they attempt to form at the ledges. A meagre and

scant observation was presented concerning precipitation on the disordered ledges in Fe-10%Cr-0.2C (w.t%) alloy.[3] In highly alloyed steels, they believe that the mobility of ledges is reduced and at the same time the solute concentration at the interface is increased. Both conditions favour the formation of precipitates on the ledges. Once the precipitation has occurred, the ledges will be pinned. The sequence of events following this pinning would presumably require the passage of subsequent ledges to overtake and unpin the ledge containing the precipitate.

Interphase precipitation is not only confined to low energy immobile interfaces which grow by the ledge mechanism leaving behind a planar array of discrete particles but also extended to high energy mobile interfaces which ultimately result in curved as well as irregular dispersions of particles due to their inherent growth characteristics. A bowing mechanism operates to form an irregular dispersion of particles when the precipitate spacing is greater than the minimum critical value whereas a quasi-ledge mechanism is believed to operate when their spacing is less than the critical value.[4,5]

The present work is undertaken with a view to exploring some of the elusive phenomena of interphase precipitation which still persist and remain unsolved and hence to provide more viable explanations so that mechanism of interphase precipitation can stand on a much more rigorous quantitative footing.

4.2 Experimental Results on Fe-5.5W-2.03Si-0.37C (wt.%) alloy

4.2.1 Isothermal Transformation at 850°C

Isothermal transformation at 850°C for 5 minutes showed about 10 volume % transformation. The resultant microstructure showed that the nucleation of α-ferrite has occurred predominantly at the austenite grain-boundaries and grew in a blocky manner to form what are known as grain boundary allotriomorphs (Fig. 4.1). Close optical examination of the γ/α interface indicated the presence of both smoothly curved, presumably incoherent, as well as facetted, semi-coherent interfaces. However, the proportion of facetted semi-coherent interface was much more than the curved one. It was also observed that the γ/α interfaces in the majority of the cases were pinned by carbides. Pinning by carbide has occurred in two different ways. Firstly, interphase precipitation

has occurred at the γ/α interface and consequently the interface has been pinned. Carbides can also pin the interface if it is already present in the austenite. Such interface showed protuberances which were formed as the γ/α interface moved across these carbides. The pinning has a direct effect on the kinetics of the γ/α transformation. It can delay the transformation and hence this approach can be effectively exploited in increasing the hardenability of alloy steels.

Many interesting phenomena were observed when this alloy was isothermally transformed at 850^{0}C for 20 minutes. Figure 4.2 shows that interphase precipitation is not only limited to the low-energy facets but it can also occur on the ledges. It was also observed that the ledges were not of the same height but they varied in height even at the same interface. Figure 4.3 shows another striking phenomenon. Pinning of low energy interface is clearly shown in this micrograph. The fact that cusps are developed where the carbides pin the facets is conclusive and direct evidence that the facets migrate normal to the facet plane without any ledge mechanism. Figure 4.4 shows that facets as well as ledges both move but the rate of migration of the facet is low compared to the ledges. This is also indicated by the fact that separation of the facet increases with distance away from ledges. So the classical view that the facet does not move at all during a diffusional process must be incorrect. Clearly as the temperature drops, the difference in mobility of the low energy and high energy interface must increase. Therefore the ledge mechanism as understood classically becomes well defined for low temperature regions. That is why we observe a very irregular ledge mechanism (Figs. 4.5 and 4.6).

Occasionally the absence of precipitation on mobile ledges was also observed (Fig. 4.7). The interphase precipitation associated with highly facetted idiomorphic ferrite was also noticed (Fig. 4.8). Figure 4.9 shows that the ledges were apparently moving in two opposite directions. It suggests that these ledges might have nucleated on the facet. Figure 10 shows the complex nature of carbide precipitation during the $\gamma \rightarrow \alpha$ transformation. Figure 4.11 illustrates that the interphase precipitation is confined to only one side of the austenite grain boundary. This supports the view proposed by Smith.[19] He proposed that it is energetically more favourable for ferrite to nucleate if it develops a coherent or semi-coherent interface (i.e. one which exhibits interphase precipitation by ledge mechanism) with one abutting austenite grain and a random or incoherent interface with the adjacent

austenite grain. Figure 4.12 shows the highly facetted α-ferrite. (These particular micrographs were taken from the alloy which had slightly different composition than the original one. The chemical composition of this new alloy was Fe-5.9W-1.95Si-0.36C (wt.%). It is believed that this effect is presumably due to the presence of silicon.

The scanning electron micrographs are shown in Figs. 4.13 and 4.14. The interphase precipitation by ledge mechanism does not always result in uniform band spacing, as shown in Fig. 4.13. It further supports the view that the ledges are not uniform in height. Direct evidence to support this view is presented in Fig. 4.2. The SEM taken from the specimen which is slightly different in composition than the original one is shown in Fig. 4.14. This specimen was isothermally transformed at 850°C for 40 minutes. Figures 4.14(a) to (d) show that the carbide precipitation has occurred on the planar facet but apparently there is no evidence of ledges. These micrographs also show that the growth has occurred mainly on one side of the boundary while on the other side its growth is restricted. The carbides present along the boundary might have exerted a pinning action to inhibit the growth on the other side of the boundary. These micrographs also show that the α-ferrite is highly facetted.

The large number of pictures have been included to demonstrate that the features observed are not peculiarities but reflect the general complexity of the carbide precipitation during the transformation.

4.2.2 Isothermal Transformation at 800°C

Isothermal transformation at 800°C for 2.5 minutes showed about 10 volume % transformation. This is the temperature at which minimum incubation period was recorded. It indicates that the nose of TTT diagram is around 800°C. The transformation has occurred predominantly at the austenite grain boundaries (Fig. 4.15). The allotriomorphs appeared as dark etched regions along the grain boundaries. Figure 4.16 needs special attention. This micrograph shows the presence of fibrous carbide associated with the interface which has migrated by ledge mechanism. Evidence of interface pinning was also noticed.

4.2.3 Isothermal Transformation at 750°C

Isothermal transformation at 750°C for 5 minutes showed 10 volume % transformation. Again the reaction has occurred mainly along grain-boundaries as expected. The aspect ratios of these allotriomorphs are quite high compared to the allotriomorphs formed at higher temperatures. A continuous layer of the transformation product was observed in the majority of cases (Fig. 4.17). Pinning of the interface by carbides has also been observed (Fig. 4.18). Fibrous carbide was also recorded (Fig. 4.19).A strong tendency towards facetting was noticed.

4.2.4 Isothermal Transformation at 700°C

The incubation period increased as the transformation temperature was further decreased. Only 6 volume % transformation occurred after holding the specimen at 700°C for 10 minutes. The transformation started at the grain boundaries, forming a continuous layer of the transformation product (Fig. 4.20). In the majority of cases, the interface appeared planar. Figure 4.21 illustrates some important crystallographic aspects of the transformation product on macroscopic scale. This micrograph illustrates the formation of allotriomorphs at the junction where three grain boundaries meet (i.e. formation of allotriomorphs at the triple point). Evidence of interface pinning was noticed, even at this temperature.

At all temperatures, the transformation started at the grain boundaries to form grain-boundary allotriomorphs. At higher temperatures separate nuclei could be seen but as the transformation temperature is lowered a continuous layer of ferrite is formed along the grain boundary. In the majority of cases, the interface appeared planar. Ledges of variable heights were observed at the highest transformation temperature (850°C). Extensive evidence of interphase precipitation was noticed at the highest temperature. Interphase precipitation was not only limited to the low energy facets but it was also extended to the ledges. No evidence of interphase precipitation was obtained optically during the early stage of transformation (10 vol.%) at all temperatures. Ledges appeared more frequently at higher temperatures as compared with lower

temperatures (on a microscopic scale). Direct evidence of the normal migration of facets was recorded at highest temperature of transformation. However, no such evidence was obtained as the transformation was reduced (i.e. 750°C and 700°C). Evidence of interface pinning was also noticed at all temperatures. It was also noticed that the aspect ratio of the allotriomorphs increased with decreasing temperatures. Absence of Widmanstätten ferrite at all transformation temperatures (850°C to 700°C) led to the conclusion that most of the allotriomorphs were bounded by low energy interfaces since Widmanstätten ferrite is believed to grow from incoherent boundaries of the allotriomorphs.[19]

Transmission electron microscopy was used to reveal the details of the microstructural features of the ferrite formed in the temperature range of 850°C to 700°C. Electron micrographs showed extensive evidence of interphase precipitation at 850°C. Figure 4.22 shows that the band spacing is not uniform. It also shows that at some stage of transformation, the ledges have combined together. The point where the two ledges join, the band spacing is doubled in size as shown by arrow in Fig. 4.22. Precipitation on the mobile ledge is shown in Fig. 4.23. With decreasing transformation temperature, it was found that the carbides had a tendency to form from supersaturated ferrite - and not by interphase mechanism (Fig. 4.24). These carbides have been identified as W_2C and M_6C [6-10]

The TTT diagram for 10 volume % transformation is shown in Fig. 4.25. The fastest reaction occurs at 800°C and the transformation starts after an incubation period of approximately 2 minutes at 800°C. The $\gamma \rightarrow \alpha$ transformation can also be described by Avrami-equation, the general form of which is given by

$$f = 1 - \exp(-kt^{\eta})$$

$$\text{where} \quad f = \frac{\text{volume fraction of } \alpha}{\text{equilibrium vol. fraction of } \alpha \text{ at temp. T}}$$

where η is a number whose value can vary from 1 to 4. The value of k depends on nucleation and growth rate and is therefore sensitive to temperature.

Figure 4.26 shows the isothermal section of Fe-Si-C alloy in the temperature range of 1000K to 1373K. Figure 4.27 shows Fe-C equilibrium diagram at constant silicon content. Both these diagrams indicate that silicon has strong tendencies to expand α-field. In addition to this silicon is also believed to decrease the solid solubility of carbides in ferrite. Both these aspects have been exploited to their full extent in the present study of Fe-5.5W-2.03Si-0.37C wt.% alloy.

Wilyman[11] studied the effect of Al and Si on isothermal transformation characteristics of Fe-V-C alloy, and came to the conclusion that these elements accelerate the interphase precipitation which is consistent with our results.

4.2.5 Step Quenching

The specimens were first austenitized at 1200°C for 30 minutes, then isothermally transformed at 850°C for 20 minutes followed by step quenching at 750°C for 10 minutes.

The optical micrographs taken from these specimens (Fig. 4.28(a) to (d)) show the evidence of interphase precipitation surrounded by a thick grey layer. It was expected that the thick grey layer was due to the formation of fibrous carbides at lower transformation temperature. However, contrary to the opinion, the electron micrographs revealed that the thick grey layer consisted of dense carbide precipitates. Absence of fibrous carbides at lower temperature further strengthen the view that most of the interfaces were semi-coherent in nature and hence prevented the formation of fibrous carbides.

Micrographs taken from the double step quenched specimens (i.e. 850°C 20 min → 750°C 20 min → 850°C) were shown in Figs. 4.29 to 4.34. These micrographs show that the carbides have precipitated by interphase mechanism as well as from supersaturated ferrite. Precipitation on the mobile ledges were also observed.

4.3 Discussion

Grain-boundary allotriomorphs were the first transformation product observed over the temperature range (850° to 700°C) of the investigation. A strong tendency towards facetting was observed in this alloy particularly at higher temperatures of transformation. Frequent evidence of ledges implies that these interfaces have been displaced by a ledge mechanism. The aspect ratio of these allotriomorphs increased with decreasing transformation temperatures since the role of grain boundary carbon diffusion in allotriomorphs lengthening then becomes more significant.

Extensive evidence of interphase precipitation was obtained using optical microscopy and SEM. These micrographs also show that the interphase precipitation is not only limited to the broad faces (i.e. low energy facets) but it can also occur on the mobile ledges. The question which immediately arises is how nucleation can occur on the migrating ledges, and once the

nucleation has occurred, how do these ledges migrate instead of being pinned? To understand this unusual behaviour, it is essential to know the migration characteristics of ledges. The migration characteristics of the individual ledge may vary due to the point effect of diffusion acting along its height. It can be anticipated that the higher the ledge height, the slower will be its speed. In the present work, the ledges are unusually very high (μm). The migration velocity of such ledges of exceptional height would be appreciably low. Under such circumstances it is possible for the embryos to develop into successful nuclei before it will be overrun by the ledges. Once an embryo turns into a successful nucleus, it pins the ledges. So a mechanism is needed to explain migration characteristics of such a ledge which has been pinned by carbides. The leading ledges, which are pinned by carbides, are unzipped by trailing ledges which overtake them. This sequence of events is repeated again and again and we get random precipitates along with planar array of interphase precipitation.

It is also possible that some of these ledges lag behind giving an opportunity for nucleation to occur. Another possibility is that during later stages of transformation, some of these ledges are forced to adopt a rational interface orientation and under these circumstances, carbides can easily nucleate on them.

It was also observed that ledges are not of the same height even at the same interface. This variation is about an order of magnitude. The variation in ledge height has also been reported earlier.[11] Variable ledge heights can be explained on the basis of migration characteristic of ledges. Ledges do not migrate with equal velocity due to overlapping diffusion fields of adjacent ledges.[12,13] The velocity of leading ledges is reduced compared to the trailing ledges due to overlapping diffusion fields. As a consequence of which, the trailing ledge catches the leading ledge and merges with it. For the interface containing three ledges, the second ledge can either merge with the first (i.e. leading ledge) or the third ledge (i.e. trailing ledge) depending on its position. If it is nearer to the first ledge, it will merge with the leading ledge. But if it is nearer to the third ledge, it will be caught by the trailing ledge and the first ledge will escape. This explains why we observe trailing ledges of more height than the leading one occasionally. As ledge multiplication occurs during the growth of ledged interfaces and we observe ledges of variable heights, the process of ledge

multiplication continues until the ledges acquire a maximum limited height. Beyond this limited height, the "point effect of diffusion" from the top to the bottom of riser starts acting and hence the ledges become unstable. At this point it is worth mentioning the paper by Bhadeshia.[14] He developed a simple equation to correlate the critical ledge height (h) with interfacial energy (δ)/area and chemical-free energy change per unit volume (ΔF_v^m). This relationship can be written as

$$h^* = \frac{\delta}{\Delta F_v^m}$$

Though the measured ledge height exceeded the predicted minimum value of h*, the calculated and experimental curves showed strikingly similar trends as a function of transformation temperature.

Frequent evidence of cusps on low energy facets was noticed at the highest transformation temperature (Fig. 4.3). Development of cusps on low energy facets led to the view that these interfaces have moved normal to the facet plane without the need of a ledge mechanism. (The cusps are developed as the interface moves across the carbides during the transformation .) So the classical view that the low energy facets do not move at all during diffusional process must be incorrect. Figure 4.4 clearly illustrates the fact that both low energy facets and ledges move during the transformation. But the rate of migration of facets is low compared to the ledges. No such evidence was recorded at lower transformation temperatures. This clearly suggests that as the temperature drops, differences in mobility of the low energy facets and ledges (i.e. high energy facets) must increase. Consequently, the ledge mechanism becomes better defined for low temperature regions.

Occasionally, fibrous tungsten carbides were observed (Fig. 4.16). The interesting point about these carbide fibres is that they appear to grow from the interface that has migrated by ledge mechanism. So far in the literature it is strongly argued that these fibres grow in association with high energy interfaces. This unusual observation needs further investigation before arriving at any conclusion.

At all transformation temperatures, the γ/α interface appeared planar in the majority of cases. A high proportion of the planar γ/α interface observed in this alloy indirectly suggests that silicon has a pronounced effect on modifying the interfacial structure during the early stage of transformation.

Since low energy facets move by a ledge mechanism, it is expected to have extensive interphase precipitation in this alloy.

So far in the literature least attention has been paid to the effect of alloying elements on the morphologies of the α-ferrite. It is usually reported that in the case of many alloy steels the morphology follows the general trends of Dube's morphological classification. The present observation does not fully support this view. It is not clear how the kinetics of the $\gamma \rightarrow \alpha$ transformation can be altered by addition of alloying elements without affecting the nature of the interface which basically controls the transformation during the early stages.[15]

At this stage the argument may appear unsound but it has got some justification and relevance too. Alloying elements may modify the interfacial structure between the parent and the product phase in order to synchronize the transformation kinetics. Those alloying elements which accelerate the transformation kinetics, particularly Al, Co, Si, may tend to develop a nucleus bounded by semi-coherent interface. Formation of semi-coherent nucleus requires considerably less thermodynamic force than those bounded by incoherent ones. The interfacial energy (δ) term is directly related to the minimum energy (ΔG^*) required to develop an embryo into successful nucleus within the parent crystal. This relationship may be expressed as follows:

$$\Delta G^* = \frac{16\pi\delta^3}{\Delta G_v^2} + \frac{n^2 E}{1-\nu}(C-C_o)$$

where ΔG_v is volume-free energy term associated with transformation. $n = (1/a)d \ln a/C$, in which a is the lattice parameter, E is Young's modulus, ν Poisson's ratio, C_o is average nucleus composition and C is the change in the nucleus composition as a function of distance.

ΔG^* is related to the rate of nucleation (J^*) which is a time dependent phenomenon. This relationship is given by:

$$J^* = Z B^* n e^{-\Delta G^*/kT} e^{-\tau/t}$$

where Z is the Zeldovich factor, B^* a frequency factor, n the number of nucleation sites and τ the incubation time.

In the above equation the dominating factor is ΔG^*.[16] So the rate of nucleation can be accelerated by minimizing the value of ΔG^* which is directly

related to the interfacial energy term. The interfacial energy term will be minimized provided the parent and product phases adopt an orientation relationship which allows low energy interfaces to develop between the phases. ΔG^* can be further reduced if the embryo develops on a crystal boundary of the parent phase.[17,18]

Though energetically it is more feasible to form a nucleus bounded by low energy semi-coherent interface, crystallographic restrictions may prevent it doing so and an intermediate situation arises in which a nucleus may develop which is neither fully semi-coherent nor totally incoherent. C.S. Smith[19] long ago proposed that the ferrite nuclei would have one coherent or semi-coherent interface with the austenite and thus normally a random or incoherent interface with the adjacent austenite grain. Recently Howell and Honeycombe (1983)[20] analysed in detail the crystallographic aspects of diffusional transformation in metals and alloys and came to the conclusion that the existence of reproducible orientation relationships implies that partial coherency can exist at the majority of the interface orientations and that a truly incoherent or disordered structure is rare. Further, Ryder et al[21] and King and Bell[22-24] also discovered that the product phase exhibited rational orientations with both abutting parent grains.

The present work supports this view, particularly when the transformation is accelerated by addition of alloying elements such as silicon.

4.4 Experimental Results on Fe-5.8W-0.4C (wt.%) alloy

4.4.1 Isothermal Transformation at 850°C

No evidence of transformation product (ferrite) was obtained at this temperature even after 8 hours at the transformation temperature. Fine precipitates of tungsten carbide within the austenite grain were observed. These carbides are possible of the type M_6C (Fe_4W_2C). In the absence of an appropriate phase diagram, it can be anticipated from microstructural observations that at 850°C, the phase field consists of $\gamma + M_6C$ only.

4.4.2 Isothermal Transformation at 800°C

About 15 volume % transformation was recorded at 800°C after 20 minutes. Nucleation started at the austenite grain-boundaries and growth occurred along these boundaries to form blocky allotriomorphs (Fig. 4.35). The rate of nucleation appeared slow compared with the growth rate. These effects resulted in developing coarse-grained ferrite. The γ/α interfaces appeared curved in most cases. In the majority of cases, the interface appeared serrated as well as ragged (Figs. 4.36 and 4.37). Evidence of carbide precipitation within the ferrite was recorded. The dispersion of these carbides appeared random. With further increase in transformation time (40 minutes), the allotriomorphs grew with a relatively low aspect ratio. Evidence of ledges was also obtained on planar interfaces in some cases. Almost all interfaces appeared either serrated or ragged due to pinning effect. A random distribution of tungsten carbide within the ferrite was noticed.

Evidence of banded structures formed by an interphase mechanism was also noticed in certain cases. The presence of ledges (Figure 4.38) in association with the banded structures indicates that these carbide dispersions have occurred on low energy interfaces which moved by the migration of ledges. This micrograph also shows that the banded structure has developed only on one side of austenite grain, while the other side of the grain shows random distribution of carbide dispersion. Figure 4.39 shows a grain-boundary allotriomorph bounded by planar interface. Cusps were frequently observed on these planar interfaces. Presence of cusps on the planar interfaces is taken as evidence of normal migration of these interfaces without a ledge mechanism. (Cusps are developed as the interface moves across the precipitate particle.)

4.4.3 Isothermal Transformation at 750°C

The minimum incubation period (8-10 minutes) was recorded at this temperature. It suggests that the nose of the TTT diagram is near 750°C. The transformation started mainly at the austenite grain-boundaries leading to the formation of grain-boundary allotriomorphs. The aspect ratios of these

allotriomorphs were high compared to those formed at 800°C. Evidence of interface pinning was also recorded at this temperature.

4.4.4 Transformation at 700°C

The $\gamma \rightarrow \alpha$ transformation started at around 40 minutes at this temperature. Only about 5 volume % transformation was recorded at this temperature (Fig. 4.40). It suggests that the rate of transformation is slowest at this temperature. The transformation started at the grain-boundary and grew rapidly along it to form the allotriomorph (Fig. 4.41). The aspect ratios of these allotriomorphs are quite high compared to those formed at 800°C or 750°C. These ferrites appeared virtually free from carbides. However, precipitation at the γ/α interface was frequently noticed. Figure 4.42 shows clear evidence of pinning of low energy interface. Cusps on these interfaces strongly suggest that these low energy interfaces have moved normal to the facet plane without a ledge mechanism.

No evidence of Widmanstätten ferrite was obtained in the temperature range of 800°C to 700°C.

TEM studies further revealed that there was less evidence of interphase precipitation in this particular alloy. Most of the carbides were formed from supersaturated ferrite. Unlike silicon-containing steels, these carbides appeared in several different morphologies (Fig. 4.43). The volume fraction of these carbides increased with decreasing transformation temperature (Fig. 4.44). The carbides were identified as M_6C (i.e. Fe_2W_4C). Clear evidence of interface pinning by tungsten carbide was recorded (Fig. 4.45).

A TTT diagram is constructed for 10 volume % transformation. This suggests that the transformation is fastest around 750°C and the incubation gradually increases as we move away from this temperature. Figure 4.46 shows a TTT diagram for 10 volume % transformation. The kinetics of $\gamma \rightarrow \alpha$ transformation is compared with the alloy containing the silicon, as shown in Figure 4.47. The figure clearly shows that silicon has a strong tendency to accelerate the transformation kinetics.

4.5 DISCUSSION

This alloy showed a tendency towards contracting the α-phase field. The

rate of transformation appeared slow compared to the alloy containing silicon. These two effects are mainly due to the presence of a higher percentage (0.4 wt.%C) of carbon in the alloy. The Ae_3 temperature for this alloy is around 800°C.

Grain-boundary allotriomorphs were the first transformation product to appear at virtually all austenite grain-boundaries throughout the temperature range of investigation. No evidence of Widmanstätten ferrite was recorded even at temperature as low as 700°C. It indicates that with increasing carbon content, the temperature for formation of Widmanstätten ferrite decreases. The condition required for developing Widmanstätten ferrite depends on two factors, in the case of plain carbon steel.[25] With increasing carbon content, T_w (i.e. temperature for start of Widmanstätten ferrite) also decreases. Further, an appreciable amount of undercooling below Ac_3 curve is a pre-requisite for the formation of Widmanstätten ferrite. In the present case, it appears that none of these conditions are satisfied.

At the highest transformation temperature (800°C), the rate of nucleation appeared slow compared to their growth, which led to coarse-grained ferrite. The aspect ratio of these allotriomorphs appeared low compared to those formed at lower transformation temperature (700°C) as expected for volume diffusion controlled growth of ferrite.

Frequent evidence of curved interfaces was noticed at all temperatures. It appears that in the majority of cases, the ledge mechanism did not play an important role in determining the growth kinetics of the transformation product in this particular alloy in the temperature range of 800°C to 700°C.

Evidence of interface pinning was noticed throughout the temperature range of investigation. Serrated interfaces developed due to pinning action by those carbides which have formed by an interphase mechanism. Ragged protuberances were developed as the interface moved across the carbides which were already present in the austenite. Both these mechanisms of interface pinning can be utilized to delay the transformation kinetics and hence to increase the hardenability of many alloy steels.

Cusps were frequently observed in association with planar interfaces. It is anticipated that those cusps were developed as the planar interfaces moved normal to itself without the ledge mechanism.

Random distribution of alloy carbide (M_6C) within the ferrite was noticed for transformation at $800^{0}C$. These carbides were either formed from supersaturated α-ferrite or by precipitation at the incoherent γ/α interface. However, the ferrites formed at lower temperature ($700^{o}C$) were virtually free from carbides. This may be due to high supersaturation of ferrite formed at lower temperature as compared to the ferrite formed at higher temperatures.

It was also observed in limited cases that on one side of the grain, banded carbide dispersion appeared, whereas on the other side random dispersion of alloy carbide was noticed. Ledges were seen in association with the banded structure. This strongly implies that these banded carbides were formed on the low energy interface which moved by ledge mechanism. A random dispersion of alloy carbides was formed possibly by precipitation at incoherent γ/α interfaces.

4.6 Conclusions

1. Silicon has a pronounced effect on enhancing interphase precipitation at high transformation temperatures. It expands the α-phase-field and lowers the solid solubility of the alloy carbides in ferrite. In addition, it has a strong tendency towards developing a high proportion of low energy facets which move by ledge mechanism. It can be anticipated that these factors may combine to enhance interphase precipitation in Fe-5.5W-2.03Si-0.37C (wt%) alloy. It also accelerates the kinetics of the $\gamma \rightarrow \alpha$ transformation.

2. Interphase precipitation is not only limited to the less mobile low energy facets but it can also occur on more mobile high energy facets (i.e. ledges).

3. Ledges may vary in height even at the same temperature and this variation may be on order of magnitude.

4. Near the highest transformation temperature (i.e. just below Ae_3) both low energy facets as well as ledges move. The rate of migration of low energy facets is low compared to the ledges. As the temperature drops,

differences in mobility of the low energy facets and ledges must increase so the ledge mechanism may predominate for low temperature regions.

5. The alloy without silicon showed a tendency to contract the α-phase-field. Random dispersion of tungsten carbides (M_6C) was frequently observed. These carbides have either formed from super-saturated α-ferrite or by interphase precipitation at the incoherent γ/α interface and not at the semi-coherent interface.

6. Pinning of the γ/α interface by tungsten carbide was recorded at all temperatures of transformation in Fe-5.8W-0.4C alloy. Serrated interface indicates that the pinning has occurred due to interphase carbide precipitation at the incoherent γ/α interface. Ragged or protuberance on the interface developed as the γ/α moved across the carbide particles present in the austenite.

7. The γ → α transformation was slower than in the alloy containing the silicon. Slower transformation rate is attributed to the two main factors: (a) high percentage of carbon (i.e. 0.4 wt.%C (b) lower mobility of the γ/α interface due to pinning action.

8. Only in rare cases, the banded carbide dispersions were noticed in Fe-5.8W-0.4C (wt.%) alloy.

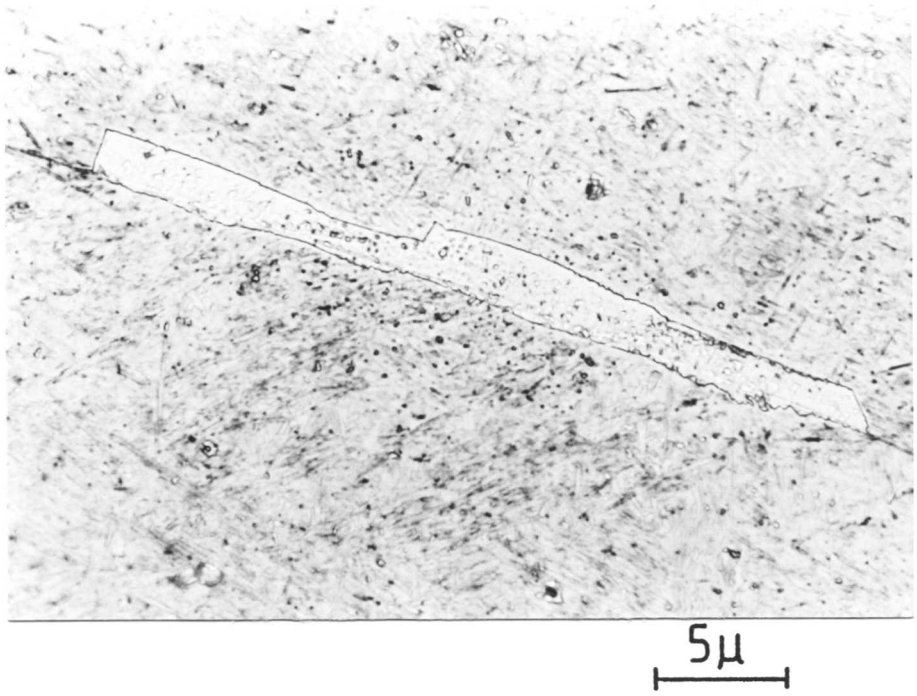

Fig. 4.1(a) Showing grain-boundary allotriomorphic ferrite. (Isothermal transformation at 850°C for 5 minutes.

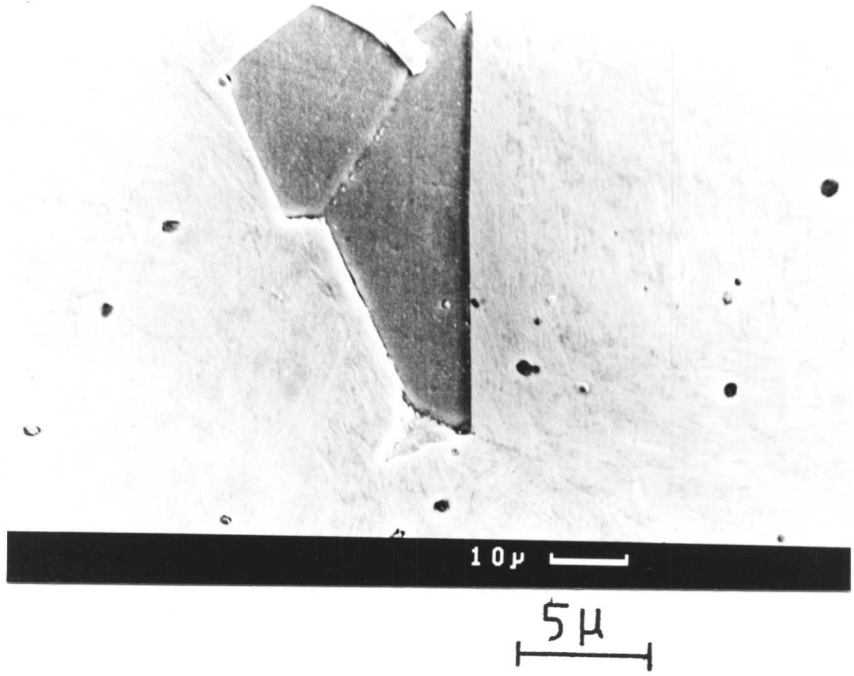

Fig. 4.1 (b) Highly facetted α - ferrite (isothermal transformation at 850°C for 5 minutes).

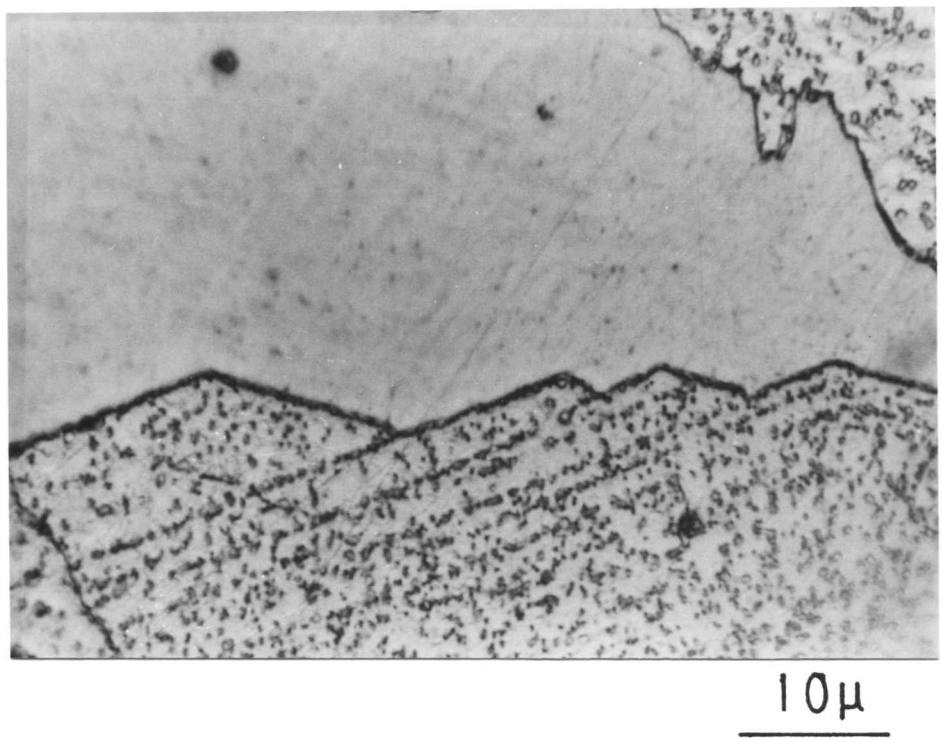

Fig. 4.2 Showing precipitation both at the low energy facets and ledges. Random distribution of alloy carbides are clearly apparent within the banded carbide dispersions. (Isothermal transformation at 850°C for 20 minutes.

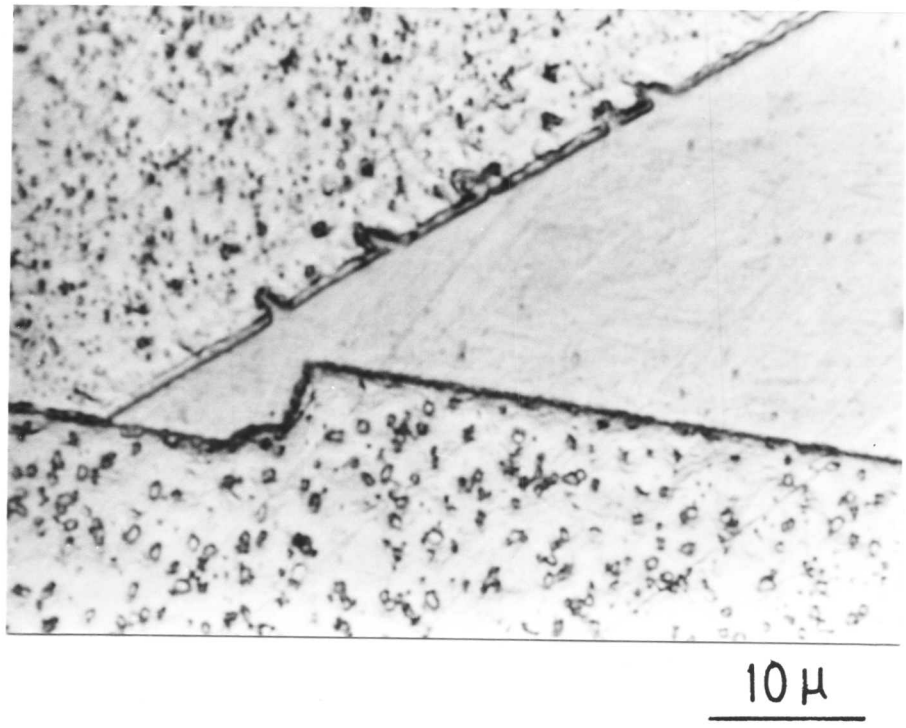

Fig. 4.3 Showing cusps on low energy facets. (Isothermal transforamation at 850°C for 20 minutes.

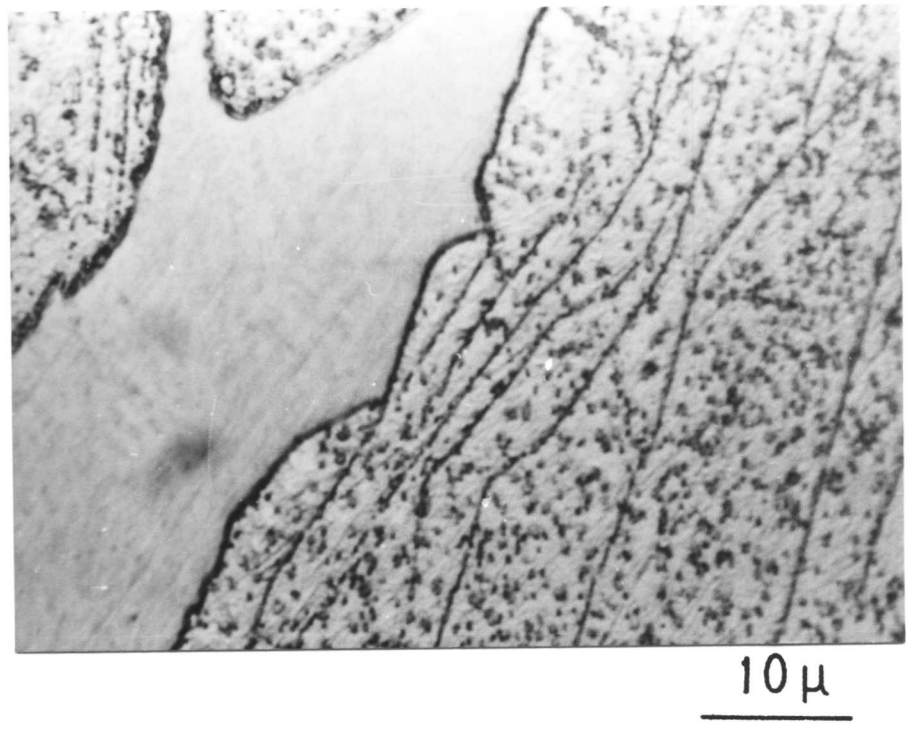

Fig. 4.4 Shows that low energy facets as well as ledges both move. (Isothermal transformation at 850°C for 20 minutes.)

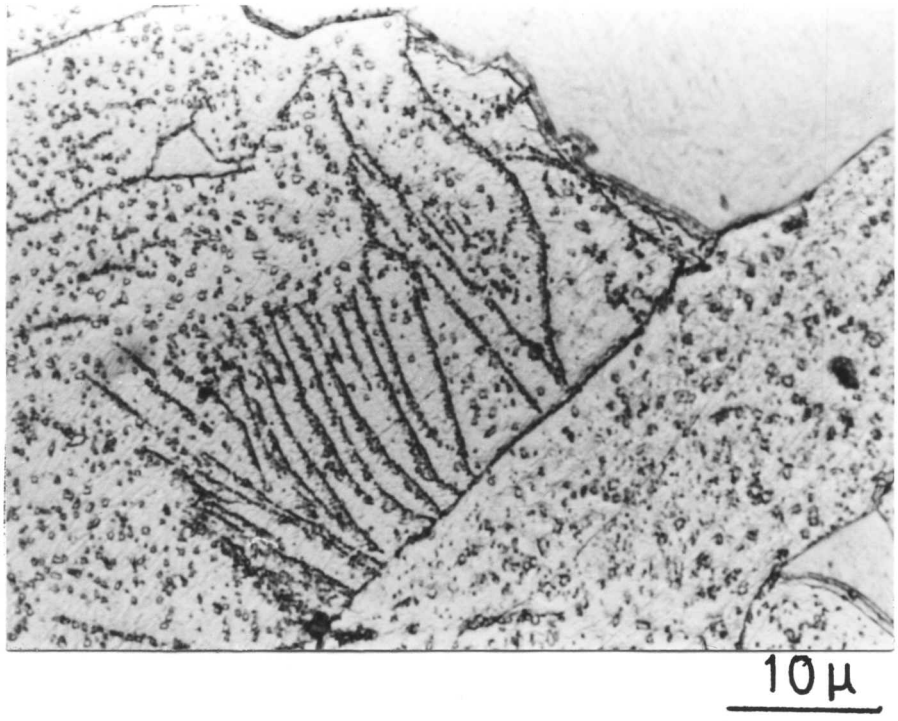

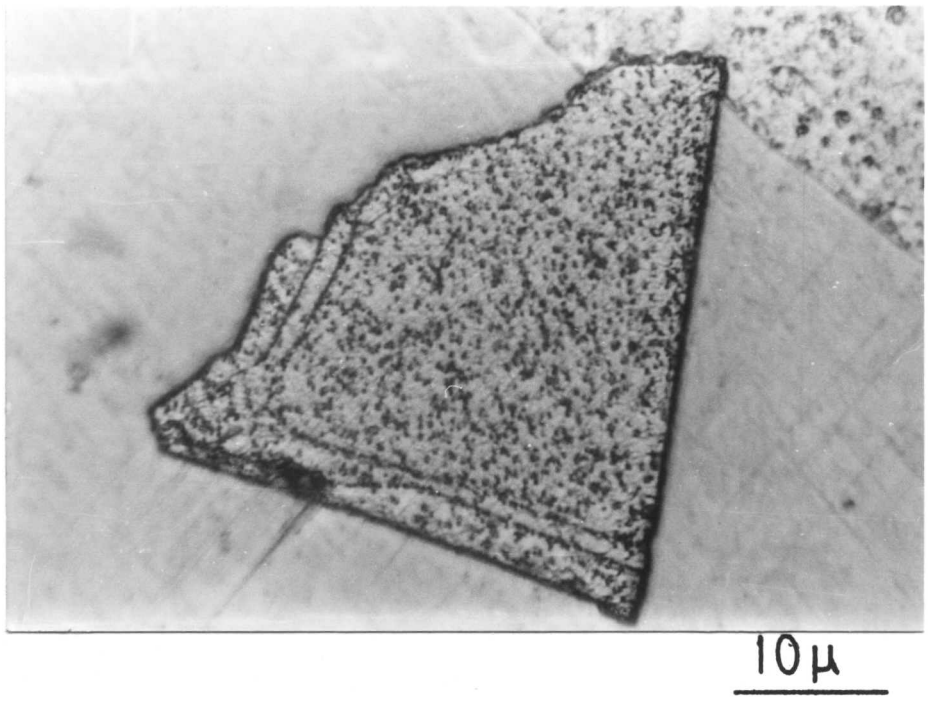

Figs. 4.5 and 4.6 showing an irregular ledge mechanism.
(Isothermal transformation at 850°C for 20 minutes.)

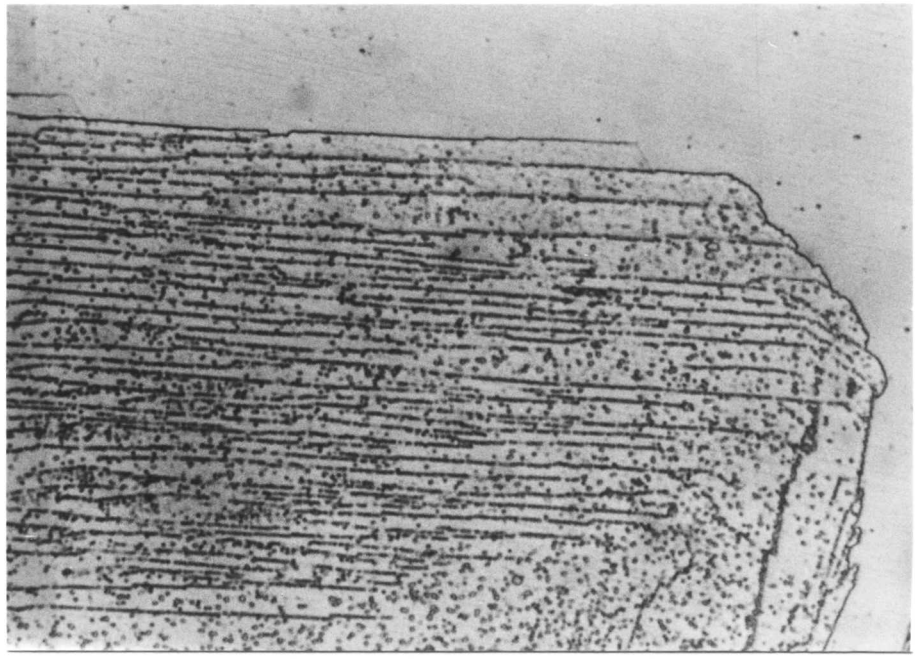

Fig. 4.7 Showing absence of precipitation on mobile ledges.

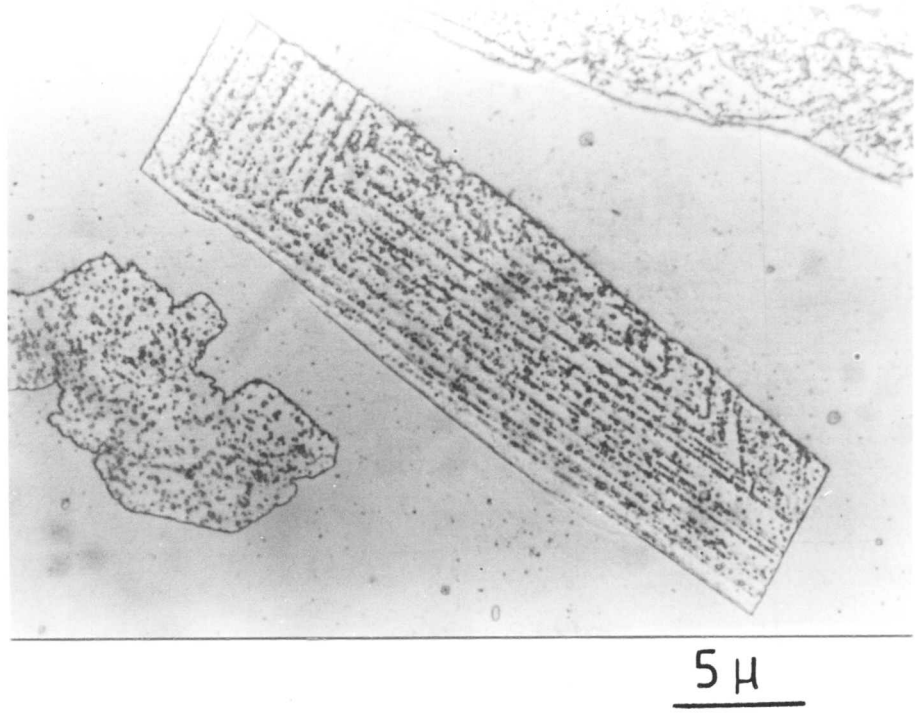

Fig. 4.8(a) The interphase precipitation associated with highly facetted idiomorphic ferrite is evident in this micrograph.

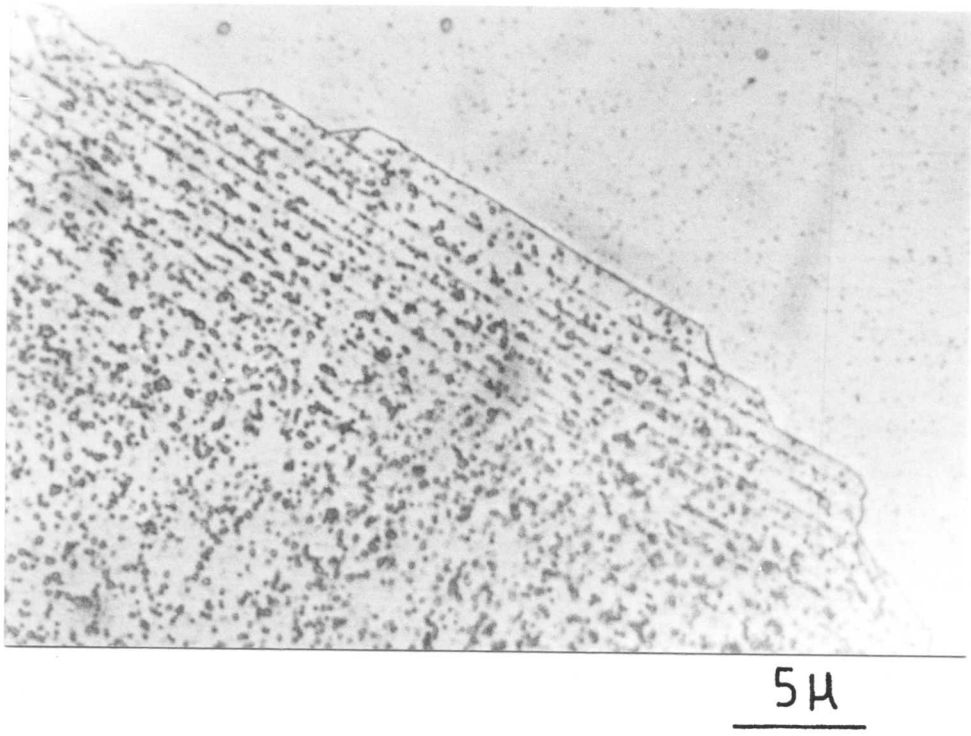

Fig. 4.9 Ledges are moving in two opposite driections on the same interface.

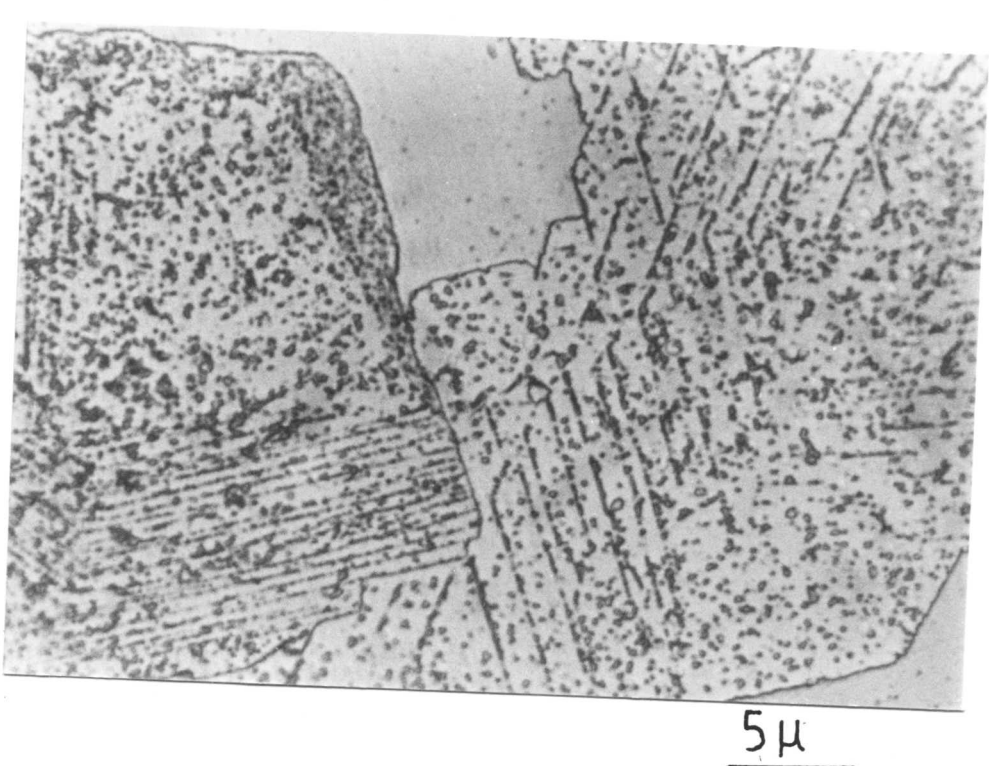

Fig. 4.10(a) Complex nature of carbide precipitation during the $\gamma \rightarrow \alpha$ transformation is apparent in these micrographs.

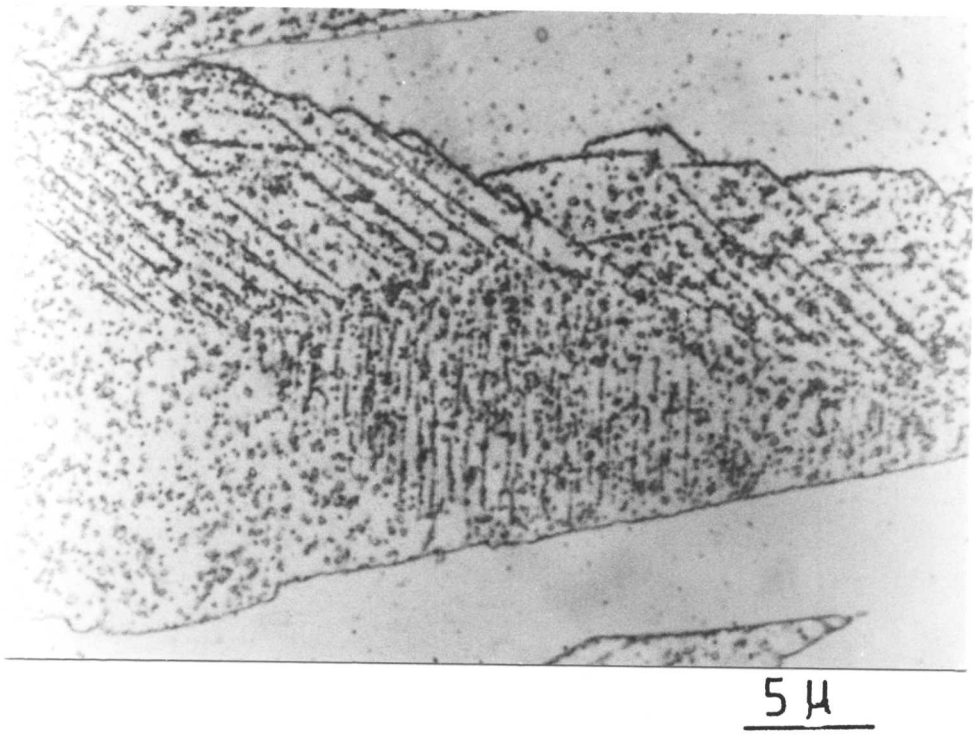

Fig. 4.10 (b)

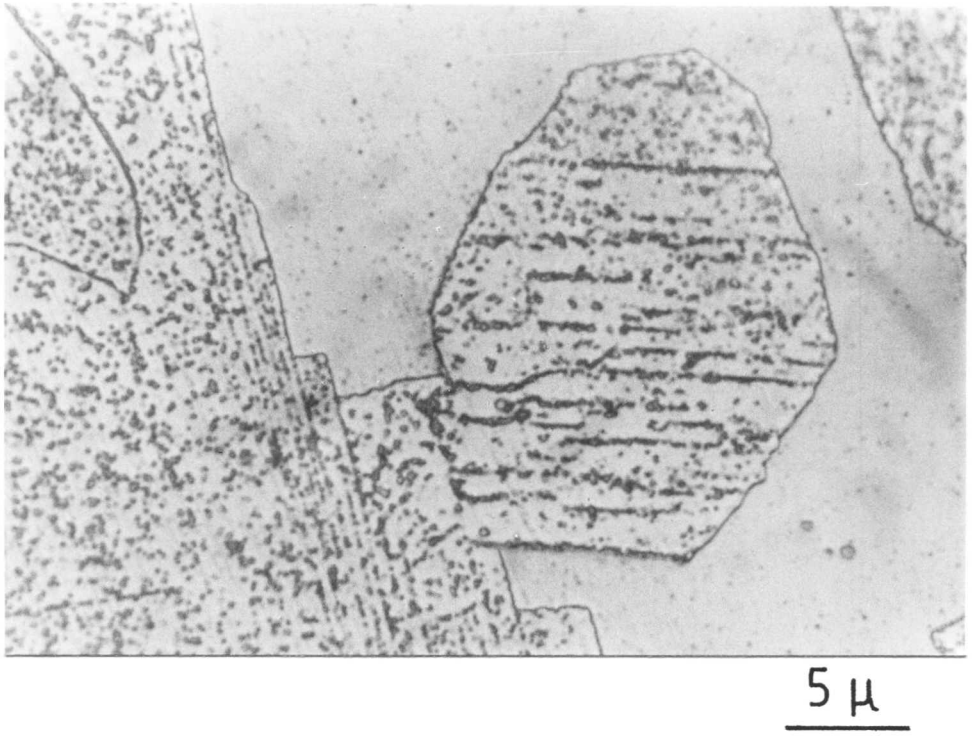

Fig. 4.10 (c)

Fig. 4.10 (b) and (c) Complex nature of carbide precipitation during the $\gamma \rightarrow \alpha$ transformation is apparent in these micrographs.

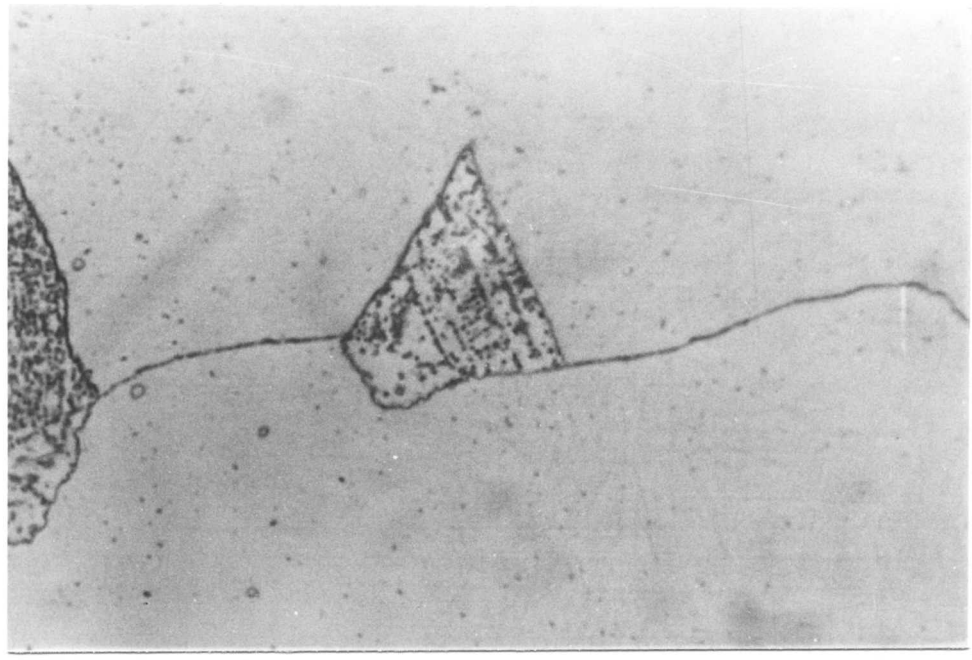

Fig. 4.11 The grain-boundary allotriomorph showing interphase precipitation to only one side of the grain-boundary.

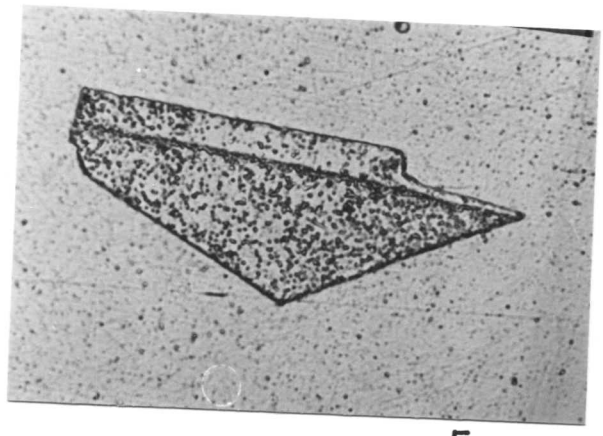

(a)

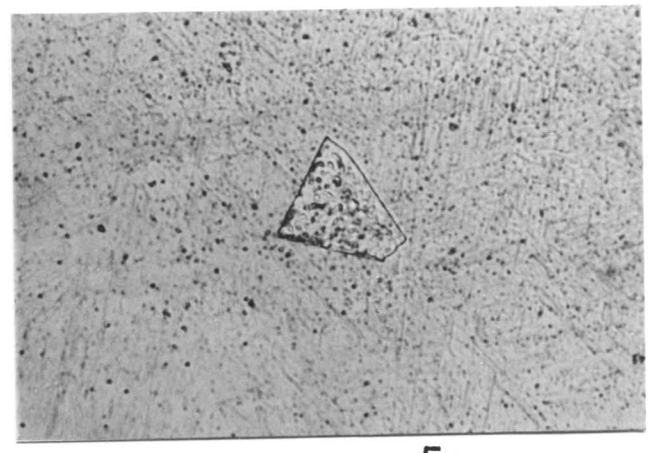

(d)

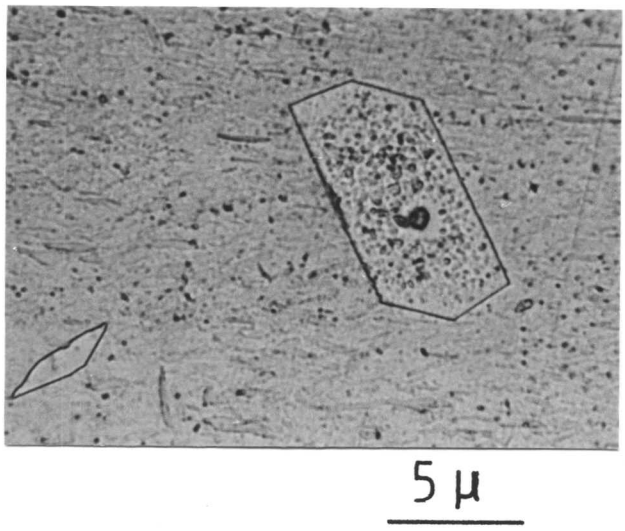

(b)

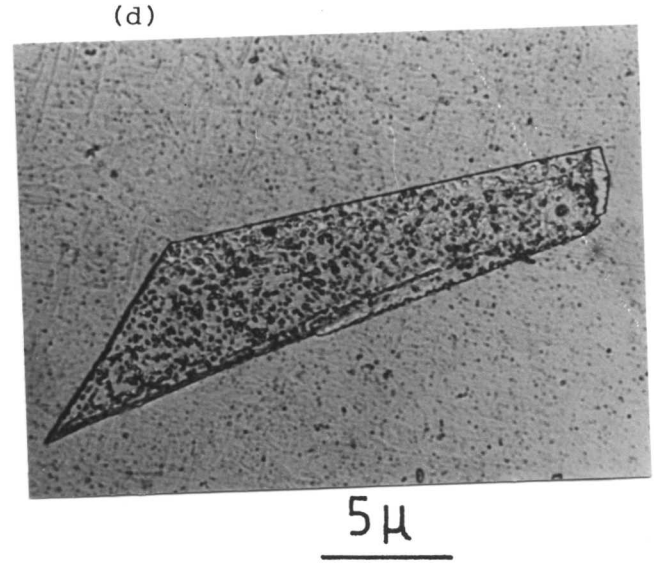

(e)

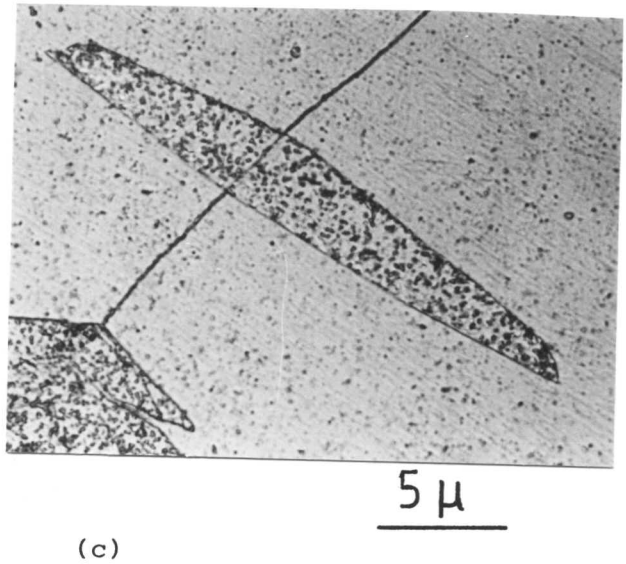

(c)

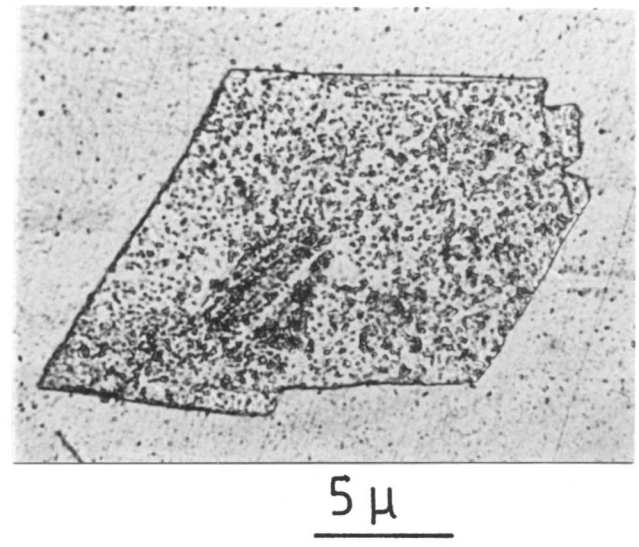

(f)

Fig. 4.12(a) to (f) Showing highly facetted α-ferrite.

(a)

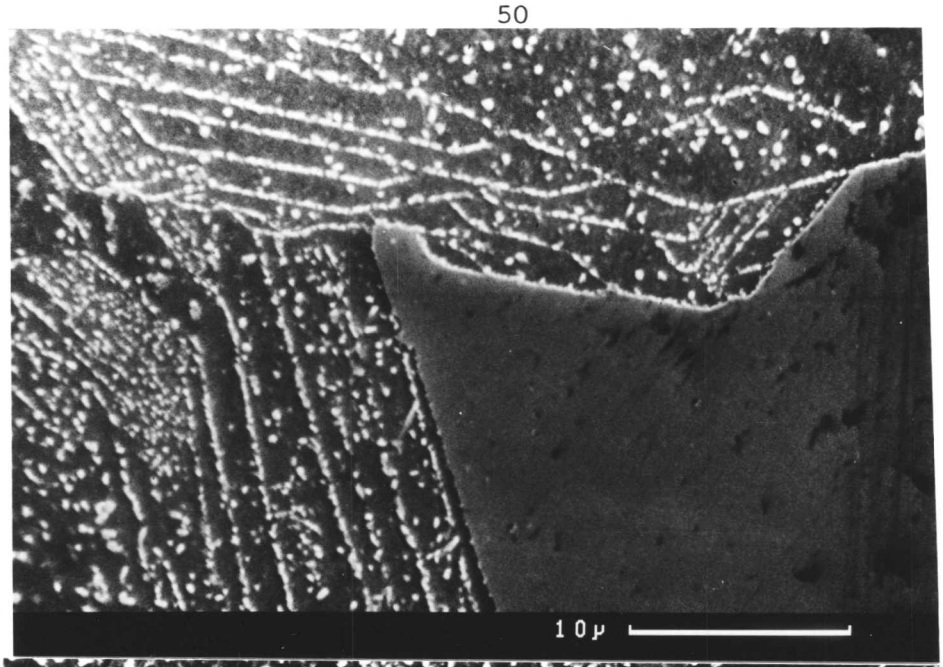

(b)

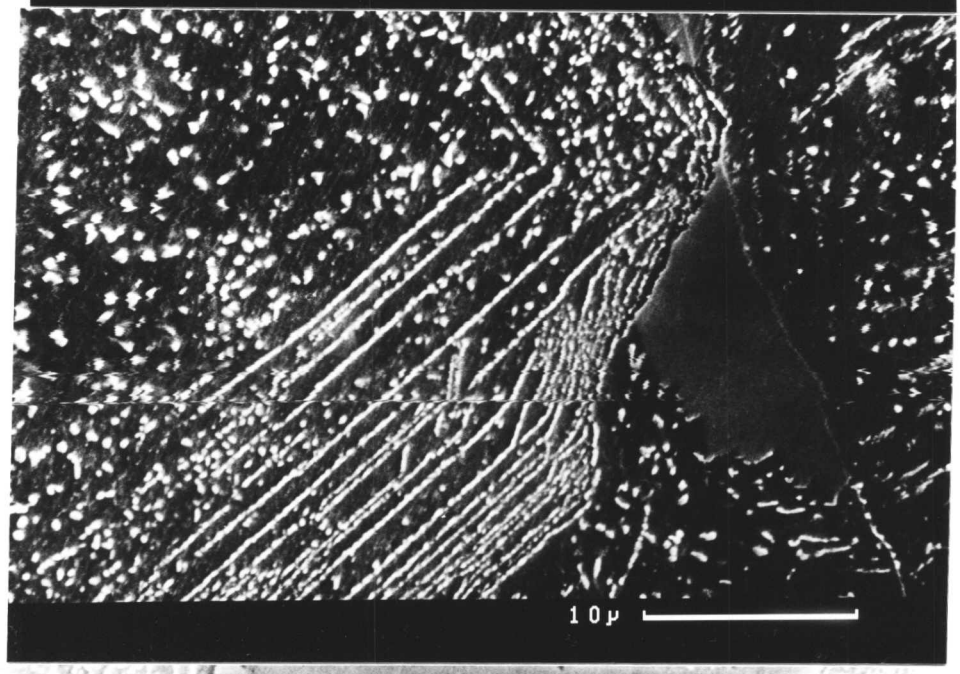

(c)

Fig. 4.13(a) to (c) Showing variation in the band spacing. Random carbide precipitation is also visible.

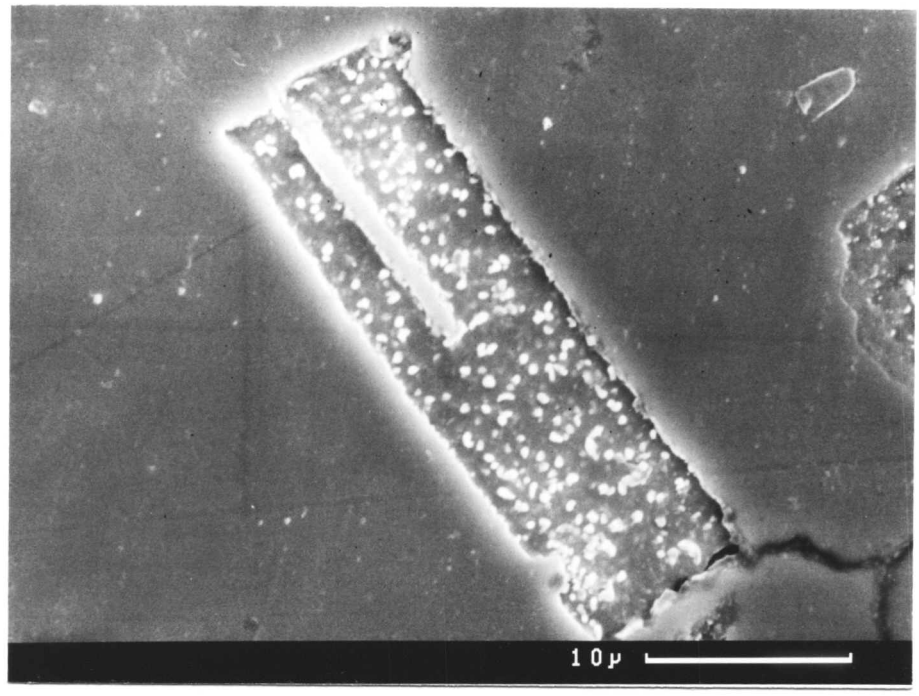

(a)

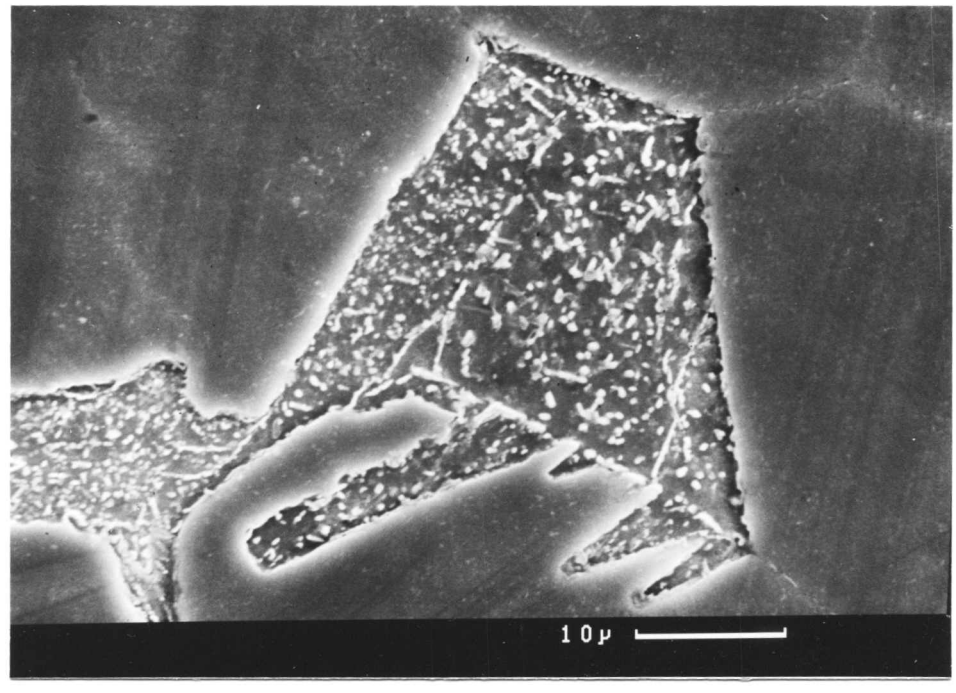

(b)

Fig. 4.14(a) to (b) Showing carbide precipitation along the planar low energy facets. But there is no evidence of ledges on these interfaces.

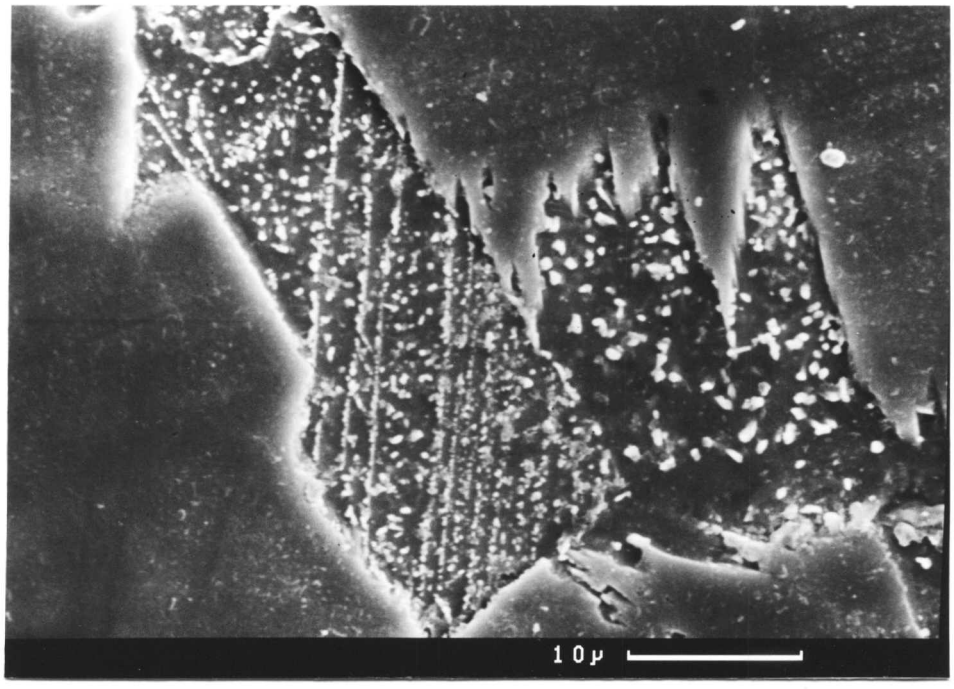

(c)

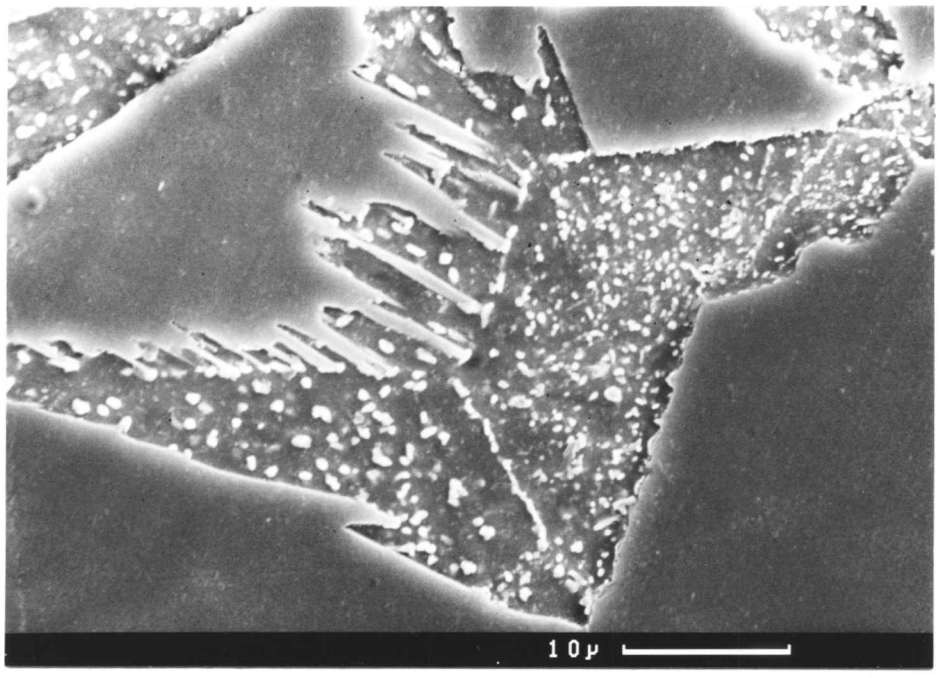

(d)

Fig. 4.14 (c) and (d) Showing carbide precipitation along planar low energy facets. But there is no evidence of ledges on these interfaces.

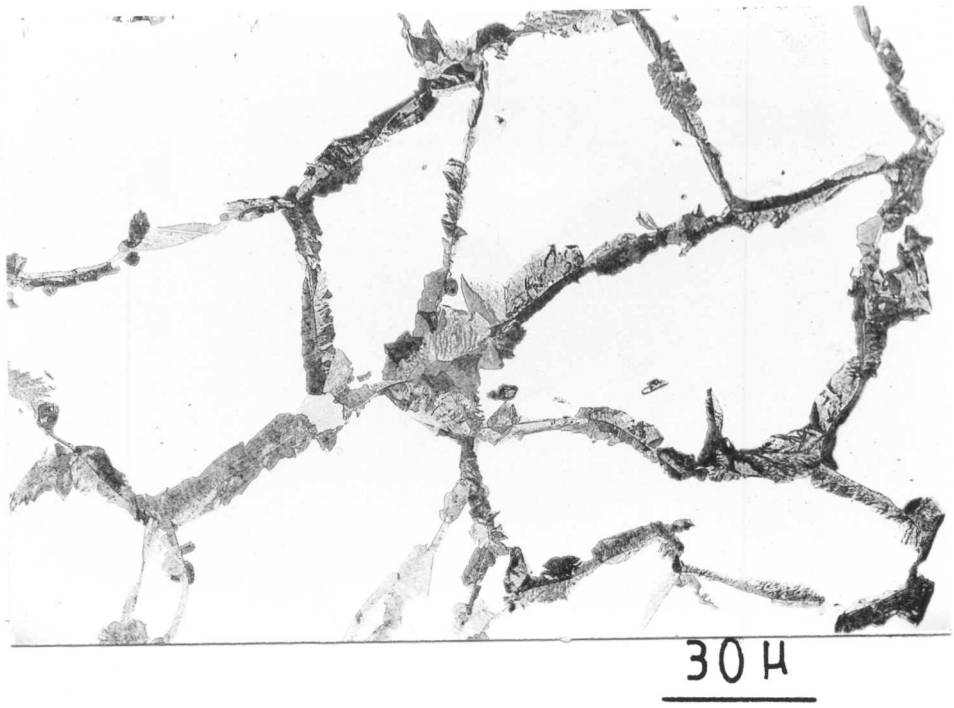

Fig. 4.15 Showing dark etch grain-boundary allotriomorphic ferrite.

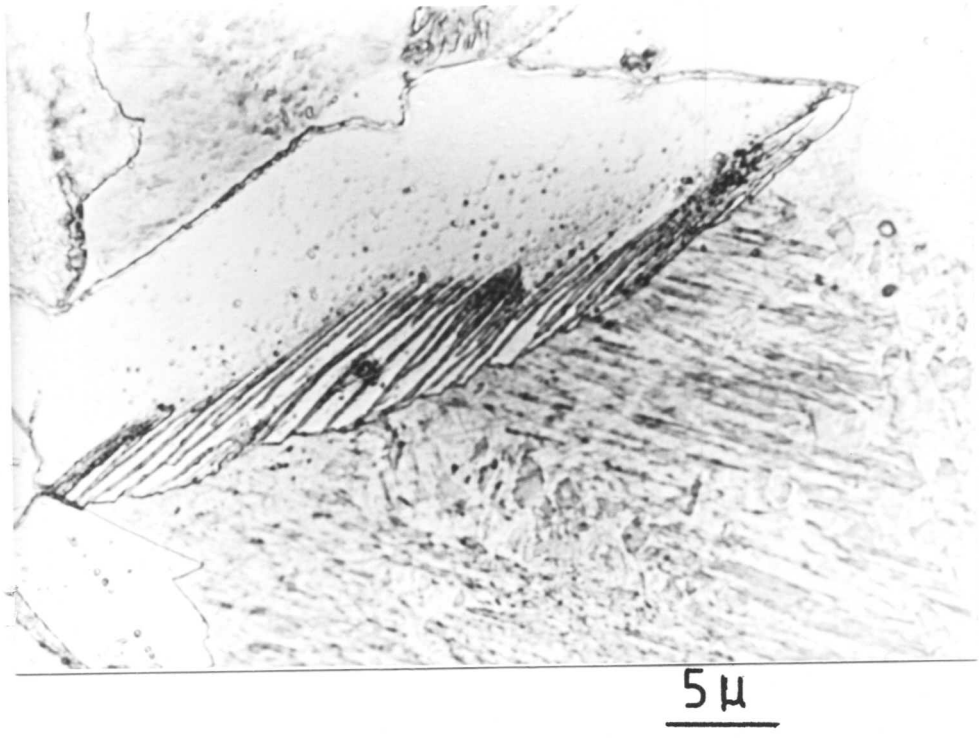

Fig. 4.16 Showing fibrous carbides formed in association with the facet which has been moved by a ledge mechanism.

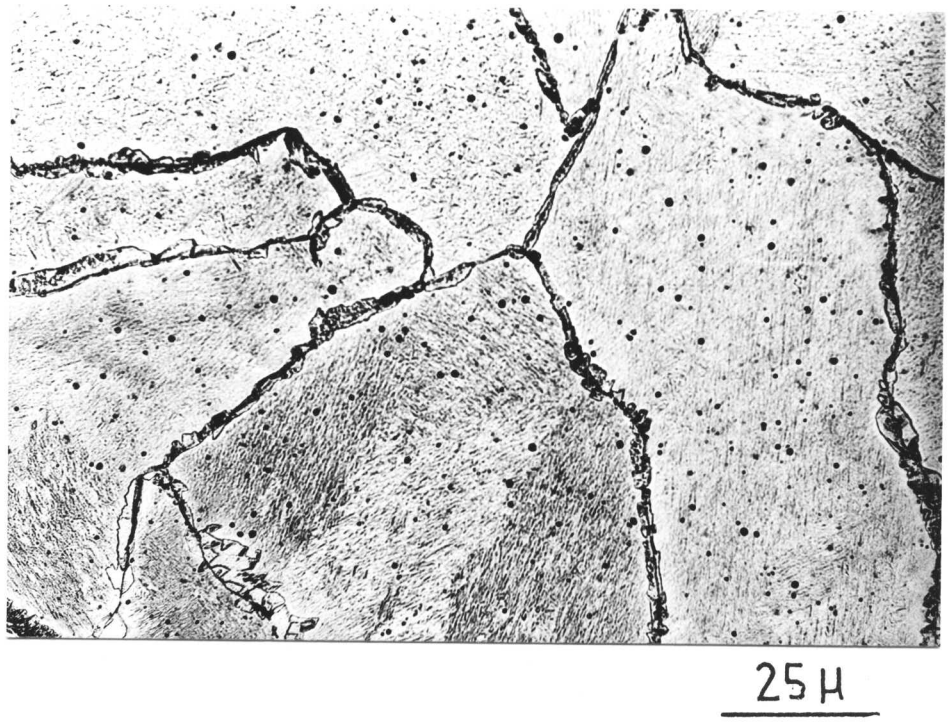

Fig. 4.17 Showing grain-boundary allotriomorphs having high aspect ratio. (Isothermal transformation at 750°C for 5 minutes.)

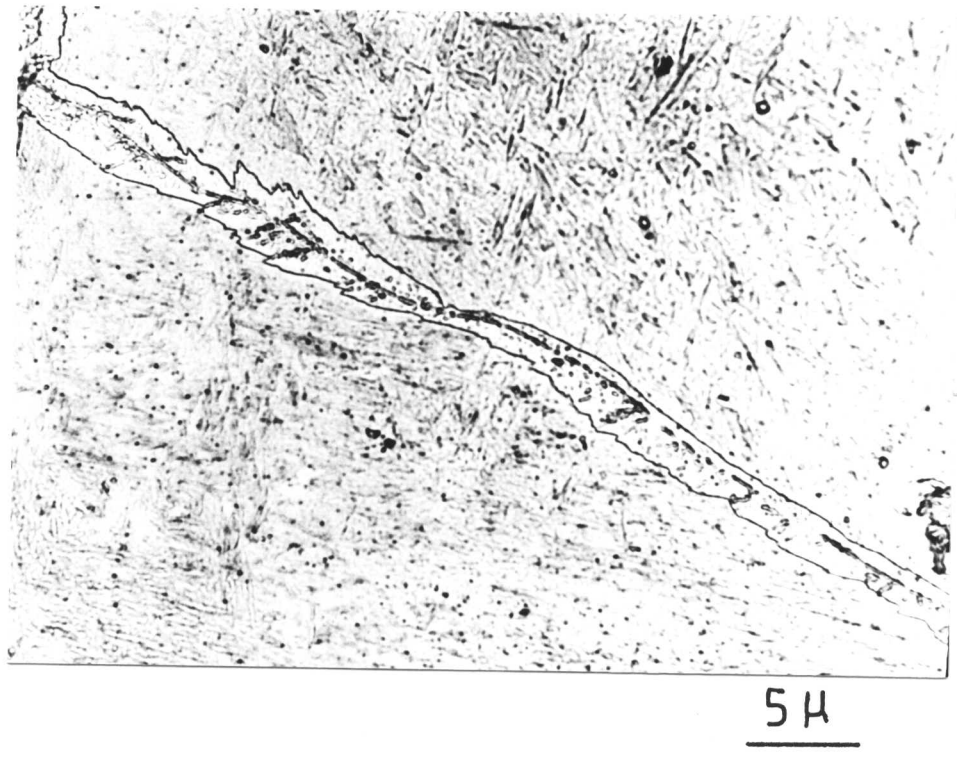

Fig. 4.18 Showing the serrated interface arising as a result of interface pinning by alloy carbides. (Isothermal transformation at 750°C for 5 minutes.)

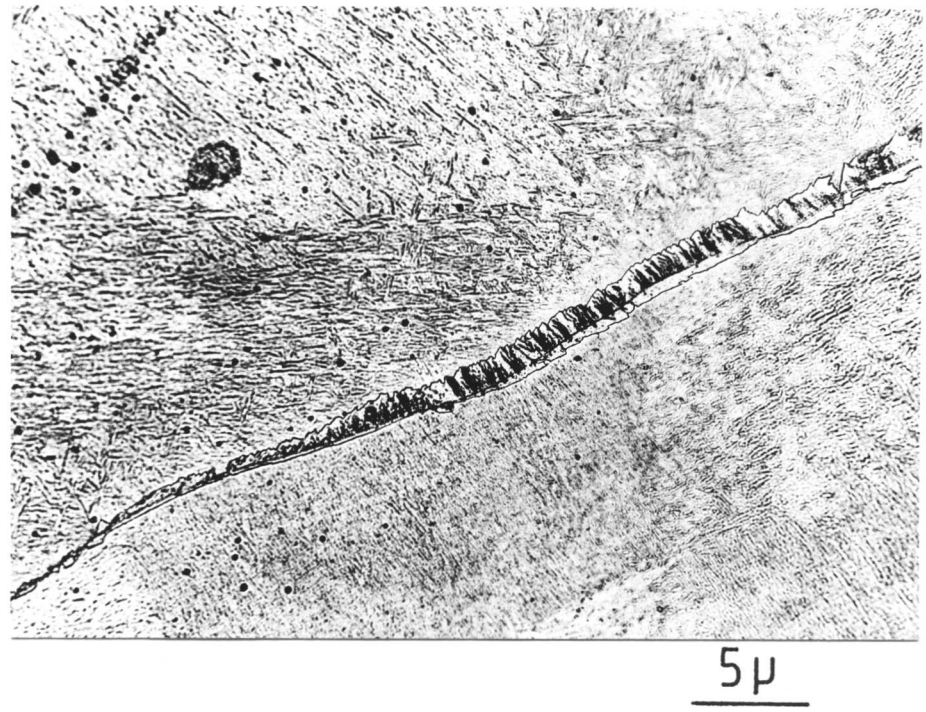

Fig. 4.19 Showing fibrous carbides formed on one side of the boundary. (Isothermal transformation at 750°C for 5 minutes.)

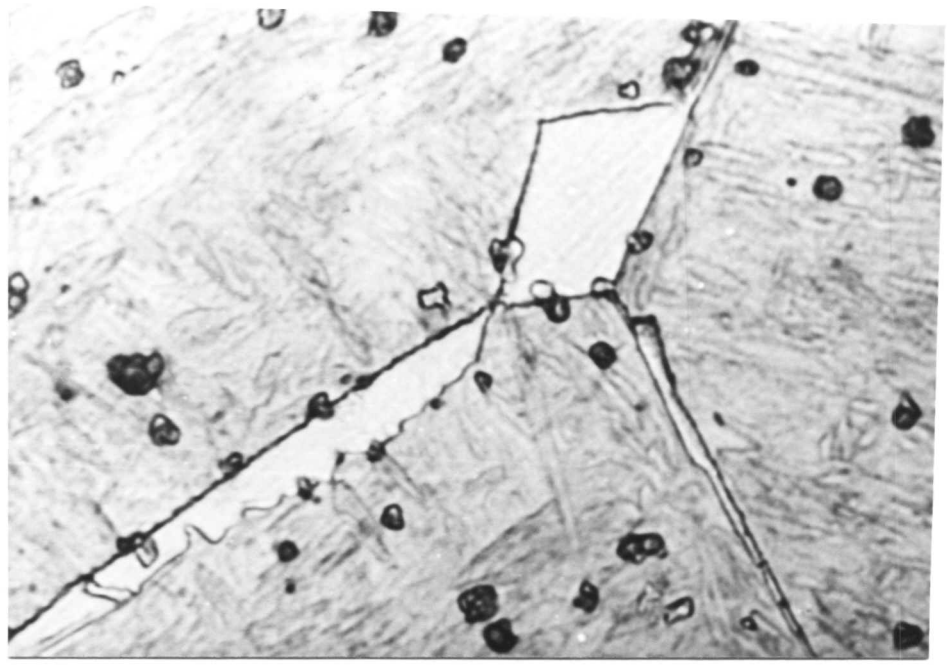

Fig. 4.20 Showing grain-boundary allotriomorphs formed during the early stage of transformation. (Isothermal transformation at 700°C for 10 minutes.)

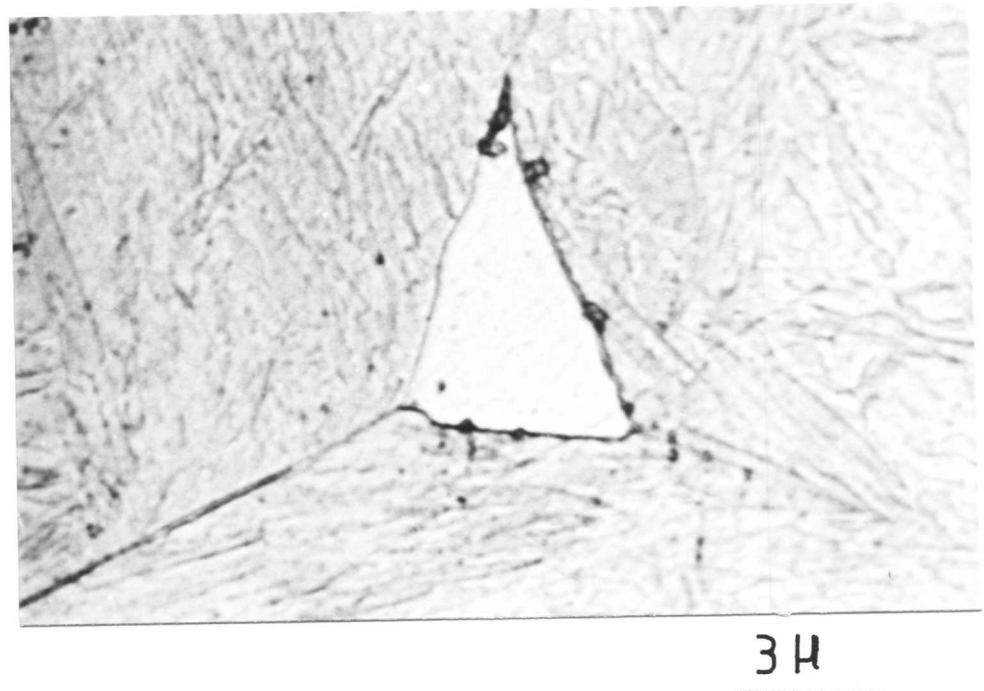

Fig. 4.21 Showing grain-boundary allotriomorphs formed at the junction where three grain-boundaries meet. (Isothermal transformation at 700°C for 10 minutes.)

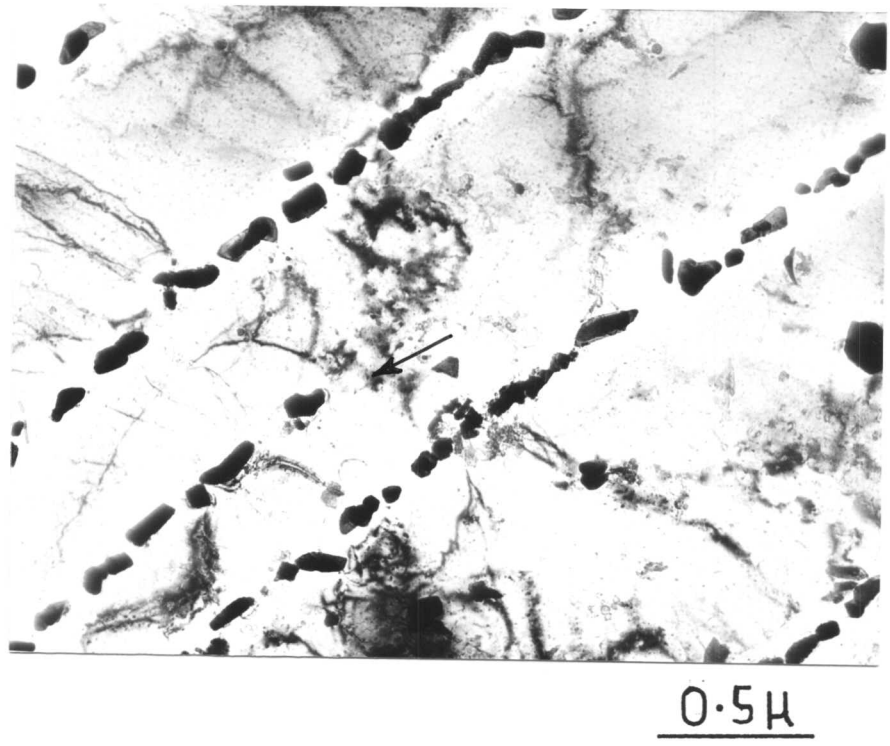

Fig. 4.22 Shows evidence of interphase precipitation. (Isothermal transformation at 850°C for 20 minutes.) Thin foil micrograph.

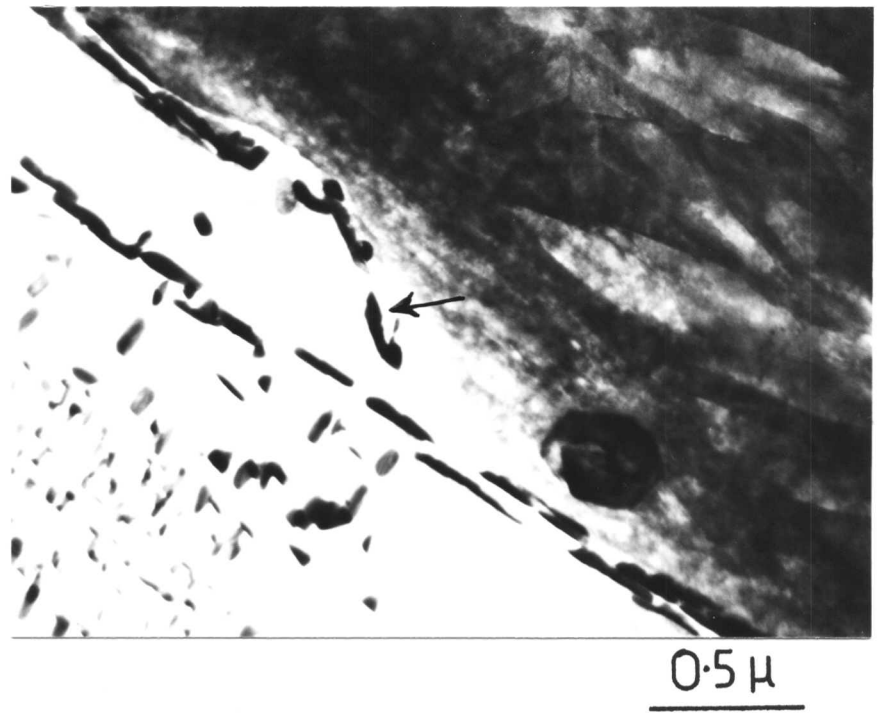

Fig. 4.23 Showing precipitation on the mobile ledge.

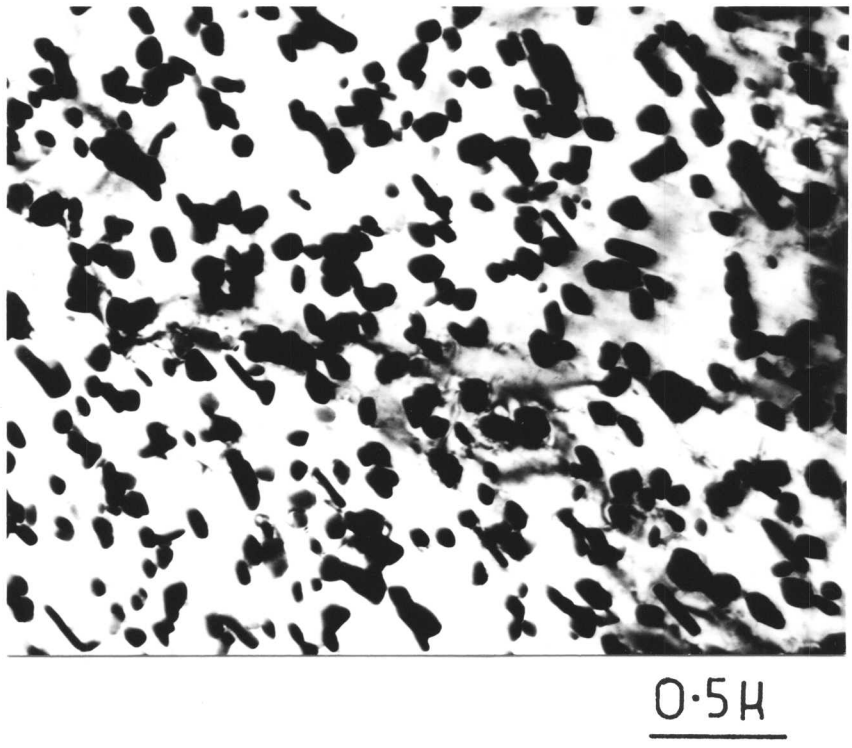

Fig. 4.24 Carbide precipitation from super-saturated ferrite. (Isothermal transformation at 750°C for 5 minutes.)

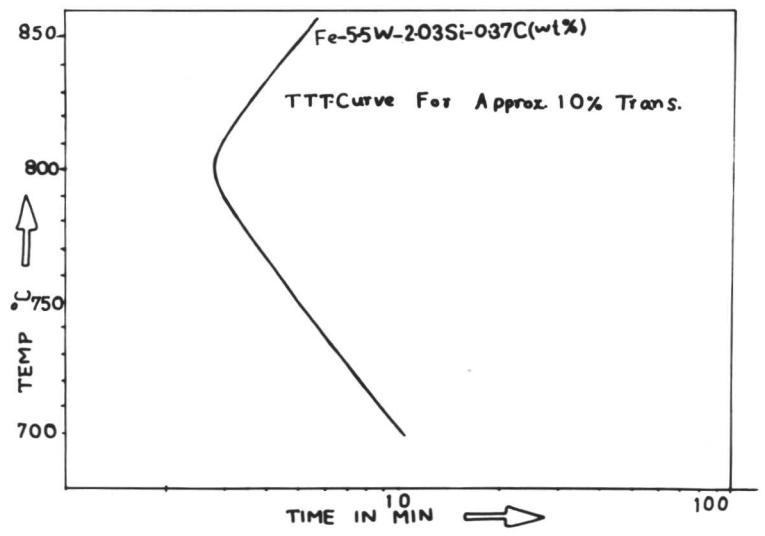

Fig. 4.25 : TTT diagram for 10% transformation in Fe-5.5W-2.03Si-0.37C (wt%) alloy.

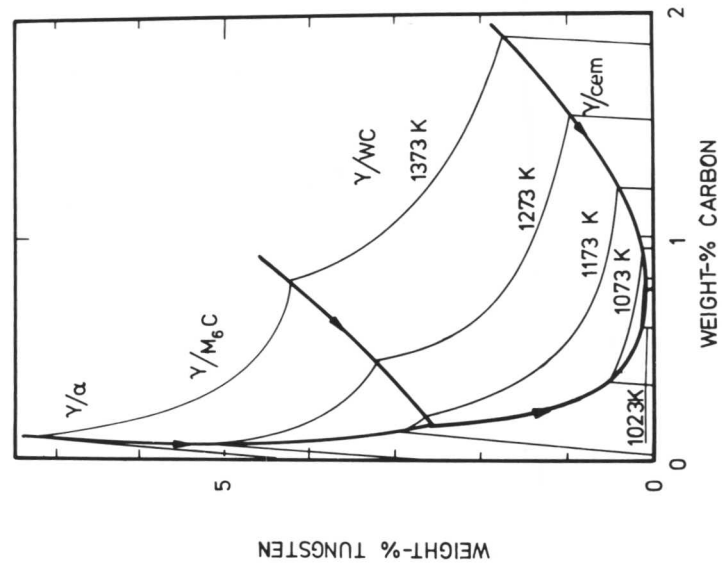

Fig. 4.26 Isothermal section of Fe-Si-C alloy in the temperature range of 1023K to 1373K.

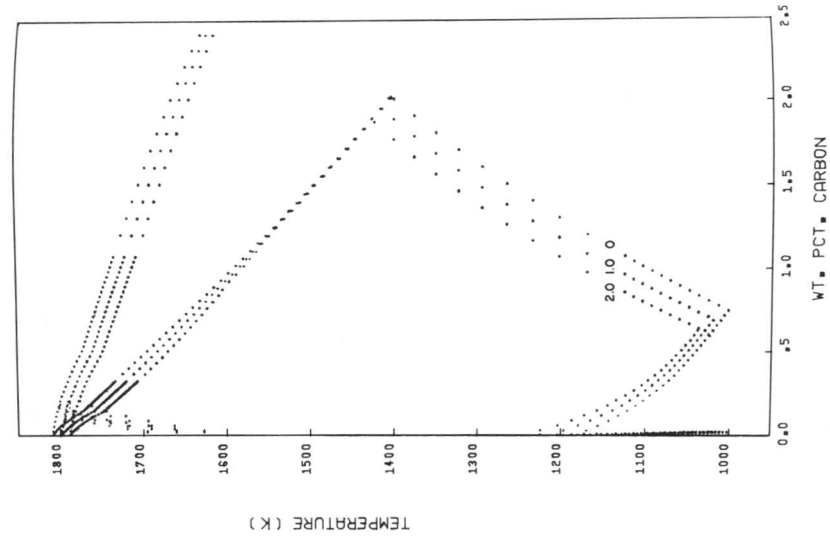

Fig. 4.27 Fe-C equilibrium diagram at constant silicon content.

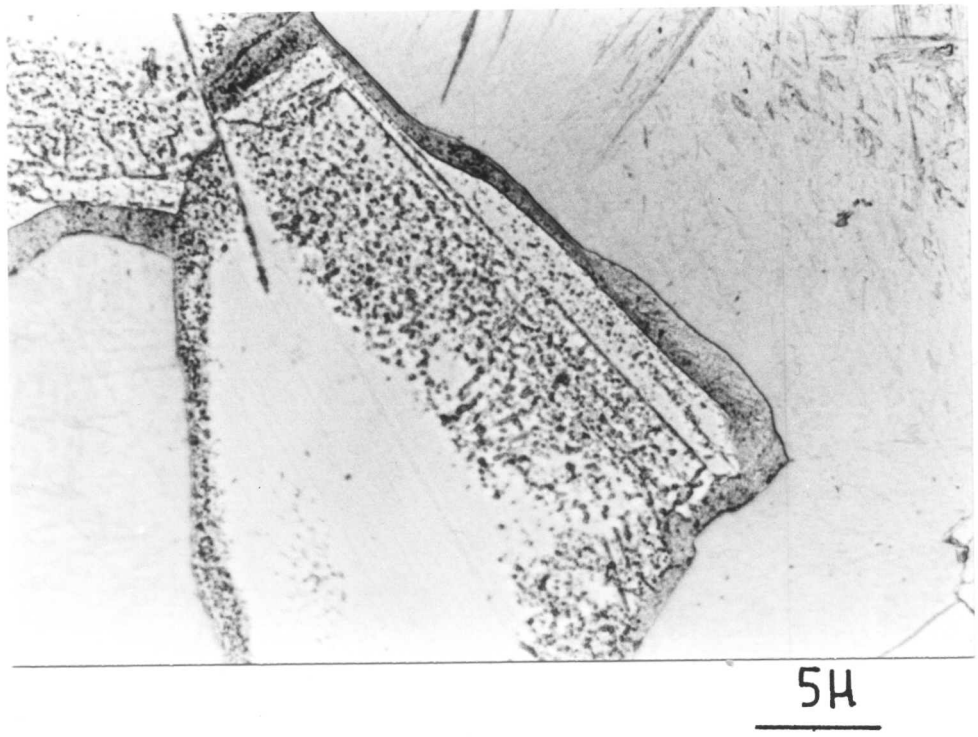

(a)

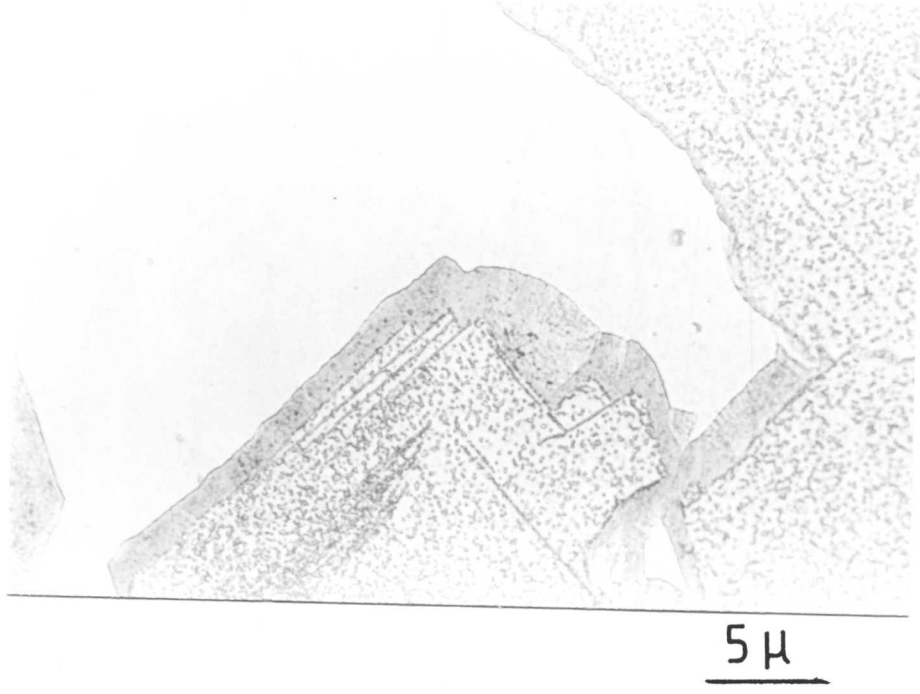

(b)

Fig. 4.28(a) to (b) Interphase precipitation surrounded by a thick grey level. (Isothermal transformation at 850°C, followed by step quenching at 750°C.)

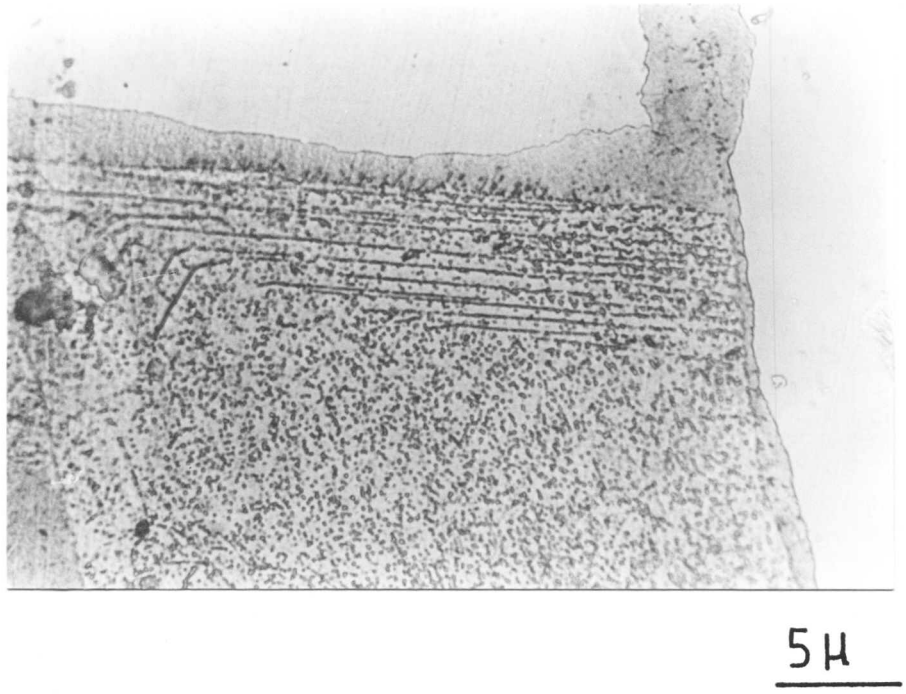

(c)

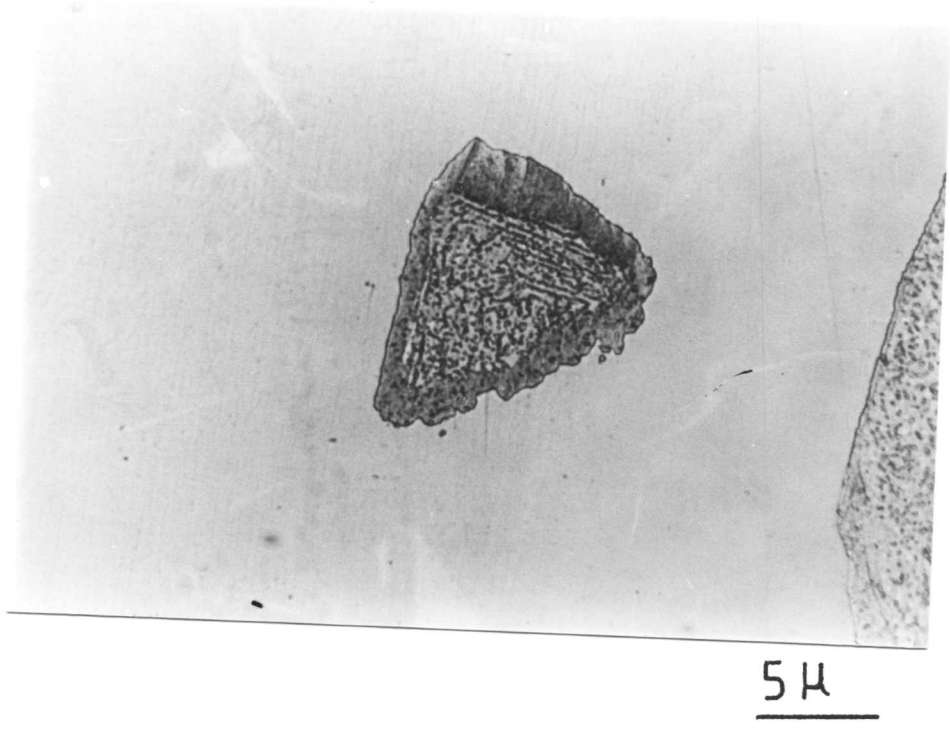

(d)

Fig. 4.28 (c) and (d) Interphase precipitation surrounded by a thick grey level. (Isothermal transformation at 850°C, followed by step quenching at 750°C).

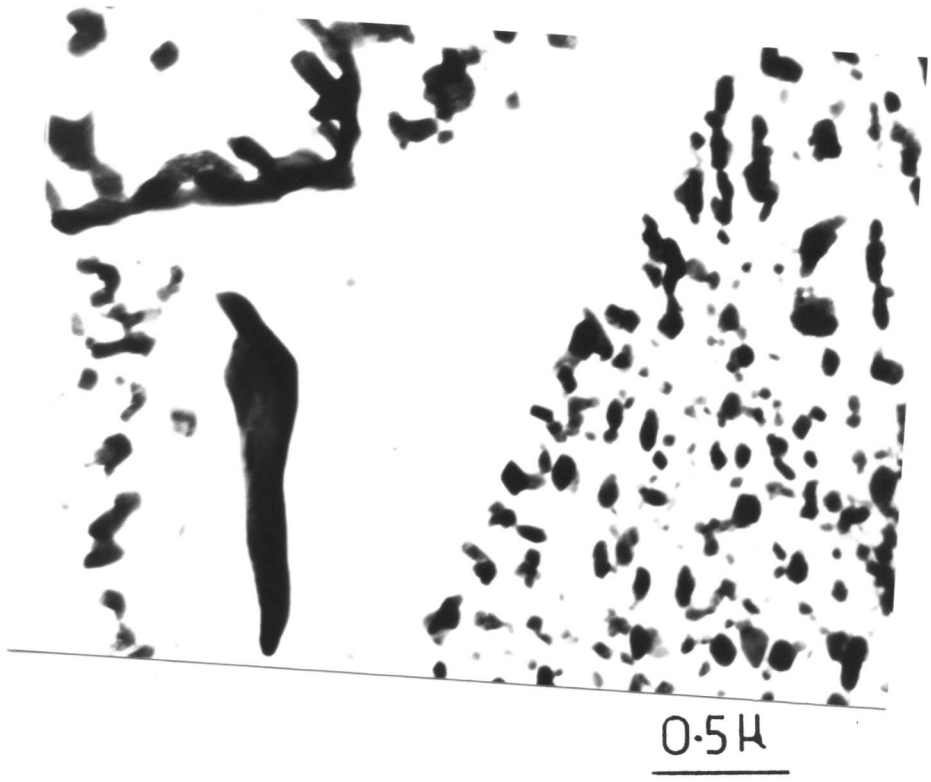

Fig. 4.29 Showing dense carbide precipitation on only side of the micrograph. (Isothermal transformation at 850°C for 20 minutes, followed by step quenching at 750°C.)

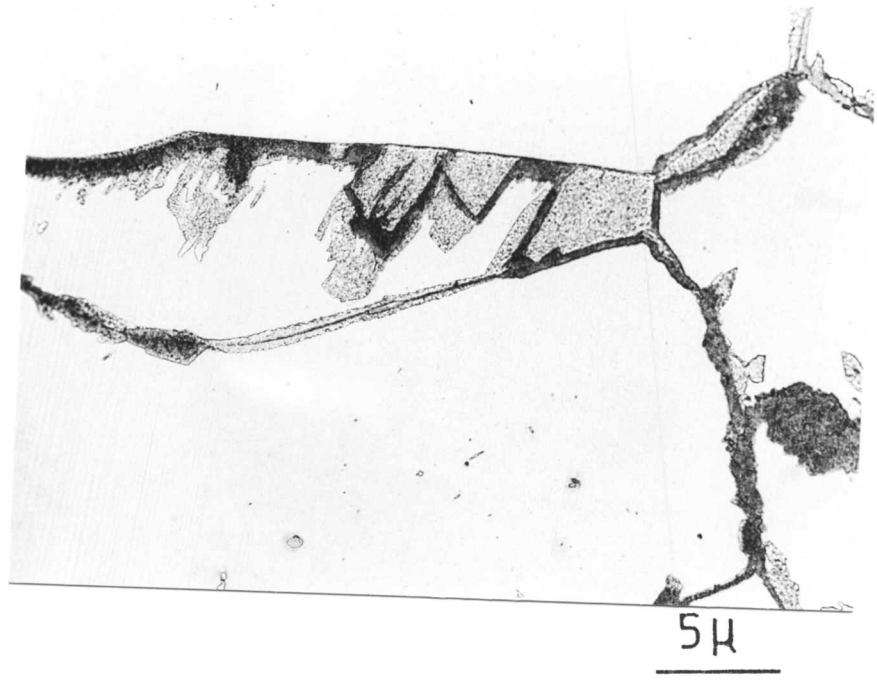

Fig. 4.30

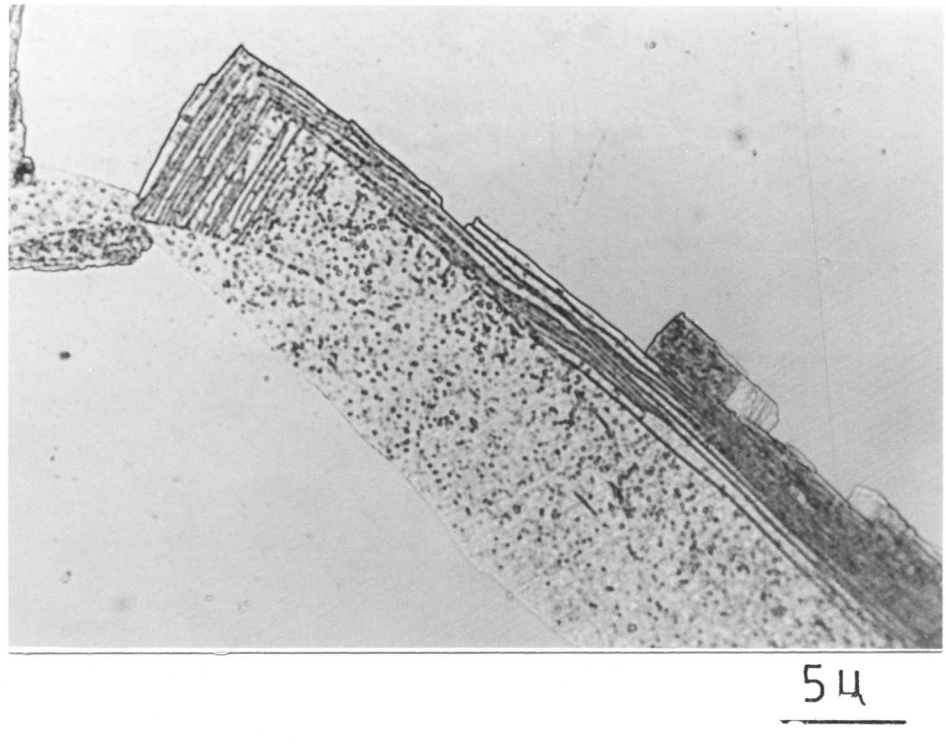

Fig. 4.31

Fig. 4.30 and 4.31 Showing carbide precipitation during double step quenching (i.e. 850°C → 750°C → 850°C). In certain areas there is a dense distribution of carbide whereas in some areas the interphase precipitation is more dominant.

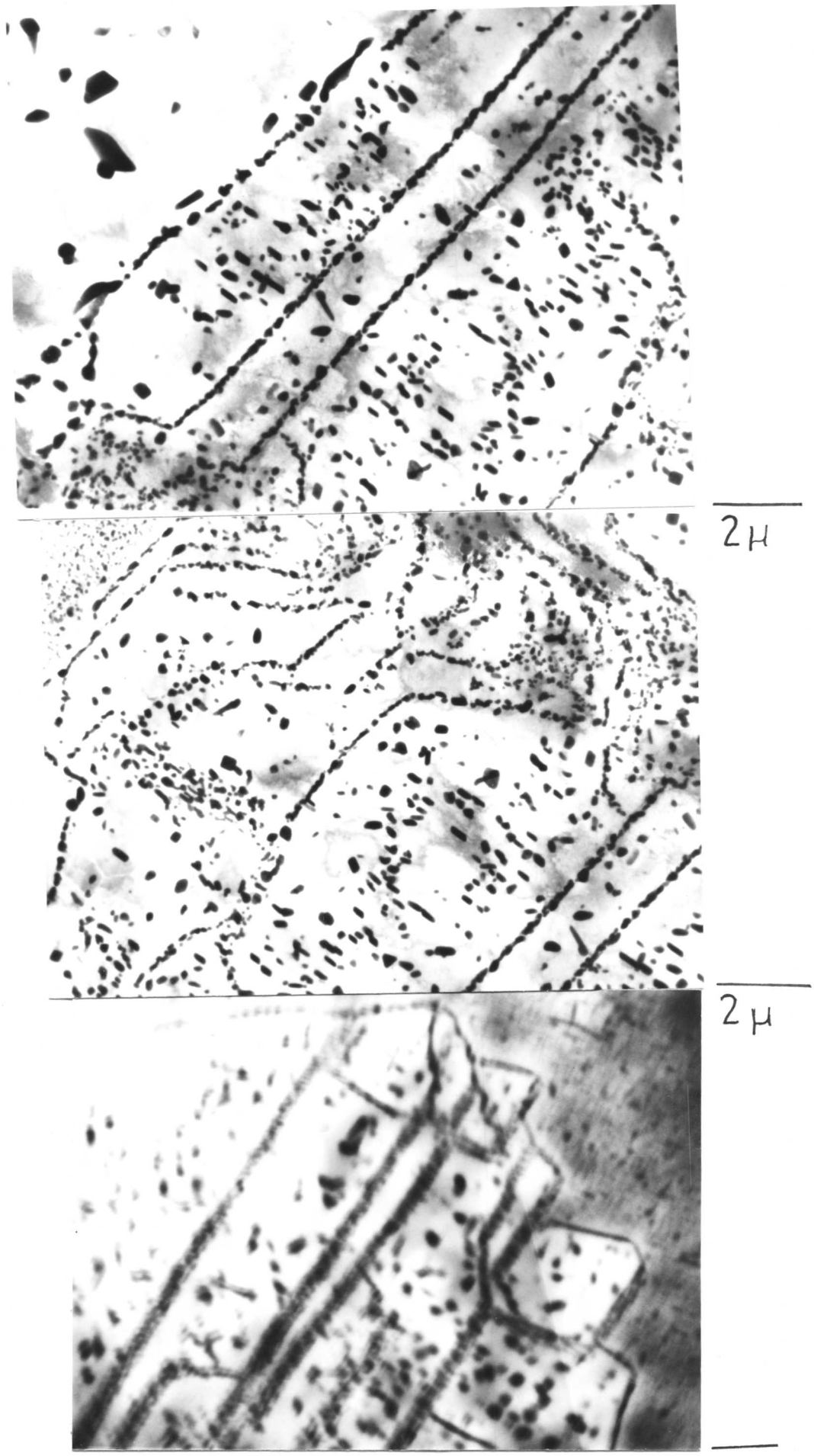

Fig. 4.32 to 4.34: Microstructure developed by double step quenching.

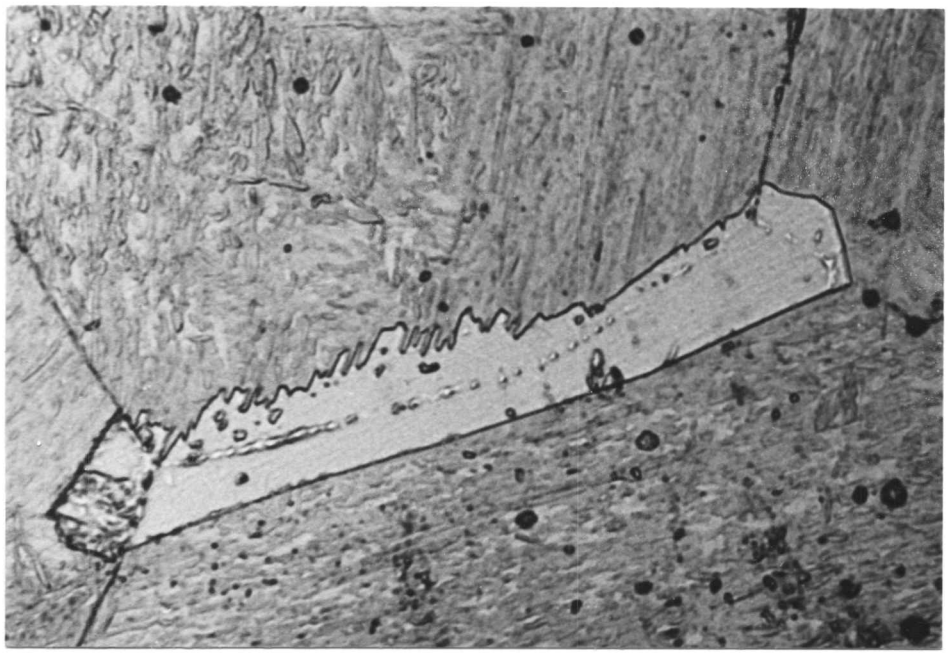

(a)

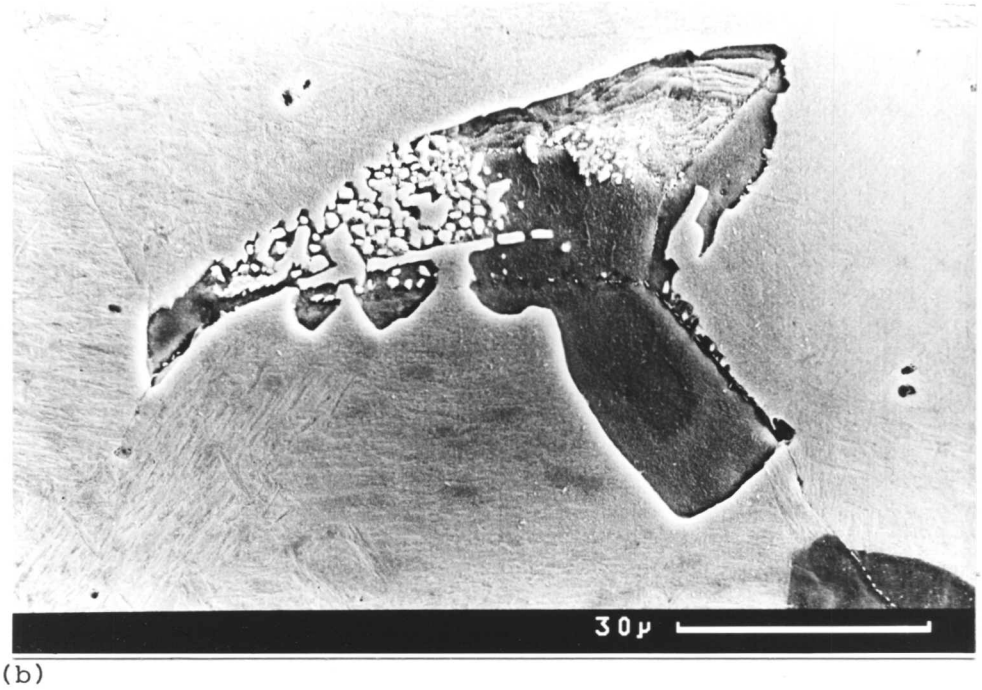

(b)

Fig. 4.35 (a) and (b) Ragged interface formed as a result of pinning by carbides. (Isothermal transformation at 800°C for 20 minutes.)

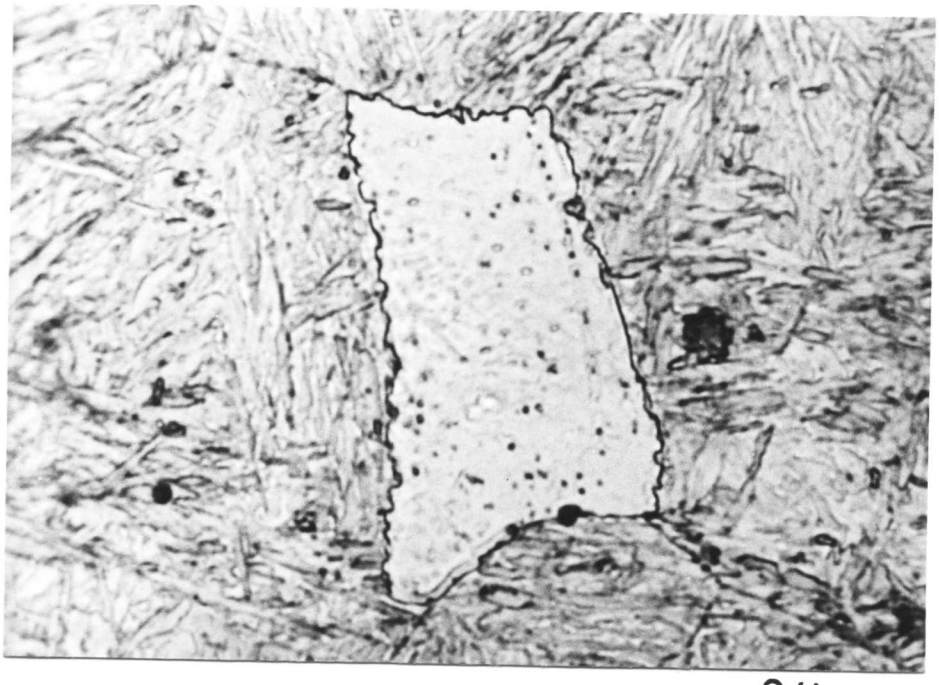

(a)

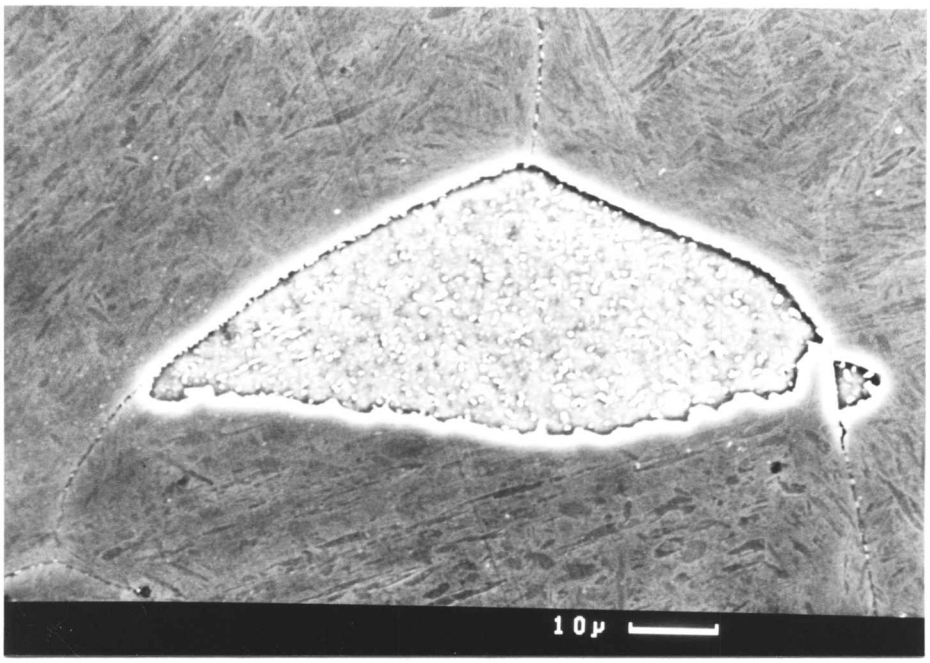

(b)

Fig. 4.36(a) and (b) Showing serrated interface formed as a result of interphase precipitation. (Isothermal transformation at 800°C for 40 minutes.)

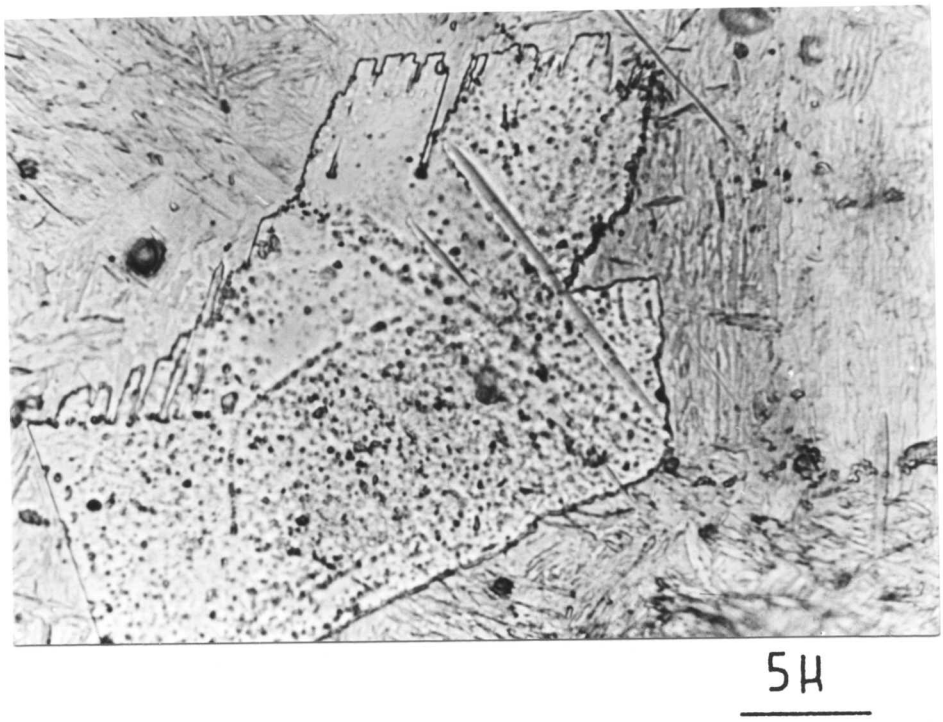

(a)

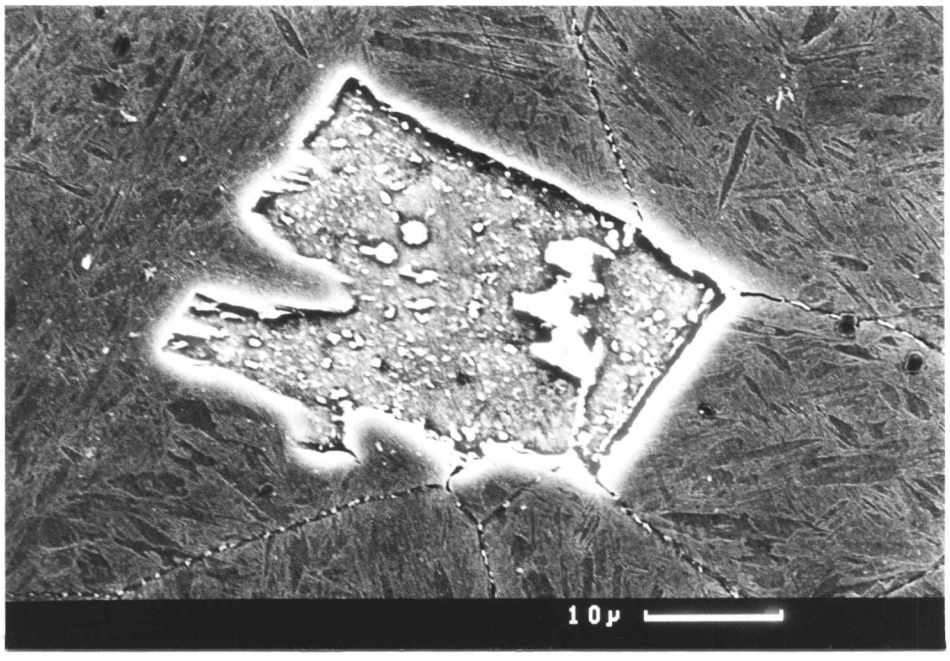

(b)

Figure 4.37(a) and (b) Showing ragged interface formed as a result of pinning by carbides. (Isothermal transformation at 800°C for 40 minutes.)

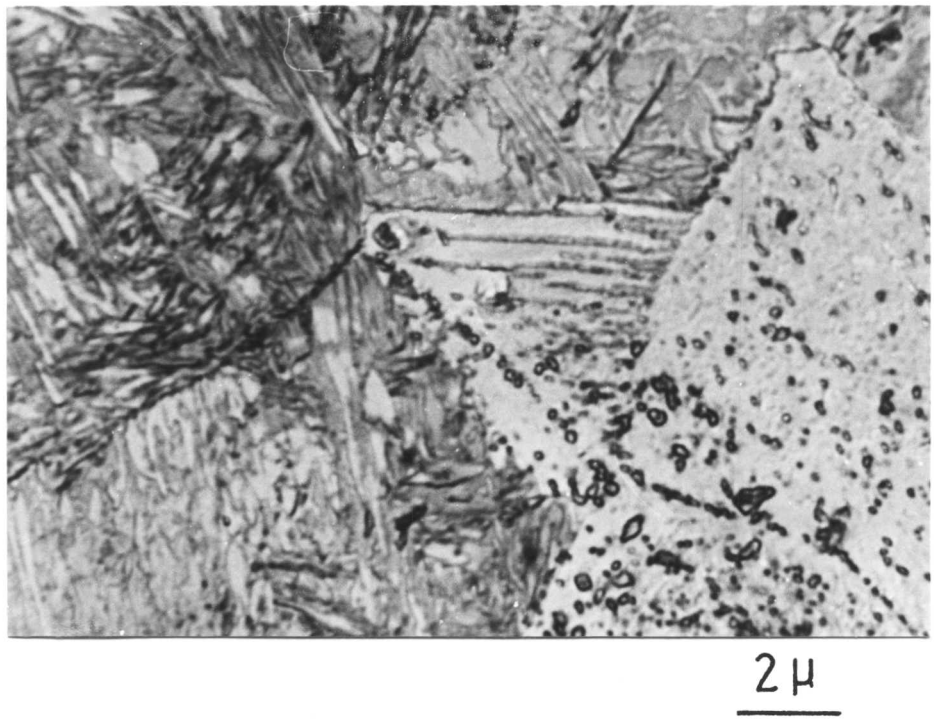

Fig. 4.38 Showing interphase precipitation associated with ledge mechanism. (Isothermal transformation at 800°C for 80 minutes.)

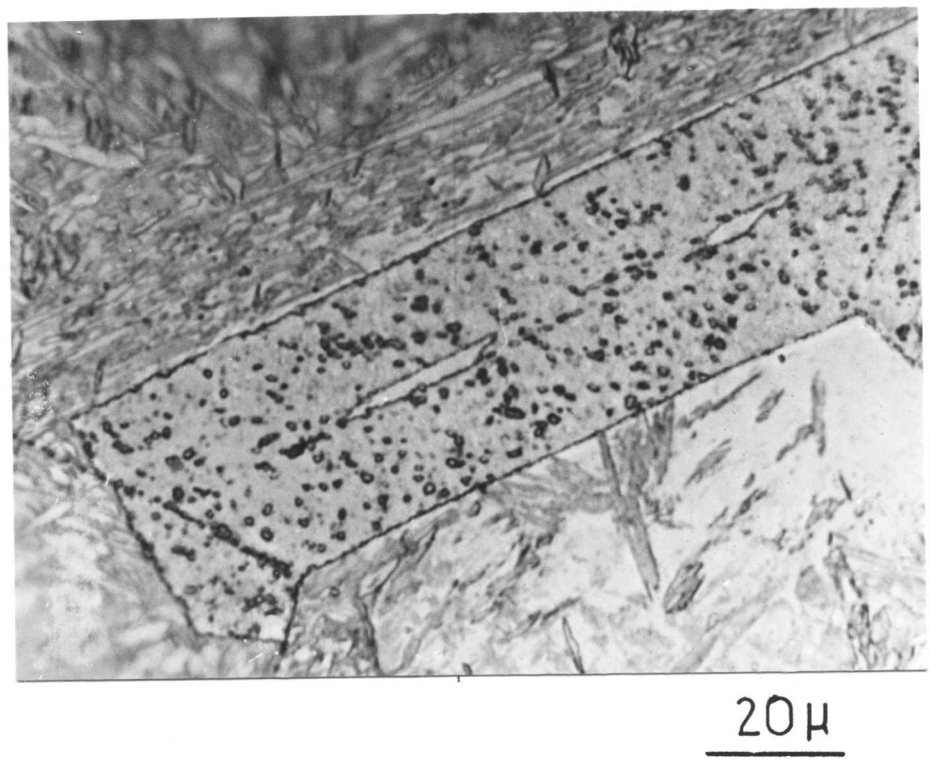

Fig. 4.39 Showing cusps on the low energy facets. (Isothermal transformation at 800°C for 80 minutes.)

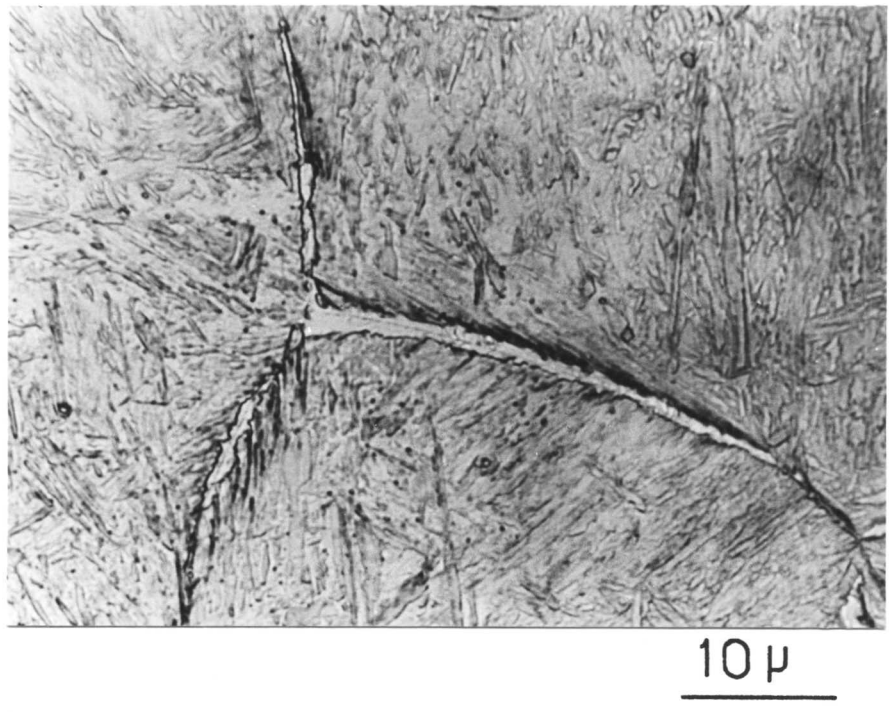

Fig. 4.40 Showing grain-boundary allotriomorphs with high aspect ratio. (Isothermal transformation at 700°C for 40 minutes.)

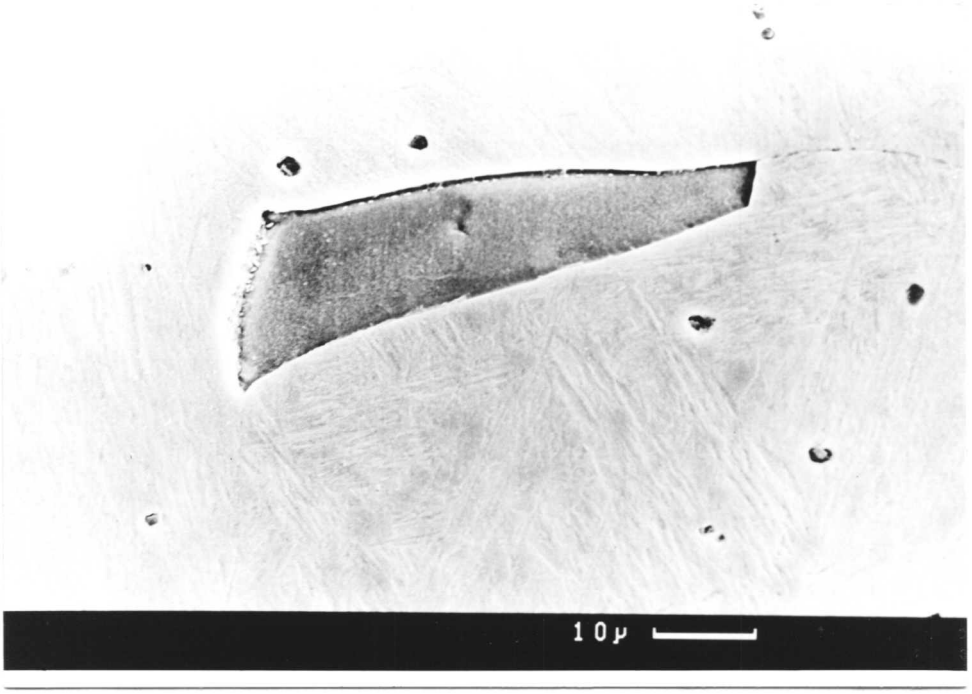

Fig. 4.41 Showing grain-boundary allotriomorphs. (Isothermal transformation at 700°C for 40 minutes.)

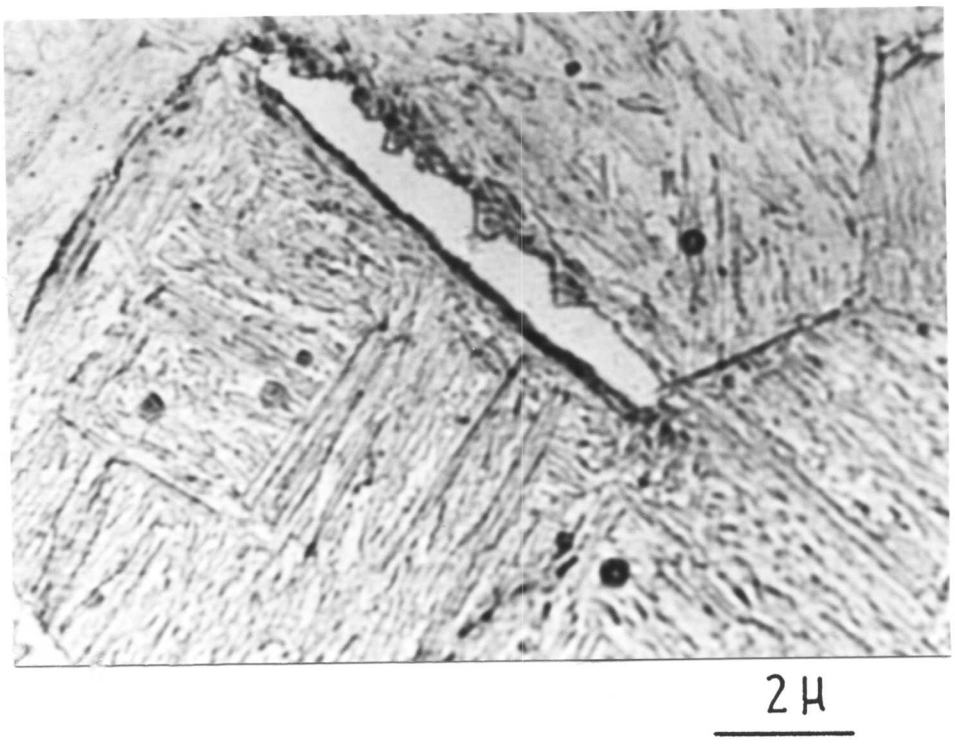

Fig. 4.42 Showing cusps on the low energy facets. (Isothermal transformation at 700°C for 40 minutes.)

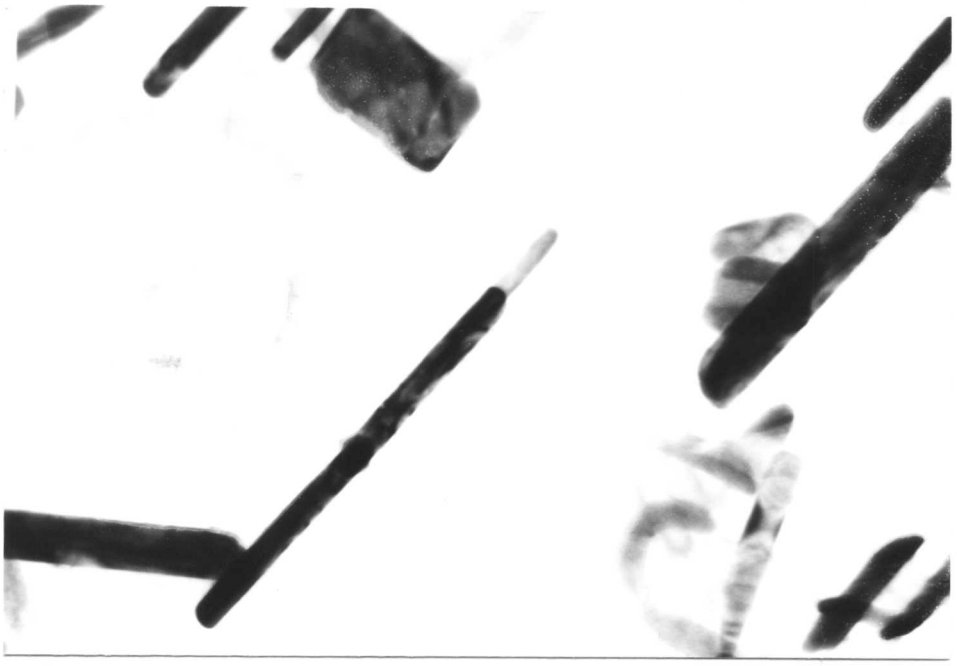

(a)

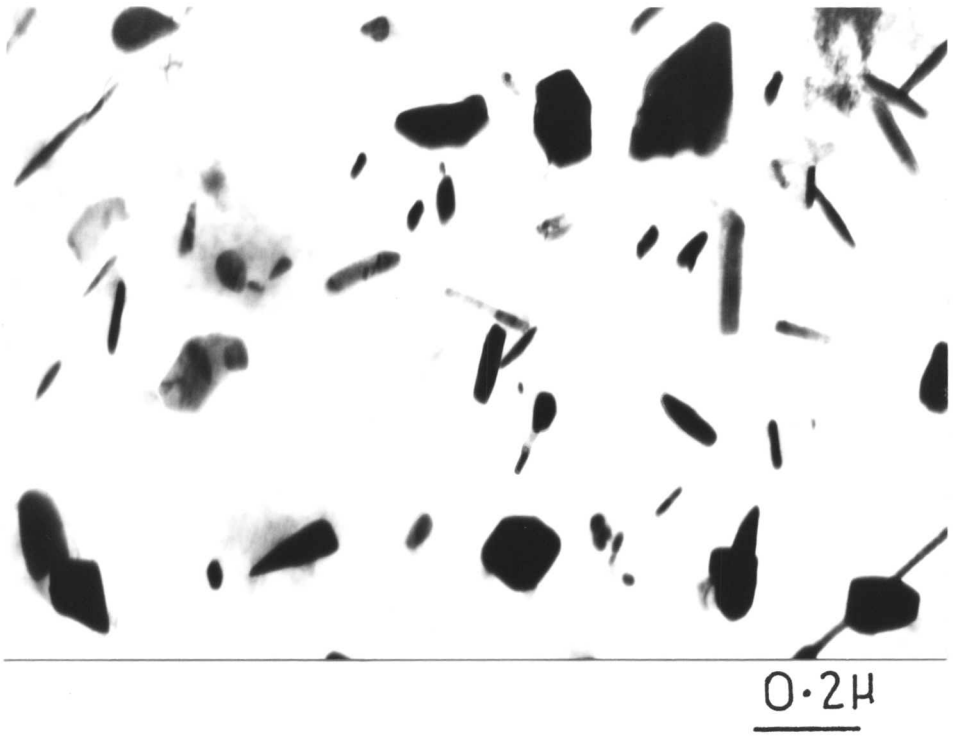

(b)

Fig. 4.43(a) and (b) Showing carbides in several different morphologies. (Isothermal transformation at 800°C for 40 minutes.)

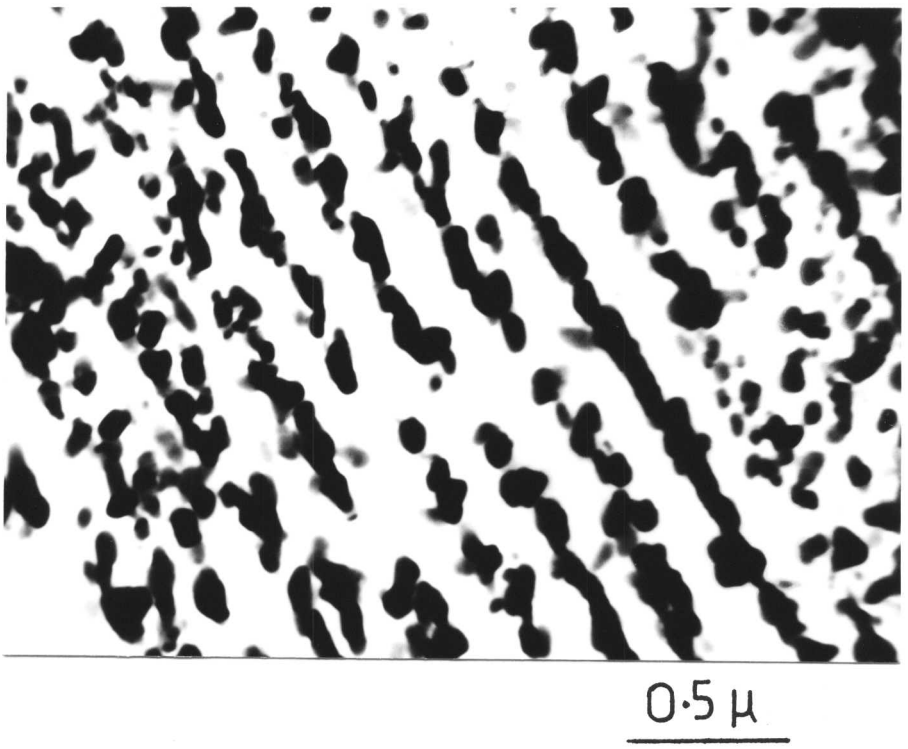

Fig. 4.44: TEM micrograph showing higher volume fraction of tungsten carbide at 750°C compared to that obtained at 800°C

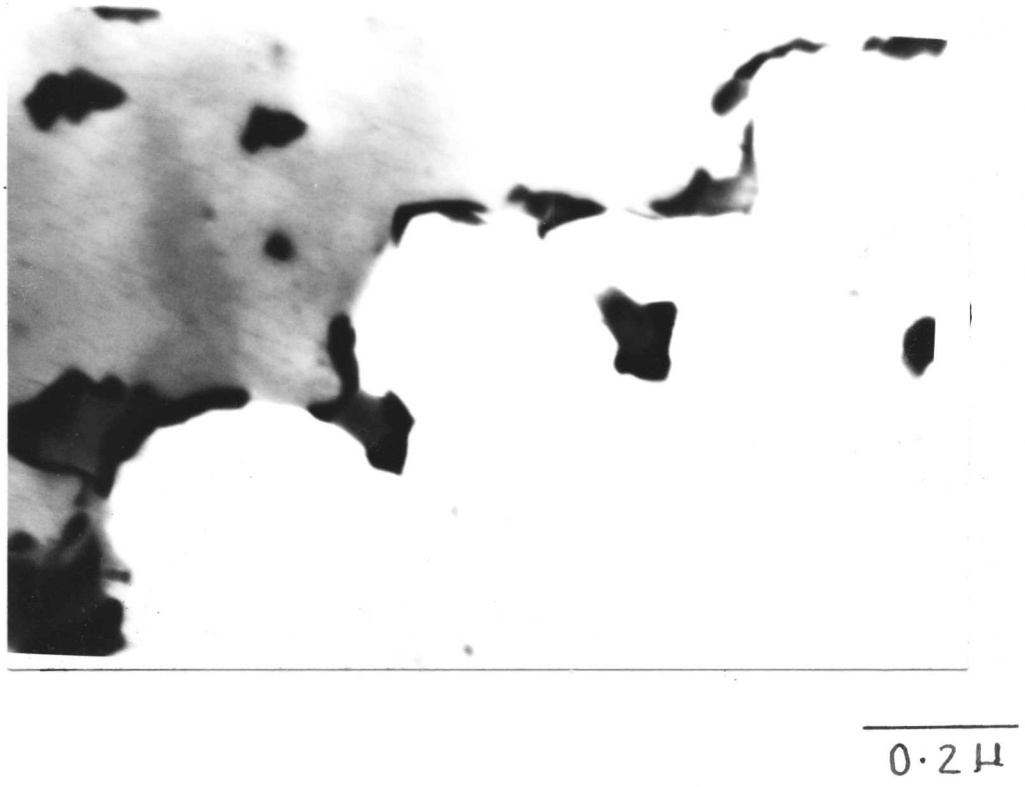

Fig. 4.45 Interface pinning by tungsten carbide.
(Isothermal transformation at 800°C for 40 minutes.)

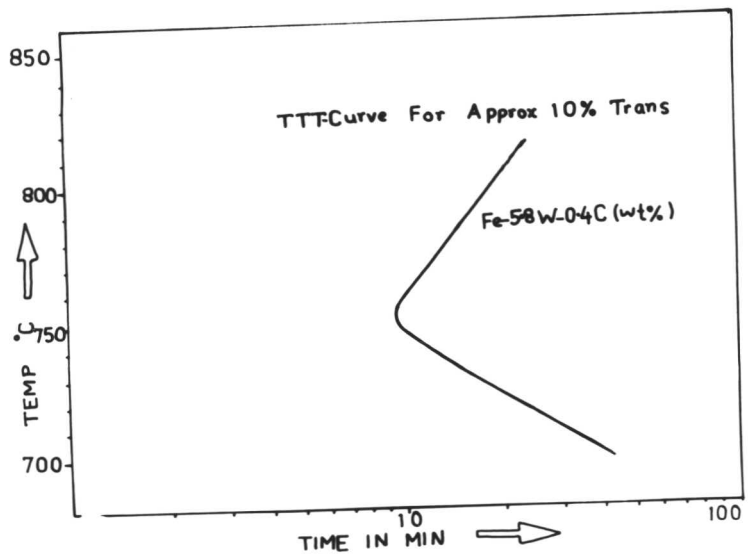

Fig. 4.46: TTT diagram for 10% transformation in Fe-5.8W-0.4C (wt%) alloy.

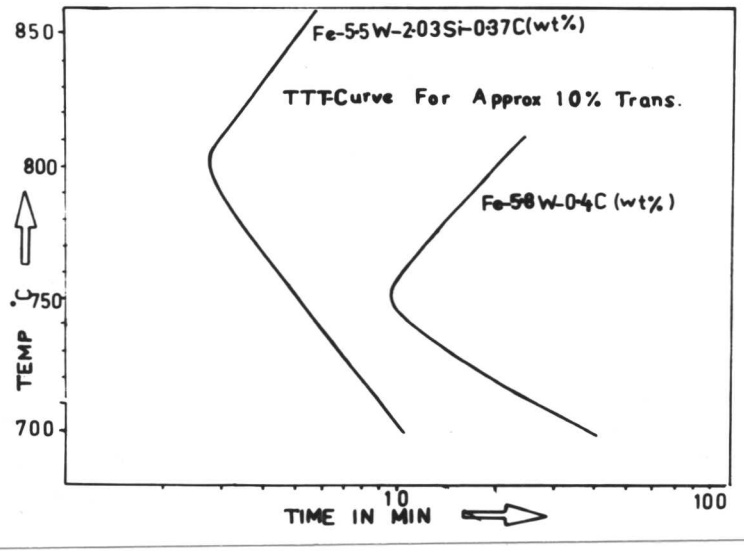

Fig. 4.47: TTT diagram showing effect of Si on the $\gamma \rightarrow \alpha$ transformation in Fe-W-C alloy.

CHAPTER V

The Austenite → Ferrite transformation in Fe-5W-0.23C (wt%)

5.1 INTRODUCTION

The austenite can decompose by several diffusional mechanisms to give rise a variety of microstructures. The resultant microstructure is sensitive to both temperature of transformation and the composition of the alloy. By controlling these two variables, one can control the mechanism through which diffusional transformation can proceed. Several microstructures can develop by variation of temperature and composition, including proeutectoid ferrite proeutectoid cementite, pearlite and bainite. Among these the proeutectoid ferrite reaction has received much attention in the past few decades.

Study of the $\gamma \rightarrow \alpha$ transformation is not only limited to the binary Fe-C system but also extended to the ternary Fe-C-X system where X is a substitutional alloying element such as Cr, Mn, Mo, Ni, Si, Co, Au, Ti, V, etc. This reaction starts predominatly at grain boundaries when the alloy is held below Ae_3 temperature. At low supersaturation (i.e. small undercooling, ΔT), grain boundary allotriomorphs are formed which grow rapidly along the grain boundaries but thicken more slowly. The growth kinetics of grain boundary allotriomorphs have been studied with the help of thermionic electron emission microscopy[1] (1967). The rate of thickening is parabolic in accordance with the relationship

$$S = \alpha_1 t^{1/2}$$

where S = half-thickness, t = growth time, and α_1 is the parabolic rate constant. Hillert [2] developed an expression for the lengthening rate of allotriomorphs with the assumption that the transformation is basically volume diffusion-controlled. The form of the expression is

$$G_L = \frac{D_\gamma (x_\gamma^{\gamma\alpha} - x_\gamma)}{4r^1 (x_\gamma - x_\alpha^{\alpha\gamma}) \sin \phi}$$

where $x_{\gamma}^{\gamma\alpha}$ = equilibrium mole fraction of carbon in austenite at interface

x_{γ} = mole fraction of carbon in alloy

$x_{\alpha}^{\alpha\gamma}$ ≃ equilibrium mole fraction of carbon in ferrite at the $\alpha/\alpha + \gamma$ phase boundary

r^{1} = radius of curvature of the allotriomorphs adjacent to the grain junction

ϕ = equilibrium growth angle determined by the relative energies of the interphase and grain boundaries

However, the recent work[3, 4] has shown that the lengthening is parabolic with respect to time. The rate constant describing the lengthening process is simply α_1 divided by the thickness to length ratio (i.e. aspect ratio) of the allotriomorph. Both the rate of nucleation as well as the rate of growth of these allotrimorphs increases with decreasing temperature due to increasing thermodynamic driving force, however diffusivity decreases. At sufficiently high undercooling, Widmanstätten ferrite develops. The reason for the transformation from grain boundary allotriomorphs to Widmanstätten side plate with increasing undercooling is not well understood. It has been suggested[5] that the relative rates at which semi-coherent and incoherent interfaces can migrate vary with undercooling. At small undercoolings, it is proposed that both semi-coherent and incoherent interfaces can migrate at the same rates, while at large undercoolings only incoherent interfaces can make full use of the increased driving force. However it does not explain the surface relief effect associated with formation of W_s. The other morphologies which develop during the $\gamma \rightarrow \alpha$ transformation are sensitive to temperature and composition and can be described on the basis of morphological classification proposed by Dubé and further extended by Aaronson, the details of which are discussed in Chapter II.

The $\gamma \rightarrow \alpha$ transformation in alloy steels has stimulated much interest in the intervening decades. This transformation provides a direct route of strengthening (in contrast to the use of quenched and tempered steels) by interphase-precipitation of alloy carbides. Alloy carbides are precipitated periodically at the advancing γ/α interface in order to accommodate the solid solubility associated with the decomposition of austenite and hence termed

"interphase precipitation". This form of precipitation appears generally in a banded structure which can be planar, curved or irregular. Planar banded structures are formed when precipitation occurs on low energy semi-coherent interfaces which are displaced by a ledge mechanism. Curved and irregular dispersion of carbides are formed in association with high energy incoherent interfaces. The resultant band spacing can be controlled by either varying the isothermal transformation temperature or by proper choice of alloying elements. At temperatures close to the nose of the T.T.T. diagram, the reaction proceeds rapidly and so the band spacing will be very fine. Similar effect is expected with alloying elements that will accelerate the transformation. However, another kind of carbide formation has also been observed in isothermally transformed steels. These carbides appear fibrous; they grow normal to the incoherent interphase-boundary and are usually observed as the transformation temperature is lowered.

The concept of interphase carbide precipitation has been exploited in the present chapter to investigate the $\gamma \rightarrow \alpha$ transformation in Fe-5W-0.23C (wt%) alloy. Special attention has been given to understand the carbide precipitation at the advancing γ/α interface by partially transforming the specimen at various temperatures. The effects of a small addition of titanium (0.14wt%) on the transformation characteristics of this alloy has been studied briefly.

5.2 Experimental Results on Fe-5W-0.23C (wt%) alloy:

5.2.1 Transformation at 850°C.

Isothermal transformation at 850°C for 2.5 minutes showed approximately 0.2 per cent volume fraction of transformation. Nucleation of proeutectoid ferrite was found to occur primarily at the austenite grain boundaries. The γ/α interface appeared curved as well as planar. Frequent evidence of ledges on the planar interfaces implies that these interfaces have moved by a ledge mechanism (Figure 5.1) although the ledge movement seems irregular. Apparently curved interfaces also showed a tendency towards facetting. This may be as a result of an interface adopting lower energy configurations and it is interesting to speculate whether these facetted interfaces also move by the propagation of ledges[6]. When the time of transformation was increased to 5 minutes at this temperature, the vol. fraction of transformation rapidly increased to 0.6 percent of its equilibrium value. The interfaces in the majority of cases appeared to be planar. Presence of ledges of variable height was noticed. Apparently intragranular ferrite bounded exclusively by planar interfaces was also observed in many cases (Figure 5.2a). Figure 5.2b deserves special attention. It clearly shows the evidence of interface pinning by carbides. Figure 5.2b shows the presence of residual austenite (now martensite) in ferrite. The residual austenite in ferrite has formed as the interface has moved through the carbides. The presence of residual austenite seems to indicate that the precipitate pinned the γ/α interface and then these boundaries were forced to move around the particles by bowing, leaving behind the residual austenite. This is somewhat similar to the Orowan bowing mechanism for looping of dislocations around precipitates. Practically no evidence of precipitation in ferrite was recorded during the early stages. The formation of such a carbide-free ferrite is attributed to the appreciably higher solubility of tungsten carbide in ferrite at this temperature. Carbides free ferrites have also been reported in Fe-Mo-C[7], Fe-V-C(N)[8] and more recently in Fe-Nb-C[9] alloys during this early stages of transformation. Some interesting features were observed when the time of transformation was increased to 20 minutes at 850°C. Carbides were formed at the γ/α interface but appeared to grow in austenite to form a planar array of tungsten carbide (M_6C) (Figure 5.3) in austenite. The reaction can be written as

$$\gamma \rightarrow \alpha + \gamma_1 \rightarrow \alpha + \gamma_2 + M_6C \quad (1)$$

With increasing time of transformation, all the austenite (γ_1) was replaced by $\gamma_2 + M_6C$. During the later stages of transformation all γ_2 was replaced by ferrite and finally the resultant structure consisted of α-ferrite + M_6C. The whole sequence of reaction can be written as

$$\gamma \rightarrow \gamma_1 + \alpha \rightarrow \gamma_2 + M_6C + \alpha \rightarrow M_6C + \alpha \quad (2)$$

The microstructural changes which occurred during the isothermal transformation at 850°C are shown in Figures 5.2 to 5.4 and schematically in Figure 5.5.

5.2.2 Transformation at 800°C

Isothermal transformation at 800°C for 1.5 minutes showed about 5 volume % transformation of its equilibrium value. The reaction mainly started at the austenite grain boundries. The grain boundary allotriomorphs showed a tendency towards facetting (Figure 5.6a). Some evidence of Widmanstätten ferrite was also recorded (Figure 5.6b) at this temperature. This Widmanstätten ferrite has grown along martensite trace direction. Figure 5.6c illustrates some important crystallographic aspects of allotriomorphs formed at the junction where three grain boundaries meet. This micrograph indicates that this allotriomorph is crystallographically related only to two abutting grains. (Planar interface is taken here as tentative evidence of a rational orientation relationship between parent and product phase on a macroscopic scale.) With increasing time of transformation (2.5 minutes), the allotriomorphs grew more rapidly along the grain boundaries and thickened slowly. Most of the interfaces appeared planar. Frequent evidence of ledges indicates that these interfaces have moved by ledge mechanism. With further increase in time (5 minutes, 10 minutes) these allotriomorphs developed to form equiaxed ferrite due to impingement effects. The aspect ratio of allotriomorphs increased with decreasing temperature as expected. Ferrites thus formed during early stages were virtually free from carbides. Clear evidence of pinning was recorded (Figure 5.6d-f). This pinning has resulted while the interface has moved across the carbide particles, during transformation. This aspect of interface pinning can be utilized to delay the transformation and hence to increase the hardenability of alloy steels. Some evidence of carbide precipitation was also recorded during the latter stage of transformation (i.e. 40 minutes and 20 minutes) (Figure 5.6g). However, these carbides have precipitated from supersaturated ferrite and not by interphase mechanism. This has been further confirmed by TEM (Figure 5.6h).

5.2.3 Transformation at 750°C

When the transformation temperature was further reduced to 750°C, the reaction started mainly at the austenite grain boundaries to form allotriomorphs, the aspect ratio of these allotriomorphs was further increased. Approximately 15 volume % transformation occurred when the specimen was held at this temperature for five minutes. The interface appeared both planar and curved. However, in the majority of cases, the interface appeared planar. The ferrite grains were again free from carbides during the early stages of transformation.

5.2.4 Transformation at 700°C

With further decrease in temperature (700°C), the incubation period increased. Only 10 volume % transformation was recorded after 10 minutes at this temperature. The transformation mainly started at grain boundaries to form grain boundary allotriomorphs. The aspect ratio of these allotriomorphic ferrite also increased. The amount of transformation increased with increasing time as expected. Again these ferrites were free from carbides. With further increasing time, the amount of transformation increased without any evidence of precipitation.

In the temperature range of 850°C to 700°C the $\gamma \rightarrow \alpha$ transformation exclusively started at austenite grain boundaries to form what are known as grain boundary allotriomorphs. Grain boundary allotriomorphs are defined as crystals which nucleate at the grain boundaries and their morphology does not reflect their crystalline symmetry. A tendency towards facetting was recorded at all temperatures of transformation. Frequent evidence of ledges indicates that the planar interfaces have been displaced by migration of ledges. Evidence of facetting even on the curved interfaces was recorded from time to time. Facetting on these curved interfaces may be due to the interface adopting a low energy configuration. It can be speculated that these interfaces also require a ledge mechanism to operate for their growth. The aspect ratio of these allotriomorphs increased with decreasing transformation temperature as expected. At all temperatures, the transformation proceeded with the formation of carbide free ferrite. During the later stages of transformation at 850°C, carbide precipitation at the interface was noticed. But no such carbide dispersion was observed at lower temperatures. However, some evidence of carbide was observed during the later stages of transformation at 800°C (40 minutes and 80 minutes). But these carbides have precipitated from supersaturated ferrite and not by an interphase mechanism.

TEM investigations were done to study the $\gamma \rightarrow \alpha$ transformations. Figure 5.7 shows rod-shaped tungsten carbide (M_6C) which were formed during the later stages of transformation at 850°C. These tungsten carbide particles have been identified as η-carbide[10, 11, 12]. The η-carbide is represented by M_6C (Fe_4W_2C) and has a complex cubic structure. This structure contains 112 atoms per unit cell viz 96M and 16C[13]. The lattice parameter of η-carbide is 11.04 Å.

A TTT diagram for 10 volume % transformation is shown in Figure 5.8. It indicates that minimum incubation period lies between 800°C and 850°C.

Table V shows the change in microstructure as a function of transformation temperature and time.

5.3 The effects of a small addition of titanium (0.14 wt%) on transformations in Fe5.9W-0.21C (wt%) alloy: Titanium forms a carbide which has a NaCl-type structure, whose composition varies between $TiC_{0.6}$ to TiC due to vacancies in the carbon sublattice[14]. The solubility limit of titanium carbide in austenite can be estimated by using the relationship[15]:

$$\text{Log}_{10}\left[\text{Ti}\right]\gamma\left[\text{C}\right]\gamma = -\frac{7000}{T} + 2.75$$

where $\left[\text{Ti}\right]\gamma$ and $\left[\text{C}\right]\gamma$ are wt% concentrations in austenite.

This expression enables the estimation of the amount of titanium used up in forming titanium - carbide at a particular austenitizing temperature, the remainder being in solid solution.

Titanium carbide (like niobium carbide) forms preferentially along the grain-boundaries and hence inhibits austenite grain-growth.

However its precise role on the kinetics of $\gamma \rightarrow \alpha$ transformation is not established. The present investigation was carried out to study the influence of Ti on the kinetics of the $\gamma \rightarrow \alpha$ transformation. The specimens were isothermally transformed in the range of 900°C to 700°C after austenitizing at 1200°C for 30 minutes. The volume fraction of α in partially transformed specimens was quantified by using the image analyse Quantimet 720. Figs. 5.9 & 5.10 show the microstructures that were developed at a fixed interval of time at each isothermal temperature, both in alloys with and without titanium. Figure 5.11 shows that titanium is effective in retarding the kinetics of the $\gamma \rightarrow \alpha$ transformation.

In order to investigate the details of the microstructure of α, TEM studies were done. At all temperatures, the decomposition of austenite started with nucleation of virtually carbide-free α-ferrite (Fig. 5.12). But during the later stages of transformation, carbides were precipitated either by an

interphase precipitation mechanism or from supersaturated ferrite.

5.4 Discussion: The $\gamma \rightarrow \alpha$ transformation started primarily at the austenite grain-boundaries by nucleation of proeutectoid ferrite. Smith[16] proposed a simplified crystallographic relationship between ferrite nuclei and austenite. According to him, a ferrite nucleus would form with a rational orientation relationship with one abutting grain and an irrational orientation relationship with the other adjacent austenite grain. The usual orientation relationship between austenite and ferrite is approximately represented by the Kurdjumov-Sachs relationship. This allows parallelism of the closest packed planes in the two structures, perhaps giving a degree of atomic misfit. Hillert[17] observed that in the majority of cases, the proeutectoid ferrite allotriomorphs had straight interfaces with both abutting grains, indicating partial coherency with both grains. He proposed that the ferrite nuclei may be closely related to form highly coherent interface with one austenite grain and still related to the other grain, forming an interface with lower coherency. Ryder et al.[18] also observed that during fcc → bcc transformations in Co-20 wt% Fe alloy, the grain-boundary nucleated product phase was crystallographically related to both adjacent parent grains. King and Bell[19,20] reported similar observations while working on 0.41C wt% steel. A recent elegant and extensive review by Howell and Honeycombe[21] strongly suggests the existence of partial coherency at the majority of interfacial orientations and that a truly incoherent structure is rare. The present observation indicates that the grain-boundary allotriomorphs are bounded by planar interfaces in the majority of cases. Frequent evidence of ledges implies that these interfaces have been displaced by a ledge mechanism[22]. Curved interfaces also showed a tendency towards facetting. This may be as a result of the interface adopting a lower energy configuration and it is interesting to speculate whether these facetted interfaces also move by the propagation of small steps[6].

The aspect ratio of the grain-boundary allotriomorphs increased with decreasing transformation temperature. This may be attributed to the diffusivity of C in austenite (D_C^{γ}) as a function of temperature. Thickening of the allotriomorphs is controlled by the volume diffusion of carbon in austenite[22]. As the temperature of transformation is decreased D_C^{γ} also decreases and consequently the rate of thickening is gradually reduced. This results in an increasing aspect ratio of the allotriomorphs with decreasing temperature since the role grain-boundary carbon diffusion in allotriomorph lengthening then becomes more significant.

At all transformation temperatures, the reaction started with the formation of carbide free ferrite. The formation of such a carbide free ferrite is

attributed to the appreciably lower supersaturation of tungsten carbide in ferrite at this temperature. During later stages of transformation at 850°C (20 minutes), evidence of carbide precipitation was noticed, at the γ/α interface. With increasing time of transformation, these carbides grew into the austenite. The sequence of reaction is represented by equations (1) and (2) and schematically shown in Figure 5.5. The reason for the transition from clean ferrite to ferrite + tungsten carbide may be explained on the basis of continued carbon enrichment of austenite during the $\gamma \rightarrow \alpha$ transformation. As the transformation proceeds, C is continuously rejected ahead γ/α interface in the austenite. Ultimately the carbon content of the austenite near the γ/α interface is sufficiently increased to induce $\gamma_1 \rightarrow \gamma_2 + M_6C$ reaction.

Sakuma and Honeycombe[9] while working on Fe-Nb-C alloys tried to analyse the reason for transition from clean ferrite to ferrite + alloy carbide by recording the micro-hardness of isothermally transformed alloys as an index of the 'C' content of austenite. The increase in micro-hardness of martensite with increasing time is attributed to the increase in the carbon content of austenite[22]. Figure 5.13 shows schematically the carbon concentration profile near the moving interface[9] under two different circumstances. Figure 5.13a shows a steady state carbon concentration profile which is achieved under high driving force operating in lower temperature ranges. But at high temperatures, the carbon concentration profile will change with time due to its increased diffusivity (Figure 5.13b). Under this condition, the migration rate of the interface will gradually decrease and thus provide an opportunity for precipitation at the γ/α interface during the latter stage of transformation.

The reason for transition from clean ferrite to ferrite + alloy carbide can be explained on the boundary migration rate and nucleation rate of carbide on the boundary[23]. According to the analysis,[23] favourable conditions for carbide nucleation will be created only when the migration rate is low. The migration rate of an interface continuously changes with time during the isothermal transformation in Fe-X-C[24]. Growth rate of grain-boundary allotriomorphs during the isothermal transformation of austenite in ternary system has been divided into three stages: an initial no-partition stage which includes a parabolic growth rate and subsequent non-parabolic stage and the final stage in which partitioning of substitutional alloying elements occurs[25, 26]. During the first stage, no partitioning occurs due to the greater difference between the diffusivities of C and X. Experimental evidence of no partition growth of ferrite allotriomorphs has been reported in many ternary Fe-C-X alloys[27].

As the transformation proceeds, the supersaturation or the driving force for transformation decreases and eventually reaches a point where appreciable partitioning of substitutional element X between the parent and product phases must occur. Coates[24] used the concept of local equilibrium at the moving interface to explain the above phenomenon. When the degree of undercooling is high, local equilibrium is maintained without partitioning of alloying element. Under this condition (NP-L.E) the rate of reaction is controlled by the fast diffuser 'C' and the ferrite inherits the alloy content of austenite. Local equilibrium with partition (P-L.E) occurs when the transformation rate is slow and the transformation is mainly controlled by the slower diffuser 'X'.

Titanium seems to have a retarding effect on the kinetics of the $\gamma \rightarrow \alpha$ transformation. On austenitizing at 1200°C, titanium carbides are preferentially formed along the austenite grain-bounderies. Some carbides are also precipitated within the grains. The presence of copious precipitation of titanium carbide reduces the number of available sites for the nucleation of α and hence reduces its nucleation efficiency. Once the nucleation has occurred the carbides present within the austenite grain offer resistance to the growing γ/α interface by a pinning action.

5.5 Conclusions:

1. In the present study, the majority of the interfaces appeared planar in partially transformed specimens. More frequently ledges were observed on these planar interfaces. Facetting was also observed on the curved interfaces. It suggests that the ledge mechanism plays a significant role in controlling the mobility of the γ/α interface during the transformation.

The mobility of the such interfaces will depend both on the frequency with which the ledges are nucleated as well as their ability to move during the transformation.

2. The $\gamma \rightarrow \alpha$ + carbide reaction is found to occur in at least two distinguishable stages. The first stage involves the formation of allotriomorphic ferrite, and the carbon partitioning accompanying this reaction induces the precipitation of carbides in the austenite ahead of the γ/α interface. The ferrite subsequently engulfs the carbides as the remaining austenite transforms further to ferrite. This sequence of events has been tentatively interpreted in terms of local equilibrium theory.

3. Ti showed tendency to suppress the kinetics of the $\gamma \rightarrow \alpha$ transformation in the temperature range of 700°C to 900°C.

Showing change in microstructure as a function of isothermal temperature

Change in microstructure as a function of isothermal

Temperature °C	Time in minutes	Vol.%	Nature of Interface	Presence of Ledges	Aspect Ratio	Pr
	2.5	18 - 21%	Both Planar & Curved	Frequently	Low equiaxed	
	5	55 - 67%	"	Less	"	
	10	69 - 72%	"	Less	"	
	20	74 - 78%	"	"	"	
850°C	40	slightly increased	"	"	"	
	80	"	"	"	"	
	320	100%	Curved mostly	No	"	
	500	100%	"	No	"	
	1.5	3 - 5%	Both Planar & Curved	Frequently	Increased	
	2.5	6 - 8%	"	"	Increased	
	5	34 - 37%	"	Less	Equiaxed	
800°C	20	37 - 41%	"	Less	"	
	40	39 - 44%	"	Less	"	
	80	slightly increased	"	Less	"	
750°C	5	12 - 15%	Both Planar & Curved	Frequently	Increased	
700°C	10	8 - 10%	Both Planar & Curved	Frequently	Increased	

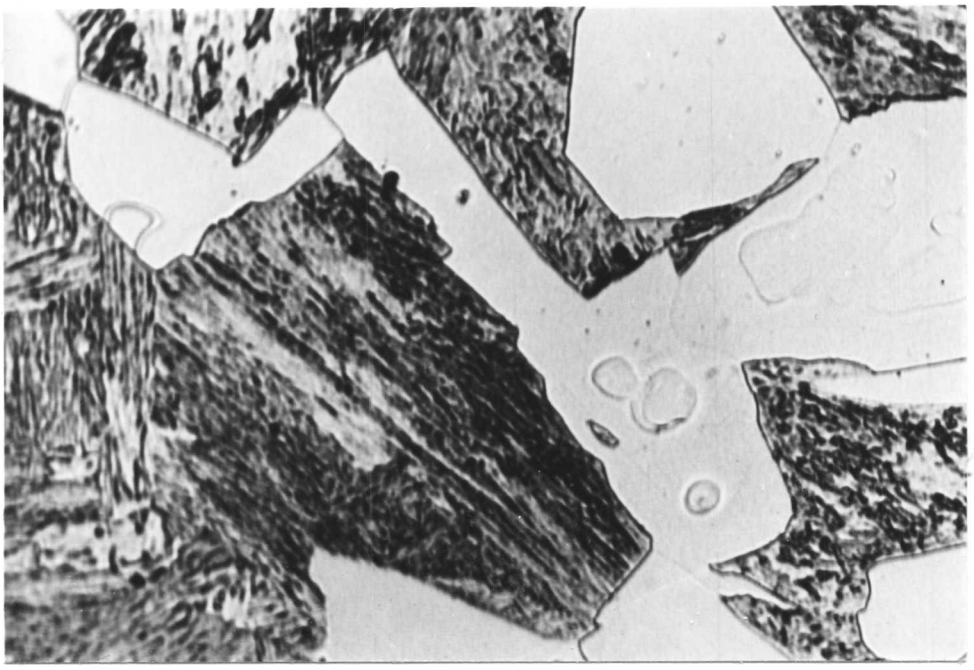

Figure 5.1: High proportion of planar boundary (i.e. semi-coherent γ/α interface) is depicted in this micrograph. Presence of ledges implies that these interfaces have been displaced by ledge mechanism. (850°C/2.5 Min).

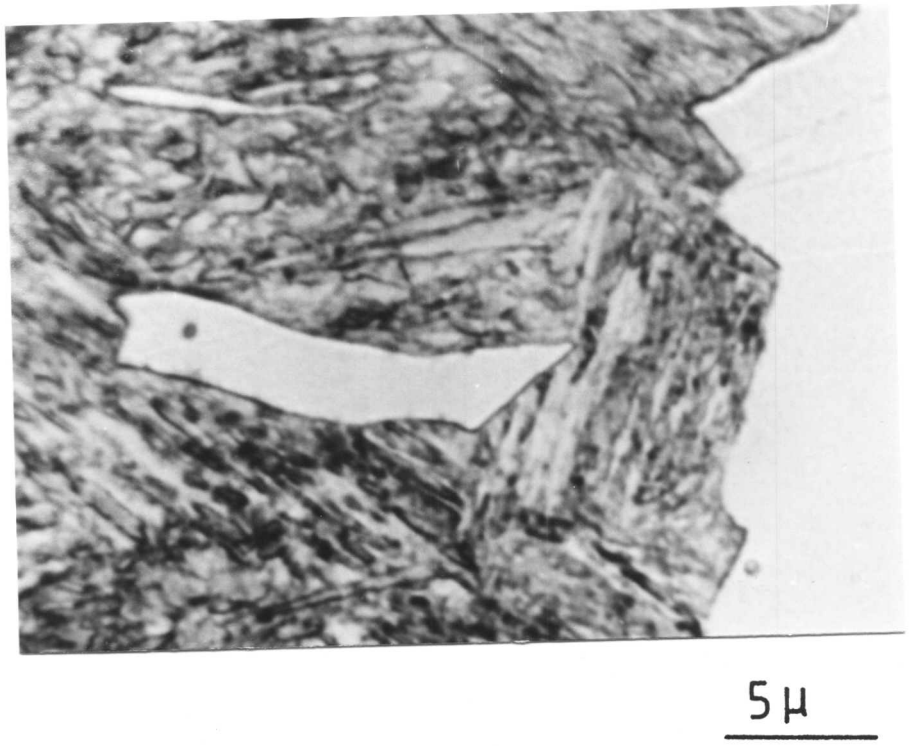

Figure 5.2a: Intragranular ferrite bounded exclusively by planar interfaces. (850°C/5 Min).

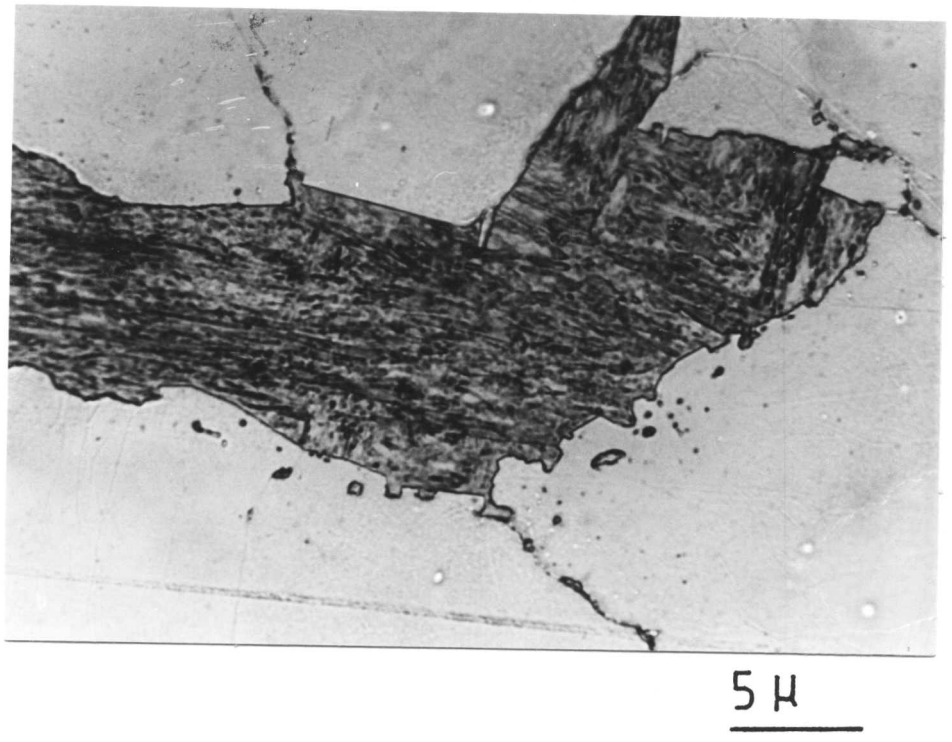

Figure 5.2b: The moving γ/α interfaces have been pinned by tungsten carbide. This results in formation of ragged interface. Some entrapped austenite are also present within the ferrite grain (850°C/5 Min).

Figure 5.3a: Precipitation of tungsten carbide at the γ/α interface. These carbides appear to grow in the austenite. (850°C/20 Min).

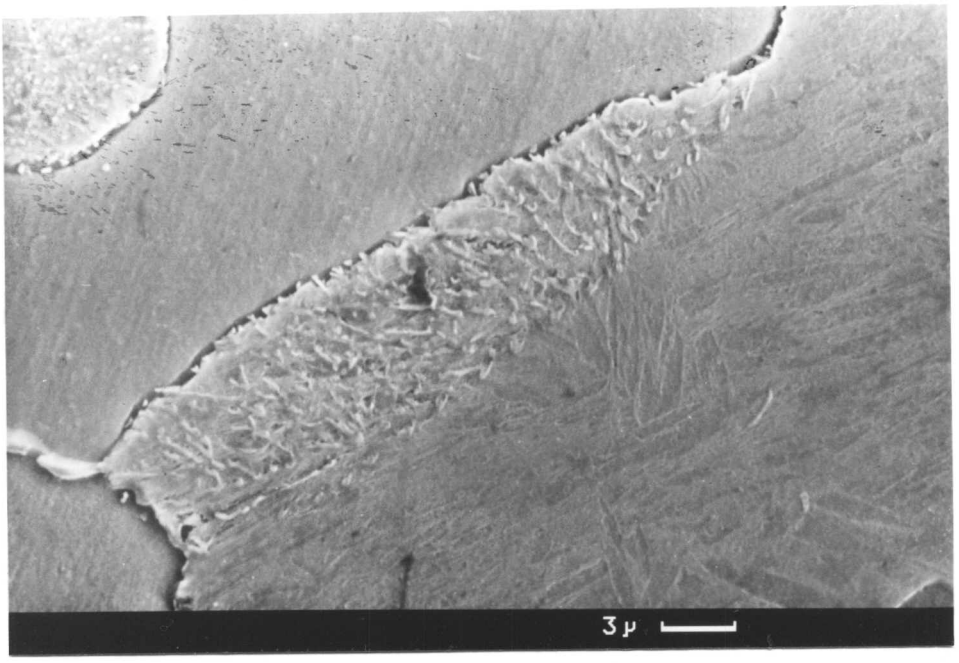

Figure 5.3b: Scanning micrograph showing growth of tungsten carbide away from the γ/α interface but within the austenite grain (850°C/20 Min).

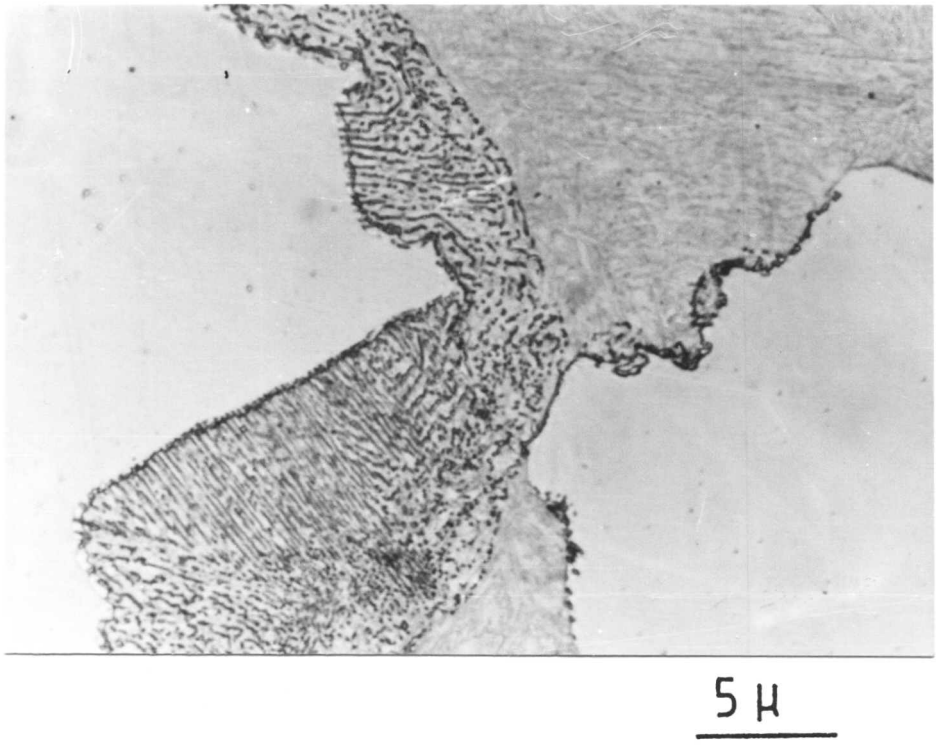

Figure 5.3c: Planar array of tungsten carbide within the austenite grain (850°C/20 Min).

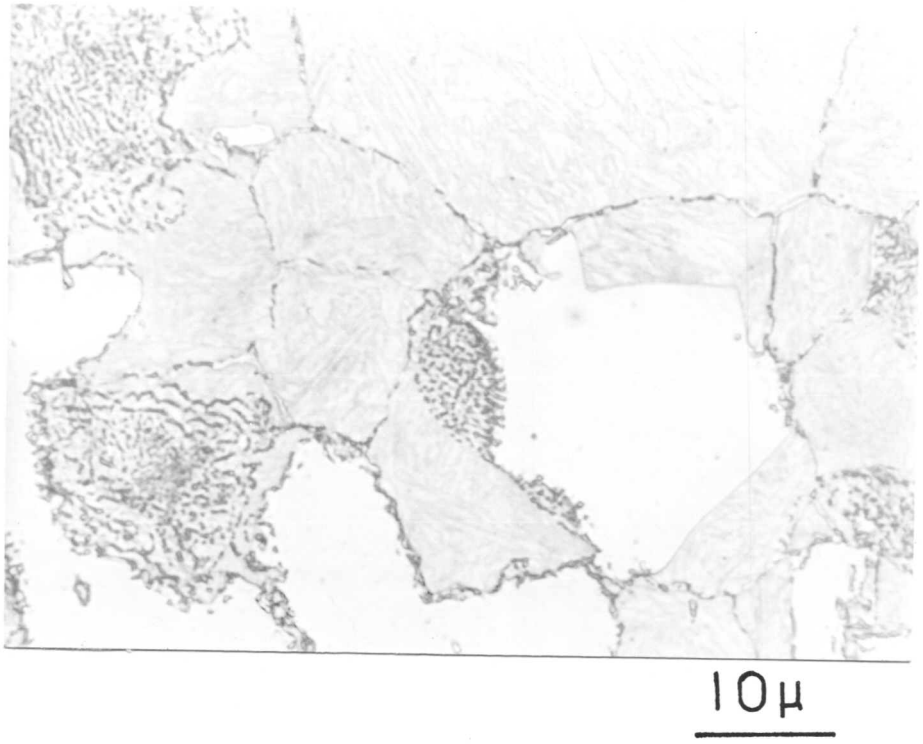

Figure 5.4a: With increasing time of transformation the carbides grew in austenite (850°C/80 Min).

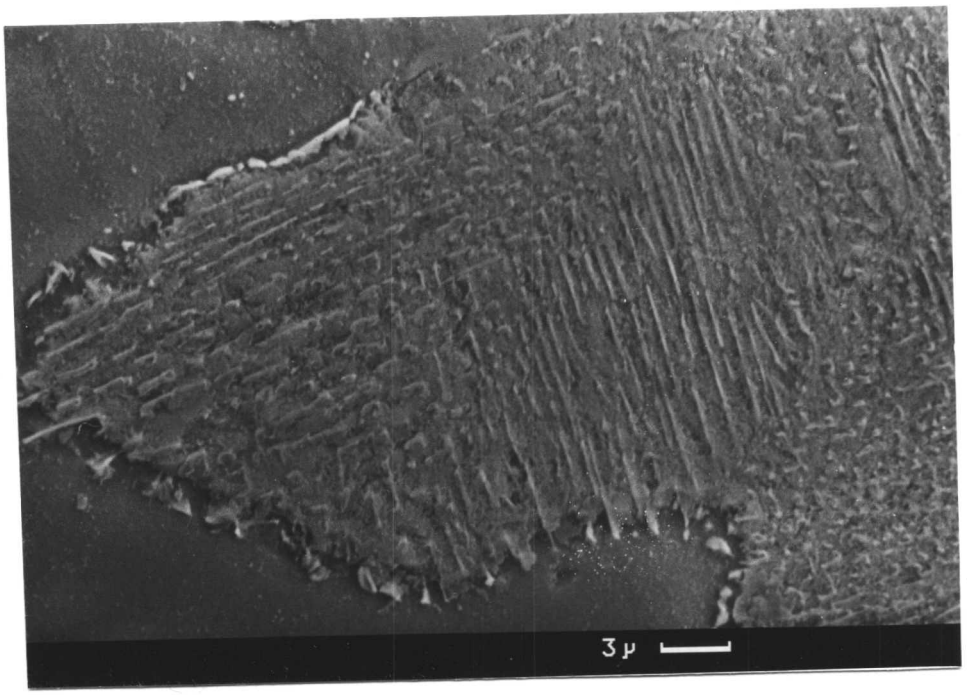

Figure 5.4b: Scanning electron micrograph showing further growth of tungsten carbide within the austenite grain (850°C/160 Min).

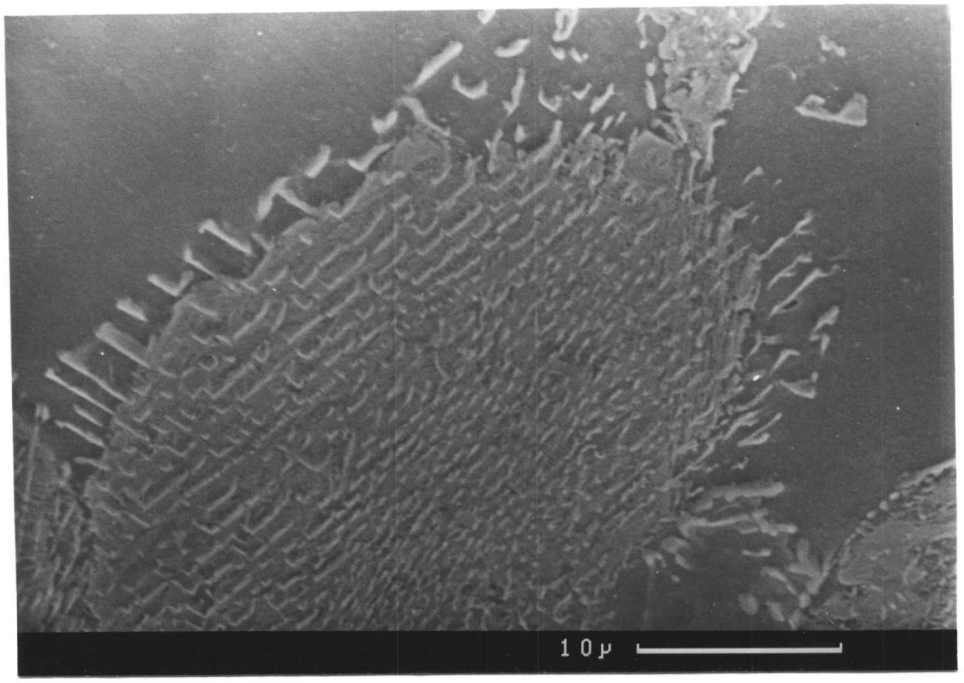

Figure 5.4c: Scanning electron micrograph showing planar array of tungsten carbides within the austenite grain (850°C/160 Min).

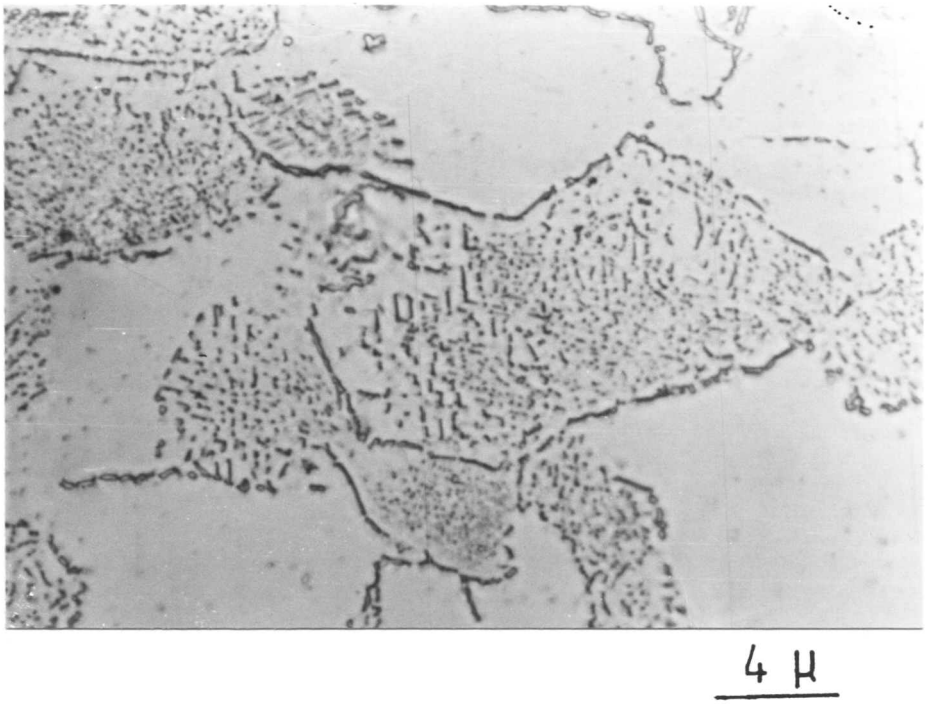

Figure 5.4d: After prolong ageing, the microstructure consisted of $\alpha + M_6C$. (850°C/320 Min).

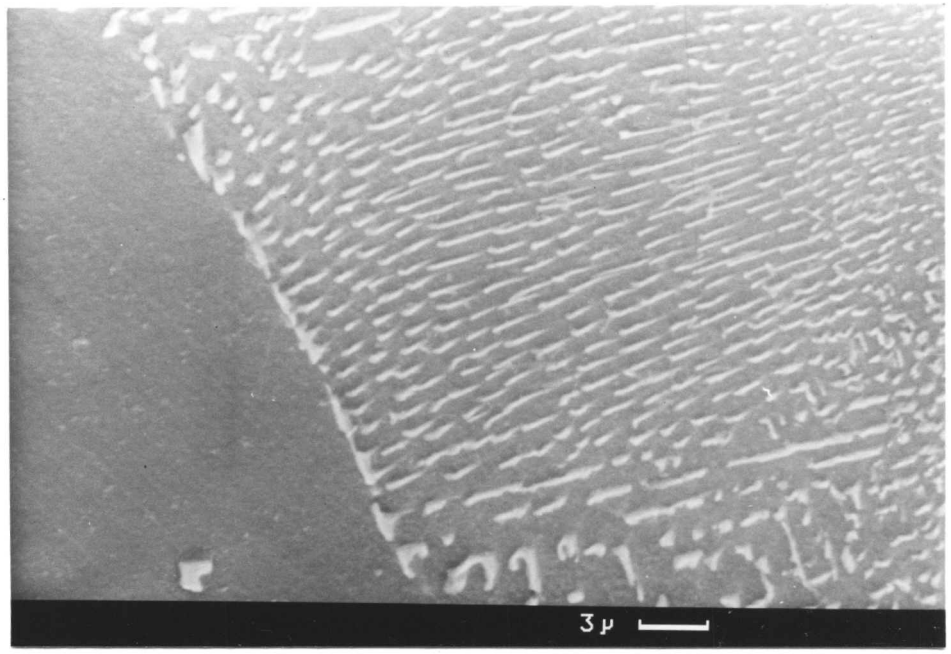

Figure 5.4e: Scanning electron micrograph showing aligned carbide dispersion (850°C/320 Min).

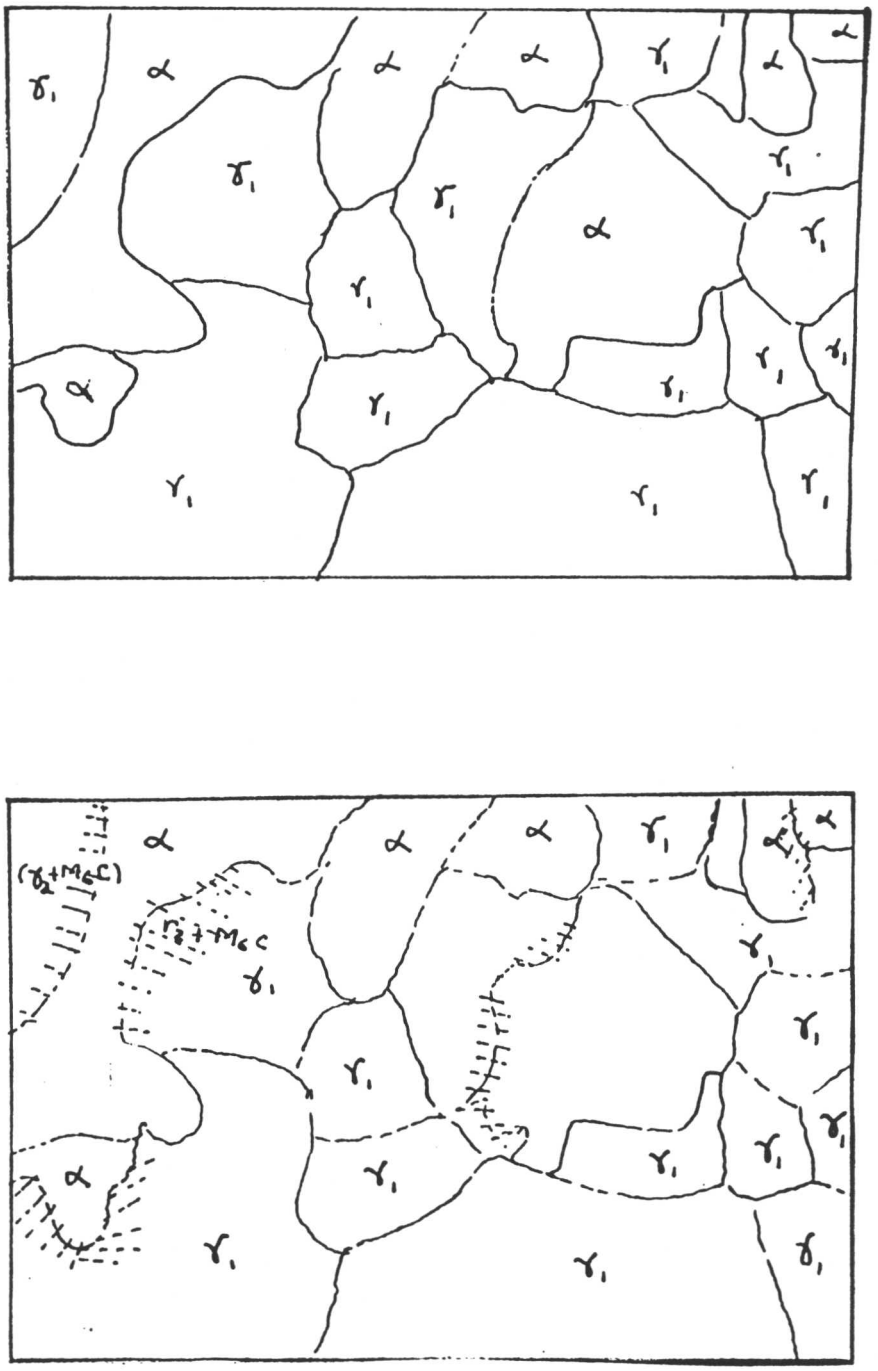

Figure 5.5: Schematic diagram showing the sequence of reaction at 850°C. i.e. $\gamma \rightarrow \alpha + \gamma_1 \rightarrow \alpha + (M_6C + \gamma_2) \rightarrow \alpha + M_6C$.

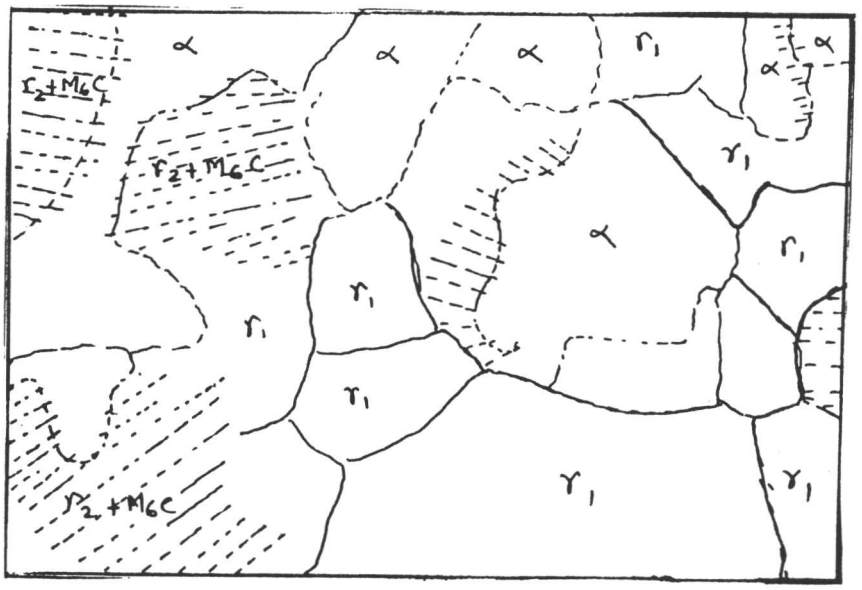

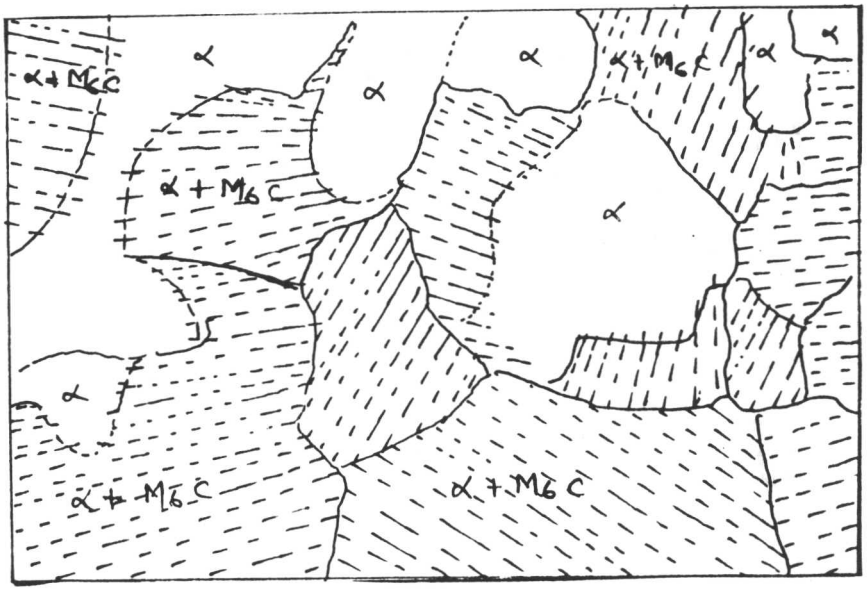

Figure 5.5: Schematic diagram showing the sequence of reaction at 850°C. i.e. $\gamma \rightarrow \alpha + \gamma_1 \rightarrow \alpha + (M_6C + \gamma_2) \rightarrow \alpha + M_6C$.

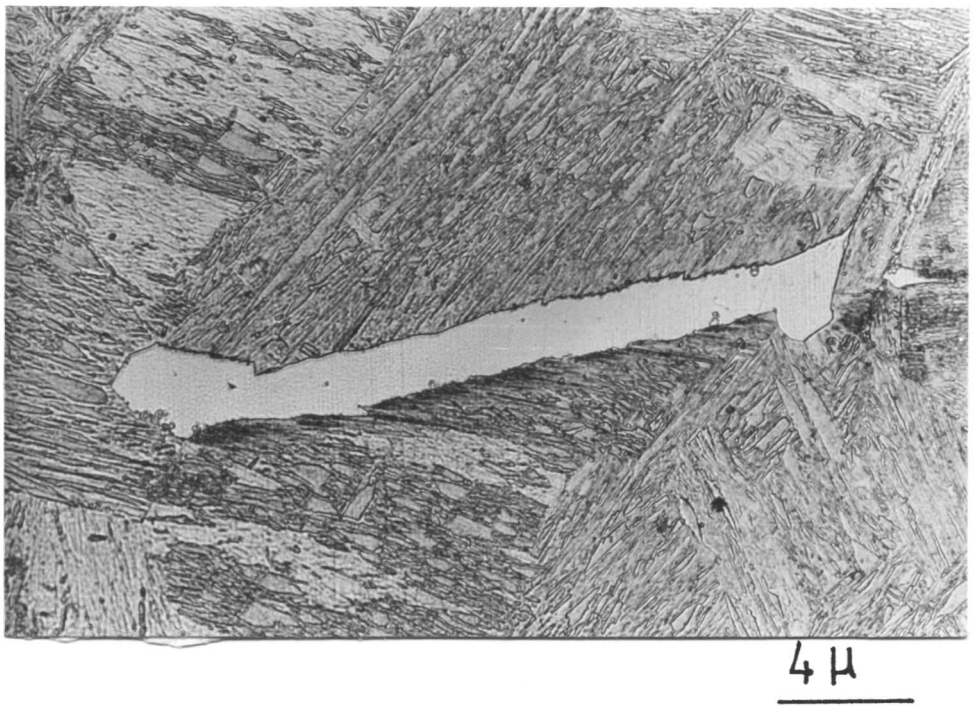

Figure 5.6a: Facetted allotriomorphic ferrite (800°C/1.5 Min).

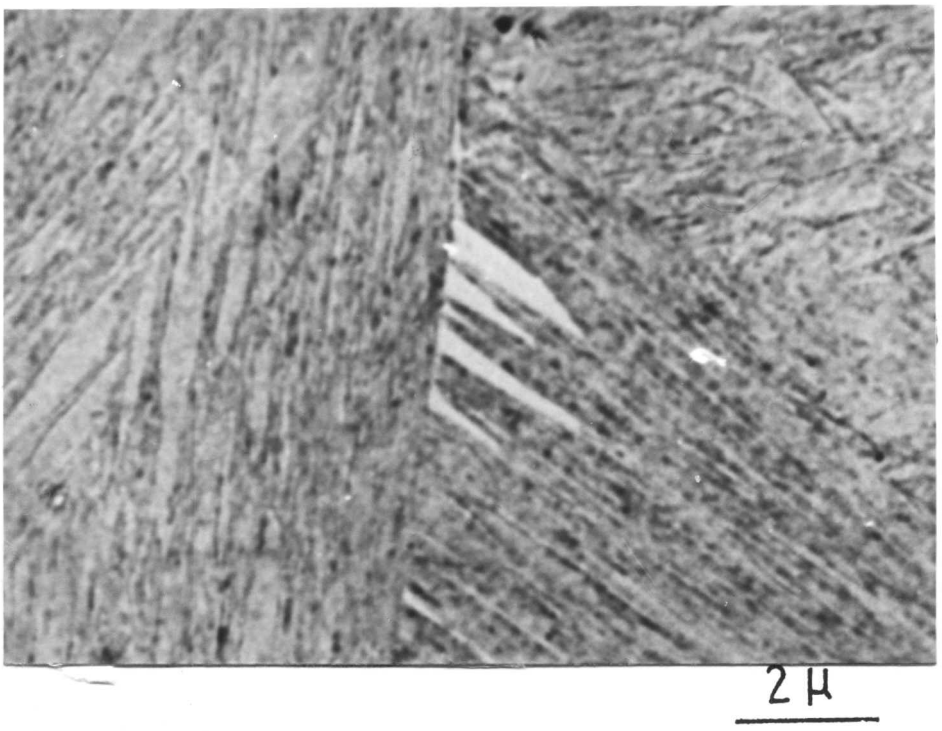

Figure 5.6b: Widmanstätten ferrite growing in the martensite trace direction. (800°C/1.5 Min).

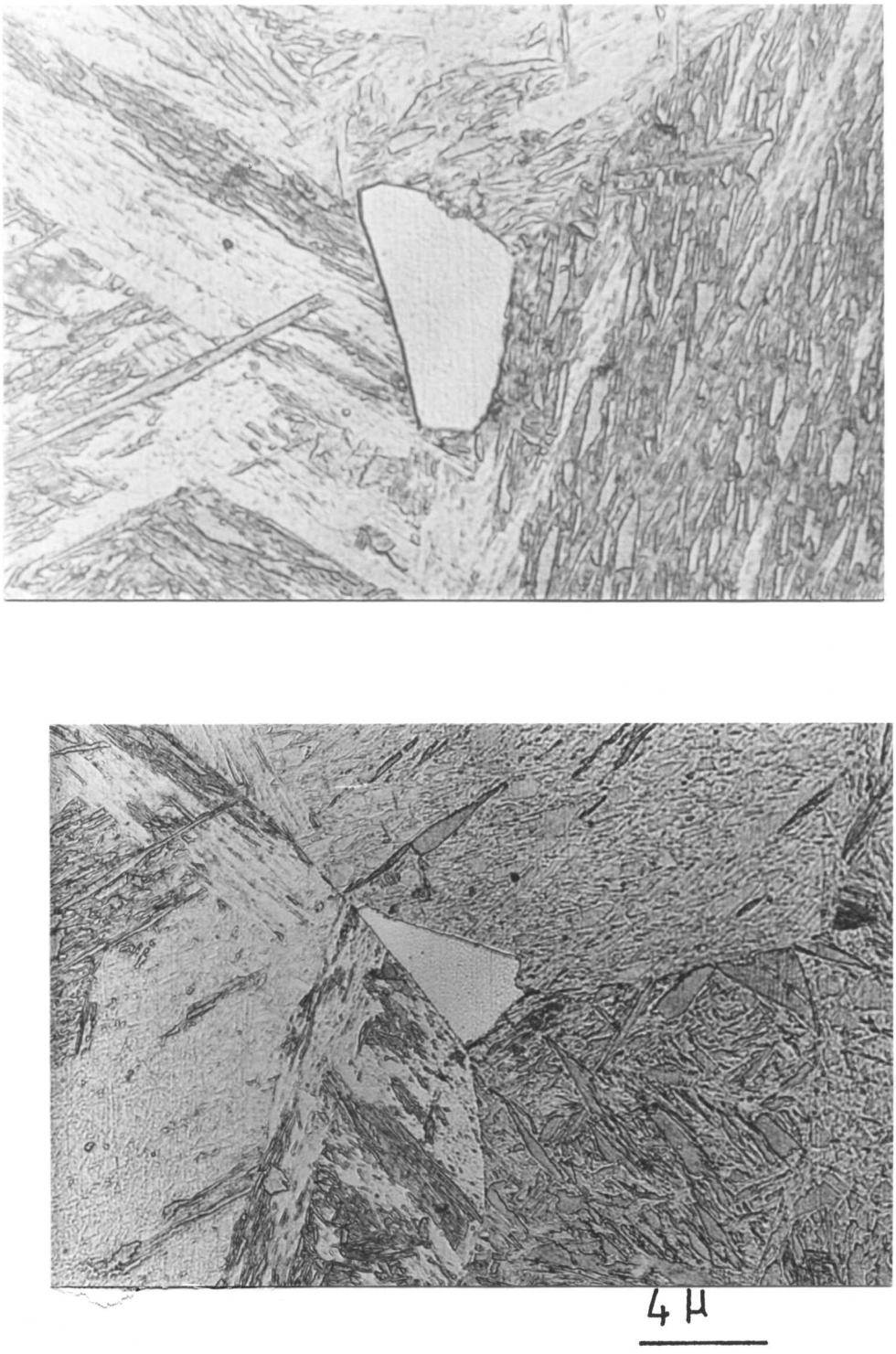

Figure 5.6c: Facetted allotriomorphic ferrite growing at the triple point (800°C/1.5 Min).

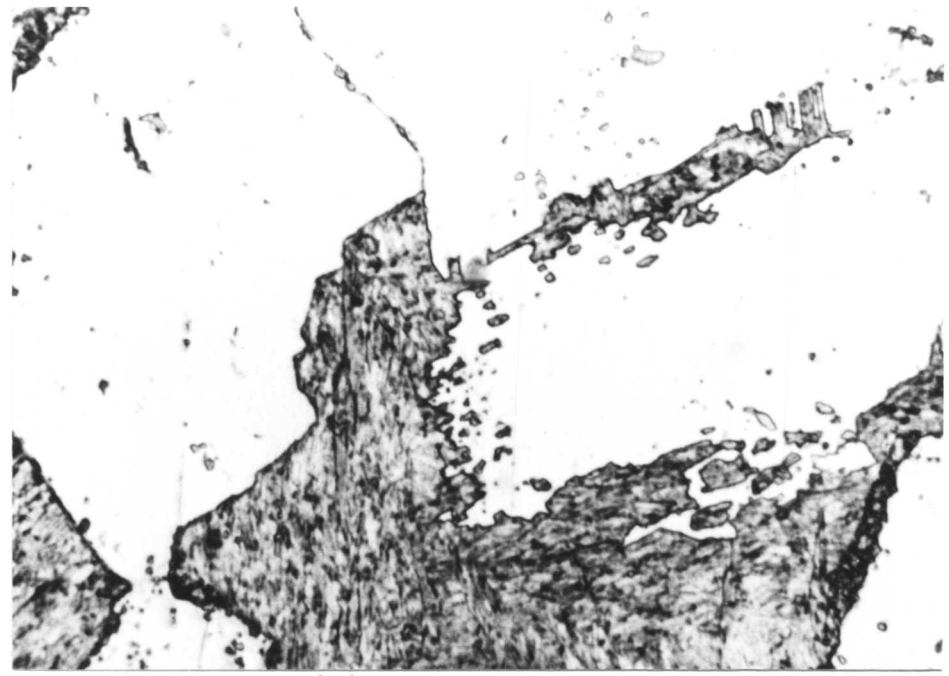

10μ

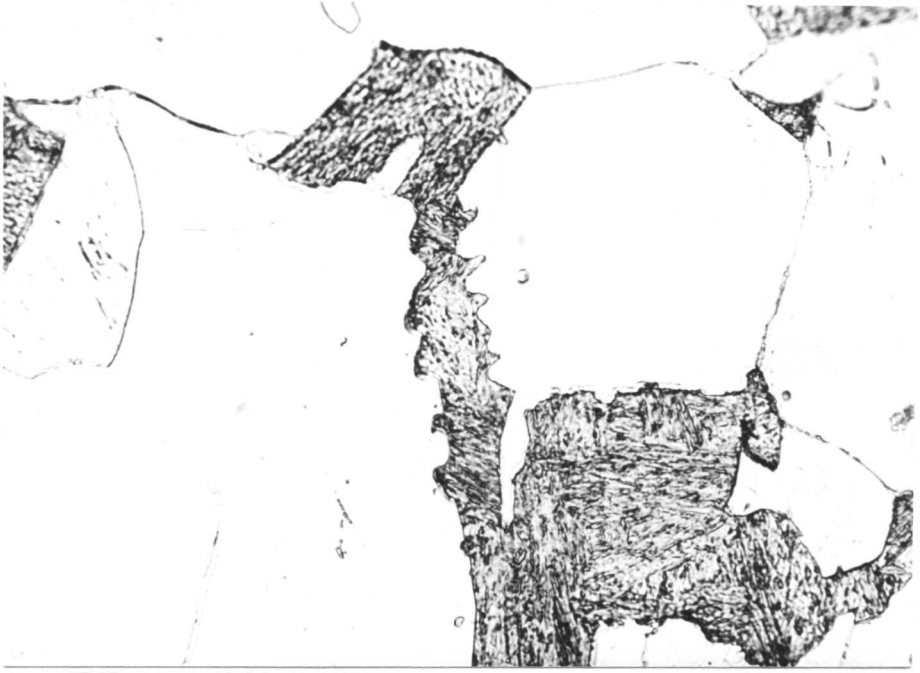

20μ

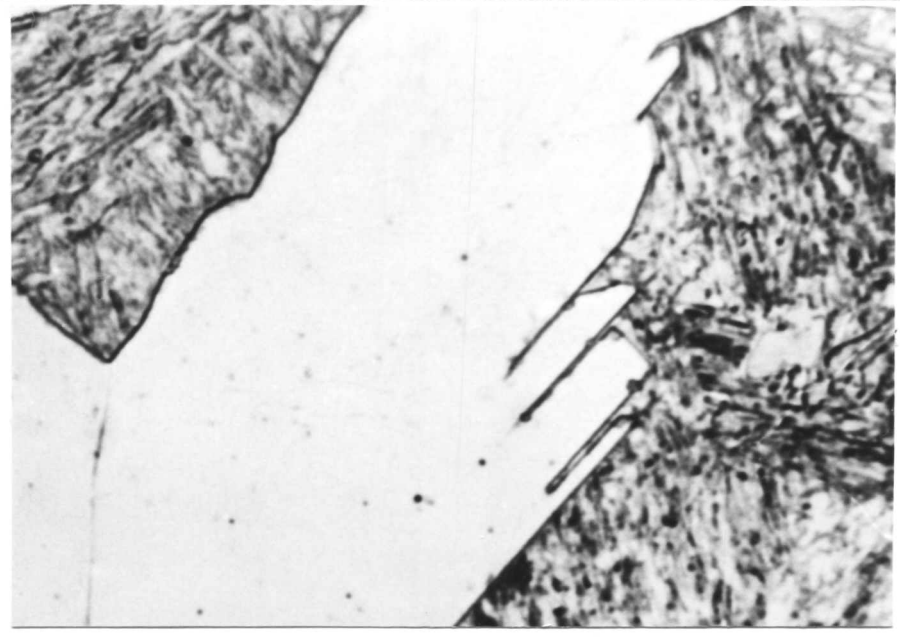

20μ

Figure 5.6d to f: Pinning of the γ/α interface by tungsten carbide.

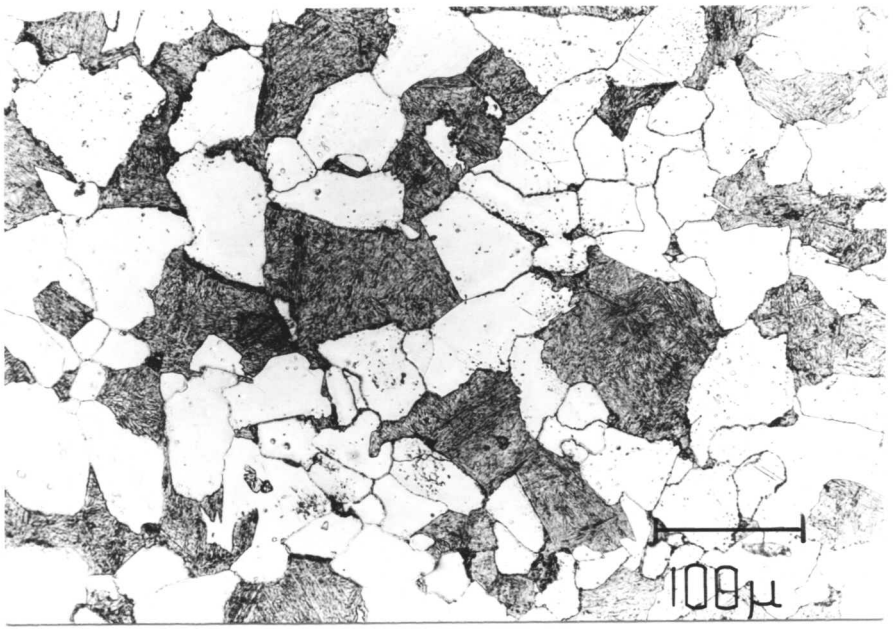

Figure 5.6g: Polygonal ferrite with evidence of carbide precipitation within the ferrite (800°C/40 Min).

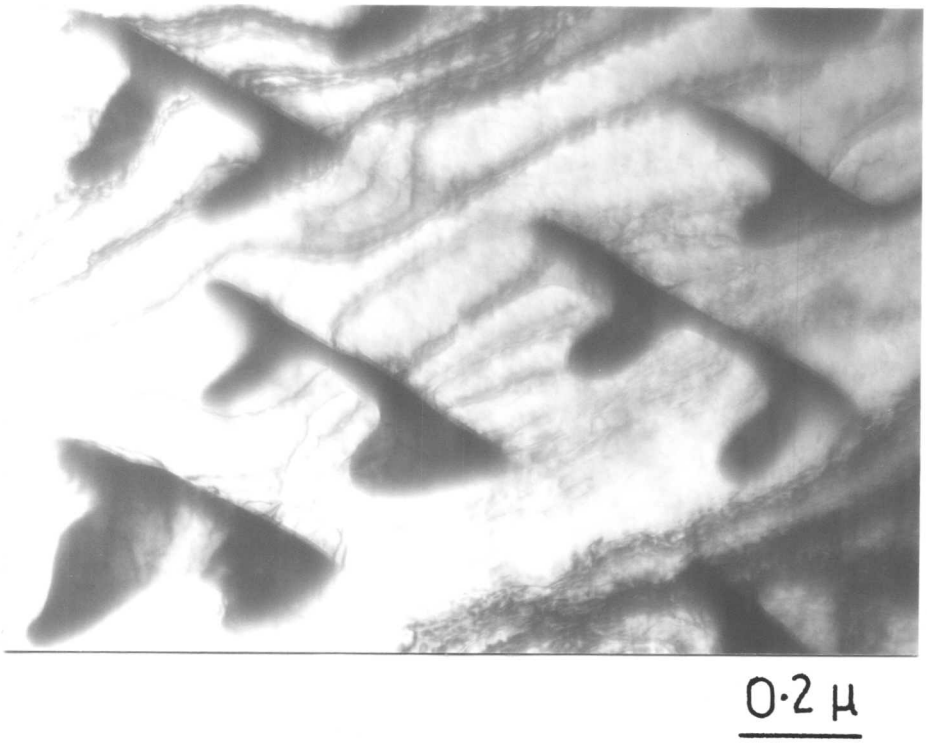

Figure 5.6h: Transmission electron micrograph showing carbide precipitation within ferrite.

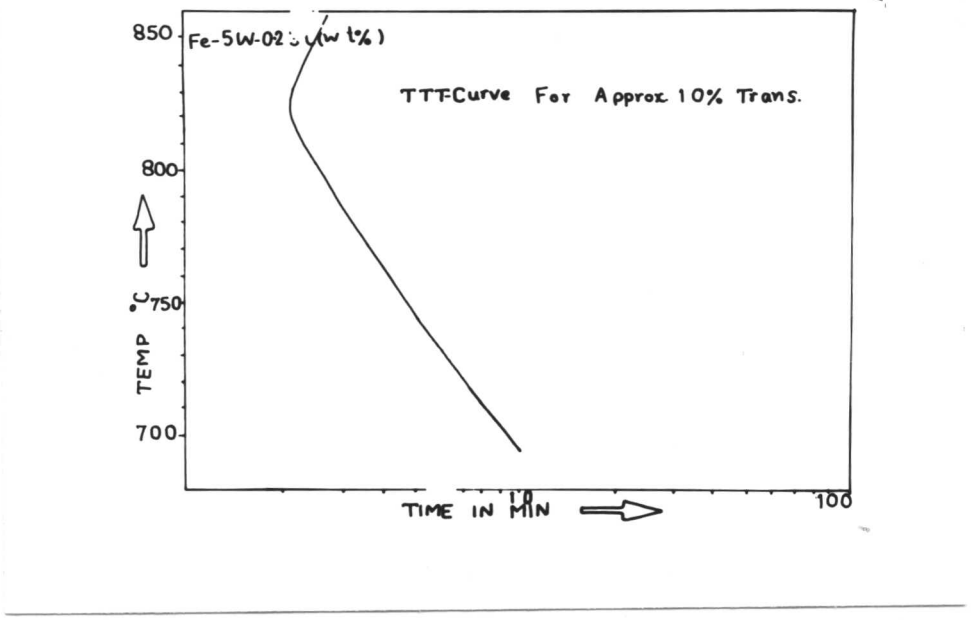

Figure 5.8: TTT diagram constucted to show approximately 10 vol.% transformation.

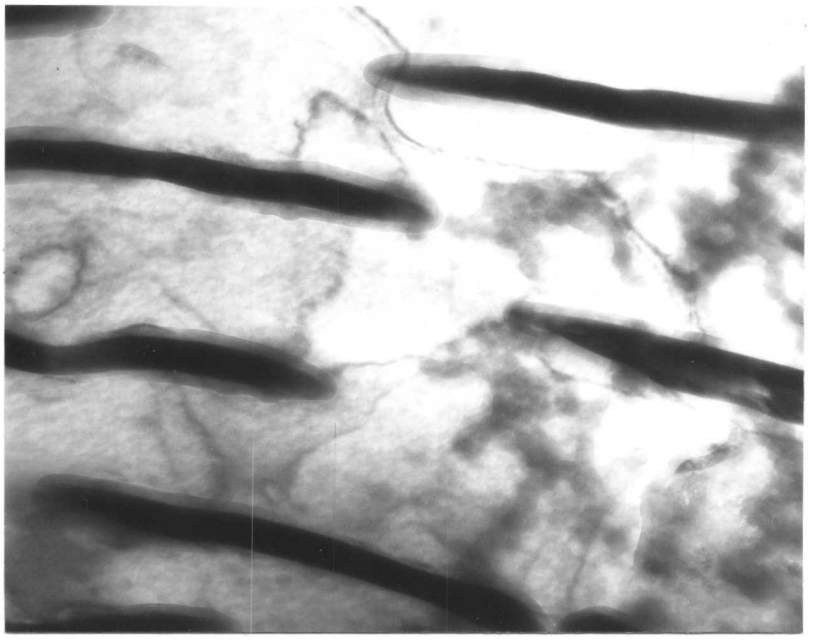

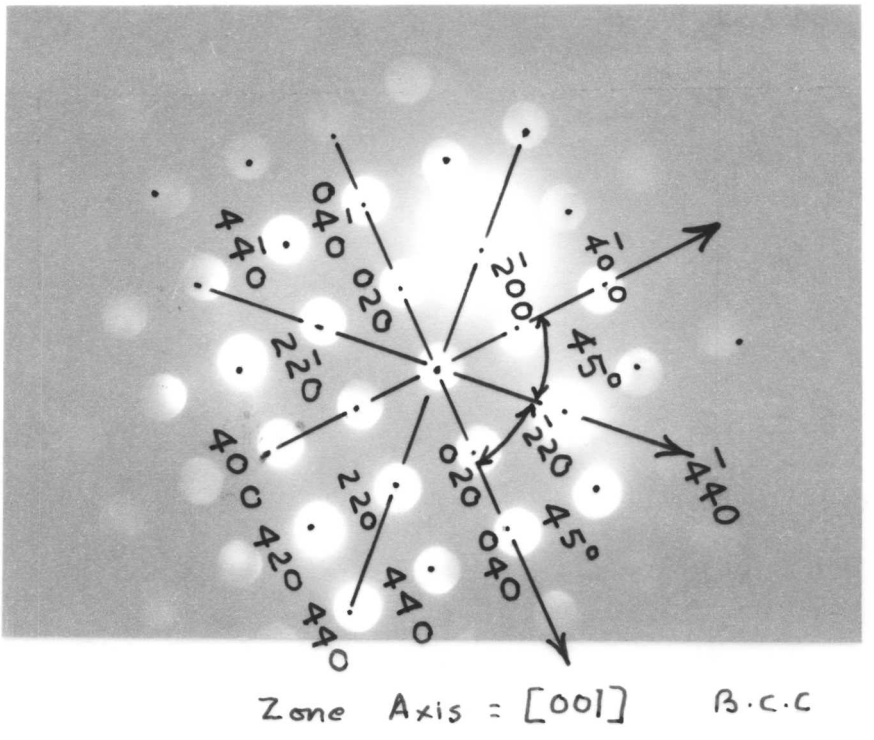

Figure 5.7(a): Transmission electron micrograph showing rod-shaped morphology of the tungsten carbide.

(b) Convergent beam diffraction pattern.

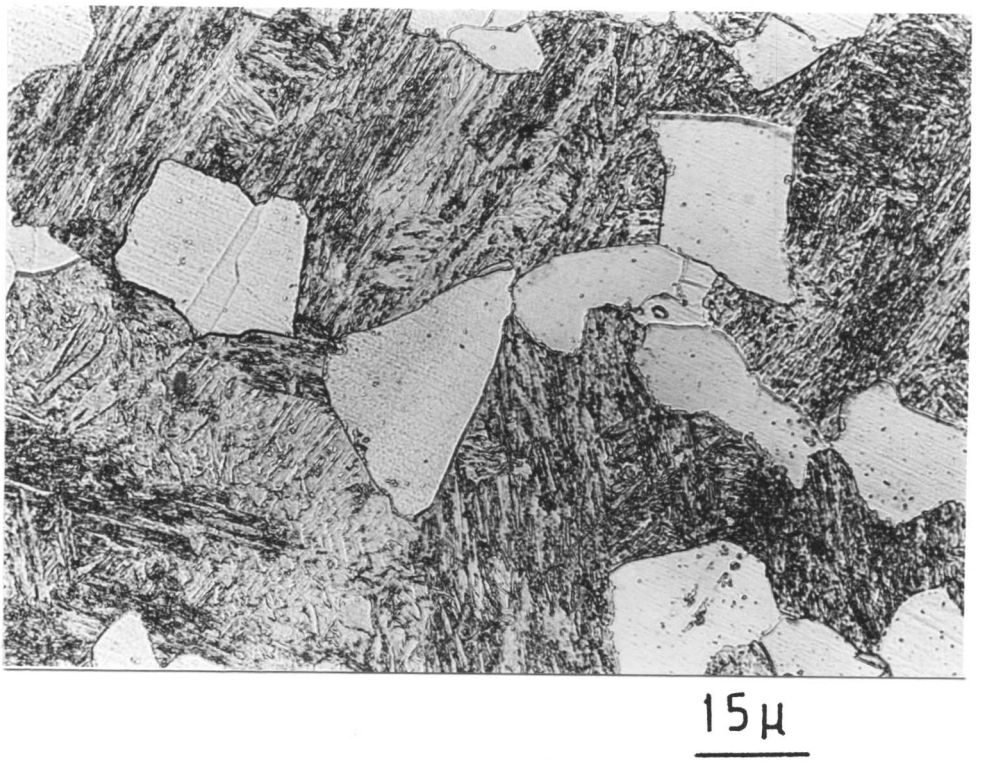

Figure 5.9a: Microstructure developed within 2.5 minutes at 850°C in Fe-5W-0.23C (wt%).

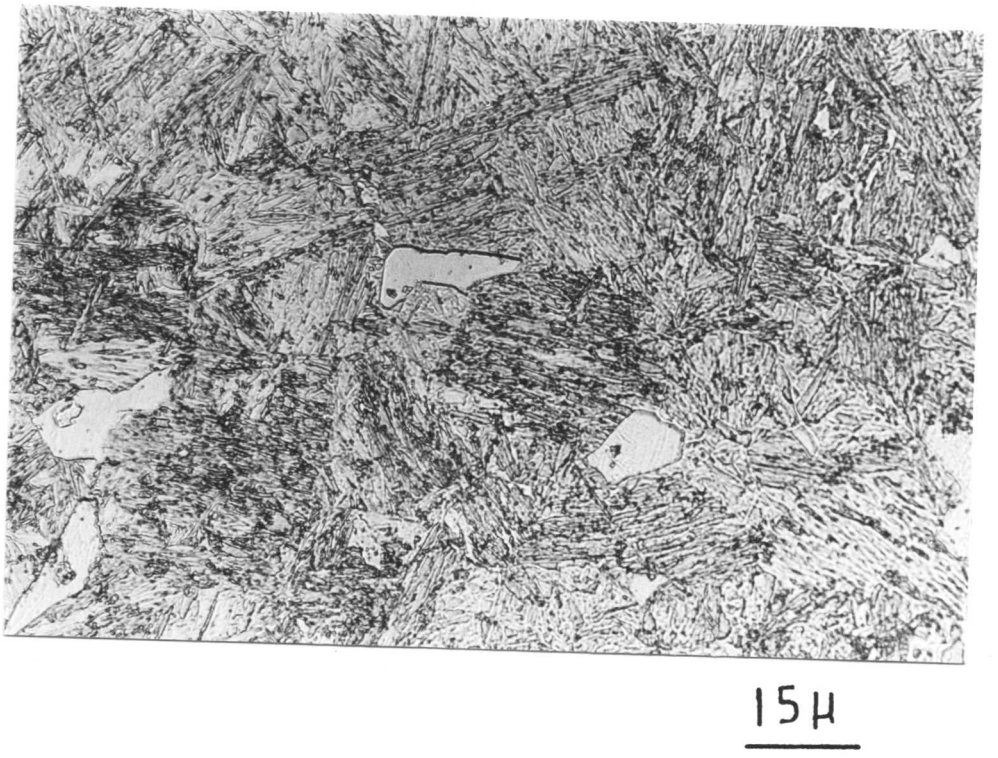

Figure 5.10a: Microstructure developed after same heat treatment as above in Fe-5.9W-0.14Ti-0.21C (wt%) alloy.

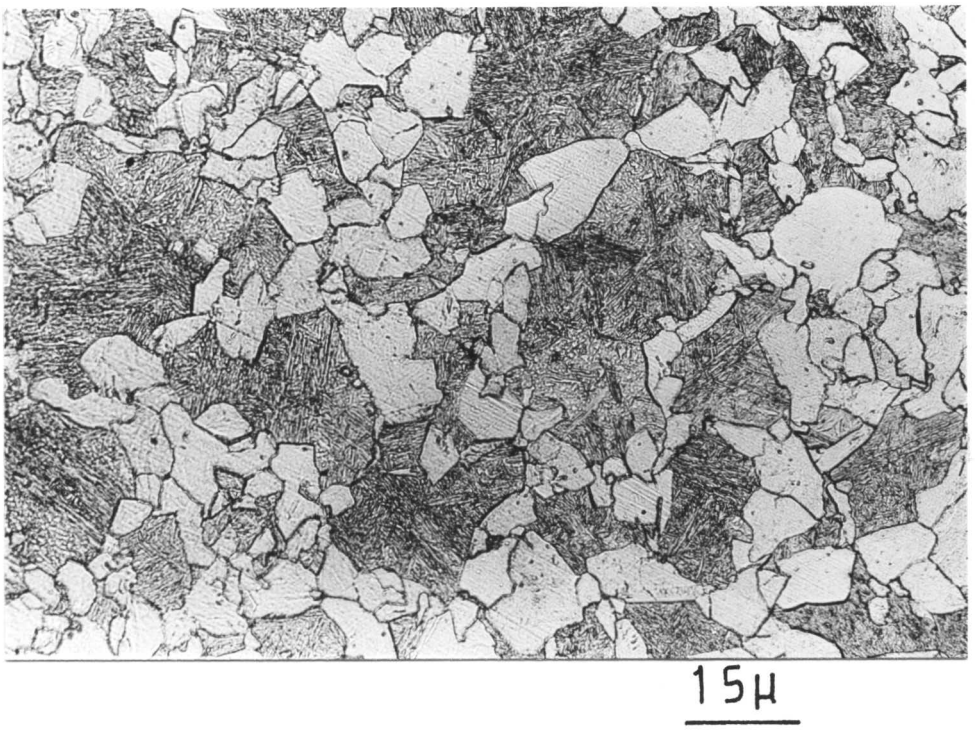

Figure 5.9b: Microstructure developed at 750°C within 5 minutes in Fe-W-C alloy.

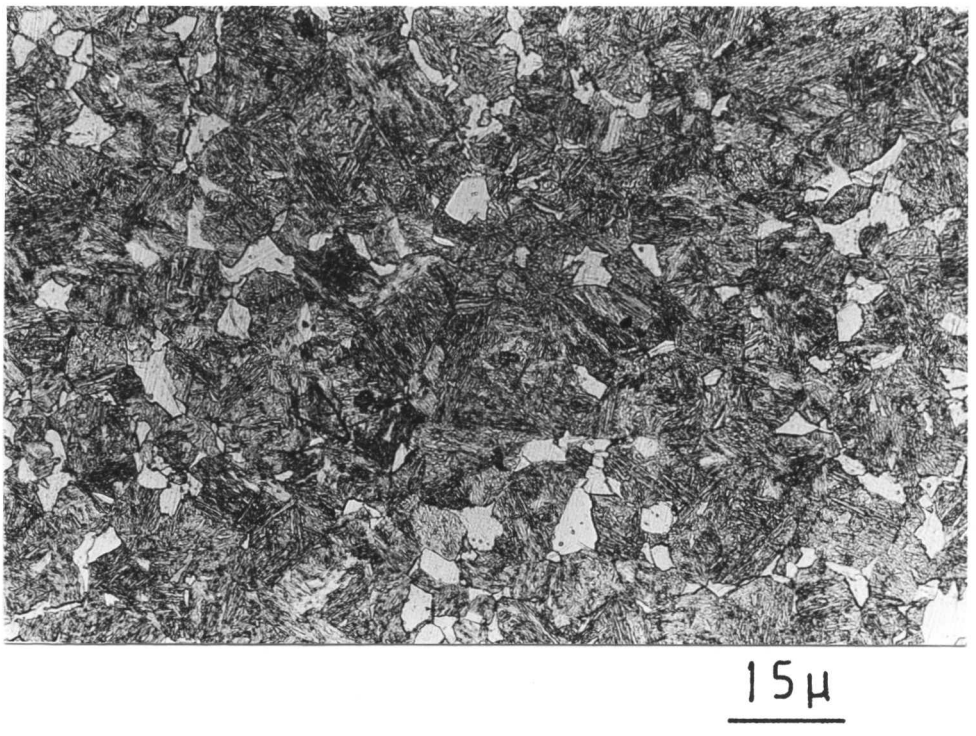

Figure 5.10b: Microstructure developed after the same heat-treatment in Fe-W-Ti-C alloy.

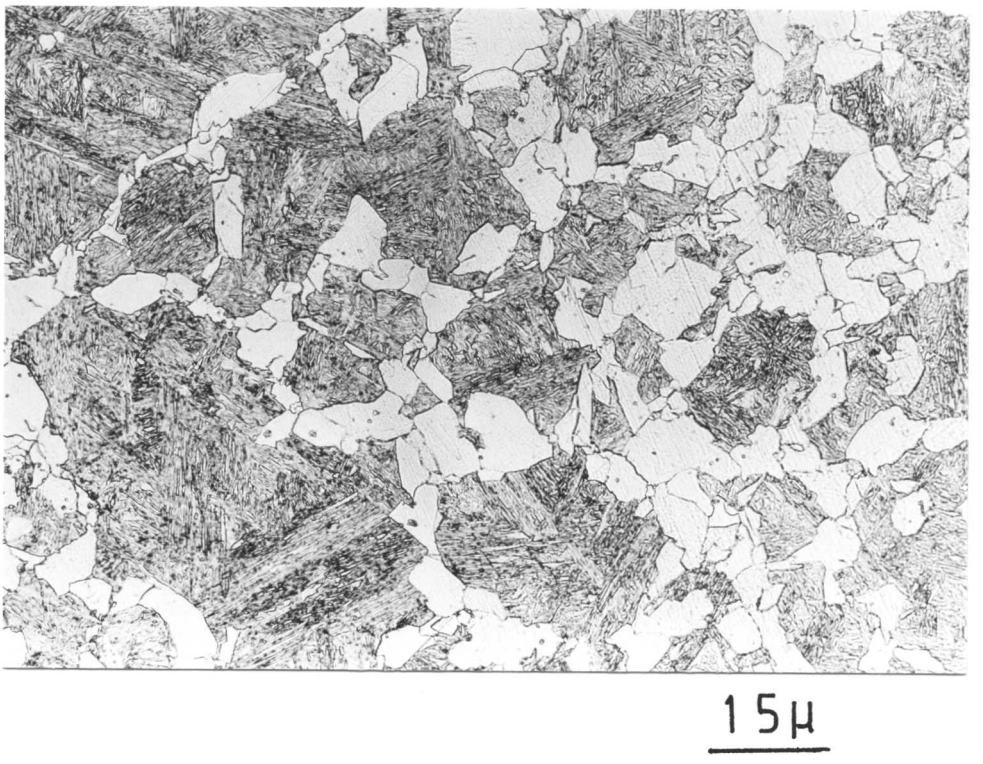

Figure 5.9c: Microstructure obtained at 700°C/10 Min in Fe-W-C alloy.

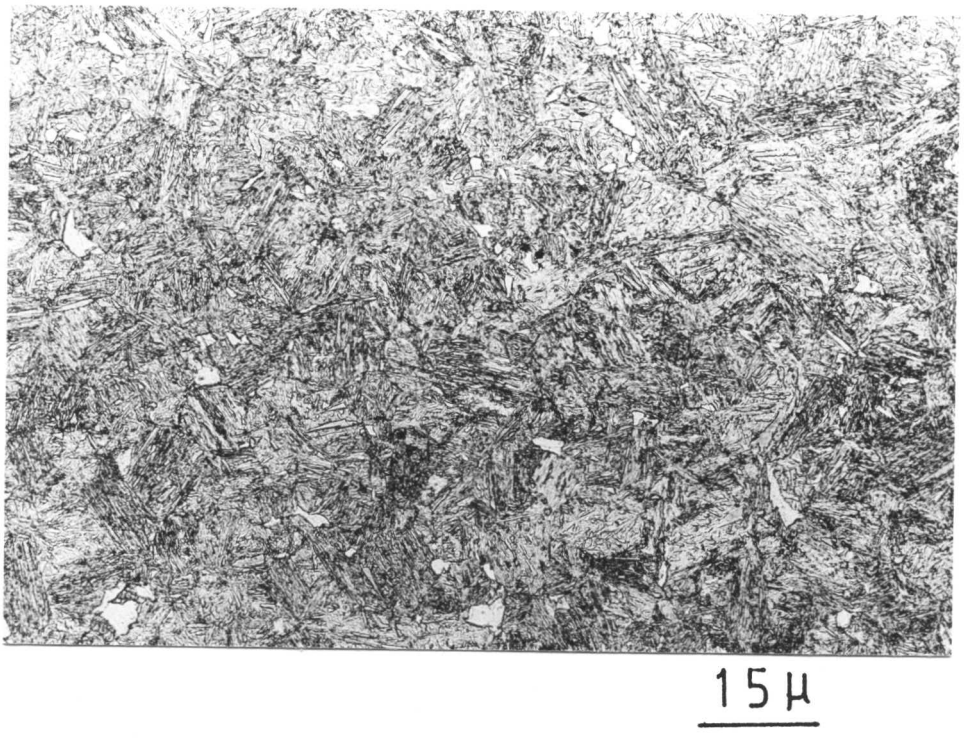

Figure 5.10c: Microstructure developed after same heat-treatment as Fe-W-Ti-C alloy.

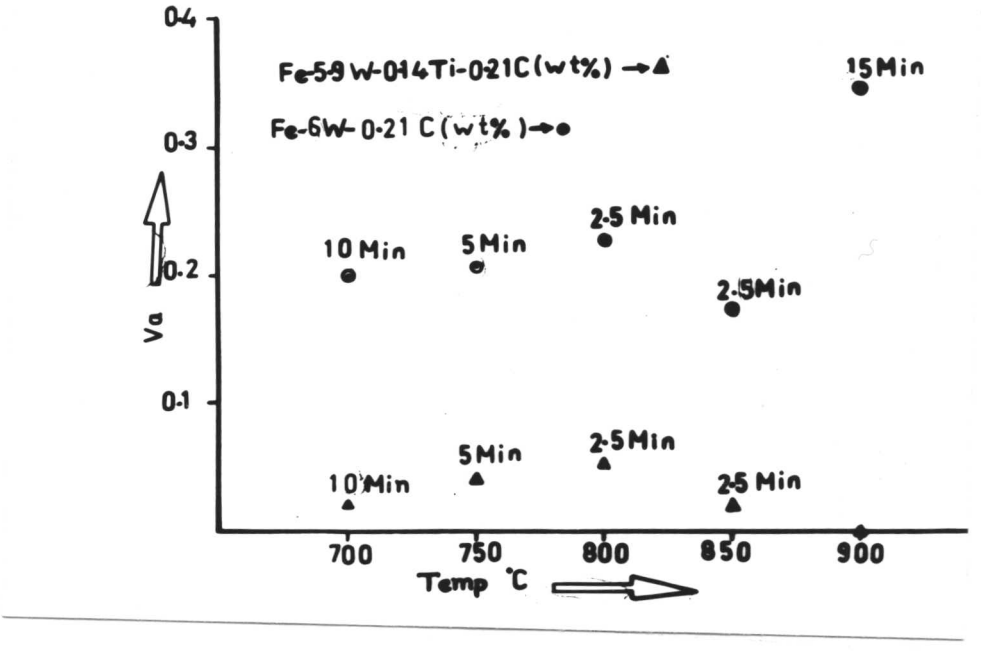

Figure 5.11: Quantitative measurement of volume fraction (Vα) at different isothermal temperature in alloy with and without titanium. It clearly shows that titanium is effective in retarding the $\gamma \rightarrow \alpha$ transformation.

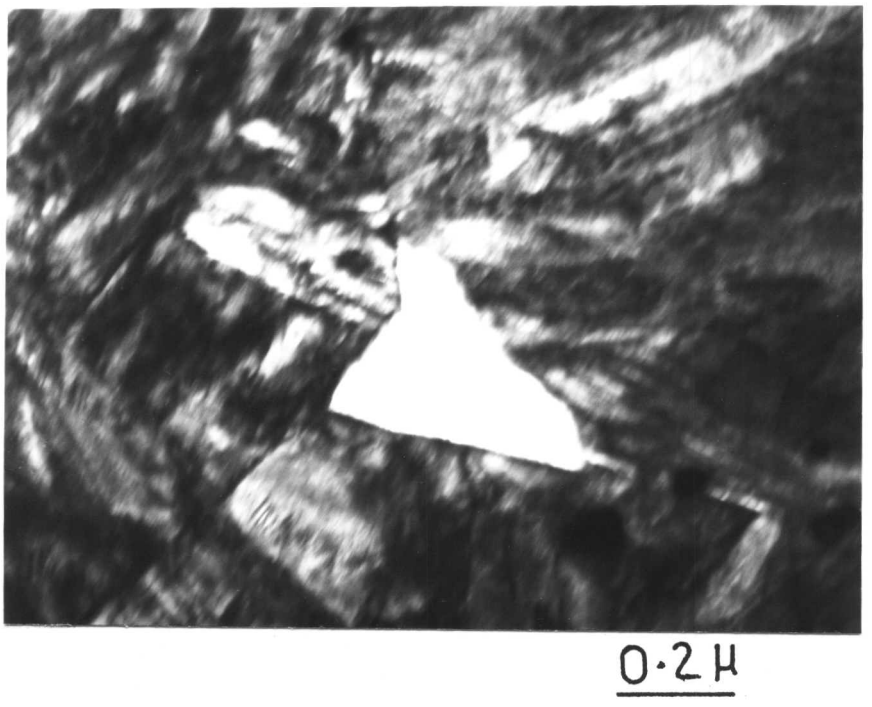

Figure 5.12: Transmission electron microscope showing carbide free ferrite formed during early stages of transformation.

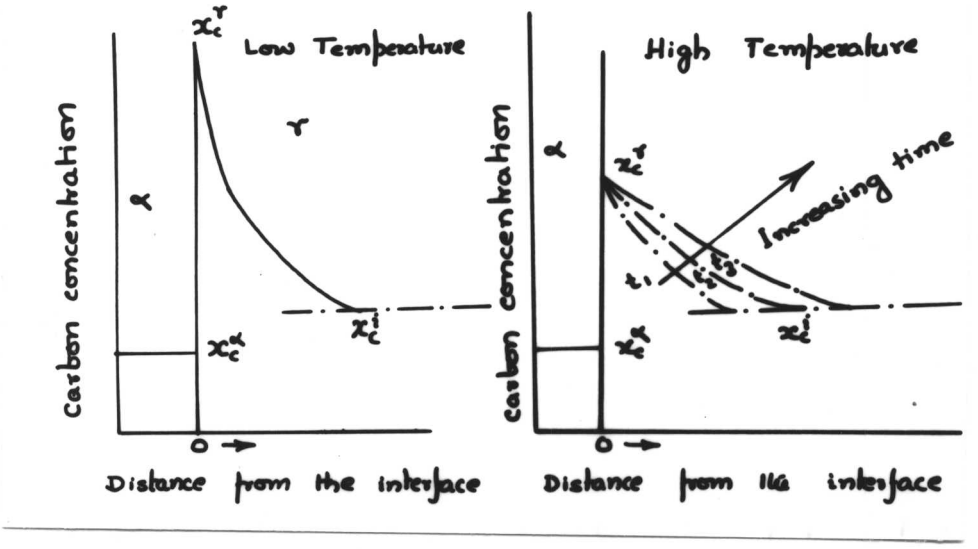

Figure 5.13: Schematic diagram showing carbon concentration profile near the moving interface under two different circumstances.

CHAPTER VI

The $\gamma \rightarrow \alpha$ transformation in Fe-5W-2.3Si-0.15C (wt%) alloy.

6.1 Introduction: To achieve the best combination of strength and toughness in alloy steels, an alternate approach of direct transformation is gaining importance. Small additions of strong carbide forming elements such as Nb, V, Ti etc, have been shown to increase the strength and toughness of low carbon low alloy steels at room temperature by forming a fine dispersion of carbides through the process of interphase precipitation as well as by grain refinement[1,2,3]. Detailed structural studies have revealed that these carbides are nucleated at the semicoherent γ/α interface and appear as bands representing successive stages of the transformation front[4]. The size and spacing of the carbide precipitation depend on the isothermal transformation temperature, the alloy composition, the volume fraction of carbide and the rate at which the decomposition of austenite takes place[5]. In addition to interphase precipitation, there is another kind of carbide morphology which forms at relatively lower temperatures. This carbide appears as fibres[6]. These fibrous carbides nucleate on the incoherent γ/α interface and grow normal to the interphase-boundary as fine fibers often only 500Å diameter. These two types of carbide morphology are competitive, often occurring together in the same specimen and even in the same original austenite grain. However, variation in heat-treatment or alloy composition can markedly alter the proportion of two morphologies observed. At sufficiently high undercooling these two modes of carbide precipitation are superseded by formation of supersaturated ferrite. The carbides are precipitated on dislocations by aging process from these supersaturated ferrites. Dislocations are generated during the transformation and act as a preferential nucleation sites. The pioneering work by Honeycombe and his students[7-16] led to important advances in our understanding of these microstructures which develop during the $\gamma \rightarrow \alpha$ transformation. They presented convincing evidence to elucidate the various mechanisms of carbide precipitation by performing extensive series of well conceived experiments.

The present investigation aimed to characterize and if possible, elucidate the transformation behaviour of Fe-5W-2.3Si-0.15C (wt%) alloy in the temperature range 850°C to 700°C. This alloy is similar in composition to that used in chaper V except that it contains Si and slightly less amount of carbon. This particular composition was selected to examine the effect of silicon on the transformation characteristics. To our surprise, the microstructure in this particular alloy is quite different from that obtained at

in Fe-5W-0.23C (wt%) alloy. This change in microstructure is attributed to the presence of silicon.

6.2 Experimental Results:

6.2.1 Isothermal Transformation at 700°C: The $\gamma \rightarrow \alpha$ transformation at this temperature was much faster than in the similar alloy without Si . Isothermal transformation at 700°C for 5 minutes showed approximately 15 vol.% transformation. The $\gamma \rightarrow \alpha$ transformation started predominatly at austenite grain-boundaries to form grain-boundary allotriomorphs (Figure 6.1a). The rate of thickening appeared low compared with that of lengthening, leading to high aspect ratio for those allotriomorphs. In the majority of cases, the interface appeared planar and facetted. Occasionally interface pinning was noticed (Figure 6.1b). Fine carbides were also detected within the austenite grain.

Many interesting features appeared when the time of transformation was increased to 10 minutes at 700°C. The $\gamma \rightarrow \alpha$ transformation achieved its equilibrium value within 10 minutes whereas the alloy without Si showed only 10 vol.% transformation. Grain-boundary allotriomorphs developed rapidly to form equiaxed ferrite. A fine dispersion of alloy carbides (tungsten carbide, M_6C/W_2C) was noticed within these ferrite grains in contrast to those formed in Fe-W-C alloy. More interesting is that these carbides were enveloped by a precipitate free zone (PFZ) (Figure 6.2a). The width of the PFZ appeared constant (6 to 8μm) in the majority of cases, although sectioning effects are not taken into account. However, no PFZ was observed near the α/α interface (Figure 6.2a arrowed). A dark grey rim appeared along the γ/α interface which grew in the austenite. The thickness of the rim was not uniform, indicating that the rate of growth varied even within the same grain. The interface of this growing grey rim occasionally showed the presence of ledges (Figure 6.2c). The interface of the growing rim showed evidence of pinning (Figure 6.2b).

With further increase in time to 40 minutes at 700°C, the fine dispersion of carbides within the ferrite grew in size and became more apparent using optical microscopy (Figure 6.3a). These carbides appeared to be of the Widmanstätten type (Figure 6.3b). The width of PFZ remained almost constant. The dark grey rim grew in thickness (Figure 6.3c,).

With further increase in time to 80 minutes at 700°C, the dark grey region grew in thickness and finally consumed the whole austenite grain (Figure 6.4a). However, in some cases, a dark etched region appeared ahead of this growing rim during the latter stage. No such microstructural features were observed in Fe-5W-0.23C (wt%) alloy.

Electron microscopy was employed to get microstructural details of this growing rim. The rim was found to contain dense distribution of carbides in different morphologies. Most of these carbides are very fine but some of them are relatively coarse and elongated (Fig. 6.5a). In certain areas it was observed that these carbides are arranged in rows (Fig. 6.5b). Probably these rims have formed by a discontinuous reaction. With increasing time of transformation, the coarse carbides grew rapidly in dimension - whereas the fine carbides appeared to resist growth (Fig. 6.5a and b). After long ageing treatments (i.e. at 700°C for 40 to 80 minutes), the resulting microstructure show two interfaces at some places. The primary interface of the discontinuous reaction was followed by a secondary discontinuous reaction (Fig. 6.5c). The second discontinuous coarsening reaction appeared to have the same two phase, but during this step carbide dispersion is much finer. The region containing finer dispersion of carbides was bounded on one side by previously existing grain-boundary (Fig. 6.5c). The carbides formed from supersaturated ferrite are shown in (Fig. 6.5d). Non-uniform distribution of carbides is apparent in this micrograph. Widmanstätten type of carbides were also observed in certain areas of ferrite (Fig. 6.5e).

6.2.2 Isothermal Transformation at 800°C was much faster as expected. Within 1.5 minutes about 50 volume % transformation occurred. The incubation period appeared to be minimum at this temperature. Grain boundary allotriomorphs formed at this temperature showed a tendency towards facetting. (Fig. 6.6a). Frequent evidence of ledges was also recorded. The height of the ledge appeared to vary even at the same interface. Close optical microscopy observations indicated the presence of carbides at the γ/α interface.

Fine carbides were also noticed within the austenite as well as inside the ferrite. At high magnification, fibrous carbides were noticed (Figure 6.6b-c). These fibrous carbides appeared to grow in association with low energy facets which have moved by a ledge mechanism.

6.2.3 Clear evidence of interphase precipitation was obtained when the specimen was transformed at 850°C (Figure 6.7a). The band spacing varied even within the same grain. Occasionally, fibrous carbides were observed (Figure 6.7b). Random or irregular dispersions of alloy carbides were also noticed frequently along with banded dispersions.

SEM taken from these specimens are shown in (Fig 6.8a-h). Figure 6.8a-d show sheets of precipitates. It suggests that the precipitation has occurred on a semi-coherent interface which moves by a ledge mechanism. However, in certain areas the precipitates are not arranged perfectly in rows (Fig. 6.8e-h).

Probably these carbides have formed on an incoherent interface. It is also apparent from these micrographs that the band spacing is not uniform. The variation in band spacing is about an order of magnitude.

TEM studies were done to examine the γ/α interface responsible for banded dispersion of carbides. Fig. 6.9 shows that the ledge mechanism operating during formation of banded carbide dispersion. The variable band spacing is shown in Fig. 6.9.

6.2.4 Step Quenching.

Step quenching was tried in order to ascertain the effect of transformation temperature on the transformation product. The specimen was first held at 700°C for 20 minutes followed by upquenching at 800°C for 3.5 minutes. Figure 6.10 shows that one side of the interface contains a dark etched region while the fine dispersion of alloy carbide was noticed on the other side of the interface. The dark etched region consisted of a fine dispersion of carbides rather than fibrous carbides.

6.3 Discussion: At all temperatures, the reaction was much faster compared to Fe-5W-0.23C (wt%) alloy.

The $\gamma \rightarrow \alpha$ transformation started predominantly at austenite grain-boundaries to form allotriomorphs. The aspect ratio of these allotriomorphs was high at 700°C. It indicates that the rate of thickening is very slow compared to lengthening at this temperature. The interface appeared planar in the majority of cases. Planar interfaces are taken as evidence of low energy facets on a macroscopic scale. Evidence of ledges implies that the ledge mechanism plays a dominant role in determining the transformation kinetics over a wide range of temperatures. The high proportion of planar interfaces observed over a wide range of temperature, implies that partial coherency can exist at the majority of interface orientations and that a truly incoherent structure is rare[17].

It was also observed that interfaces were pinned by carbides. The pinning occurred mainly due to the carbides already present in the austenite. The protuberances were developed as the interface moved across the carbide particles already present in austenite.

At high transformation temperatures (850°C), the carbide precipitation occurred predominantly by an interphase mechanism. In contrast, complete absence of carbide precipitation by an interphase mechanism was observed in Fe-5W-0.23C alloy (Chapter V) at this temperature. It is believed that the presence of silicon causes a significant drop in solid-solubility of carbides in ferrite. Consequently these carbides are precipitated during the $\gamma \rightarrow \alpha$ transformation

by a ledge mechanism and the resultant carbides are generally aligned (Fig. 6.7 to 6.9). Two distinct modes of carbide precipitation were noticed at 700°C. A fine dispersion of carbides was noticed within each ferrite grain. These carbides have formed from supersaturated ferrite by an ageing process. However, there was another kind of precipitation phenomenon noticed at this temperature. A grey rim appeared to form along the γ/α interface. The formation of rim is analogous to that of the discontinuous precipitation.

In discontinuous precipitation the heterogeneous nucleation of grain-boundary precipitates takes place with concurrent boundary migration. The reaction product is a two-phase lamellar cell which consumes the supersaturated matrix. The reaction is discontinuous in so far as there are discrete changes in crystallographic orientation and chemical composition at the advancing reaction front. The discontinous precipitation reaction is expressed as:

$$\gamma \rightarrow \gamma^1 + \beta$$

where the depleted matrix γ^1 phase has the same structure as the initial supersaturated solid solution γ, differing from it only in composition. The precipitating phase β can be an intermetallic phase[18], a solid solution of another lattice structure[19] or a solid solution of the same lattice structure[20].

The initiation of the discontinuous reaction has been the subject of many investigations and there are two proposed mechanisms for the initial migration of boundaries leading to discontinuous precipitation.Tu and Turnbull[21] have proposed the so called pucker mechanism in which facetted nuclei of the precipitating phase form at the grain-boundary with a low energy interface with one of the grains. The system then reduces its energy by a puckering of the grain bounday. The boundary then migrates to regain its minimum length and also leaves both sides of the precipitate with a low energy relationship with the one grain. It is believed that during migration further precipitation occurs because of favourable orientation of the boundary. Hence the process is self sustaining. The pucker mechanism has been unequivocally demonstrated to operate in many discontinuous reaction.

Fournelle and Clark[22] on the other hand suggested that boundary migration occurs due to its curvature in the direction required for grain growth. Allotriomorphs on grain-boundary act as a pinning centres and lead to cell formation. The process is not auto-catalytic in any respect and is self-sustaining almost immediately, due to the establishment of a chemical free energy difference across the advancing interface. Precipitate/matrix orientation habit plane is of little importance in this mechanism. This

mechanism was first established in Cu-In[22].

Optical metallographic observations followed by TEM showed that the rim nucleated along the γ/α interface. As the ageing continues, the precipitation reaction proceeds through the formation of duplex cells containing α matrix and the carbides. During the growth of cells, the multiplication of the cells occurs mainly by the nucleation of new lamellae at the cell boundary (Fig. 6.5a), the progressive development of the microstructure for different periods of time at 700°C is displayed in Figs. 6.1 to 6.4. After a long ageing time, two interfaces in the discontinuous cells were observed. Such two step coarsening of the discontinuous product in the duplex cell has been frequently reported in the past. A recent observation is due to Fournelle[23] in Fe-10%Ni-6% Ti wt% alloy.

Definite conclusions regarding the mechanism of nucleation of the discontinuous cells in this alloy are not possible. However, it is anticipated that the mechanism of nucleation suggested by Fournelle and Clark is operative in this alloy. This is further supported by the fact that the carbides observed at the γ/α interface are non-facetted rather than facetted as required in Tu and Turnbull's model.

Precipitate free zones (PFZ) surrounding the ferrite grains were observed at 700°C width of the PFZ remained constant during the latter period of transformation. Precipitate free zones are often observed adjacent to grain-boundaries in age hardening alloys. Originally these zones were attributed to localized depletion of solute because of preferential precipitation at the grain-boundaries[24]. Depletion of vacancies during the nucleation of matrix precipitate might control the formation of PFZ[25,26]. Microanalysis results have confirmed that the PFZ in this particular alloy have developed due to solute depletion rather than depletion of vacancies. This solute depletion is believed to occur by partioning of carbon and alloying element (i.e. C, W and Si) to the growing rim.

6.4 Conclusions:

1. At high transformation temperatures (850°C), banded carbide dispersions appeared. The band spacing was not uniform. This reflects the tendency towards variable ledge height responsible for such dispersion.
2. Random dispersions of alloy carbides were also noticed along with the banded structure.
3. In the majority of cases, the interface appeared planar.
4. At lower transformation temperatures (700°C) the mechanism of interphase precipitation was completely suppressed. A random dispersion alloy carbides formed from supersaturated ferrite during the later stages of transformation

and not by a ledge mechanism.

5. PFZ's surrounding ferrite grains were also noticed. Formation of PFZ's was attributed to localized depletion of solute because of preferential precipitation at the grain-boundaries.

6. Dark grey rims appeared to form at the γ/α interfaces but grew in the austenite. Finally all the austenite grains were replaced by these grey constituents. It is believed that these grey rims are formed by a discontinuous precipitation reaction.

7. The presence of silicon in the alloy accelerated the $\gamma \rightarrow \alpha$ transformation. It also enhanced the tendency towards developing banded structures at the highest transformation temperatures, possibly by decreasing the solid solubility of alloy carbide in austenite at that temperature. However, its precise role in inducing the discontinuous reaction at lower temperatures is not well understood.

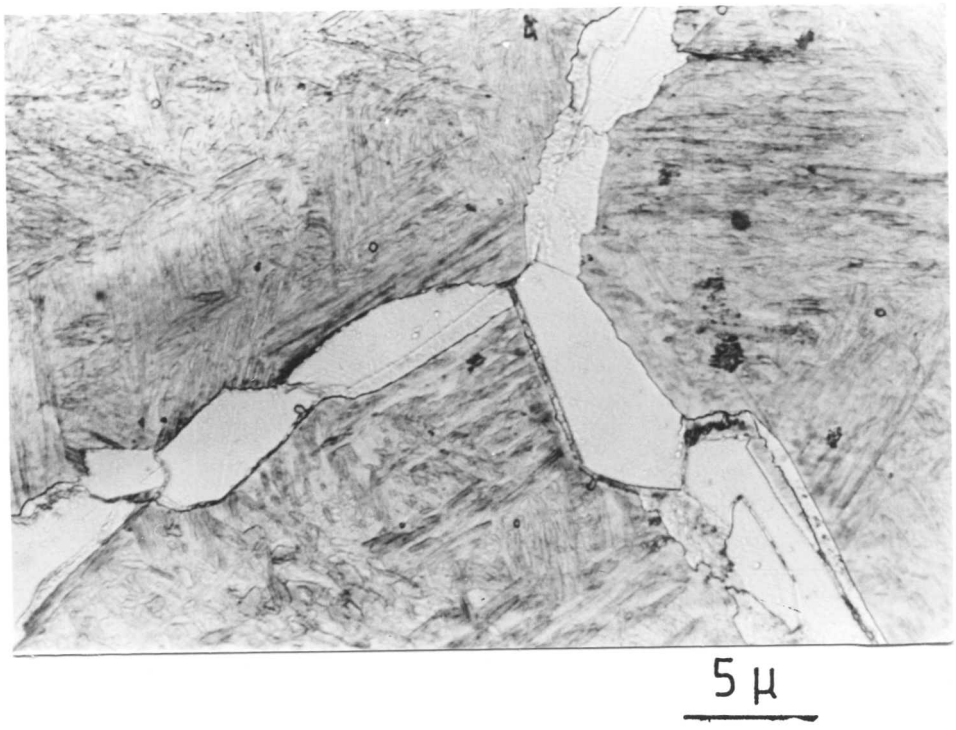

Figure 6.1a - Showing grain-boundary allotriomorphs.
(Isothermal transformation at 700°C for 5 minutes.)

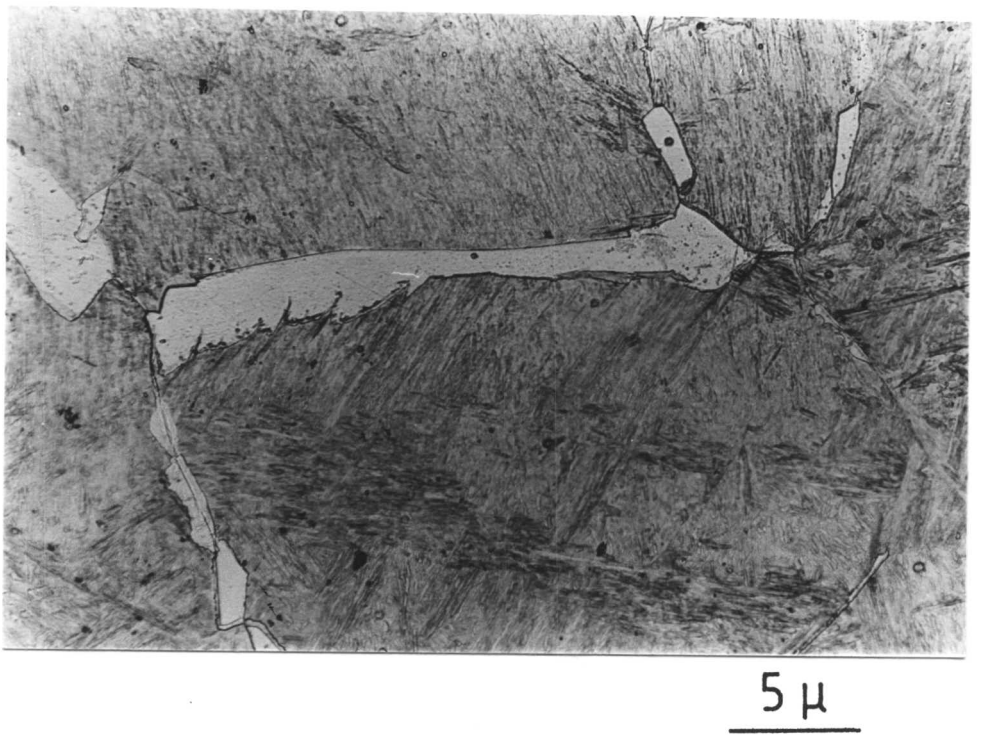

Figure 6.1b - Showing evidence of interface pinning by tungsten carbide. (Isothermal transformation at 700°C for 5 minutes.)

Figure 6.2a - Showing fine dispersion of carbides within the ferrite, surrounded by PFZ. A dark grey rim appeared to grow inside the austenite from the γ/α interface. (Isothermal transformation at 700°C for 10 minutes.)

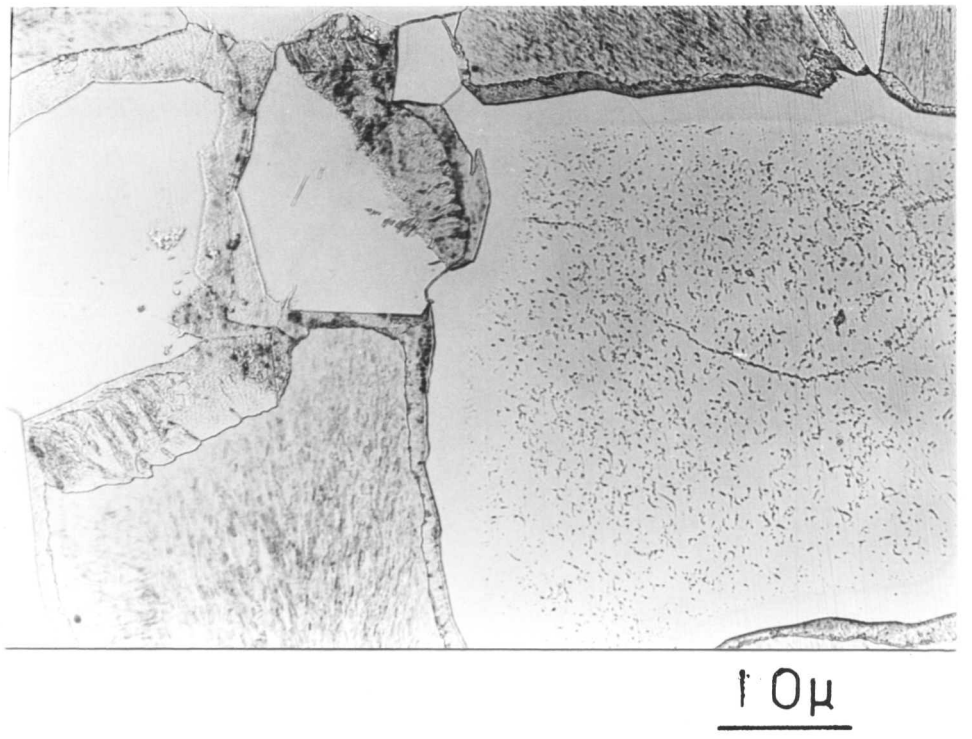

Figure 6.2b - Showing evidence of pinning at the interface of growing rim. (Isothermal transformation at 700°C for 10 minutes.)

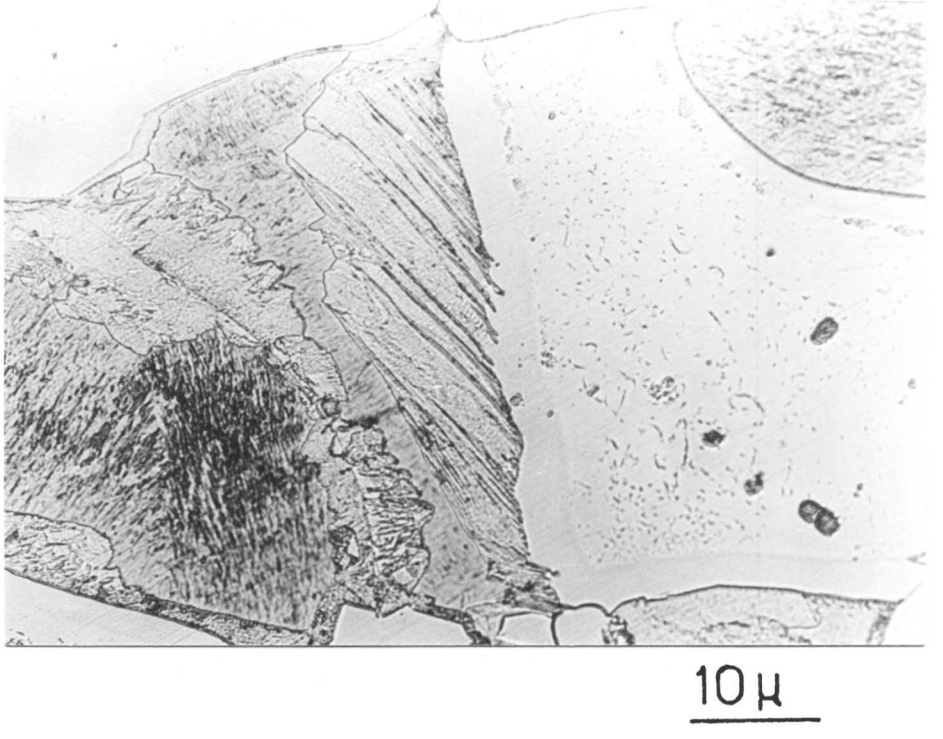

Figure 6.2c - Showing presence of ledges ahead of the growing dark grey rim. (Isothermal transformation at 700°C for 10 minutes.)

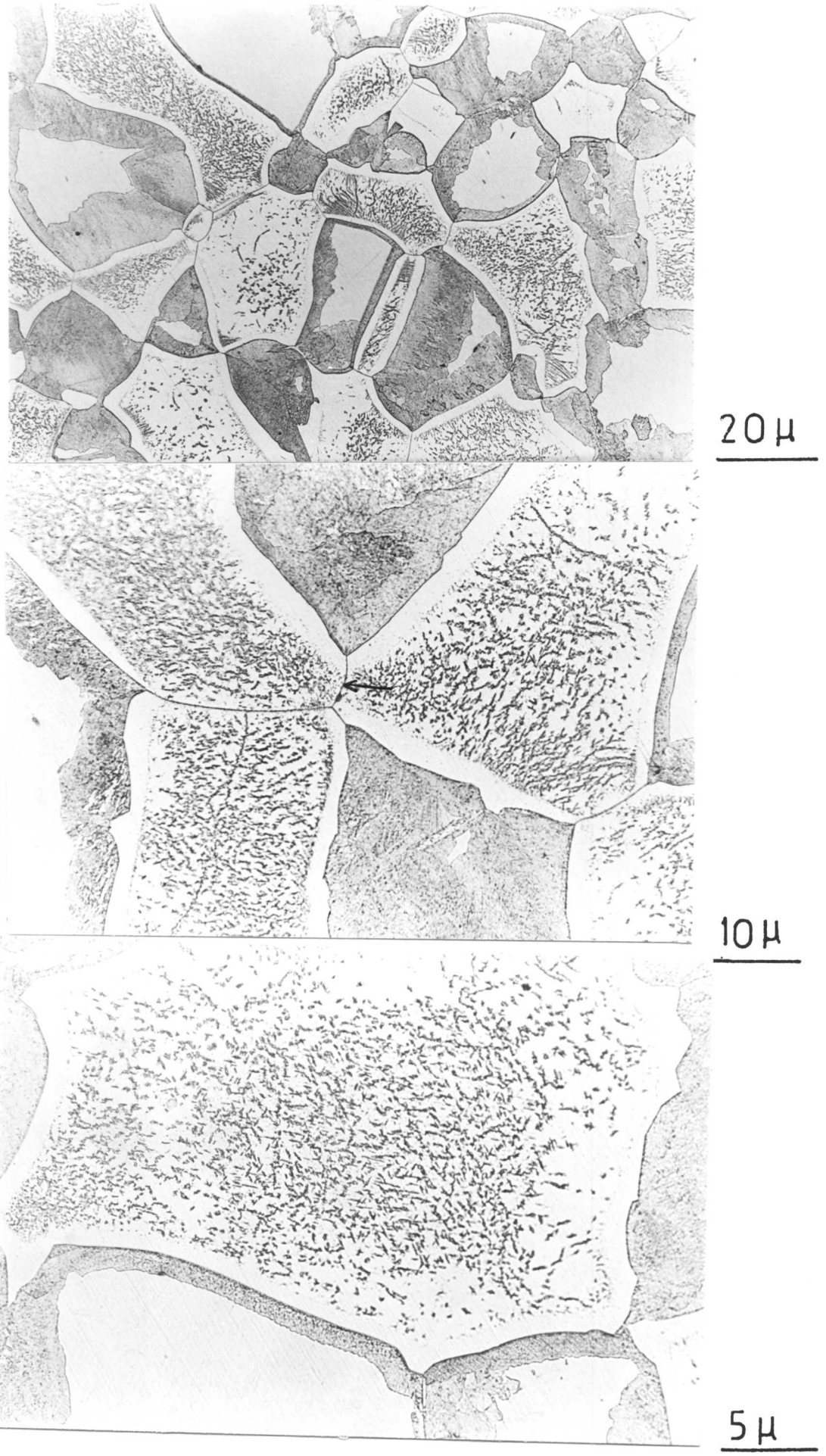

Figures 6.3a,b,c - Showing fine dispersions of carbide within the ferrite grain. The rim also grew in thickness with increasing time. (Isothermal transformation at 700°C for 40 minutes.)

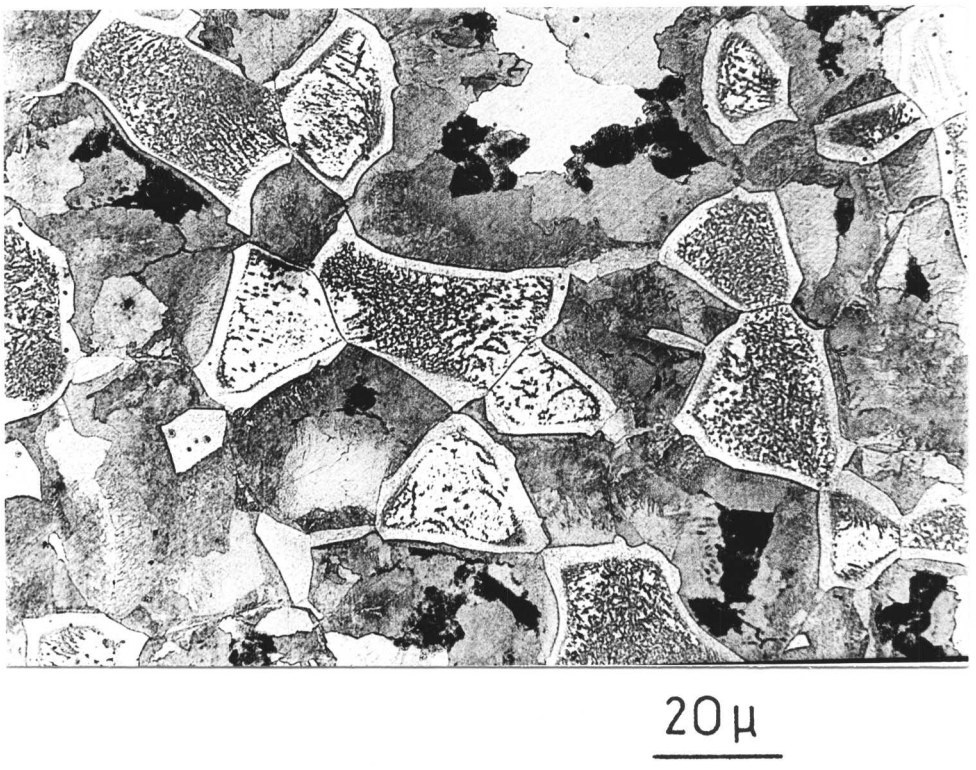

Figure 6.4 - Isothermal transformation at 700°C for 80 minutes. The dark grey rim grew further in size.

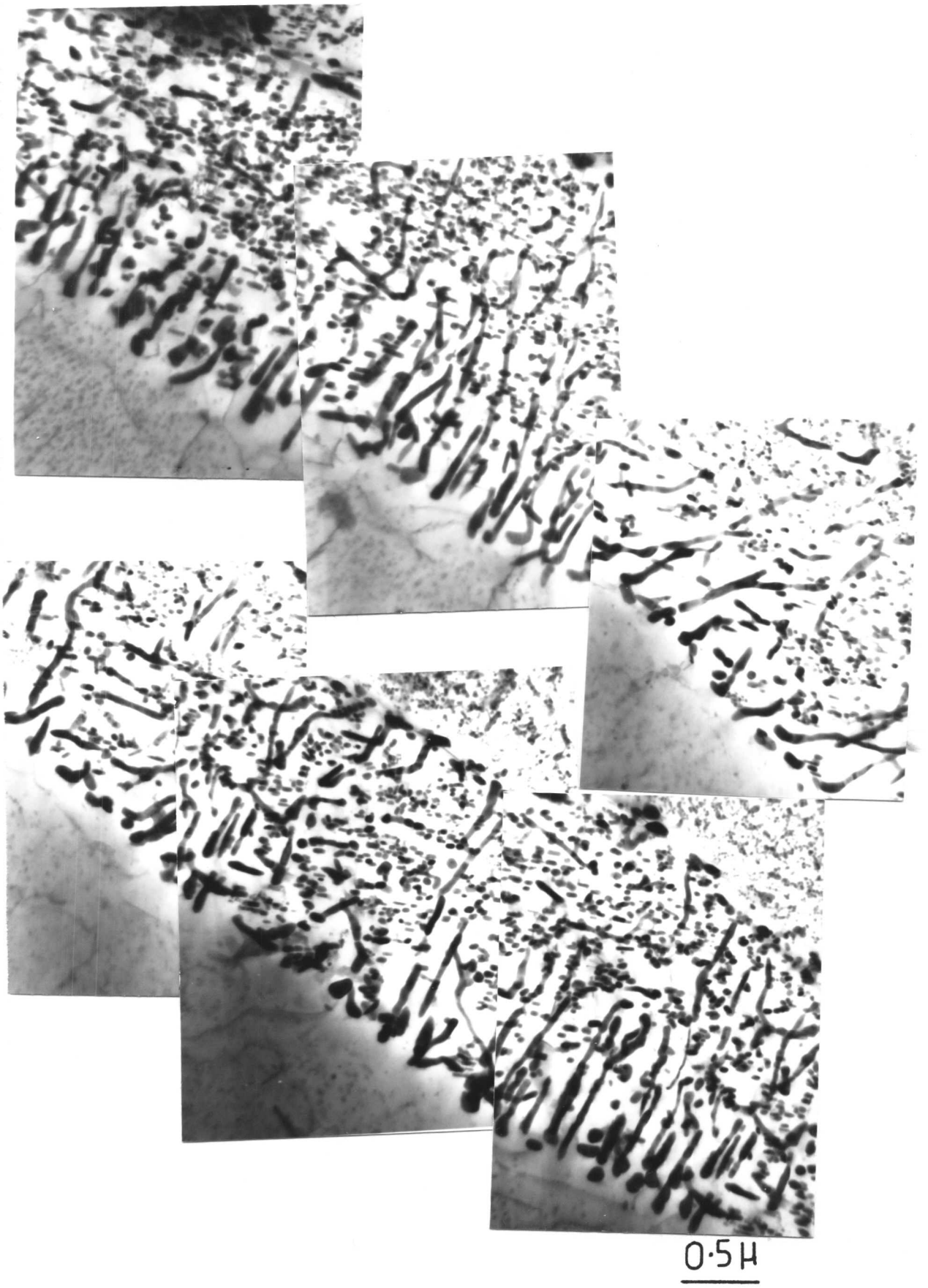

Figure 6.5a - Microstructure of the rim. It consists of fine dispersions of carbides in α. Some coarse carbides are also visible.

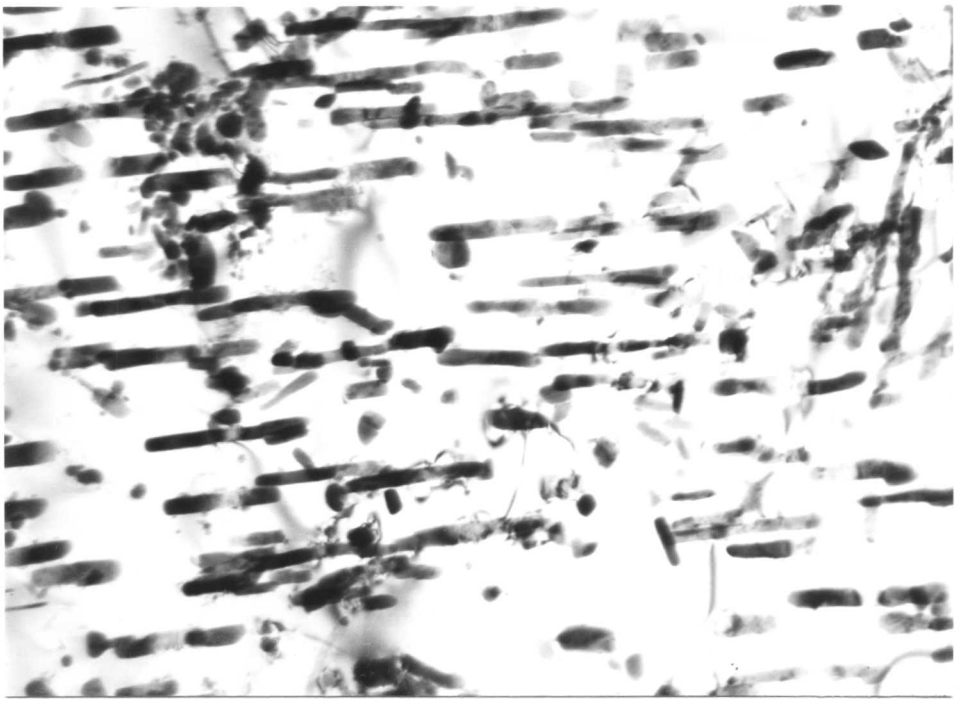

Figure 6.5b - Carbides arranged in one particular direction.

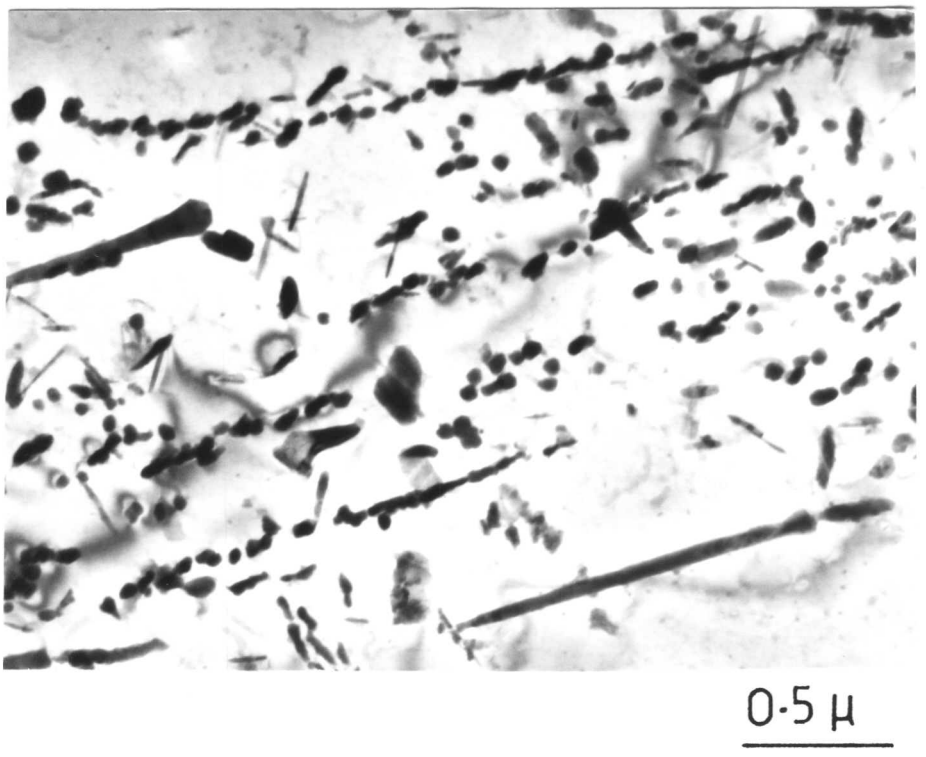

Figure 6.5d - Carbide formed from supersaturated ferrite are less dense and non-uniform in distribution.

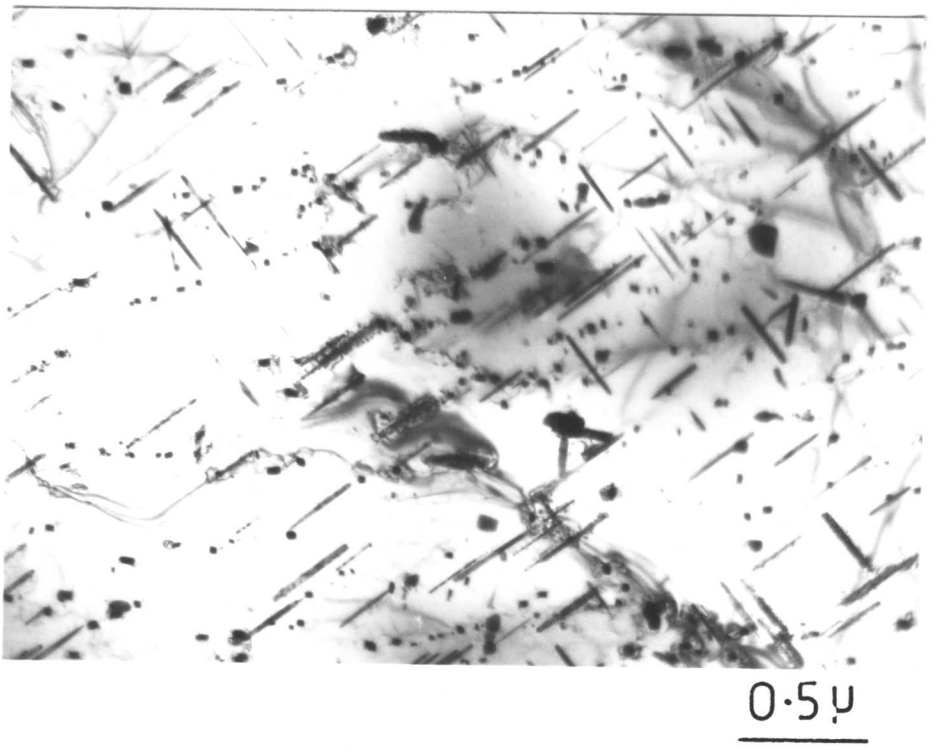

Figure 6.5e - Formation of Widmanstätten type of carbide in α.

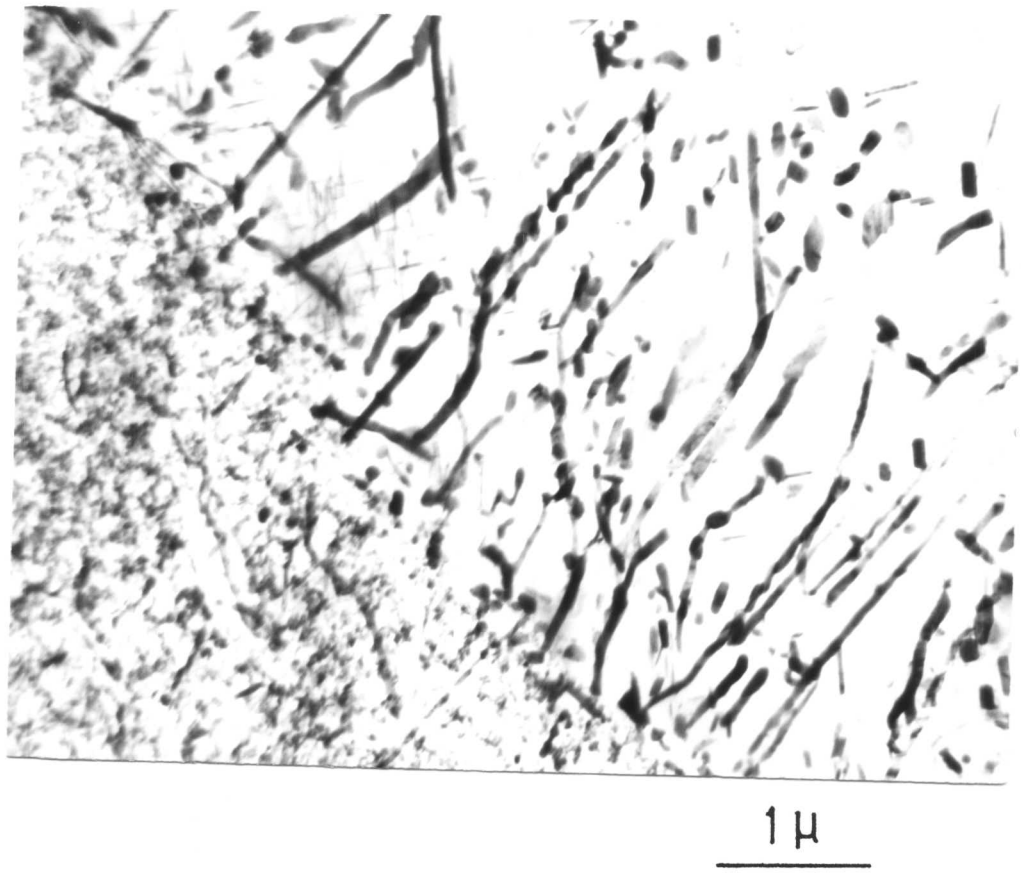

Figure 6.5c - Microstructure showing two step coarsening of the discontinuous precipitations.

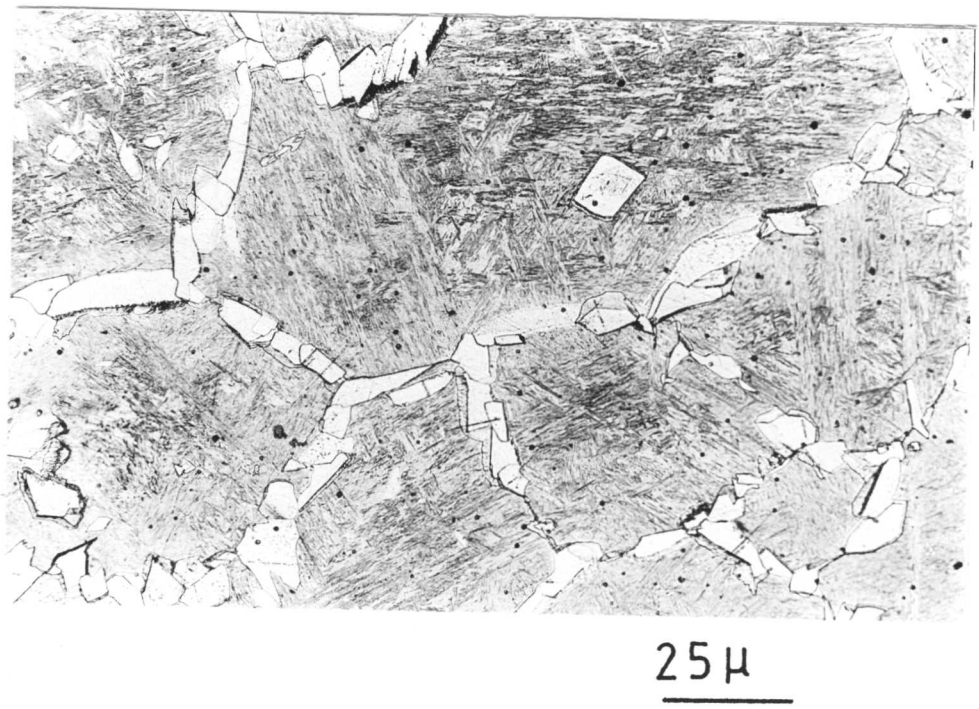

Figure 6.6a - Showing grain-boundary allotriomorphs occasionally containing ledges. (Isothermally transformed at 800°C for 1.5 minutes.)

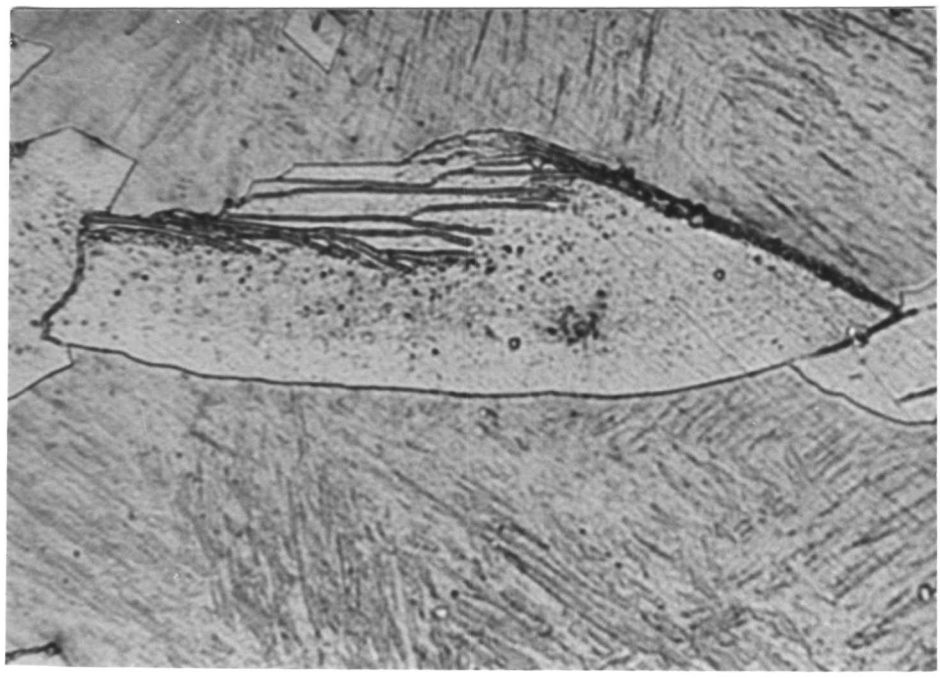

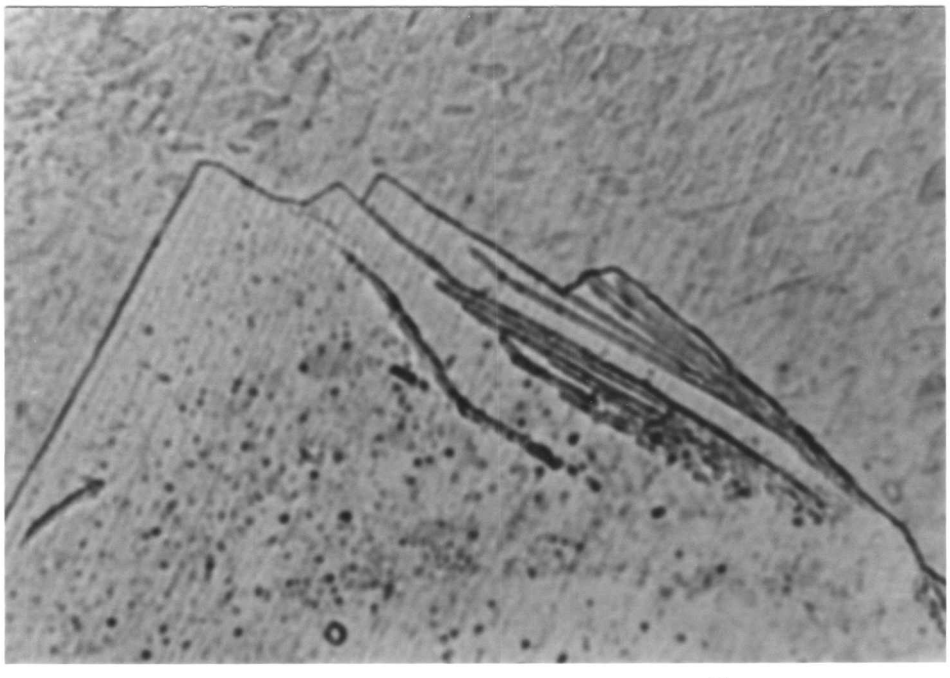

Figures 6.6b-c - Showing fibrous carbides in association with low energy interface which has moved by ledge mechanism. (Isothermal transformation at 800°C for 1.5 minutes.)

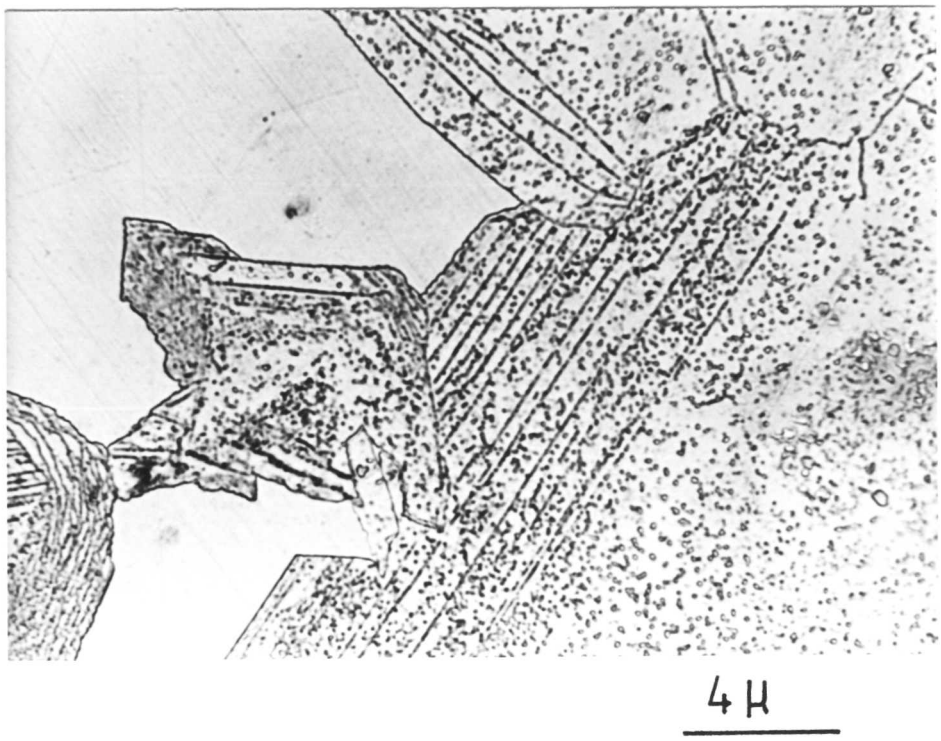

Figure 6.7a - Showing evidence of interphase precipitation at 850°C for 20 minutes.

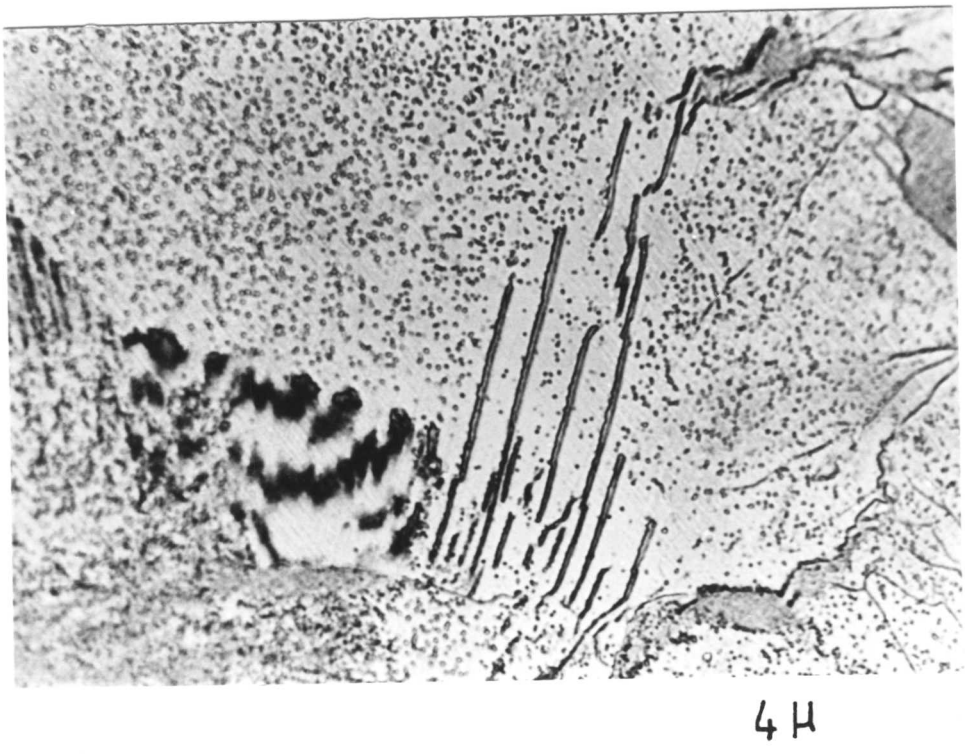

Figure 6.7b - Showing fibrous carbides as well as random dispersions of carbides. (Isothermally transformed at 850°C for 20 minutes.)

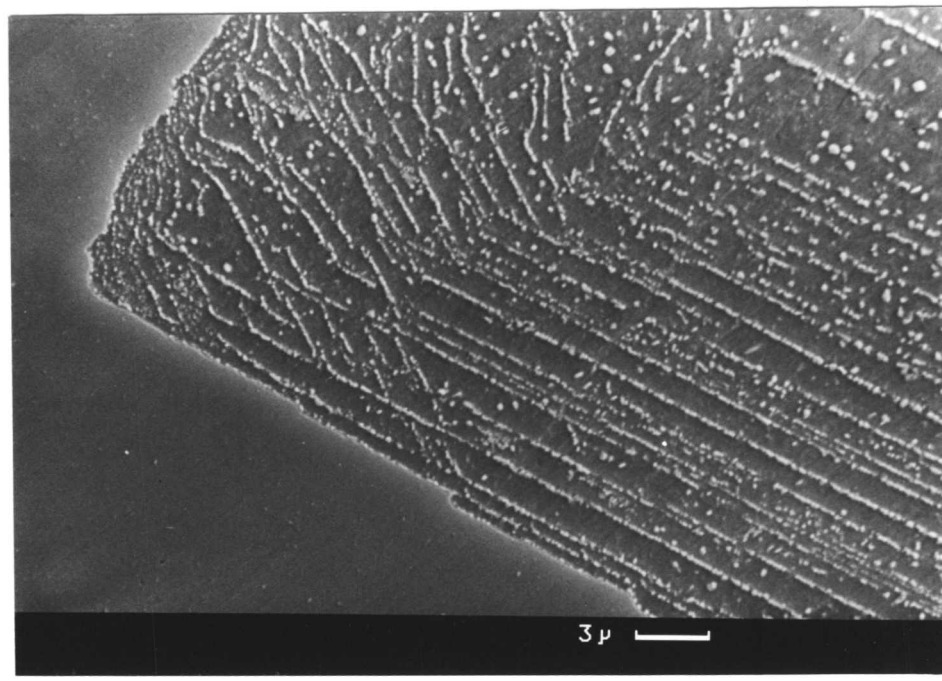

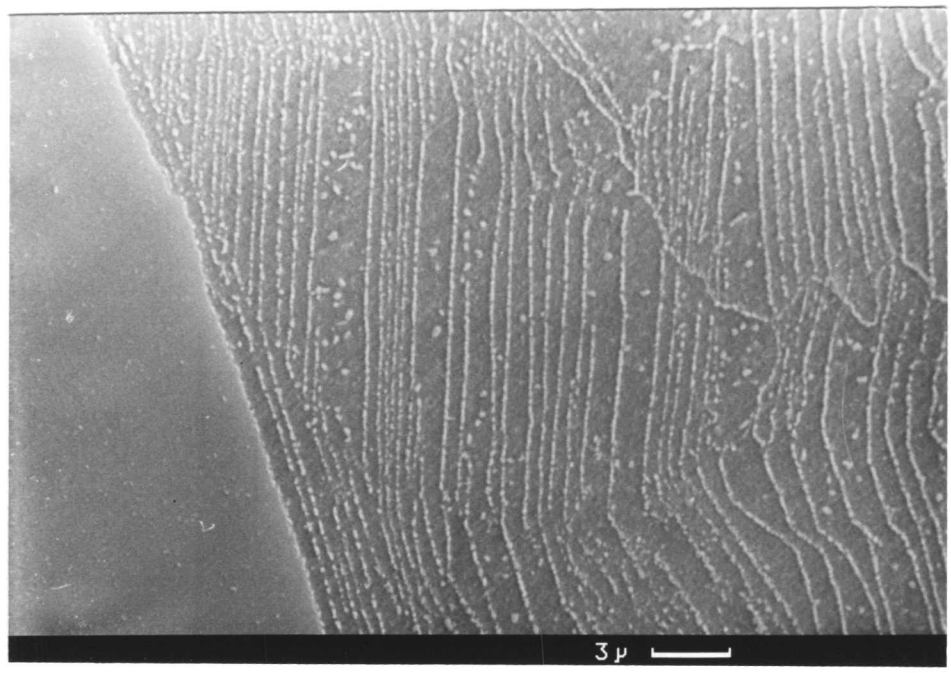

Figure 6.8a and b - Scanning micrographs showing interphase precipitation.

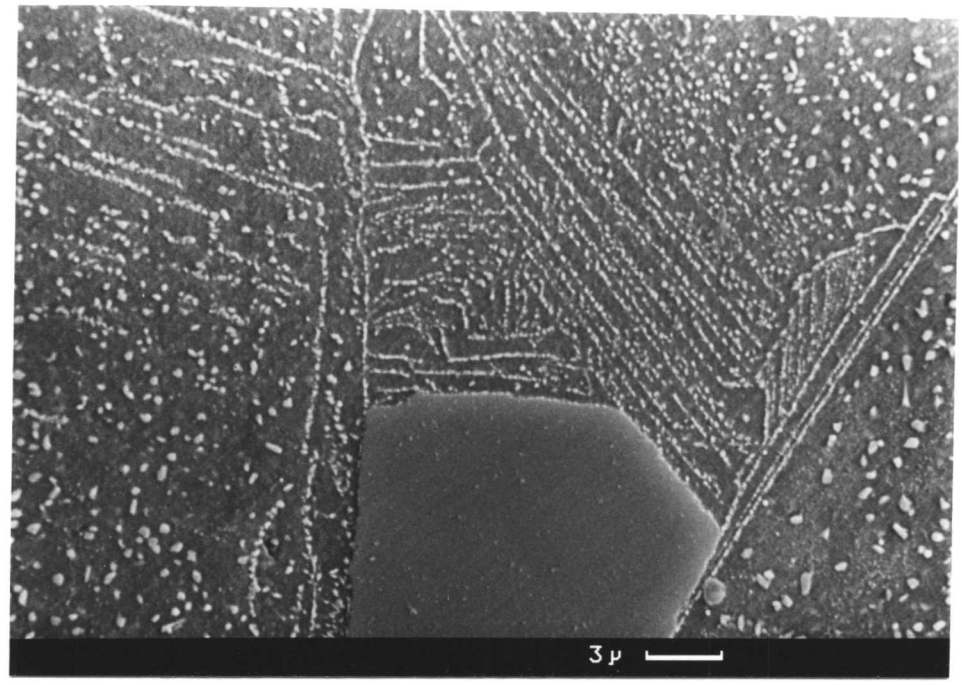

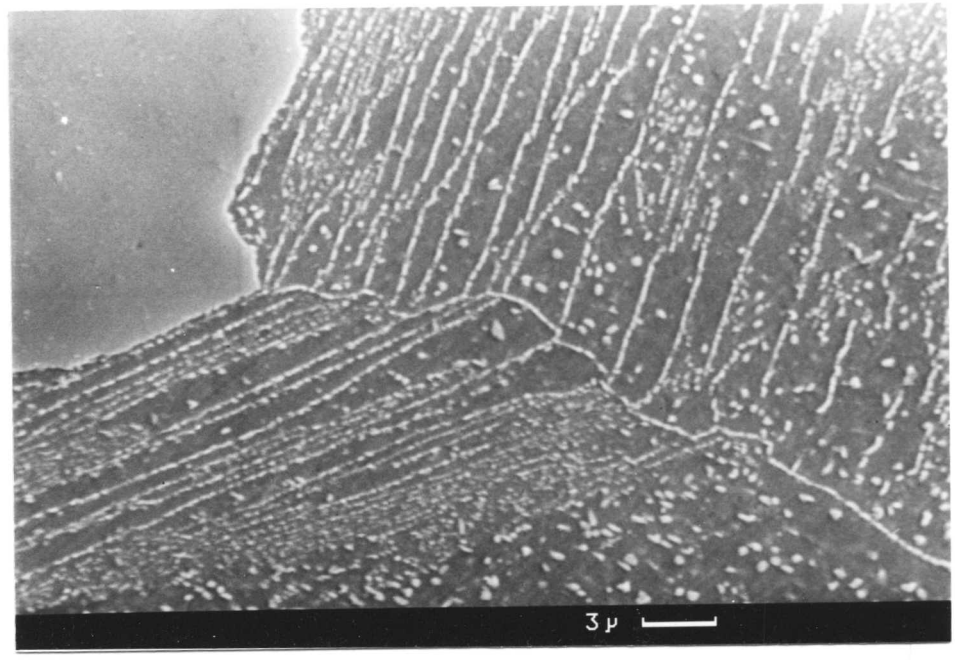

Figure 6.8c and d - Scanning micrographs showing interphase precipitation.

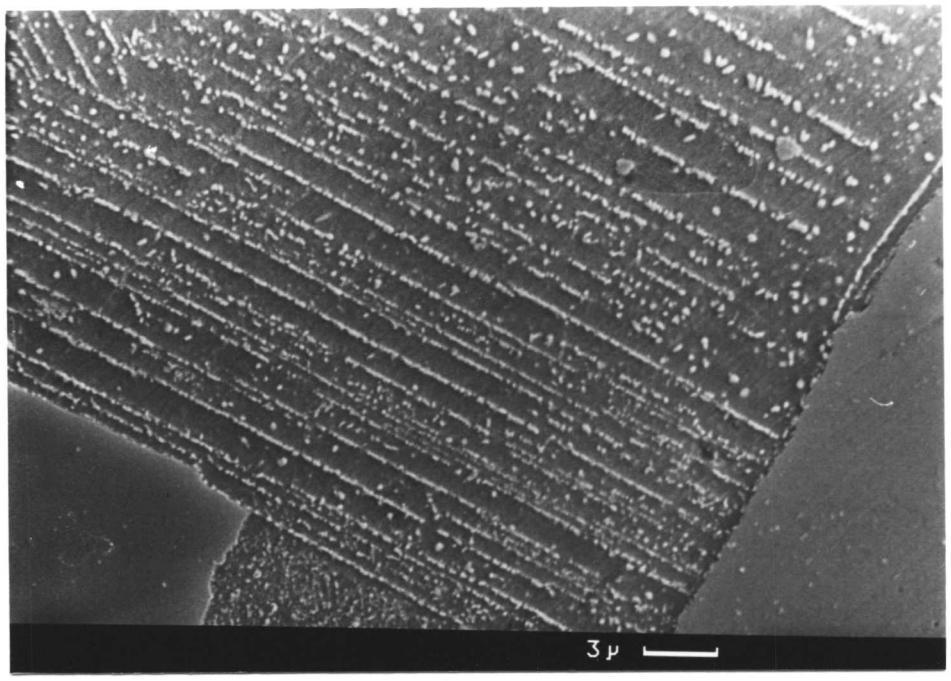

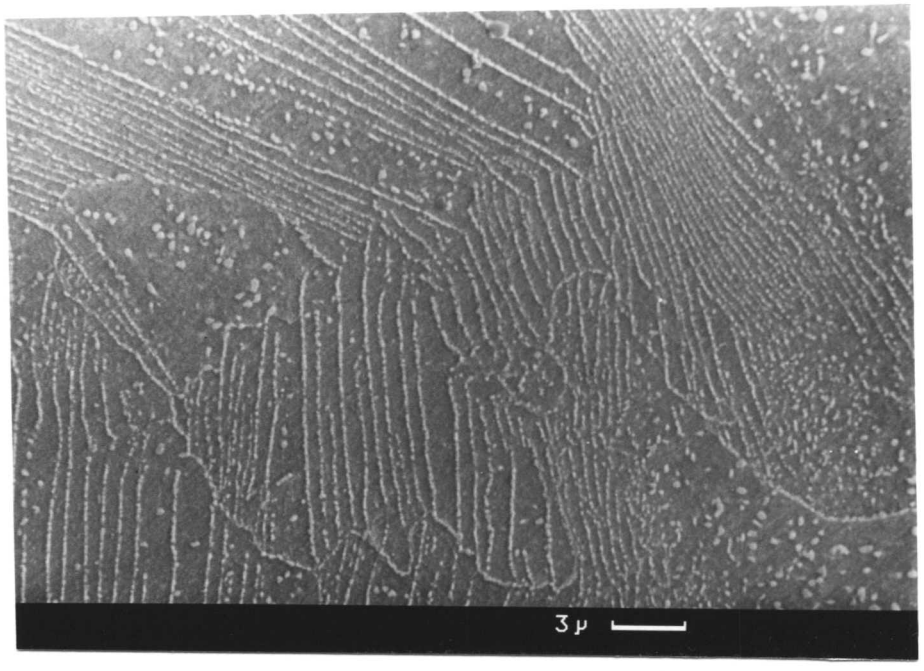

Figure 6.8e and f - Scanning micrographs showing interphase precipitation.

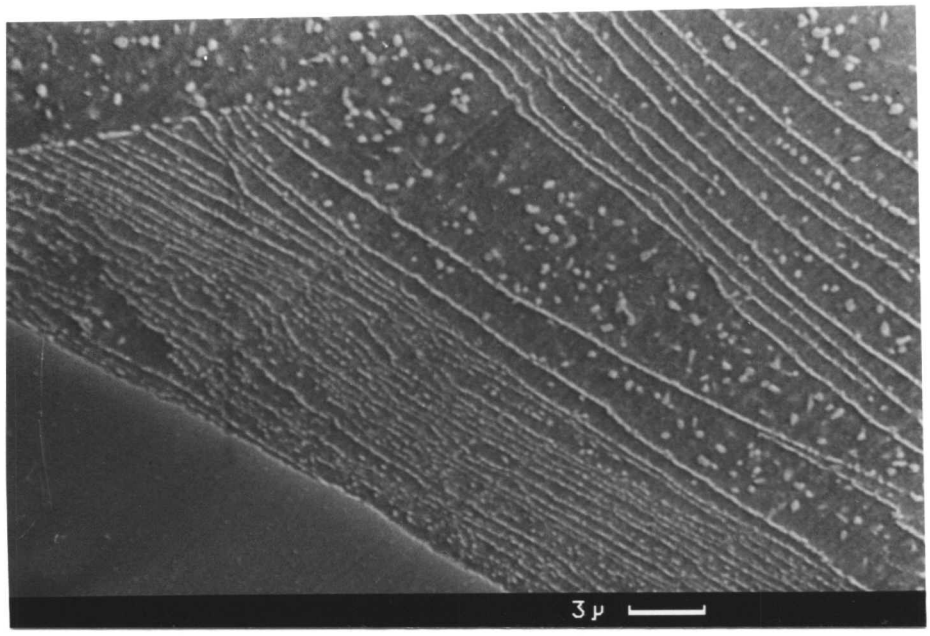

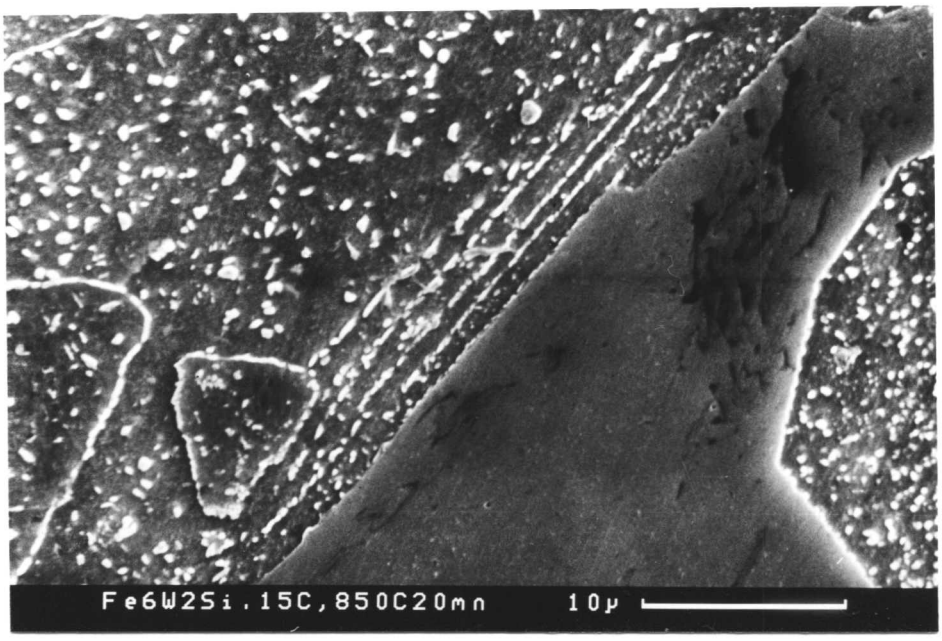

Figure 6.8g and h - Scanning micrographs showing interphase precipitation.

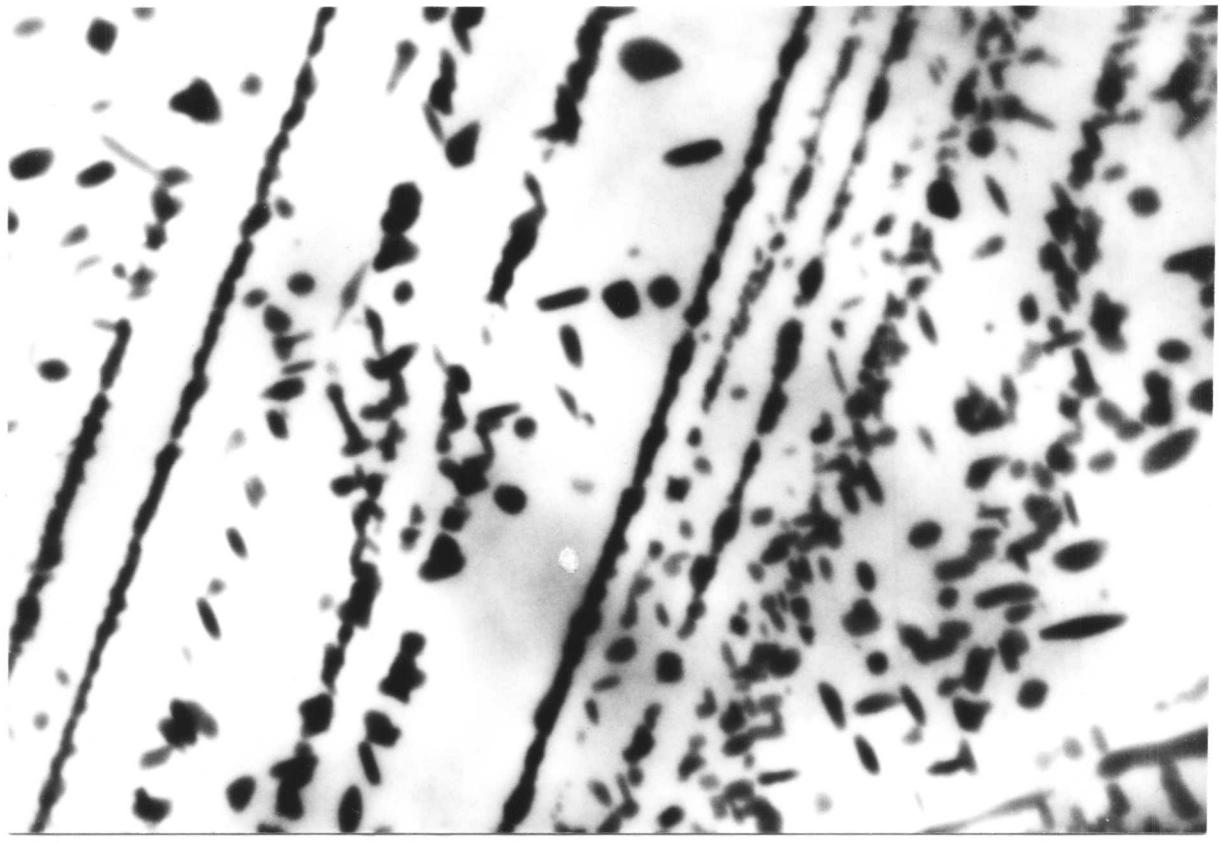

Figure 6.9 Variable band spacing is apparent in this micrograph. (TEM).

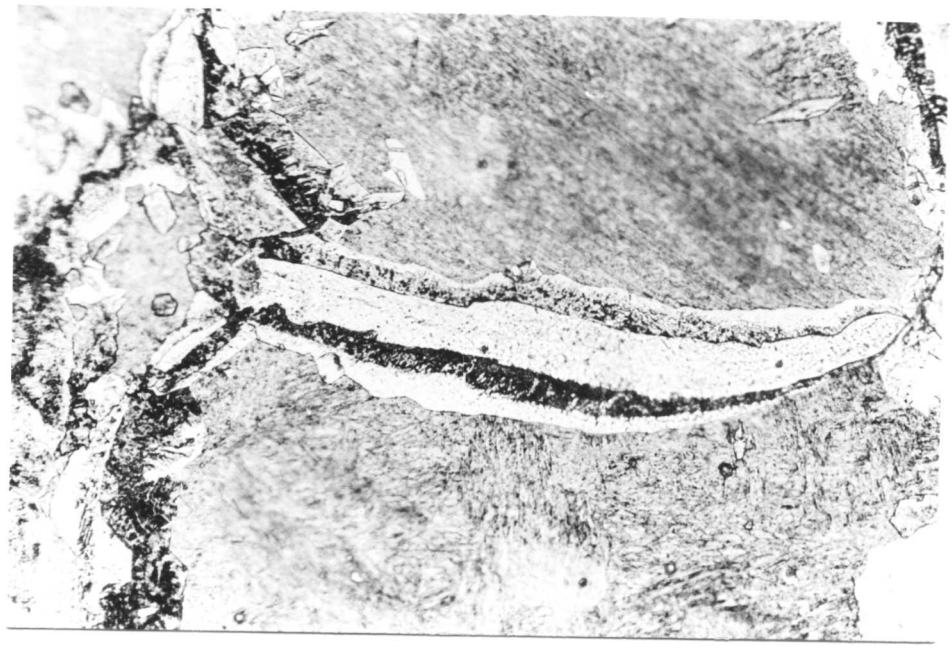

Figure 6.10 - Isothermal transformation at 700°C for 20 minutes followed by upquenching at 800°C for 3.5 minutes.

CHAPTER VII

THE INFLUENCE OF CARBIDE PRECIPITATION ON THE NUCLEATION OF ALLOTRIOMORPHIC FERRITE IN Fe5.8W-0.5C (wt%) ALLOY.

7.1 Introduction: Strong carbide forming substitutional alloying elements such as niobium sometimes significantly increase the hardenability of steels even when used at concentrations well below 0.1 wt%[1-4]. The increase in hardenability is unexpected, since the formation of niobium carbide (NbC) at austenite grain boundaries restricts grain growth during austenitization. The resulting fine grained structure should provide a larger number density of grain-boundary sites for the heterogeneous nucleation of ferrite, an effect which should accelerate the $\gamma \rightarrow \alpha$ transformation and hence reduce hardenability. In spite of this, Nb is known to retard the nucleation of α ferrite, although the mechanism by which it does so is not clear. Niobium carbide forms very thin plate-like particles which grow along the austenite grain boundaries; these particles are in general difficult to detect, especially if their presence has to be related to some coarse feature of the microstructure (such as ferrite grains during the early stages of their growth).

In this work, we used an Fe-W-C alloy to examine the influence of carbide precipitation on the heterogeneous nucleation of ferrite at austenite grain boundaries. In this alloy, tungsten carbide (WC/M_6C) can preferentially precipitate at the austenite grain boundaries (in the form of coarse, globular particles as well as lamellar rod like particles) which can easily be resolved using optical microscopy. The kinetics of the $\gamma \rightarrow \alpha$ change have been studied over a range of isothermal transformation temperatures under two circumstances: firstly, in the presence of copious WC/M_6C precipitation at the austenite grain-boundaries, and when such carbide precipitation has occurred to an extent which covers only a small proportion of the austenite grain boundaries. At low undercooling (i.e. at temperature close to Ae_3) the kinetics of transformation have been expressed both in terms of the rate of nucleation as well as with respect to volume fraction transformed. But at higher under coolings, the kinetics have been only expressed in terms of volume fraction as it became extremely difficult to recognise individual ferrite due to rapid impingement even during the early stages of transformation.

7.2 Experimental Procedure: The Fe-W-C alloy used was prepared as a 65g Argon-Arc melt using high-purity constituents and was homogenised at 1300°C (± 5) for 2 days in a quartz tube under a partial pressure of argon; the composition of the alloy (analysis carried out after homogenisation) was found to be Fe-5.8W-0.5C(wt%);the high alloy content was chosen to ensure sufficient hardenability for the heat-treatments discussed below, even when some of the W and C was tied up as carbide. The alloy was swaged down to 3mm diameter rod and cut into 10mm lengths for further heat-treatment. Specimens were all electrolytically plated with Ni, to a thickness of about 75 μm, prior to heat-treatment, in order to prevent surface degradation and surface nucleation. The heat treatments used were as follows:

A. After sealing in a quartz tube under a partial pressure of argon, the alloy was heated in the (γ + WC/M_6C) phase field at 1200°C (± 5) for 30 minutes; this avoided the development of any coarse-grained structure which might exhibit strong orientation texture not typical of normal practice. It was then transferred into a furnace at 900°C (± 5) (i.e. γ + WC) where it was held for 5 hours to induce the formation of WC at the austenite grain boundaries. The quartz tube was then transferred to a fluidized bed maintained at a pre-specified isothermal temperature (i.e. 800°C, 750°C and 700°C) to promote the formation of ferrite and at the end of a specified interval of time, the quartz tube was rapidly broken and the specimen quenched into water to prevent further reaction. To fully explore the transformation characteristics, three distinct isothermal transformation temperatures were selected. The first one was 800°C which is just below Ae_3 of the alloy. This isothermal transformation temperature was selected to induce a slow rate of nucleation and growth of ferrite to ensure a small equilibrium volume fraction of ferrite and to avoid nucleation site saturation and problems with impingement between adjacent growing particles. The second isothermal temperature was 750°C near the nose of the TTT diagram and the third one was at 700°C a temperature well below Ae_3. These two temperatures were selected to see the effect of increasing driving force (i.e. change in free energy per unit volume, ΔG_v) on the transformation characteristics.

B. As above, but with the alloy held at 900°C ± 5 for only 5 minutes before the isothermal treatment. This heat-treatment was designed to permit the formation of only a small amount of carbide-phase so that much of the ferrite could then nucleate from the γ/γ grain boundaries. The alloy could, after austenitisation, have directly been transferred to the fluidized bed at

isothermal temperature but there would then have been uncertainties about the time taken for the specimen to reach the isothermal temperature.

All the stereological measurements were performed on light optical images using a Quantimet 720 image analysing system. Nucleation was characterised by counting the number of ferrite grains per unit area of plane section; we note that this cannot be converted into nuclei per unit volume without making specific assumptions about the ferrite particle shapes.

7.3 Results and Discussion: Fig. 7.1 (a) and (b) illustrate the microstructures obtained when the specimens were subjected to isothermal treatment at 800°C under the two different conditions of pre-precipitation in the (γ + WC) phase field. These micrographs clearly indicate the marked difference in the transformation kinetics under these two conditions of heat-treatment. SEM pictures Fig. 7.2 (a) and (b) taken using a CamScan 4 give an idea about the percentage of grain-boundary area occupied by the carbide (WC/M_6C). While about 65-70% of grain-boundaries are covered with carbide in the heavily pre-precipitated alloy, only about 10% of these are covered when the time of pre-precipitation was reduced to 5 minutes from 5 hours. TEM (Fig. 7.3) clearly shows the shape of the carbides formed on the grain-boundaries. These carbides precipitate at the grain-boundaries in the form of coarse globular particles as well as rod-like carbides.

The nucleation counts presented in Fig. 7.4 demonstrate the drastic drop in the nucleation rate of ferrite in the presence of WC at the grain-boundaries when the isothermal temperature was close to Ae_3 i.e. 800°C ($\pm$ 2). Similarly it also shows the difference in the volume fraction of ferrite obtained at this isothermal temperature. These results are contrary to the fact that WC formation leads to a depletion of solute in the matrix resulting in increased driving force for the $\gamma \rightarrow \alpha$ transformation. It seems that the nucleation of ferrite at carbide-austenite interfaces is less favourable compared to nucleation at austenite grain boundaries.

Fig. 7.5 (a) and (b) show the volume fraction (V_α) transformed at the isothermal temperature of 750°C and 700°C respectively. The plots show that the volume fraction (V_α) transformed in case of heavily pre-precipitated alloys is much higher at these isothermal temperatures. It can be anticipated that with increasing undercooling, the driving force per unit volume (ΔG_v) increases and eventually it exceeds a value required for nucleation on the austenite/carbide interface. Some workers[4,5,6] have shown that coarse grain-boundary carbides can be potent nucleation site for the formation of ferrite. They argued that these coarse carbide increase the lattice mismatch with respect to austenite resulting in high energy

interfaces conducive for nucleation of ferrite. It also locally reduces the C concentration which assists ferrite formation.

In majority of the cases, it was observed that the α is growing only one side of the boundary (Fig. 7.6). This may be due to the fact that the mobility of the carbide/ferrite interface is very restricted and hence the growth of α occurs via movement of the more mobile γ/α interface.

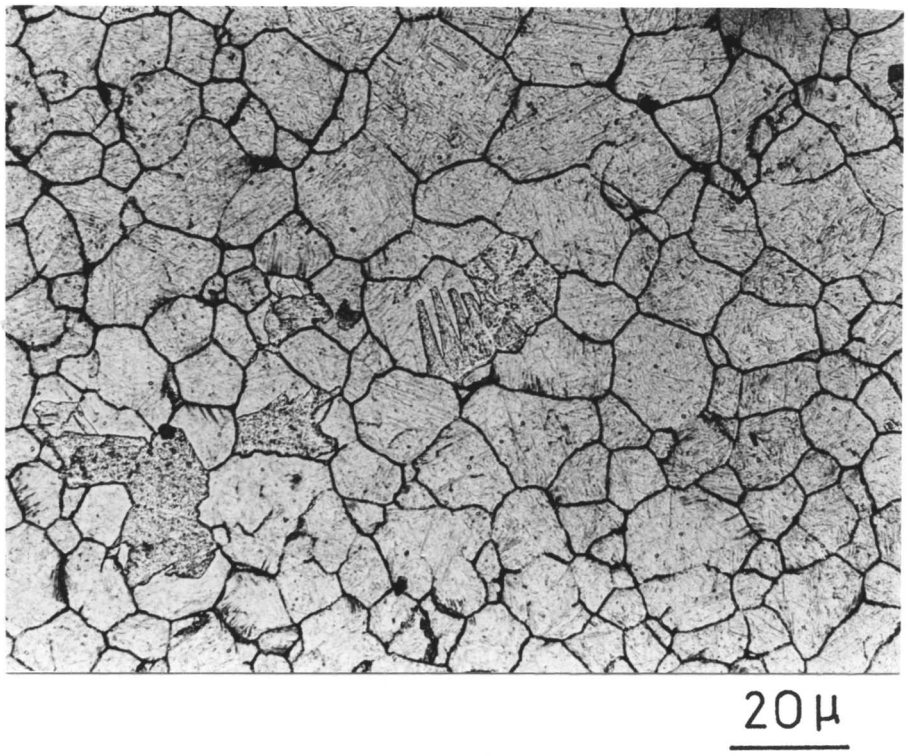

Figure 7.1a: Low volume fraction of α in heavily pre-precipitated (900°C/5 hours) specimen.

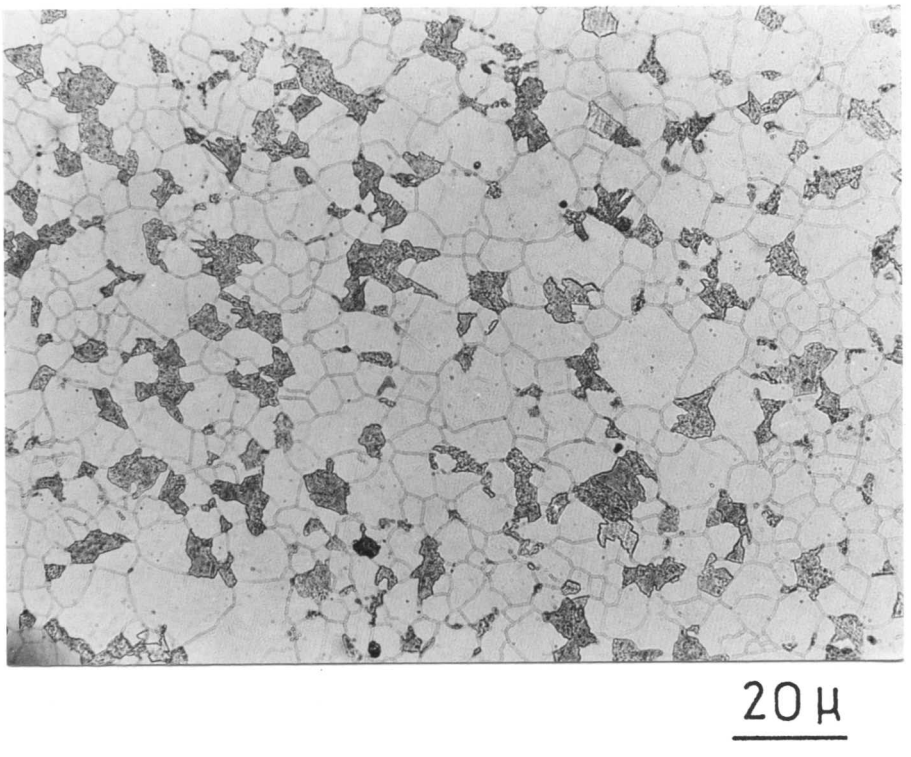

Figure 7.1b: High volume fraction of α in specimen prepreipitated for very small time (900°C/5 min).

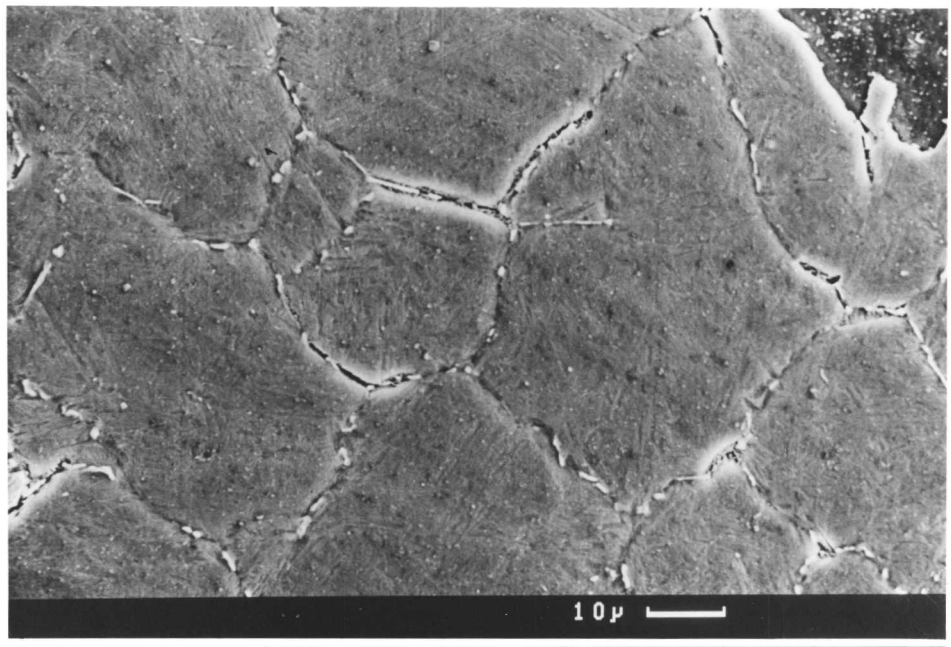

Figure 7.2a: Approximately 65 to 70% austenite grain-boundary area are covered by tungsten carbide (WC/M_6C) in heavily pre-precipitated alloy.

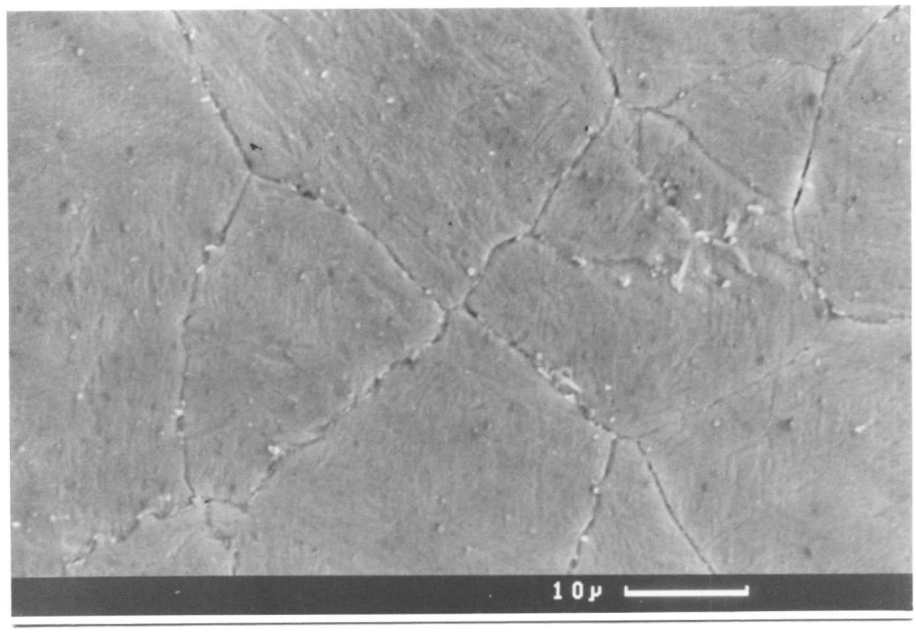

Figure 7.2b: Less than 10% austenite grain-boundary area are occupied by tungsten carbide when specimen was pre-precipitated for small time (i.e. 900°C/5 minutes).

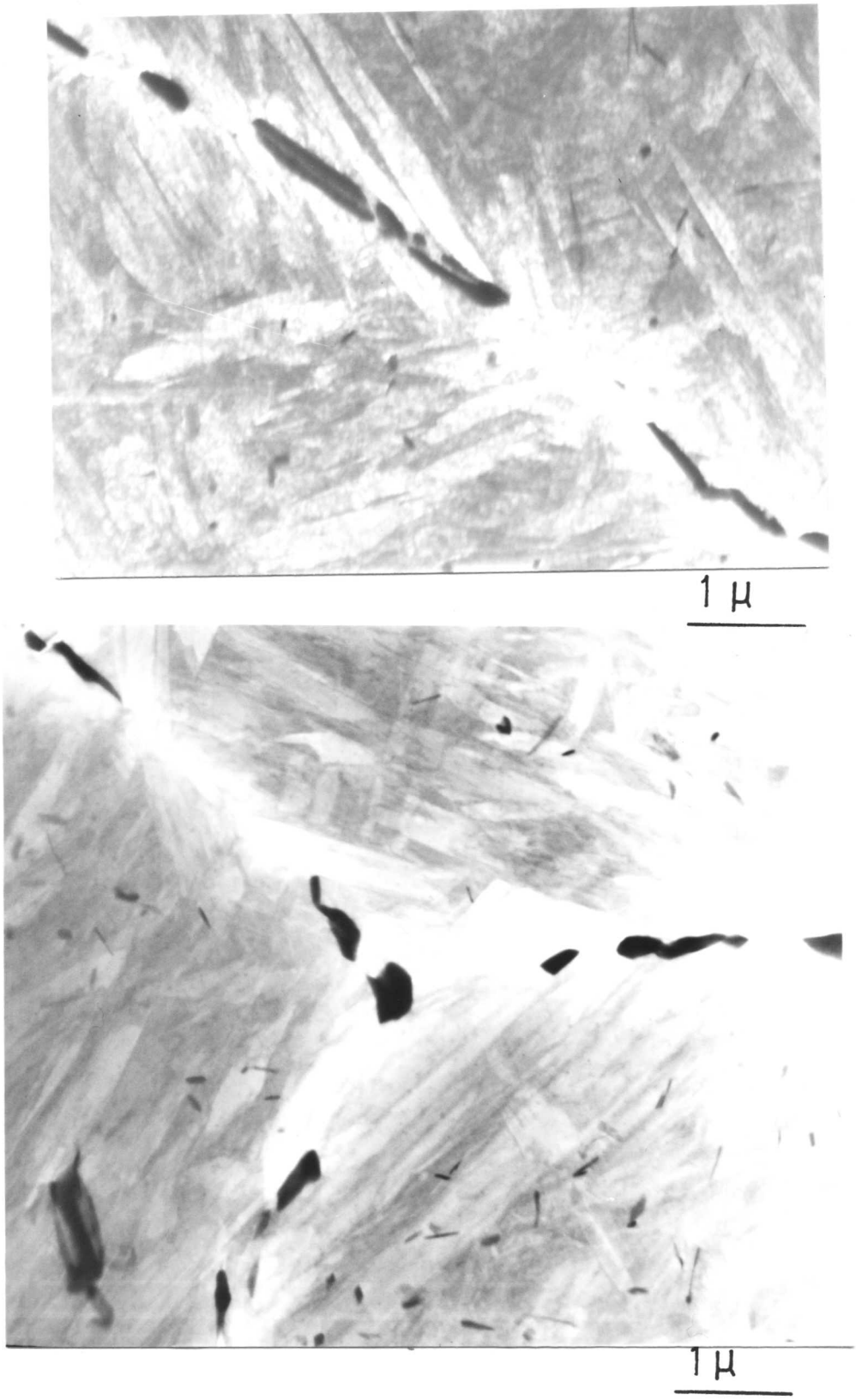

Figure 7.3a and b: Morphology of tungsten carbide varied from coarse globular to the rod like in appearance.

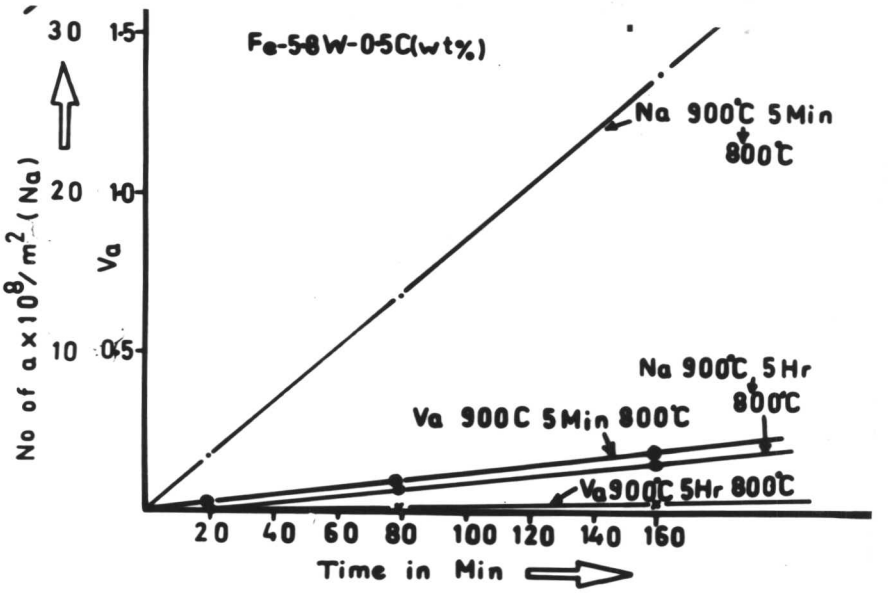

Figure 7.4: Curve showing number of α (N_α) vrs time as well as volume fraction (V_α) vrs time obtained under two different heat-treatments.

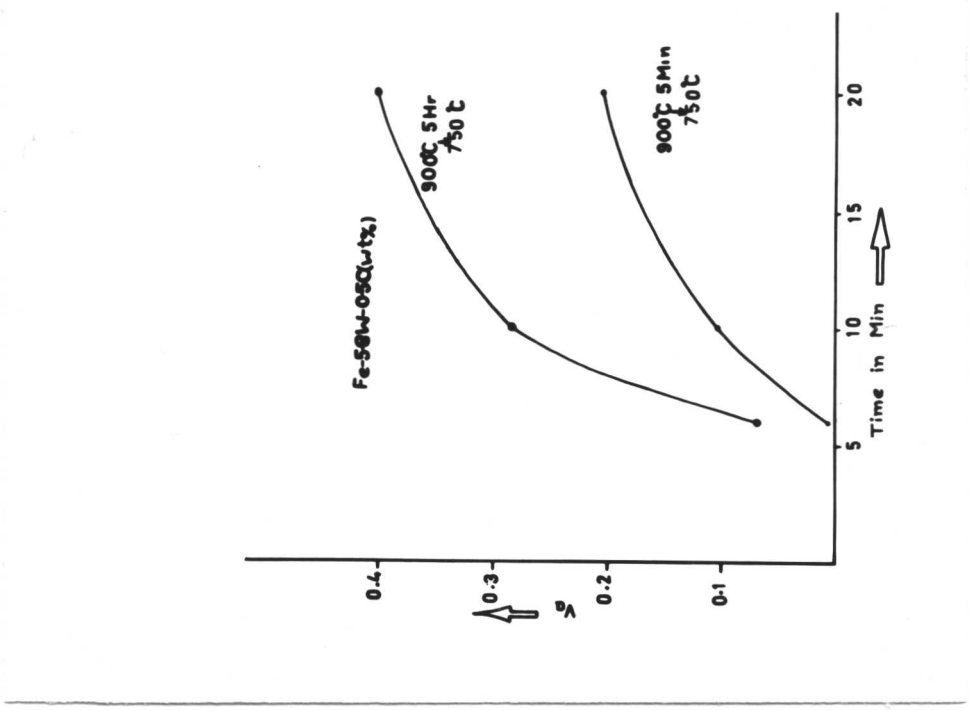

Figure 7.5a: Plot of volume fraction (V_α) vrs time for specimens isothermally transformed at 750°C under two different conditions of pre-precipitation.

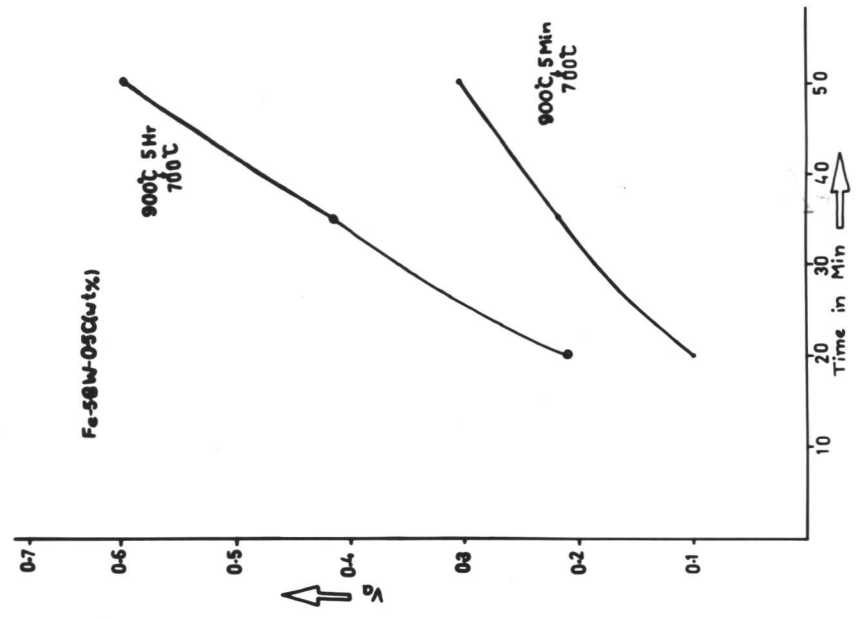

Figure 7.5b: Plot of V_α vrs time for specimens isothermally transformed at 700°C under two different conditions of pre-precipitation.

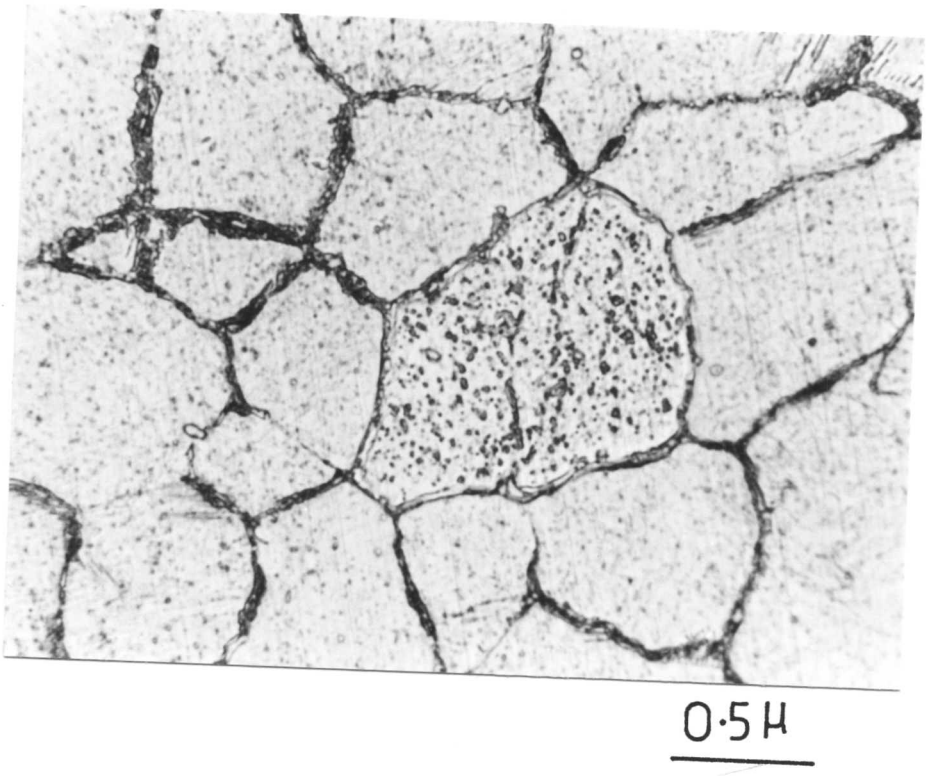

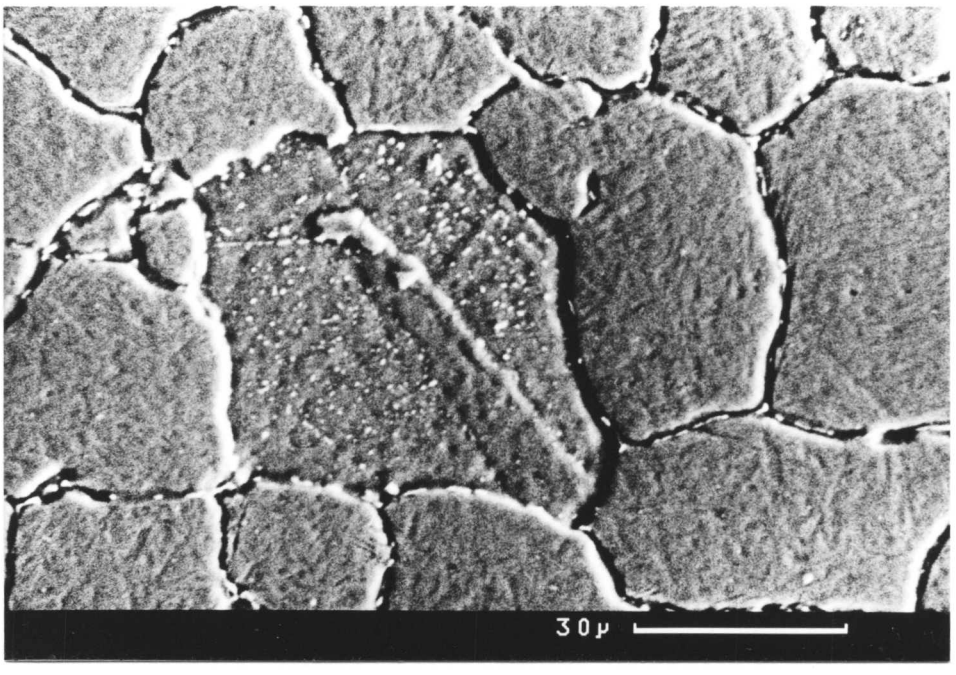

Figure 7.6a and b: Ferrite growing within one grain only.

CHAPTER VIII

THE STUDY OF GROWTH KINETICS IN Fe-2.99Cr-0.11C (wt%).

8.1 INTRODUCTION: The study of the growth kinetics of allotriomorphic ferrite in Fe-C-X ternary system has provoked considerable interest in the past two decades. Various models have been developed to predict the diffusion limited growth rate of allotriomorphic ferrite over a wide range of temperature and composition (Fig. 8.1). Diffusion limited growth refers to a situation in which the rate of growth of ferrite depends on the rate at which both carbon and substitutional alloying element (X) diffuse away from the γ/α interface and does not depend upon the nature of the processes at the interface by which atoms are incorporated in the allotriomorphic ferrite[1]. The transport or flux these atoms across the γ/α interface must be fast enough to maintain an equilibrium density of carbon and substitutional atoms in solution at the interface. The term "diffusion limited growth" has been modified and commonly used under the generic term "volume diffusion control (VDC) growth". Volume diffusion control growth means that a precipitate crystal grows in volume diffusion controlled manner as long as the growth kinetics resulting from volume diffusion in the matrix phase away from or towards the growing crystal are slower than those derived from transport across the interface boundary[2]. However, this modified definition of volume diffusion controlled growth can no longer be regarded as a unique and complete description of precipitate growth kinetics and that considerable additional information may be required in order to furnish such a description.

In recent years the growth scenario in binary and ternary systems has been examined via two different models :

(i) No partition local equilibrium (NPLE).

(ii) Para-equilibrium (PE).

8.2 Local equilibrium at the γ/α interface: The existence of local equilibrium during the growth of ferrite (α) implies that the compositions of the α and γ phases at the interface are connected by a tie line of the ($\alpha+\gamma$) phase-field in the equilibrium Fe-C-X phase diagram. This tie-line which defines the interface composition does not in general pass through the point in the ($\alpha + \gamma$) phase field which identifies the alloy composition. This is because the diffusivities of interstitial (C) and substitutional alloying elements (X) in the γ are significatly different. The appropriate tie line must be chosen to satisfy mass conservation

conditions at the moving interface and must be consistent with the partitioning behaviour of the alloying elements. Hence, the tie line corresponding to low supersaturation may lead to partitioning and long range diffusion of substitutional alloying elements. During this period, the driving force for carbon diffusion is reduced to a level which allows the substitutional element (X) flux to keep pace with the carbon flux at the interface. This situation is referred to as partitioning with local-equilibrium (PLE). The tie line for an alloy transforming at high super-saturation is such that there is virtually no partitioning of substitutional alloying elements between the γ and α and the transformation rate is controlled by volume diffusion of carbon in γ ahead of the moving interface. This situation is referred to as no partitioning with local equilibrium (NPLE).

The problem of diffusional growth of isolated α-precipitate particles in an infinite γ-matrix has been investigated in detail by Coates[3]. He assumed that local equilibrium is maintained at the $\gamma \rightarrow \alpha$ interface and then developed expressions to evaluate the interface velocity and interface composition contours. Refering to Fig. 8.2a and b $C_i^{\alpha\gamma}$ and $C_i^{\gamma\alpha}$ (i = 1, 2) are, respectively, molar concentrations in the α-precipitate and the γ-matrix at the α-γ interface. The points ($C_1^{\alpha\gamma}$, $C_2^{\alpha\gamma}$) and ($C_1^{\gamma\alpha}$, $C_2^{\gamma\alpha}$) define a unique tie line which corresponds to the α-γ interface. The tie line does not pass through the bulk composition $\bar{C}_1$, $\bar{C}_2$ because the diffusion coefficient for C (i.e. 1) and X(i.e. 2) in Fe-C-X is quite different. Coates[4] solved the problem of locating the interface tie line corresponding to a given bulk composition. and subsequently derived an expression for interface velocity as follows: Let us consider that a specimen of bulk composition ($\bar{C}_1$, $\bar{C}_2$) has been quenched from the austenite (γ) phase field into the austenite plus ferrite ($\gamma + \alpha$) phase field at a temperature T_1. Schematic T_1 ternary isotherms are shown in Fig. 8.2a where X is an α-stablizer and a γ-stablizer respectively. The equation for mass conservation at the α-γ interface under local equilibrium conditions is represented by:

$$(C_i^{\alpha\gamma} - C_i^{\gamma\alpha}) \frac{ds^*}{ds} = - J_i \Big|_{s = s^*} \quad (i = 1, 2) \qquad \ldots\ldots (8.1)$$

where J_1 = The molar fluxes of the solutes in a volume-fixed reference frame.

$$= - D_{11} \nabla C_1 - D_{12} \nabla C_2 \qquad \ldots\ldots (8.2)$$

and

$$J_2 = - D_{22} \nabla C_2 \qquad \ldots\ldots (8.3)$$

where D_{ij} (i = 1, 2; j = 1, 2) are empirical chemical diffusion coefficients and the concentrations C_i (i = 1, 2) are in moles per unit volume.

s refers to appropriate distance co-ordinate and s* is the position of the α-γ interface.

$$S^* = n_1 \sqrt{D_{11} t_1} = n_2 \sqrt{D_{22} t} \quad .. \quad .. \quad .. \quad .. \quad .. \quad .. \quad .. \quad .. \quad .. \quad (8.4)$$

where n_1 and n_2 are the growth rate constants. These growth rate constants are related by the following equations[3].

For carbon (C):-

$$f_1^k = f^k(n_1) - m\frac{D_{12}}{D_{11}}\left[f^k(n_2) - f^k(n_1)\right] \quad .. \quad .. \quad .. \quad .. \quad .. \quad .. \quad .. \quad (8.5)$$

and for X

$$f_2^k = f^k(n_2) \quad .. \quad .. \quad .. \quad .. \quad .. \quad .. \quad .. \quad .. \quad .. \quad .. \quad .. \quad .. \quad (8.6)$$

where k $\equiv$ p, c, and s for planar, cylindrical and spherical growth respectively.

f_i^k is referred to as the fractional compositions or relative supersaturations and represented by

$$f_i^k = \frac{C_i^{\gamma\alpha} - \bar{C}_i}{C_i^{\gamma\alpha} - C_i^{\alpha\gamma}} \quad (i = 1, 2) \quad .. \quad .. \quad .. \quad .. \quad .. \quad .. \quad .. \quad .. \quad .. \quad (8.7)$$

schematically it is shown in Fig. 8.3.

The functions $f^k(n_i)$ (i = 1, 2) are shown graphically in Figure 8.4.

Finally m represents the slope of the α-γ interface and given by

$$m = \frac{(C_2^{\gamma\alpha} - C_2^{\alpha\gamma})}{(C_1^{\gamma\alpha} - C_1^{\alpha\gamma})} \quad .. \quad .. \quad .. \quad .. \quad .. \quad .. \quad .. \quad .. \quad .. \quad .. \quad .. \quad .. \quad (8.8)$$

Equations (8.5) and (8.6) , can be solved to determine the growth velocity and the tie line governing interface compositions during growth since they contain only two unknown (for instance n_1 and $C_1^{\gamma\alpha}$) and the rest being determined by equation (8.4) and ternary isotherm phase-boundaries and tie lines.

The above theory for diffusion controlled growth is based on the assumption that the diffusion coefficients D_{ij} are independent of concentration. However theoretical studies[5, 6] show that the growth kinetics are influenced by the ternary diffusion interaction. It has been suggested that the weighted average diffusion coefficient is most appropriate value to use in growth rate equation i.e.

$$\bar{D}_{11} = (C - C^{\gamma\alpha})^{-1} \int_{C_1^{\gamma\alpha}}^{C_1} D_{11}(C_1)\, dC_1 \quad \ldots\ldots\ldots\ldots\ldots\ldots\ldots (8.9)$$

where C_1 represents mole fraction of carbon. The ratio D_{12}/D_{11} is also concentration dependent but Bolze et al[7], suggested that the use of a constant D_{12}/D_{11}, evaluated at the composition $\bar{C} = C_1^{\gamma\alpha}$ gives an adequate approximation to the problem.

The theory of diffusion controlled growth of α under local equilibrium conditions needs further justification to explain how can a ternary system accommodate two independent mass balances when one component (carbon) diffuses many orders of magnitude (10^4 to 10^6) faster than the other (X) Hillert[8] first realised the gravity of this situation and tried to resolve it in a rather simple way. He showed that either the fast diffuser (C) is forced to keep pace with the slow diffuser (X) by former's driving force for transformation being reduced to esentially zero or the slow diffuser is allowed to keep pace with the fast diffuser by the former's driving force for transport being raised to essentially infinity. The same concept was proposed independently by Kirkaldy[9] and co-workers[10]. To elaborate the same problem, let us consider Fig. 8.5a for low supersaturation (e.g. point A). The transformation rate is controlled by slow diffuser X. The bulk composition corresponding to this situation lies on the extrapolation of the γ-phase-isoactivity line through ($C_1^{\gamma\alpha}$, $C_2^{\gamma\alpha}$). It implies that $a_1^{\gamma\alpha} = \bar{a}_1$, where a_1 is activity of carbon. This leads to condition where driving force for fast diffuser (C) is eliminated. The amount of partitioning of X is given by $C_2^{\gamma\alpha} - \bar{C}_2$.

Let us choose a bulk composition corresponding to high supersaturation (e.g. point B) as shown in Fig. 8.5b. In this region, the transformation rate is controlled by fast diffuser C and there is effectively no partitioning of X between the precipitate and the matrix (driving force for X is infinity.) It implies that $C_2^{\alpha\gamma} \simeq \bar{C}_2$ and bulk compositions which satisfy this condition must lie on the horizontal line passing through the point ($C_1^{\alpha\gamma}$, $C_2^{\alpha\gamma}$).

In summary, the bulk composition lying on two dotted lines in Fig. 8.5a and 8.5b utilizes the same tie line. The intersection of these lines refere to a situation where transition occurs. The locus of such intersections for various tie lines generates a transition line as shown in Fig. 8.6a and b. Clearly the transition line define the two-phase field into two regions: one representing PLE (partitioning under local equilibrium) and the other NPLE (negligible partition under local equilibrium).

The growth velocity in P-LE regime is expressed from equation (8.4)

$$\frac{ds^*}{dt} = \frac{1}{2} n_2 \sqrt{D_{22}}\, t^{-\frac{1}{2}} \quad .. \quad .. \quad .. \quad .. \quad .. \quad .. \quad .. \quad .. \quad .. \quad .. \quad (8.10)$$

and in the NP-LE regime, it is given by

$$\frac{ds^*}{dt} = \frac{1}{2} n_1 \sqrt{D_{11}}\, t^{-\frac{1}{2}} \quad .. \quad .. \quad .. \quad .. \quad .. \quad .. \quad .. \quad .. \quad .. \quad .. \quad (8.11)$$

Interface composition (IC) contours: Interface contours provide a very compact means of illustrating the influences of the diffusivity ratio D_{11}/D_{22} and the precipitate morphology. (i.e. planar, cylindrical or spherical growth). Fig 8.7 shows a IC contour. The method for constructing such IC contours are discussed in details by Coates. Each bulk composition lying on this contours utilizes the same interface tie line. Every point on the IC contour represent a bulk composition which transfers with the same interface composition. As one moves along IC contour from $(C_1^{\gamma\alpha}, C_2^{\gamma\alpha})$ to $(C_1^{\alpha\gamma}, C_2^{\alpha\gamma})$ the fractional compositions f_1 and f_2 go from zero to unity.

The fractional composition ie. relative supersaturation is represented by

$$f_i^k = \frac{(\bar{C}_i - C_i^{\gamma\alpha})}{(C_i^{\alpha\gamma} - C_i^{\gamma\alpha})} = \frac{(\bar{C}_i - C_i^{\gamma\alpha})}{(C_i^{\alpha\gamma} - \bar{C}_i) + (\bar{C}_i - C_i^{\gamma\alpha})} \quad .. \quad .. \quad .. \quad .. \quad .. \quad .. \quad (8.12)$$

Fig. 8.8 shows the IC contours for various D_{11}/D_{22} ratio. As the D_{11}/D_{22} ratio increases the IC contours bulges more and more away from the tie line and finally breaks up into two straight lines $f_1 = 0$ and $f_2 = 1$ when D_{11}/D_{22} approaches infinity. In the region of $f_1 = 0$, the driving force $(\bar{C}_1 - C_1^{\gamma\alpha})$

for diffusion of the fast diffuser (C), component, is negligible (referring to equation (8.12) and hence it keeps pace with the slow diffuser, component 2 (i.e. X). Accordingly in this region transformation is controlled by slow diffuser (X). The amount of partitioning of component (i.e. X) is given by $C_2^{\gamma\alpha} - \bar{C}_2$. In the region where $f_2 \simeq 1$, $C_2^{\alpha\gamma} - \bar{C}_2 \simeq 0$ from equation (8.12) and hence the slow diffuser, component 2 (X), is keeping pace with the fast diffuser, component, by virtually eliminating the partitioning of the slow diffuser. Accordingly in this region, the transformation rate is determined by the fast diffuser, component (i.e. C).

The intersections of two straight lines $f_1 = 1$ and $f_2 = 0$ defines a transition from growth rate control by component 2 (X) to control by component (C). The locus of such intersections for various tie lines in the given two-phase field generates a transition line which is referred to as "envelop of zero-partition". The two regions of two-phase field thus defined are designated as the PLE (i.e. partioning under local equilibrium conditions) and NPLE (negligible partitioning under local equilibrium condition) regimes as shown in Fig. 8.6.

Interface velocity (IV) contours: Interface velocity contours provide a very powerful means of understanding the growth kinetics in Fe-C-X system. The effect of substitutional alloying element (X) as well as the relative supersaturation f_i^k on kinetics can be explained on the basis of this diagram.

An interface velocity contour is a line in the two-phase field of a ternary isotherm every point of which defines a bulk composition which transforms at the same rate for an assumed precipitate morphology. Fig. 8.9 show contours corresponding to various tie line in the given two-phase field. The interface velocity increases from zero to infinity as one move along IC from $f_i^k = 0$ to $f_i^k = 1$. The points corresponding to identical velocity on the various IC contours are joined to generate IV contours. The construction of IV contours is shown schematically in Fig. 8.9. The construction clearly shows that in PLE region the IV contours radiate from the Fe-C $(\gamma+\alpha)/\gamma$ phase boundary while in the NPLE region, they emerge from the Fe-X $\alpha/(\gamma+\alpha)$ phase boundary. This disposition of the IV contours results from a direct consequence of the system accommodating the two mass conservation conditions either forcing C to keep pace with X(PLE) or allowing X to keep pace with C (NPLE).

In Figs. 8.10a and b are shown schematic IV contours on Fe-C-X ternary isotherms in which X is a γ- and α- stablizer respectively. If X is a γ-stablizer, the vertical arrow in Fig. 8.10a indicates that progressive additions of X, holding the C constant, should continuously reduce the ferrite growth. It can be anticipated that well known enhancement of

hardenability induced by γ-stablizer (e.g. Mn, Ni, etc) is in part due to a reduction in proeutectoid growth rate. In the case X is α stabilizer (e.g. Si, Al), then its progressive additions at constant C level will result in increased growth rate of ferrite as shown in Fig. 8.10b.

8.3 Para-Equilibrium: Hultgren[11] introduced the term "Para-Equilibrium" to describe the kinematically constrained local equilibrium where the two adjoining phases are in local equilibrium with respect to the carbon only, the iron and the alloying element (X) being too sluggish to redistribute. In other words the ratio of the alloying element (X) and the solvent (Fe) remain constant across the α/γ interface and hence the tie lines in para-equilibrium region exists as "component rays" of the mobile species. The growth rate of the ferrite is exclusively controlled by volume diffusion of carbon ahead of the α/γ interface in the austenite matrix. Hillert[12] and Rudberg[13] introduced the same concept of unique kinetic state which deviates strongly from the true local equilibrium and the transformation proceeds under pure carbon diffusion control, local equilibrium being maintained across the interface with respect to carbon only. Aaronson, Domain and Pound[14] discussed the same concept under designation "No partition Equilibrium".

Hillert,[12] Rudberg,[13] Aaronson et al,[19] Gilmore et al[15] and Bhadeshia[16] treat the situation of para-equilibrium condition in a clear and concise way and developed the thermodynamic expression to calculate the para-equilibrium phase boundaries as follows:-

Thermodynamic condition for para-equilibrium:-

$$G_1^{-\alpha} = G_1^{-\gamma} \quad \ldots\ldots (8.13)$$

$$\text{And} \quad G_2^{-\gamma} - G_2^{-\alpha} = -\left(G_0^{-\gamma} - G_0^{-\alpha}\right)\frac{C_0}{C_2} \quad \ldots\ldots (8.14)$$

$$G_i^{\gamma} = G_i^{\circ\gamma} + RT \ln \alpha_i^{\gamma} \quad \ldots\ldots (8.15)$$

where $\frac{C_0}{C_2}$ = Ratio of the solvent mole fraction to the immobile solute mole fraction along the component ray in question.

G_i = Partial molar free energy of respective component in the phase concerned. $G_i^{o\gamma}$ is the free energy of the i in its standard state.

Substitation of eqn. (8.15) into equ. (8.13) and equ. (8.14) yields the follow two expressions between the four composition variables which in turn define one tie line of the para-equilibrium diagram.

$$\frac{{}^{o}\Delta G_1^{\alpha\rightarrow\gamma}}{RT} = \ln \frac{C_1^{\alpha}}{C_1^{\gamma}} + \ln \frac{x_1^{\alpha}}{x_1^{\gamma}} \quad .. \quad .. \quad .. \quad .. \quad .. \quad .. \quad .. \quad .. \quad .. \quad .. \quad (8.16)$$

or

$$\frac{{}^{o}\Delta G_2^{\alpha\rightarrow\gamma}}{RT} - \ln\frac{C_2^{\alpha}}{C_2} - \ln\frac{{}^{\alpha}_{2}}{{}^{\gamma}_{2}} = -\frac{C_0}{C_2}\frac{G_0^{\alpha\rightarrow\gamma}}{RT} - \ln \frac{C_0^{\alpha}}{C_0^{\gamma}} - \ln \frac{x_0^{\alpha}}{x_0^{\alpha}} \quad (8.17)$$

where x represents activity coefficient in the phase concerned.

The third condition necessary to solve for the four unknown concentrations corresponding to the requirement that C_0/C_2 be a constant along the carbon component ray. Hillert showed the PE phase boundaries lies inside equo-phase diagram as shown in Fig. 8.11. The activity coefficients for dilute solutions may be explained[17] as

$$\ln\gamma_1 = e_{11} C_1 + e_{12} C_2 \quad .. \quad .. \quad .. \quad .. \quad .. \quad .. \quad .. \quad .. \quad .. \quad .. \quad (8.18)$$

$$\ln\gamma_2 = e_{12} C_1 + e_{22} C_2 \quad .. \quad .. \quad .. \quad .. \quad .. \quad .. \quad .. \quad .. \quad .. \quad .. \quad (8.19)$$

$$\ln\gamma_0 = -\frac{e_{11}}{2} C_1^2 - e_{12}C_1 C_2 - \frac{e_{22}}{2} C_2^2 \quad .. \quad .. \quad .. \quad .. \quad .. \quad .. \quad .. \quad (8.20)$$

where e_{ij} is known as Wagner interaction parameters.

These are two possible ways in which the volume diffusion controlled growth of allotriomorphic ferrite may occur. e.g. (NPLE) and (PE). Purdy and Kirkaldy[18] designed an elegant experiment to continuously monitor the movement of the γ/α interface by use of a diffusion couple. They found the interface position to vary in proportion to the square root of time indicating diffusion controlled interface motion. Furthermore, their experimentally determined parabolic growth rate constant (i.e. slope of maximum half thickness vrs square root of time) matched accurately with the theoretically calculated value based on local equilibrium model (NPLE) in Fe-Mn-C alloys. Those are important and accurate results and support the for growth mechanism by NPLE. Except these two results, all other reported data on parabolic rate constant differ

significantly from the theoretical value[20, 21, 22, 23]. The reasons for such discrepancies are explained on the basis of facetting, solute-drag like effect, interphase-carbide precipitation, stereological error and interaction of clusters with moving interfaces.

The transition from local-equilibrium to para-equilibrium:-

In the NPLE region of the two-phase field, the distribution of X involves a narrow zone of enrichment (viz γ stabliser) or depletion (α stablizer).

This narrow zone is generally referred to as spike or diffusion zone. This diffusion zone or spike must be pushed ahead of the α-γ interface as the transformation proceeds. Currently, considerable discussion[10, 14, 24, 25] is centered about the question of whether or not this diffusion zone exists for transformations in the system Fe-C-X. It is conceivable that at very high growth rates the diffusion zone becomes so thin as to exist only mathematically and in reality disappears completely.

For situation in which a narrow diffusion zone is involved in the growth of ppt particle, the Zener[26] approximation is a useful means of estimating the diffusion zone thickness. The diffusion zone is approximated by a triangle of height $(\bar{C}_1^{\gamma\alpha} - C_1^{\gamma\alpha})$ and width ΔS is determined by an overall mass balance of the form

$$V_p (C_1^{\alpha\gamma} - \bar{C}_1^{\alpha\gamma}) = \tfrac{1}{2} A_p \Delta S (\bar{C}_1^{\gamma\alpha} - C_1^{\gamma\alpha}) \quad \ldots\ldots (8.21)$$

where A_p = Ppt area

V_p = Ppt volume

ΔS = Average diffusion zone thickness.

$$V = \frac{2D_{22}}{\Delta S} \qquad \text{where } \frac{ds}{dt} = V$$

$$\text{or } \Delta S = \frac{2D_{22}}{V} \quad \ldots\ldots (8.22)$$

The criteria to distinguish between NPLE and PE is based on the value of ΔS. If ΔS is more than 50 A^0, the precipitate (i.e. α) grows under no-partition local equilibrium condition. Local equilibrium is no longer established at the interface if the concentration profile (i.e. ΔS) in the parent phase ahead of an advancing interface becomes less than 10 A^0. Under such circumstances, the growth of α is believed to occur by para-equilibrium mechanism. Hence it is conceivable that at high supersaturation, the thickness of the diffusion zone becomes thin enough to lose its physical

existence and the growth will occur under para-equilibrium mechanism.

8.4 Calculation of Parabolic Growth Rate using para-equilibrium model: The position of the α/γ interface as a function of time, under carbon diffusion-controlled mechanism, can be described by the equation[5, 27].

$$q = \alpha_1 t^{\frac{1}{2}} \quad .. \quad .. \quad .. \quad .. \quad .. \quad .. \quad .. \quad .. \quad .. \quad .. \quad .. \quad (8.23)$$

where q = Half thickness of the allotriomorphic ferrite

t = Time in seconds

α_1 = Parabolic growth rate constant for one dimensional growth.

α_1 is obtained by solving the following equation:-

$$\left\{2\,(C^{\gamma\alpha} - \bar{C})/(C^{\gamma\alpha} - C^{\alpha\gamma})\right\}\left\{(\underline{D}/\pi)^{\frac{1}{2}}\right\} = \alpha_1\left\{\exp \alpha_1^2/(4\underline{D})\right\}\left\{1 - \mathrm{erf}\left[\alpha_1/(2\underline{D}^{\frac{1}{2}})\right]\right\} \quad (8.24)$$

where $C^{\gamma\alpha}$ = Para-equilibrium carbon content in the austenite (γ) which is obtained from the line Ae_3' are given in Appendix II (Ref[28-30]) The Ae_3' line represents $\gamma/(\gamma+\alpha)$ para-equilibrium-phase-boundary.

$C^{\alpha\gamma}$ = Para-equilibrium carbon content in the ferrite (α). Since 'C' content in α is too small it is obtained by the line Ae_1 of the Fe-C diagram.

$\bar{C}$ = Average carbon content of the alloy.

The term $\underline{D}$ is a weighted average diffusivity of carbon in α and it is given by [15, 27].

$$\underline{D} = \int_{C^{\gamma\alpha}}^{\bar{C}} D\,dx/(\bar{C} - C^{\gamma\alpha}) \quad .. \quad .. \quad .. \quad .. \quad .. \quad .. \quad .. \quad .. \quad .. \quad (8.25)$$

where D is the diffusivity of carbon in γ. The value of D depends upon the amount of carbon in austenite as well as the substitutional alloying concentration[31].

Bhadeshia[32] developed a successful computer program to calculate parabolic growth rate constant under para-equilibrium condition. The program

has been extensively used in the present investigation to calculate parabolic growth rate constant under PE mechanism for Fe-C-X alloys.

8.5 Experimental Results on Fe-3.05Cr-0.11C (wt%) alloy: The details of the heat treatment are given in chapter 2 section 3.3.

Isothermal transformation at 750°C showed that the nucleation of α started heterogeneously at prior austenite grain boundaries with subsequent growth occurring rapidly along the grain-boundaries, resulting in a thin layer (Fig 8.12). This morphology of the ferrite is referred to as allotriomorphic ferrite. Optical microscopy revealed that the observable nucleation of α at 750°C started only after 40 seconds. However, dilatometry experiments were done at several isothermal temperatures to determine the exact incubation period and the time taken to achieve 95% of equilibrium volume fraction of the transformation. The results from the dilatometry experiments will be discussed later on in this section. The α/γ interface of the allotriomorphic ferrite appeared ragged in some cases Fig. 8.13. Allotriomorphic ferrite which formed at grain boundary triple junctions appeared more or less triangular in the plane of observation Fig 8.14. Two out of the three interfaces appeared planar (i.e. semi-coherent) in such allotriomorphs. During the early stages of transformation no carbide was detected even using TEM. Prolonged transformation, (i.e. 750°C/3 min) showed the precipitation of carbide. (Fig. 8.15.) In order to determine the parabolic growth rate the maximum half-thickness (t/2) of the allotriomorphic ferrite was measured at successive intervals of time. The parabolic growth rate constant at 750°C was 0.8 $\mu m/\sqrt{sec}$ (see Fig. 8.16).

Isothermal transformation at 700°C again showed heteregeneous nucleation of α at the prior austenite grain-boundaries with subsequent allotriomorphic growth Fig. 8.17. Evidence of interface pinning was also noticed (Fig 8.18) frequently along the interface at this temperature. Occasionally evidence of Widmanstätten ferrite was noticed along highly curved grain boundaries (Fig 8.19.) Fig. 8.16 shows the plot of maximum half thickness (t/2) vrs square root of time. From the slope of this curve the parabolic growth rate constant was determined as 0.3 $\mu m/\sqrt{sec}$. TEM showed that the allotriomorphs formed during the early stages of transformation were free of carbide (Fig. 8.20)

With further decrease in isothermal temperature (i.e. 650°C) a slight decrease in the parabolic growth rate was observed as shown in Fig. 8.16. Parabolic growth rate constant (α) estimated in this case was 0.225 $\mu m/\sqrt{sec}$. Optical micrographs taken at successive intervals of time are shown in Fig. 8.21 to Fig. 8.22. Fig. 8.20 shows faceted allotriomorphs while Fig. 8.21 serrated interface. Along some highly curved grain-boundaries Widmanstätten ferrite was observed Fig. 8.23. The Widmanstätten ferrite plates appeared

to grow along the martensite trace direction. No evidence of carbide precipitation was recorded during the early stage of transformation Fig. 8.24. However the allotriomorph appeared to be highly faceted in some cases.

When the specimens were isothermally transformed at 610°C, they showed an increasing tendency to form Widmanstätten ferrite. However, the Widmanstätten ferrite always showed a tendency to form on highly curved grain boundaries. (Fig. 8.25 and Fig. 8.26.) The plates appeared to grow in martensitic trace direction. Evidence of faceting on the planar γ/α interface was noticed in many cases Fig. 8.27. TEM shows again carbide free ferrite Fig. 8.28. Evidence of interface pinning is shown in Fig. 8.29. Again the curve was plotted between maximum half-thickness vrs square root of time to determine the parabolic growth rate constant. The value thus obtained was 0.28 $\mu m/\sqrt{sec}$.

The value of the parabolic growth rate constant determined at each temperature was plotted against temperature and compared with the theoretically calculated values based on the paraequilibrium model. The plot is shown in Fig. 8.30.

The volume fraction (V_α) at each isothermal temperature was measured and plotted against time Fig. 8.31. The volume fraction was measured by image analysis on a Quantimet 720 machine. In order to reduce the statistical errors 10 fields were measured from each specimen.

In order to construct a TTT diagram, dilatometry experiments were conducted in the temperature range of 600°C to 800°C. The graph was plotted between relative length change ($\frac{\Delta L}{L}$) vrs time for each isothermal temperature (Figs. 8.32a to d). From this graph, the times for start of transformation (Ts) and termination of transformation were obtained and used for construction of the TTT diagram (Figure 8.33). The TTT diagram thus constructed was compared with the calculated TTT diagram. (Fig. 8.34.) The details for calculations of TTT have been discussed in the Appendix I. The partitioning behaviours of the substitutional alloying element (Cr) over a range of isothermal transformation temperatures was studied using the ISI (Scanning electron microscopy with microanalysis facilities). ZAF-4/ FLS program was used to determine quantitatively the partitioning of Cr in α and γ More than 5 readings were taken from each specimen. Practically no evidence of bulk-partitioning was observed. Micro-analysis results are shown in Table 8.1.

In order to obtain a measure of the nucleation rate, the number of ferrite allotriomorphs observed per unit area (N_α) was plotted against time for a range of isothermal temperatures (i.e.750°C to 610°C). The plot is shown in Fig. 8.35. The slope of this curve gives a measure of the nucleation rate $(\frac{dN}{dt})$.

8.6 Discussion: The parabolic growth rate of grain boundary allotriomorphic ferrite over a range of temperature was calculated on the basis of the paraequilibrium model. The details of the calculations are explained in the introduction of this chapter. The calculated growth constants are compared with those experimentally determined (see Fig. 8.30) The plot clearly shows significant discrepancies between calculated and measured parabolic growth rate constants, particularly at lower temperatures (610°C to 700°C). Kinsman and Aaronson,[33, 34] Atkinson et al,[35] and Bradley et al,[36] have similarly found that the growth constants of ferrite allotriomorphs are significantly less than those calculated for control by the volume diffusion of carbon in austenite. It is essential to examine in detail the sources of discrepancies in the light of the experimental observations available. Sources of discrepancies may be listed as follows:-

(i) Presence of planar facets (i.e. semi-coherent interface) over a sufficient proportion of the interfacial area of the allotriomorphs: the growth rate constant was calculated with the assumption that the allotriomorphic ferrite is entirely consisted of high energy incoherent γ/α interface which moves normal to itself under diffusion control of carbon in austenite. In the present investigation the allotriomorphic ferrites observed by optical and electron microscopy showed a tendency to develop planar facets (Figs. 8.14, 8.20, 8.24, 8.27). The presence of partially coherent facets at interphase-interfaces between crystals differing in crystal structure. has already been observed and reported[37-40]. These partially coherent boundaries are displaced solely by a ledge mechanism[41, 42]. This means that the interface is stepped and atoms are transferred from one phase to the other only at these steps. Consequently the macroscopic growth of the interface results from the motion of steps such that an element of the interface remains stationary until a step passes over it, after which the interface advances through a distance equal to the step height. For these interfaces, the growth of the ferrite will be controlled by the rate of step motion as well as the ability to nucleate steps which in turn may be controlled by the volume diffusion process. Except sometimes during early stages of growth, facets migrate less rapidly than disordered-boundaries under given conditions of alloy composition and reaction temperature.[42] The presence of planar facets over a sufficient proportion of the interfacial area of the allotriomorphic ferrite is believed to be one of the reasons responsible for discrepancies.

(ii) Pinning of the γ/α interface by carbide precipitation:- "Interphase-interface precipitation" is now a well established mode of precipitation during the $\gamma \rightarrow \alpha$ transformation of alloy steels[43]. It is believed that these interphase-carbides locally pin the γ/α interface and hence restrict its mobility[44, 45, 46]. However, interphase precipitation may not have any significant effect on the mobility of the semi-coherent planar interfaces because such interfaces are solely displaced by a ledge mechanism and ledges themselves remain unaffected by carbide precipitation due to their high mobility[47]. In the case of interphase precipitation at incoherent γ/α interfaces significant retarding effect on their mobility is expected due to the pinning action of the carbides on these interfaces.

The mobility of the γ/α interface is similarly restricted by the presence of a fine dispersion of carbide in the austenite[44]. By keeping the specimen in the austenite + carbide phase field, fine dispersions of carbide in the austenite can easily be achieved. On subsequently holding the specimen in the $\gamma+\alpha$ phase field, these carbides would be expected to restrict the mobility of the γ/α interface through a pinning action.

Evidence of interface pinning was noticed (Figs. 8.18, 8.21, 8.29) over the entire range of temperature. It can be anticipated that either interphase precipitation at incoherent γ/α interfaces or the fine dispersion of carbide in the matrix (i.e. austenite) is responsible for pinning. TEM investigation did not reveal any interphase-precipitation during the early stages of transformation throughout the temperature range. Some carbides, probably Cr_7C_3[48] (which is h.c.p) were observed during the later stages of transformation Fig. 8.15. These carbides have formed by a mechanism of co-operative growth. Any effect of interphase precipitation on the mobility of γ/α interfaces is thus ruled-out in the present case. The protuberances/ serrations observed are mainly due to pinning by a fine dispersion of alloy carbides in the matrix. The restricted mobility of the γ/α interface due to the pinning action is considered as one of the major factors responsible for slower growth rate than the predicted one.

(iii) Solute-drag-like effect: Another suggestion for slower than the anticipated growth rate is solute drag like effect.[33,42,49] The substitutional alloying element 'Cr' is believed to segregate to austenite/ferrite interfaces during growth, through a "sweeping up" of Cr- atoms, and not by its diffusion through austenite. The segregated 'Cr'-atoms alter the activity of carbon in the austenite which is in contact with these interfaces[50], thereby altering the carbon concentration profile in the austenite ahead of the interface. The interface migration rate is affected by a change in the carbon concentration profile due to presence of 'Cr'-atoms at the

interface. If the substitutional solute atom (such as Mn, Cr i.e. say X in Fe-C-X alloy) reduces the activity of carbon in austenite at the interface, the carbon concentration gradient in the austenite will reduce which in turn will result in a slow growth rate. On the other hand, the opposite effect on growth kinetics is expected if the activity of carbon in the austenite is increased due to alloy (e.g. Si) segregation at the interface. This is referred to as the inverse "solute-drag-like effect",[51] the change in carbon-activity at the two-phase boundary can be estimated from the equilibrium partition coefficient $K^{\gamma/\alpha}$ of the element between the two phases[52].

$$\ln a_C^1/a_C^0 = - \frac{K^{\gamma/\alpha}\left(X_{Fe}^{\alpha} - X_{Fe}^{\gamma}\right)}{X_C^{\gamma} - X_C^{\alpha}} X_M^{\alpha} \quad \ldots\ldots\ldots\ldots\ldots\ldots\ldots\ldots (8.26)$$

where a_C^0 = Activity of carbon without alloy content.

a_C^1 = Activity of carbon with alloy content.

X_M^{α} = Bulk alloy content.

The amount of solute segregating at the interface can be estimated from the modified McLean adsorption[47] expression:-

$$C_{Cr}^{\gamma/\alpha} = \frac{C_{Cr} e^{\Delta G_b/RT}}{1 - C_{Cr} + C_{Cr} e^{\Delta G_b/RT}} \quad \ldots\ldots\ldots\ldots\ldots\ldots\ldots\ldots (8.27)$$

where $C_{Cr}^{\gamma/\alpha}$ = Concentration of Cr at the γ/α interface

C_{Cr} = Bulk concentration of 'Cr'.

ΔG_b = Absorption free-energy of Cr to the γ/α interface.

Bhadeshia[16] in his recent review on "Diffusional Formation of Ferrite in Iron and its Alloys" has raised doubts about the solute-drag-like effect on growth kinetics of ferrite. He pointed out the segregation profile of 'X' solely confined within the interface is an unrealistic assumption particularly when the interface is moving. He supported his view using Cahn's[53] theoretical work which suggests that the solute profile in the vicinity of the moving interface always extends into the region beyond the interface. Secondly, even though the concentration of X in the interface may be different than in the bulk of the austenite, its influence on the activity of carbon in austenite should be identical to that of the X-atoms present

in the bulk of the austenite due to identical partial molar free energy of X-atoms in both the interface as well as in the austenite. Otherwise, the concentration of carbon at the interface must increase to maintain this equality of partial molar free energies. This hypothesis contradicts the one proposed by Kinsman and Aaronson[33].

(iv) Interaction of clusters with interfaces:-

Sharma and Purdy[54] proposed that the formation X-C clusters in the austenite may be responsible for special solute-drag effects. Additional driving force will be needed to strip these clusters from their carbon atmospheres as the interface moves across them. They proposed that the formation of clusters would be difficult at lower temperatures since the ability to form clusters depends on the volume diffusion in the austenite. But at the same time they also proposed that these clusters would have a significant drag effect at low temperatures which is contradictory to the fact that cluster formation is difficult at lower temperatures. Activity coefficient also plays an important role in formation of clusters. In case of 'Cr' or Mo, the activity coefficient is less than unity, implying that these elements do not tend to form clusters in austenite[55].

(v) Error due to the stereology of grain-boundary allotriomorphs:-

To minimize the stereological error, the specimens were austenitized at 1250°C for one hour and fifteen minutes to develop a very large austenite grain size in which austenite boundaries lie normal to the broad faces of the specimens. This technique was suggested by Boswell et al[56]. It is most likely that the γ/α interface formed during transformation lies parallel to the original austenite boundaries. Under such circumstances, the broad face of the allotriomorphic ferrite would represent its true thickness.

However this method (i.e. optical metallography) prevents the recording of the progress of an individual allotriomorphic ferrite during isothermal transformation since measurements are taken on different specimens isothermally transformed for different time periods. In each case, the thickest allotriomorphs were measured. This could lead to significant errors if the incubation period for the nucleation of α is relatively large. The incubation periods of this alloy over a range of temperature were relatively small (Fig 8.33) to have any significant effect.

Micro-analysis: Micro-analysis did not reveal any bulk-partitioning of alloying element 'Cr' over the entire range of investigation (i.e. 750°C to 610°C) between the austenite and ferrite (Table 8.1). This result ruled out the possibility of the $\gamma \rightarrow \alpha$ transformation taking place under equilibrium conditions. But it is thermodynamically possible to achieve the equilibrium conditions at the temperatures very close to the Ae_3 temperature. The alloying element may undergo partitioning towards the equilibrium tie line even at high supersaturations but perhaps at a very late stage of transformation.[15] The partitioning of a substitutional alloying element such as 'Cr' at relatively low supersaturation occurs at a rate-controlled by the diffusivity of the alloying element and hence it is extremely slow.[3,4,10] The methods for calculating growth rate under equilibrium conditions have been discussed by several workers.

The absence of bulk-partitioning between ferrite and austenite points out two mechanisms by which the high supersaturation no-partition reaction may occur.[3,4,9,49,52] These are the no-partition local equilibrium (NPLE) mechanism and the para-equilibrium (PE) mechanism. Both mechanisms have been examined in detail in section 8.2 and 8.3. Briefly, the PE reaction refers to a situation where the alloying element, 'X' remains uniform on both sides of the growing γ/α interface and the reaction occurs by pure diffusion control. In NPLE mechanism, there is essentially no redistribution of the alloying element between the α and the γ-phase but local equilibrium at the γ/α interface is maintained according to a certain tie line in the $(\alpha + \gamma)$ two-phase field.

From the micro-analysis results, it is rather difficult to decide whether the transformation occurred by the PE mechanism or NPLE. It has been suggested that during the early stages of growth period following the nucleation event, local equilibrium does not exist at the α/γ interface and the growth is entirely interface controlled. This initial period is presumably of short duration and soon the paraequilibrium condition is follwoed by local equilibrium at the interface. As the ferrite grows in size with increasing time at the transformation temperature the PE state passes through an infinity of thermodynamically undefined non-equilibrium states and finally gives way to the local equilibrium state.[3]

Aaronson and Domain[57] studied the partitioning behaviour of the substitutional alloying element 'X' during $\gamma \rightarrow \alpha$ transformation in Fe-C-X alloys (where X = Si, Mn, Ni, Cr, Mo, Co, Al, Cu, or Pt). They could not detect the bulk-partitioning of alloying element X during the early stage at high undercooling which indicates the growth of α either by NPLE or PE mechanism.

Recently Bradley and Aaronson[47] studied the growth kinetics in Fe-C-X alloys (where X = Ni, Cr, Mn, Si). The parabolic growth-rate constant of all the alloys studied, except Si-containing steel, showed similar disagreement between the experimentally determined value and the theoretically calculated one assuming paraequilibrium model or NPLE. However, their calculations of parabolic growth constants are incorrect since they intersect at a certain temperature giving the same value by two different mechanisms. This seems to be thermodynamically inconsistent because it contradicts the facet that the PE and NPLE modes are mutually exclusive and PE growth always occurs at a slower rate compared with NPLE growth.

The nucleation of allotriomorphic ferrite predominantly occurred at grain corners, edges and faces over a range of temperatures (i.e. from 750^{o}C down to 600^{o}C) because of reduction in the overall increase in surface energy by eliminating part of the grain boundary surface area.[58] The mis-orientation of the grain-boundary also affects the sequence of nucleation events. The ferrite allotriomorphs are nucleated first on high energy grain-boundaries,[59] while the other relatively low energy boundaries are favoured for nucleation during subsequent stages of transformation. The absence of allotriomorphic ferrite on many grain-boundaries during the early stage of transformation is attributed to this kind of effect. Soon after nucleation the allotriomorphs showed a tendency for rapid growth along the austenite grain-boundaries but thickened very slowly. The high rate of lengthening, compared with that of thickening, is mainly due to enhanced diffusion due to the point effect at the tip of the allotriomorphic ferrite. At a temperature close to Ae_3 both the rate of lengthening and thickening are reduced as expected due to a low driving force With decreasing isothermal temperature, the allotriomorphs showed an enhanced tendency for lengthening compared to that of thickening. In other words, the aspect ratio (i.e. thickness to length) of the allotriomorph is found to decrease with decreasing temperature. Due to rapid lengthening, these allotriomorphs soon impinge with each other and form networks of varying completeness about the austenite grains. Since no α/α boundaries are observed on these networks of ferrite, it is anticipated that either a single ferrite nuclei forms and grows to cover the entire boundary (which is an extreme and rare case), or similarly oriented nuclei link up to form continuous grain boundary layers.[44] The limiting interfaces of the ferrite are not regular and are strongly influenced by the presence of the boundary. The symmetry of its internal structure may be quite different from that of the outer limiting interface.[16] The various morphologies which develop over a range of temperature follow the trend described by Dubé[60] and extended by Aaronson.[41] The details of the Dubé s[60] morphological classifications are discussed in the Chapter II.

Our experimental results show a constant rate of nucleation during early stage of transformation at each isothermal temperature. In order to explain the transformation kinetics it is essential to consider the well known Avrami[67] equation.

$$N = N_o \exp(-v_1 t) \quad \ldots\ldots\ldots\ldots\ldots\ldots\ldots\ldots\ldots\ldots \quad (8.30)$$

and the nucleation rate

$$\frac{dN}{dt} = N_o v_1 \exp(-v_1 t) \quad \ldots\ldots\ldots\ldots\ldots\ldots\ldots\ldots\ldots\ldots \quad (8.31)$$

where N_o = No of the nucleation sites (g.b) per unit volume present initially.

N = No of the nucleation sites available after time 't'.

v_1 = Frequency factor which gives the rate at which an individual site becomes a nucleus.

In the our case N is constant in all the cases (i.e. no of austenite grain boundaries/volume is constant since the austenitizing conditions are same. Hence there must be a significant difference in the values of v_1 i.e. rate at which an individual site becomes a nucleus. Thus it is anticipated that the value of v_1 is gradually reduced with increasing temperature due to decreased driving force (i.e. with decreasing undercooling, the driving force for transformation is also decreased).

The value of $\frac{dN}{dt}$ need not be constant throughout the isothermal reaction period. During the latter stage of transformation the value of $\frac{dN}{dt}$ may drop down primarily due to consumption of nucleation site by allotriomorphic growth[68] and secondly due to mutual impingement of regions transforming from separate nuclei[69]. Gradual drop in $\frac{dN}{dt}$ has been recorded during the later stage of transformation at each temperature (Fig. 8.35).

Figure 8.31 shows plot of V_α vrs time (t). The plot shows again that $\frac{dN_\alpha}{dt}$ may decrease during the latter stage of transformation due to mutual impingement of regions transforming from separate nuclei and also due to gradual exhaustion of available nucleation site[69].

.7 Conclusions:

1. Thickening of ferrite allotriomorphs occurred at a rate which is approximately proportional to the reciprocal of the square root of time, even when the temperature was as low as 610°C. This indicates that interface motion is diffusion controlled and does not seem to be significantly limited by interface process for temperature range of 750°C to 610°C.

2. Discrepancies between the experimentally determined value of parabolic growth rate constants and theoretically determined value based on the PE mechanism have been attributed to the presence of facetting, pinning of the γ/α interface by carbide, the possibility of growth by NPLE and perhaps a drag, interaction of clusters with interfaces and stereological error.

3. On the basis of micro-analysis results, it is not possible to prove conclusively whether the growth occurred by paraequilibrium or no partition local equilibrium mechanism. In principle it is possible to distinguish between these two on the basis of thickness of the diffusion zone. If it is less than 10 A^{o}, para-equilibrium mechanism governs the growth rate. However if it exceeds 50 A^{o}, no-partition local equilibrium mechanism controls the growth rate. These criteria are ad hoc, and need to be supported by experimental evidence.

TABLE 8.1 (cont.)

Temp °C/ Time	Cr in α (wt%)	FI	Cr in γ (wt%)	FI
700 °C/ 80 sec	2.805	0.66	2.441	0.41
	3.73	0.93	2.825	0.38
	3.617	0.78	2.416	0.74
	3.394	0.74	2.92	0.68
	3.293	0.54	2.86	0.76
650 °C/ 40 sec	3.409 (wt%)	1.10	2.898	0.56
	3.489 "	1.05	3.127	1.17
	3.289 "	0.92	3.075	0.86
	3.459 "	0.99	3.174	0.98
	3.048 "	1.36	3.013	0.93
	3.071 "	0.86	2.953	0.77
	3.221	0.96	3.219	1.26
	3.059	0.52	2.939	0.38
	3.087	0.44	2.926	1.62
	2.934	0.69	3.133	1.75
	2.88	1.12		
650 °C/ 60 sec	3.228	2.08	3.728	0.75
	3.146	1.94	3.459	1.29
	2.996	2.34	3.349	2.20
	3.211	2.25	3.369	1.6
	3.104	1.23	3.161	1.03
	2.795	1.31	3.301	1.93
	3.314	4.46	3.3032	1.83
	3.289	5.71	3.384	11.21
	3.423	2.24	3.246	13.94
	3.327	0.79	3.044	15.
	3.209	1.26	3.361	13.10
	3.531	0.55	3.077	5.69
	3.3	2.36	3.288	13.61
	3.433	9.56		
	3.597	8.59		
650 °C/ 120 sec	3.326	1.35	3.202	1.19
	3.359	1.22	3.074	2.11
	3.110	0.89	3.364	1.92
	3.056	1.11	3.578	0.85
	3.098	1.27	3.552	0.68
	3.131	1.11	3.538	0.58
	2.989	0.81	3.154	0.91
	3.115	0.97	2.948	1.31
	3.336	0.65	3.196	0.74
	2.920	0.60	3.009	1.0
			2.986	0.63

TABLE 8.1 (cont.)

Temp °C/ Time	Cr in α (wt%)	FI	Cr in γ (wt%)	FI
650 °C/ 5 min	3.167	2.16	3.034	1.6
	3.288	3.18	3.144	1.15
	3.274	3.03	3.081	2.81
	3.154	2.54	3.755	2.35
	3.210	3.23	2.914	2.30
	3.025	2.31	2.953	2.53
			3.095	2.45
610 °C/ 75 sec	3.13	0.67	2.805	1.85
	3.09	1.19	3.037	1.90
	2.532	1.01	2.575	1.37
	3.03	1.04	2.958	1.05

TABLE 8.2

610°C/ Time	No of α X $10^8/m^2$	650°C/ Time	No of α X $10^8/m^2$
40 sec	0.11 X $10^8/m^2$	20 sec	0.7789 X $10^8/m^2$
50 sec	134.4 X $10^8/m^2$	40 sec	143 X $10^8/m^2$
60 sec	209 X $10^8/m^2$	60 sec	128.2 X $10^8/m^2$
75 sec	185.8 X $10^8/m^2$	2 min	118.2 X $10^8/m^2$
90 sec	238.4 X $10^8/m^2$	5 min	372 X $10^8/m^2$
120 sec	260 X $10^8/m^2$		
700°C/ Time		750°C/ Time	
20 sec	0.667 X $10^8/m^2$	40 sec	0.4145 X $10^8/m^2$
60 sec	137 X $10^8/m^2$	60 sec	137.3 X $10^8/m^2$
80 sec	267 X $10^8/m^2$	80 sec	125.87 X $10^8/m^2$
		45 sec	0.733 X $10^8/m^2$

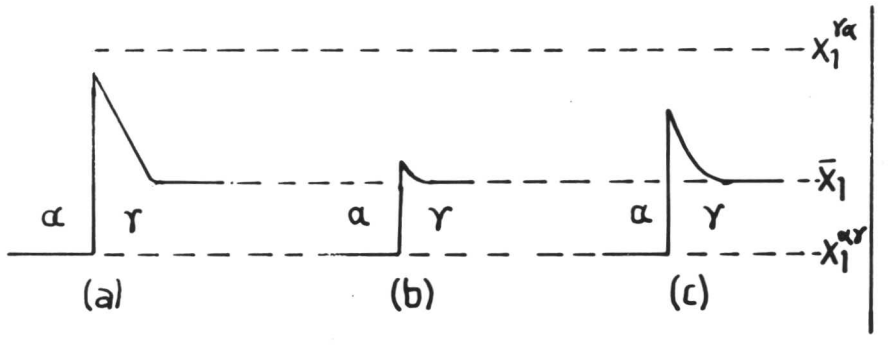

Figure 8.1: Carbon concentration profile at αγ interface moving under (a) diffusion control; (b) interface control; and (c) mixed control.

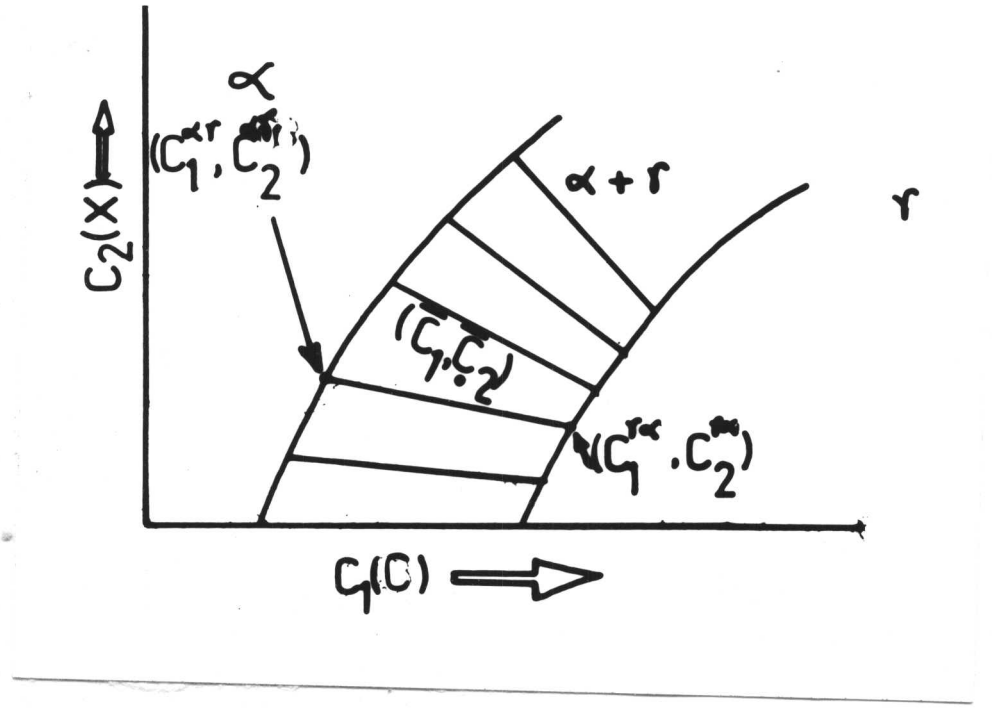

(b)

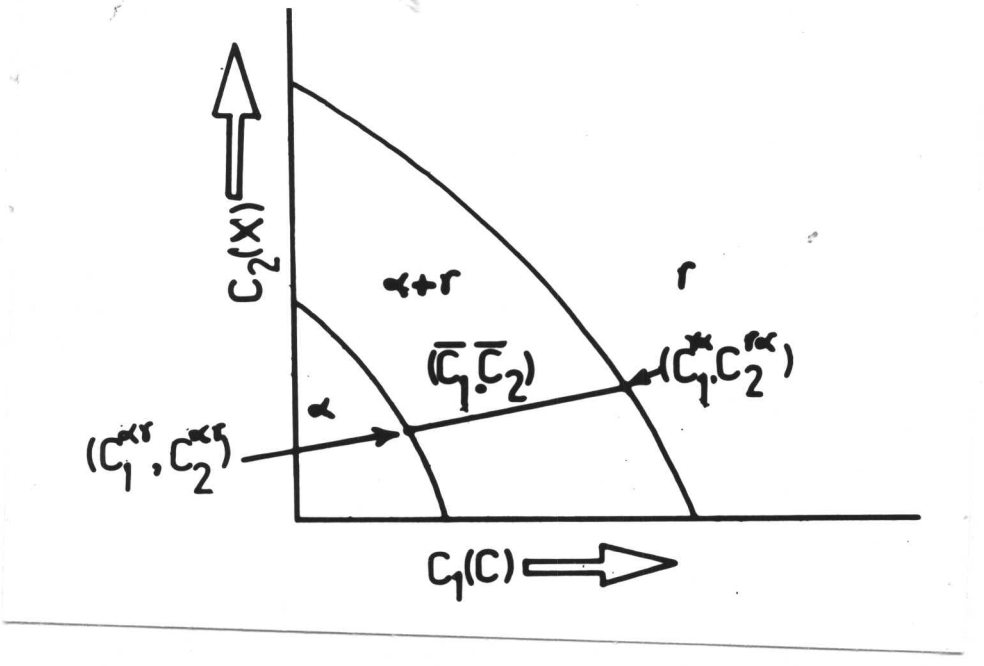

(a)

Figure 8.2: Schematic Fe-C-X isotherms showing (a) X is a γ-stabilizer (b) X is an α-stabilizer.

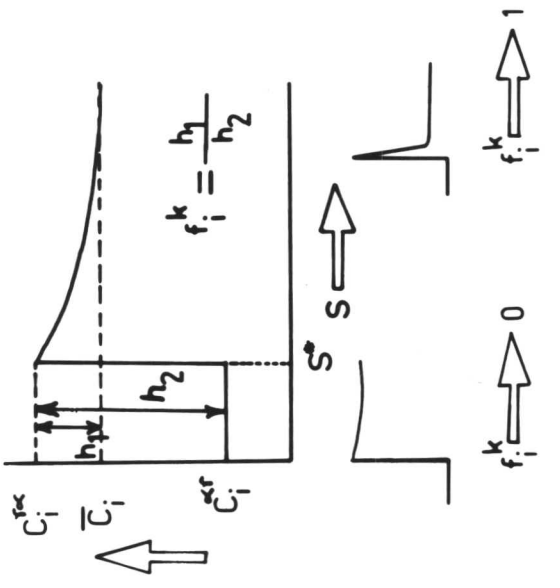

Figure 8.3: Schematic representation of the fractional composition of component i, f_2^k. The concentration distribution corresponds to $f_2^k \to 0$ or 1 are also shown.

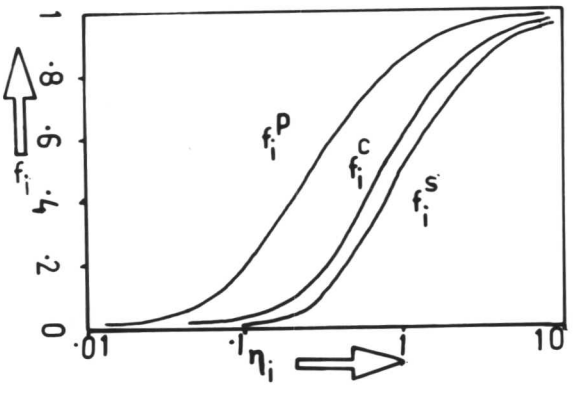

Figure 8.4: The functions f^k (n_i) vs growth rate constant n_i for planar, cylindrical and spherical growth.

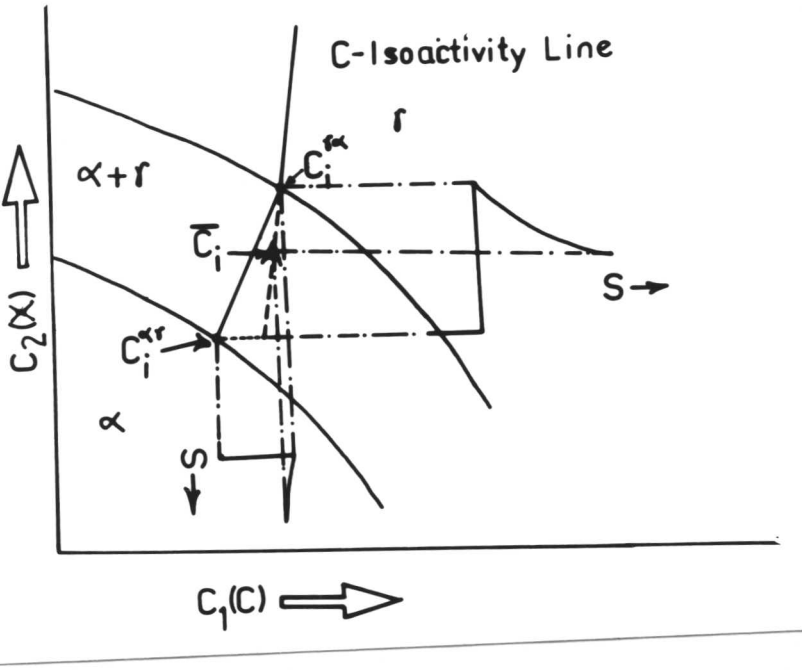

(a)

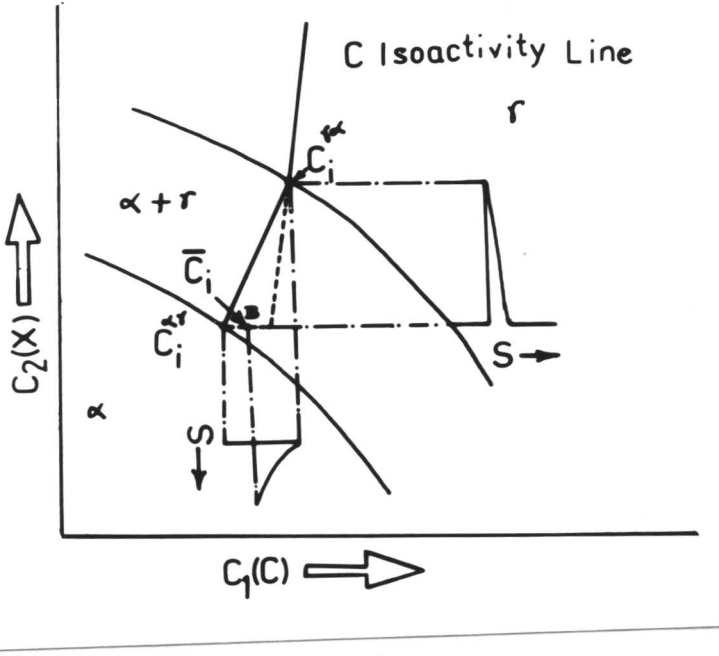

(b)

Figure 8.5: Schematic isotherm and concentration distributions depicting proeutectiod ferrite under local equilibrium at the γ/α interface, uniform C activity in the γ, partition of X between α and γ and (a) growth rate controlled by X i.e. growth via PLE mode. (b) growth rate controlled by C i.e. via NPLE mode.

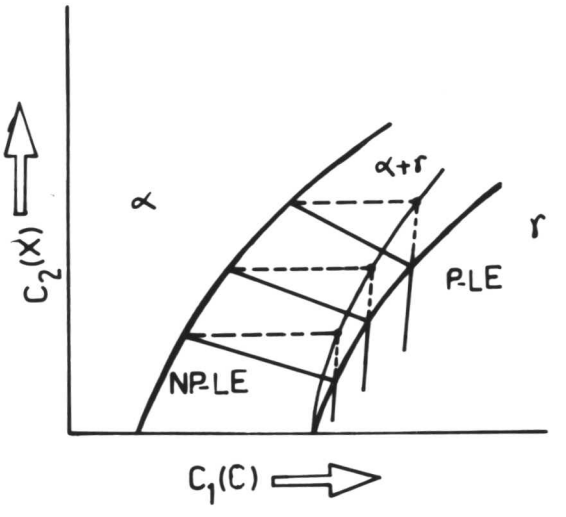

(b)

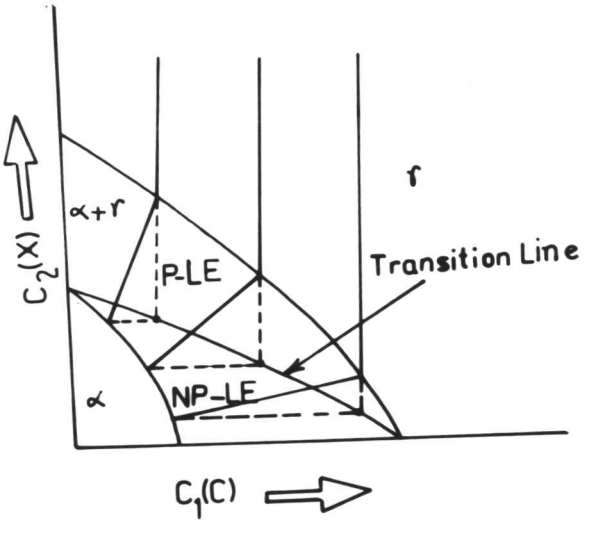

(a)

Figure 8.6: Schematic F-C-X isotherms showing NPLE and PLE regions (a) X is a γ-stablizer (b) X is an α-stablizer.

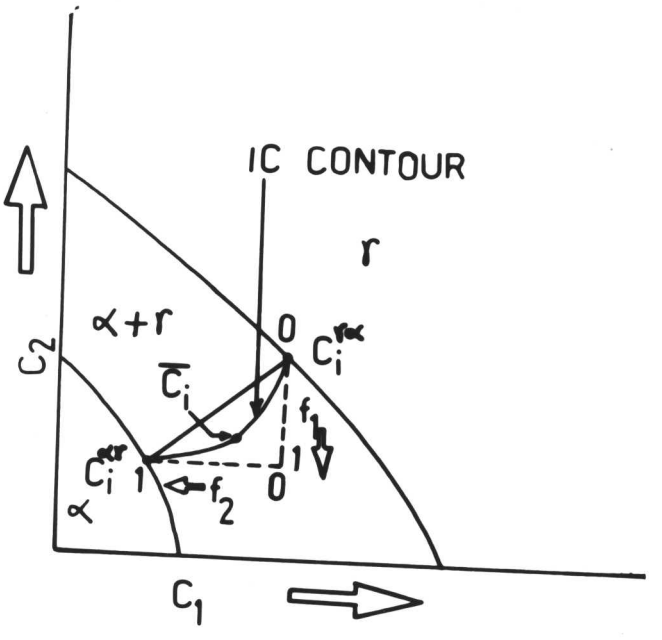

Figure 8.7: Schematic showing IC contour corresponding to a particular tie line.

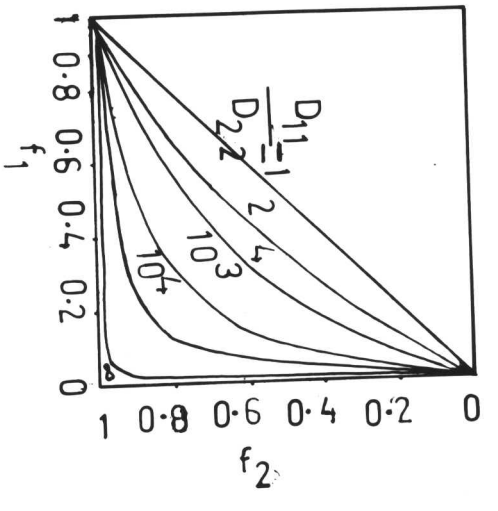

Figure 8.8: IC contours for planar growth with D_{22}/D_{11} = 1, 2, 10^3, 10^4 and ∞.

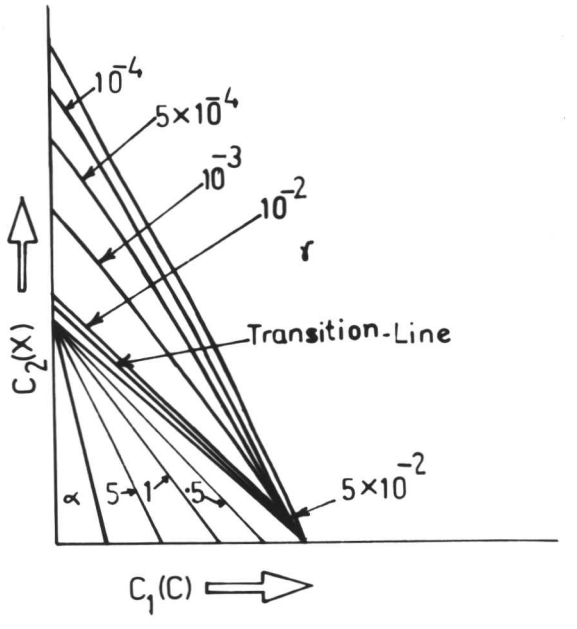

Figure 8.9: Interface velocity (IV) contours for planar precipitate growth in ($\gamma+\alpha$) field. The value of n_i corresponding to each contour is also shown.

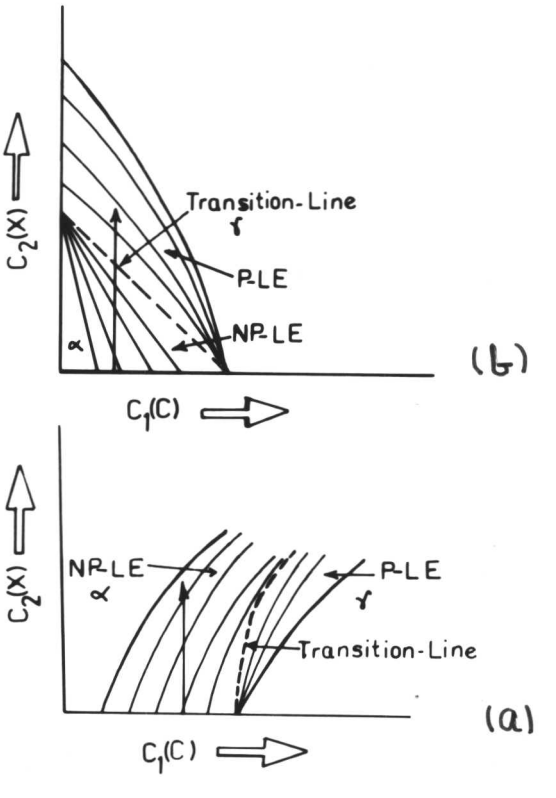

Figure 8.10: Schematic Fe-C-X isotherms showing the transition line (dotted) between NPLE and PLE growth modes and a system of IV contours. (a) X is a γ-stablizer (b) X is a α-stablizer.

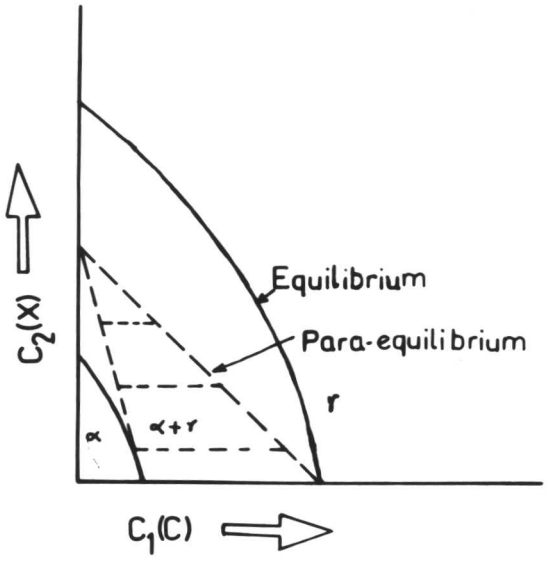

Figure 8.11: Isotherm of ternary phase - diagram. Broken line represents para-equilibrium phase boundary.

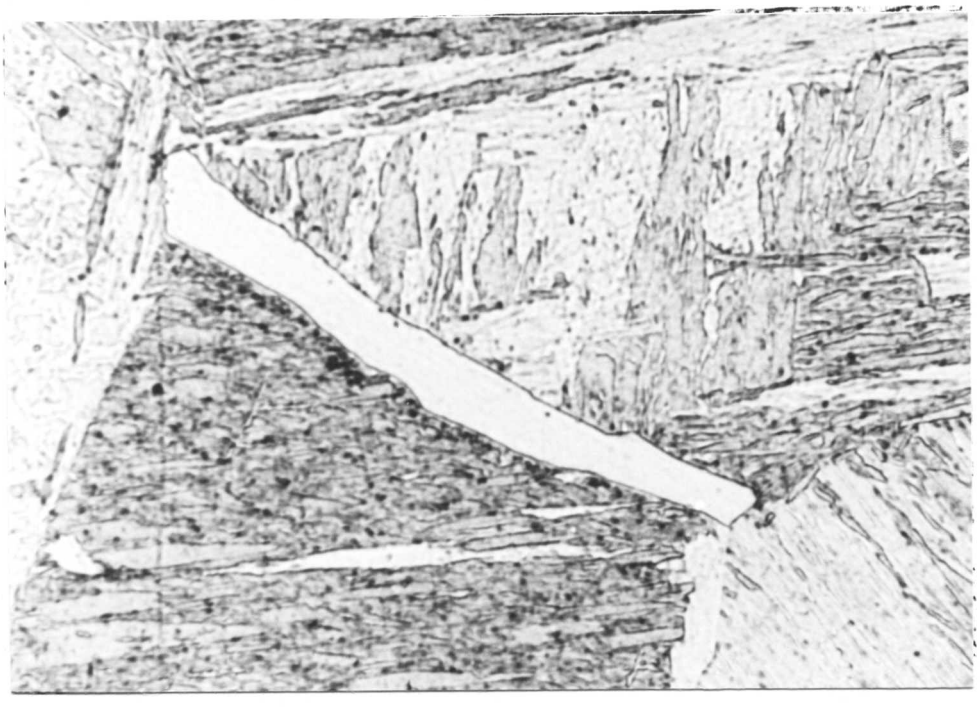

Figure 8.12: Grain-boundary allotriomorphic ferrite growing along the prior austenite grain-boundary. (750°C/40 sec).

Figure 8.13: Allotriomorphic ferrite with ragged interface. (750°C/60 sec).

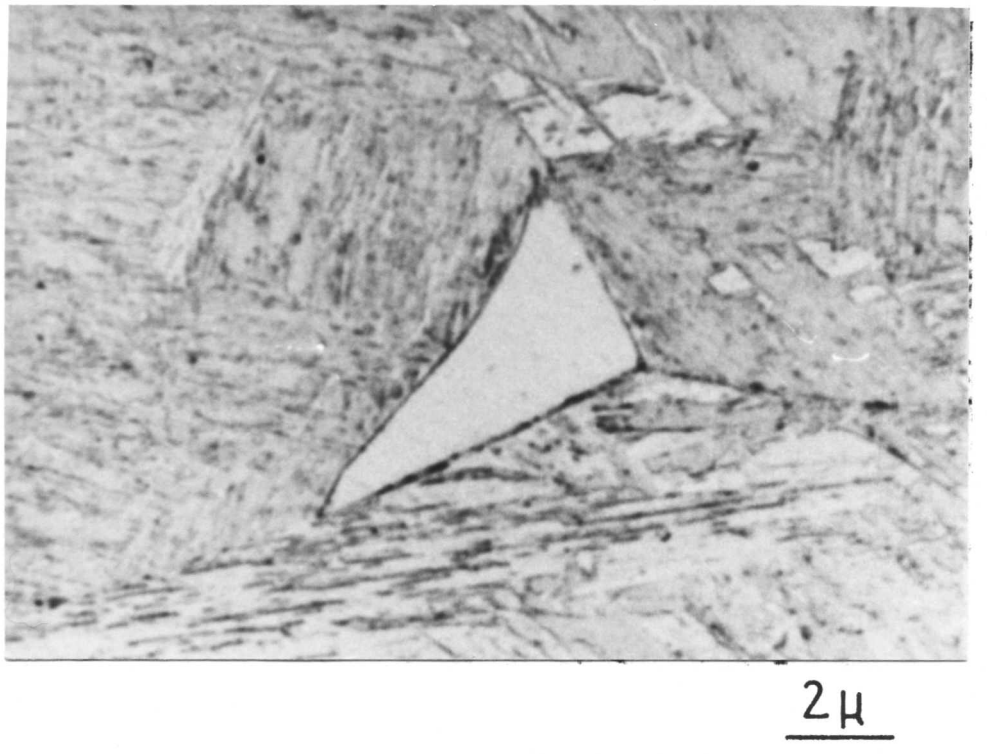

Figure 8.14: Nucleation of α at triple junction of austenite grain boundaries. (750°C/60 sec).

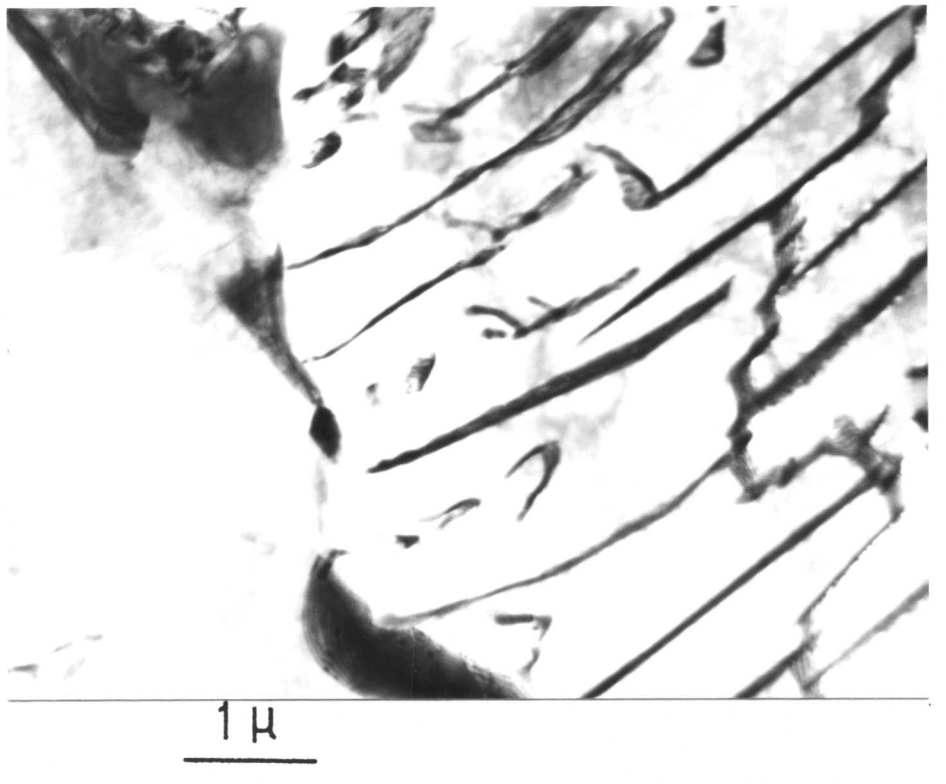

Figure 8.15: Carbide precipitation during latter stage of transformation at 750°C.

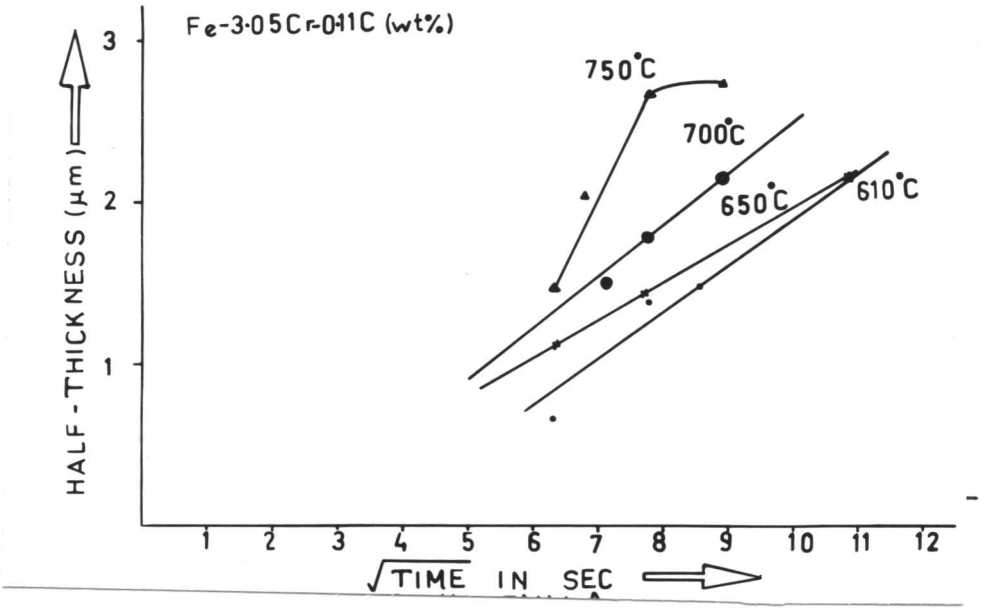

Figure 8.16: Showing a plot between maximum half thickness vs square root of time.

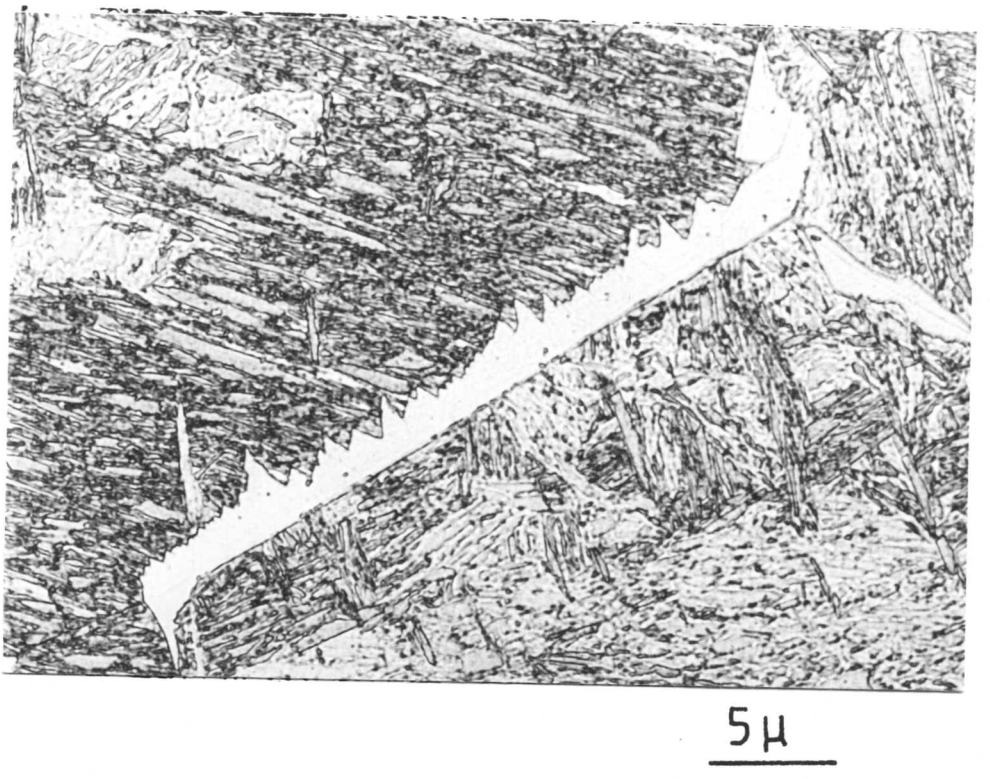

Figure 8.17: Allotriomorphic ferrite along the prior austenite grain-boundaries. (700°C/60 sec).

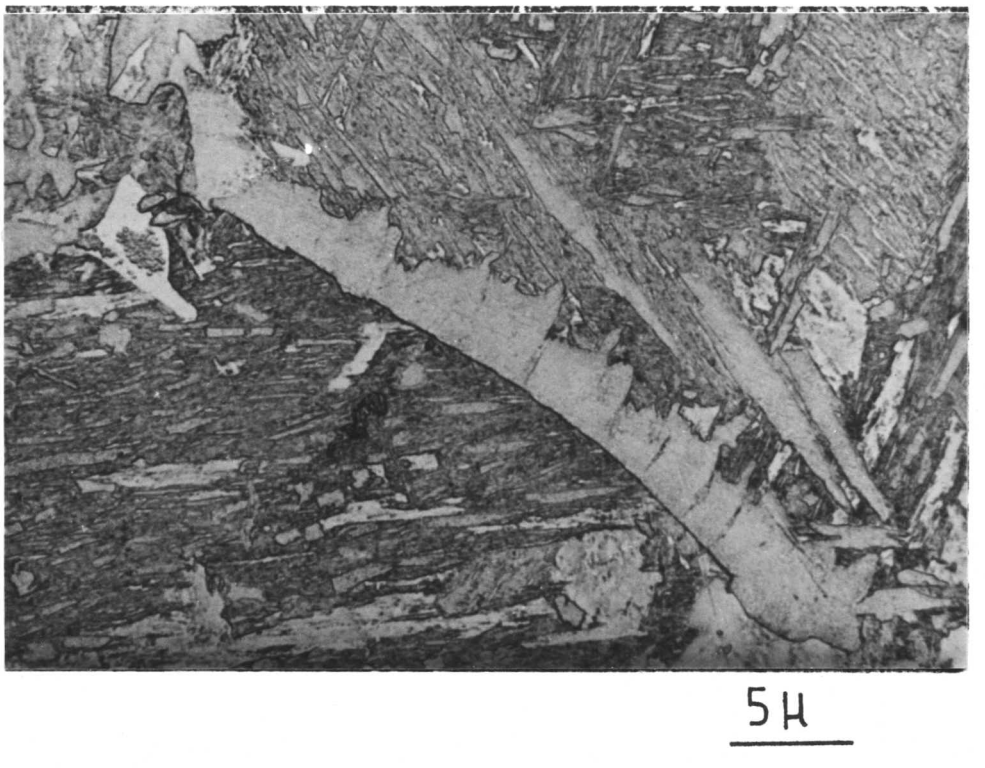

Figure 8.18: Ragged interface developed as a result of pinning by chromium carbides. (700°C/80 sec).

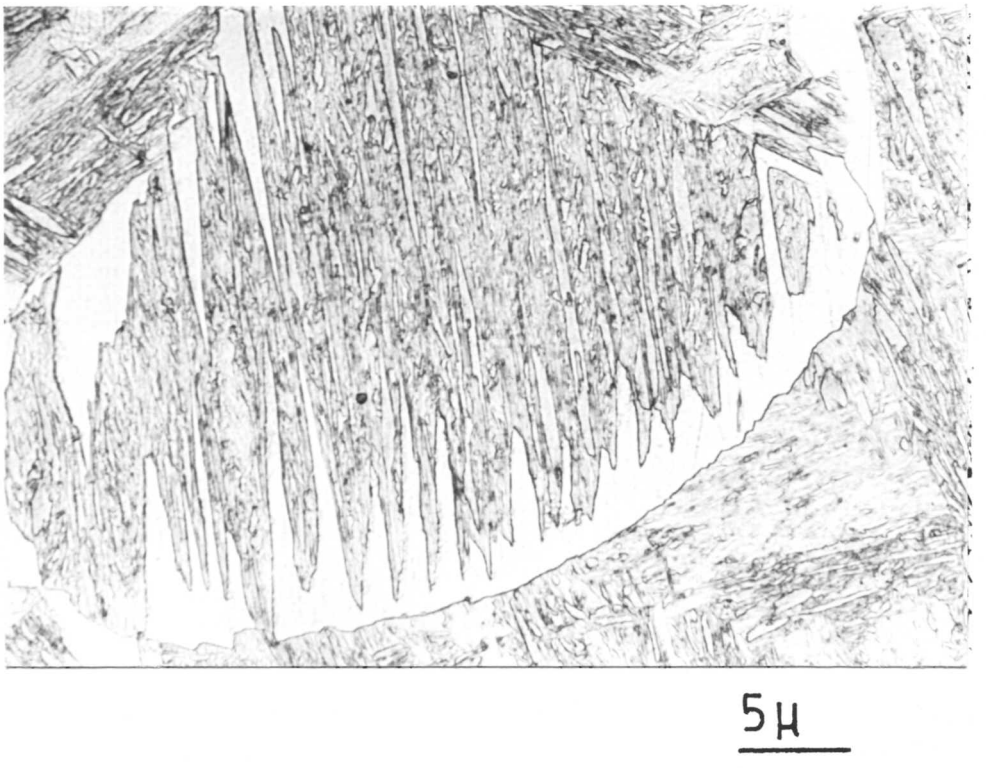

Figure 8.19: Nucleation of Widmanstätten ferrite along highly curved γ-grain-boundary. (700°C/80 sec).

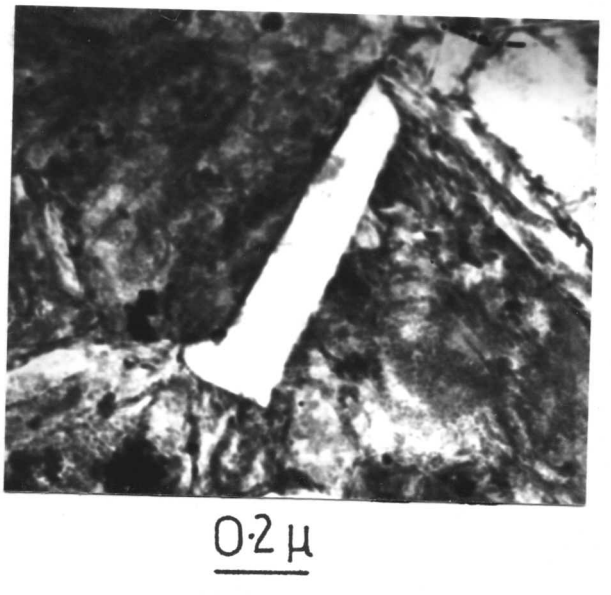

Figure 8.20: Carbide free allotriomorphic ferrite which is highly facetted. (700°C/25 sec).

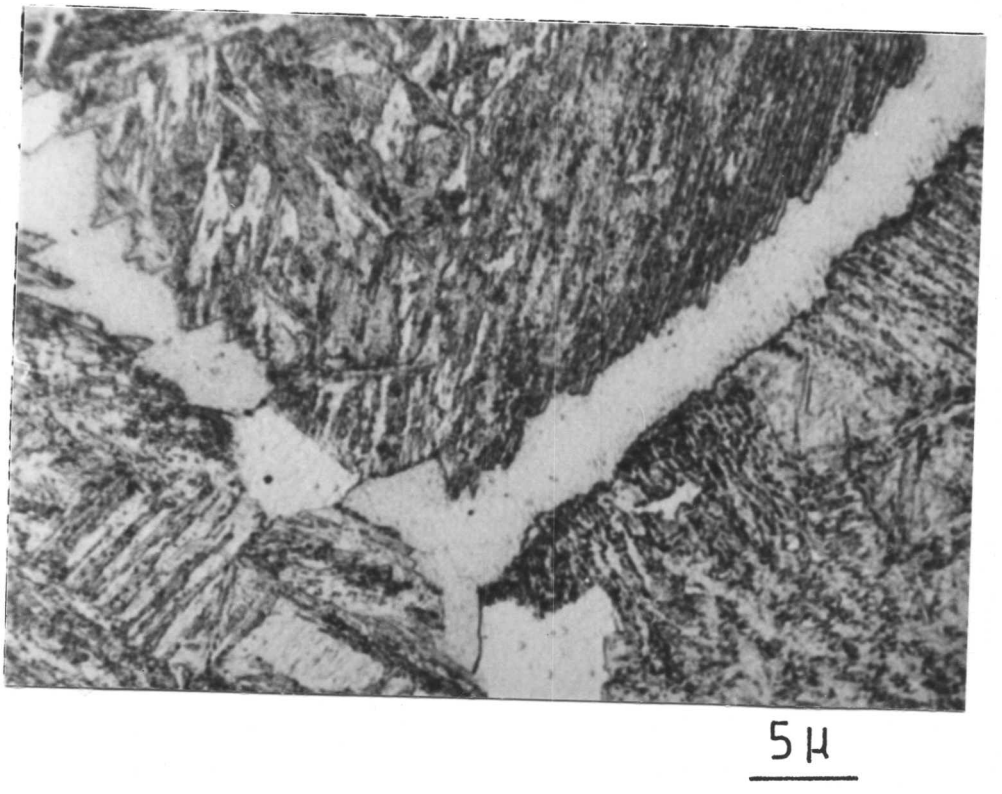

Figure 8.21: Allotriomorphic ferrite with serrated γ/α interfaces. (650°C/ 120 sec).

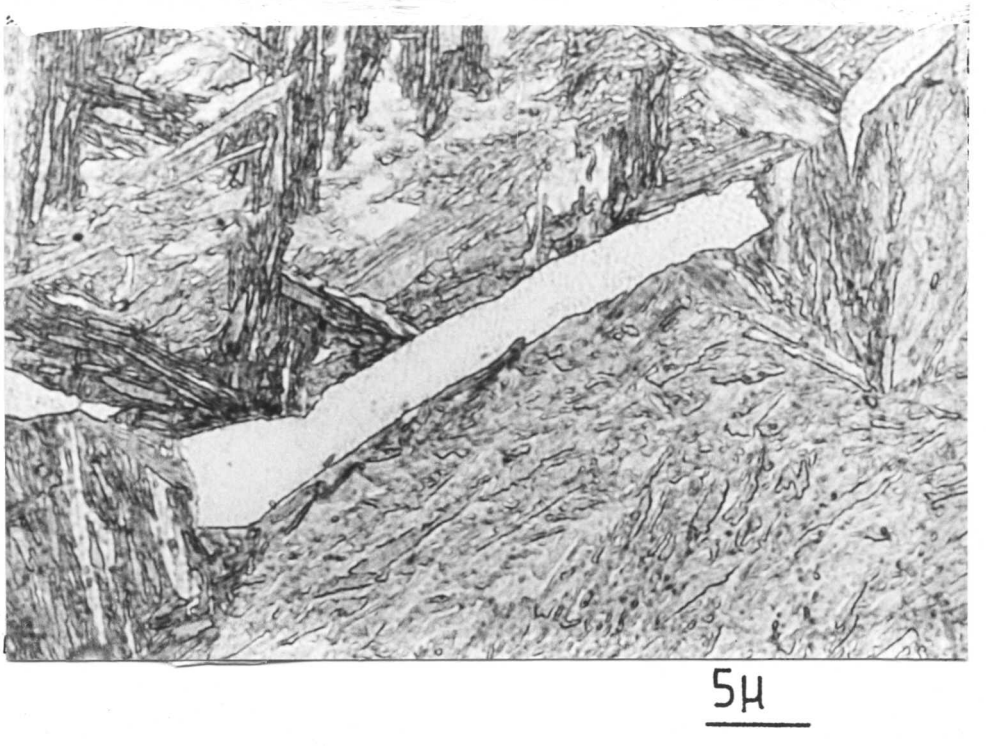

Figure 8.22: Showing facetted allotriomorphic ferrite. (650°C/40 sec).

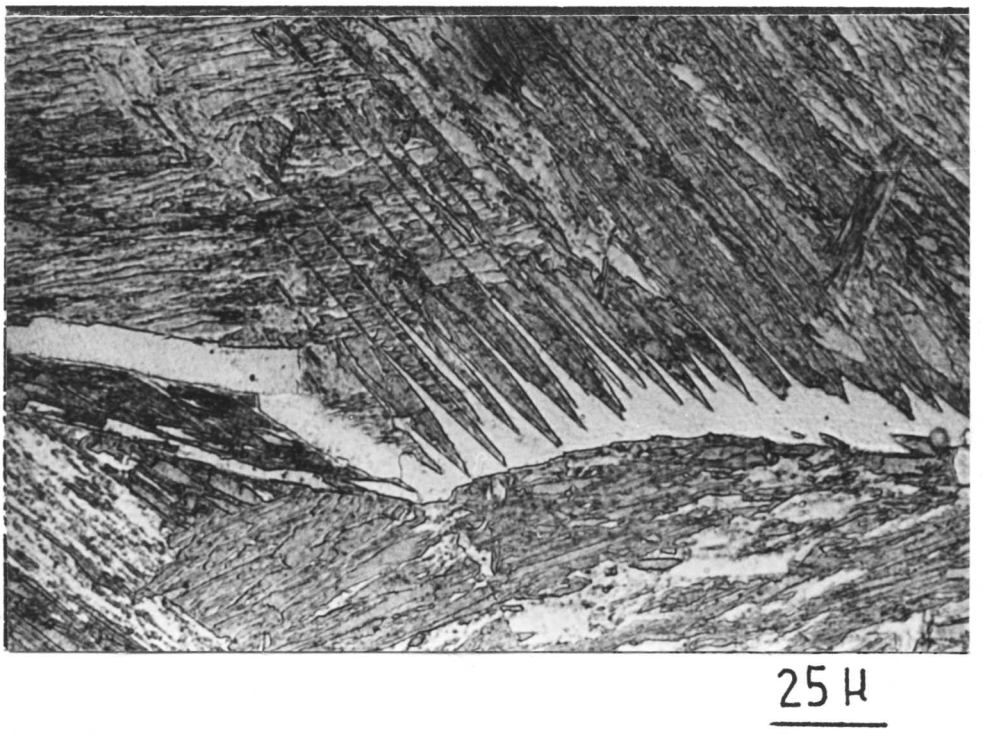

Figure 8.23: Formation of Widmanstätten along highly curved γ-grain-boundary. (650°C/40 sec).

Figure 8.24: Transmission electron micrograph showing carbide free facetted ferrite. (650°C/10 sec).

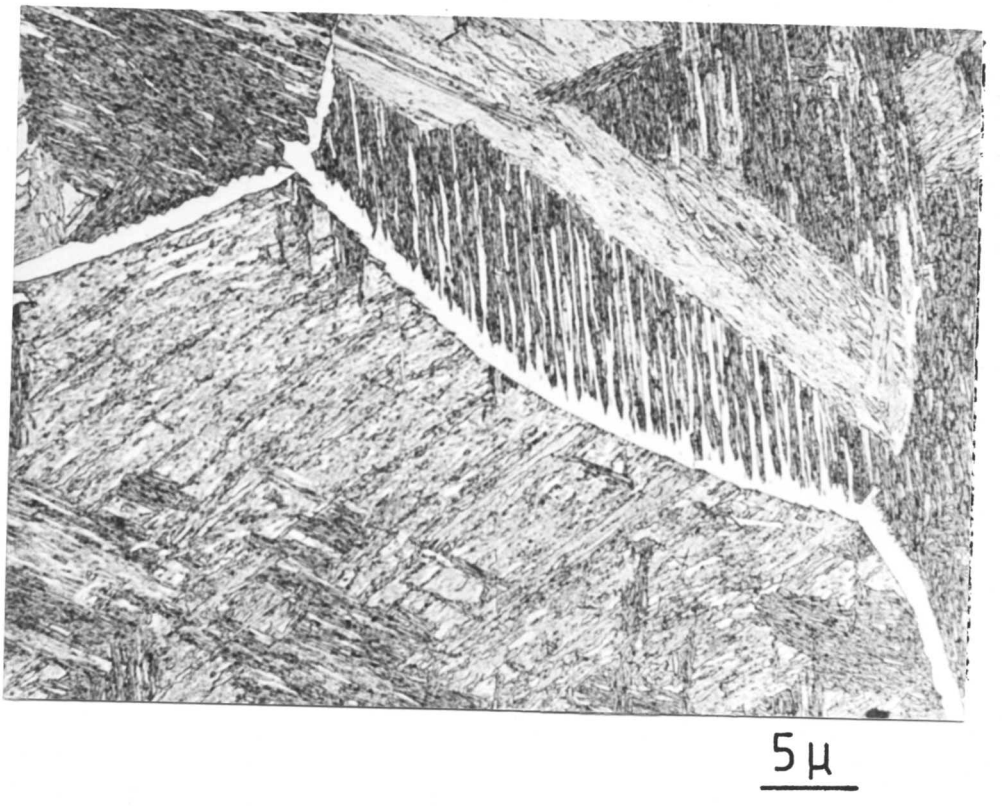

Figure 8.25: Formation of Widmanstätten ferrite along highly curved grain-boundaries. (610°C/60 sec).

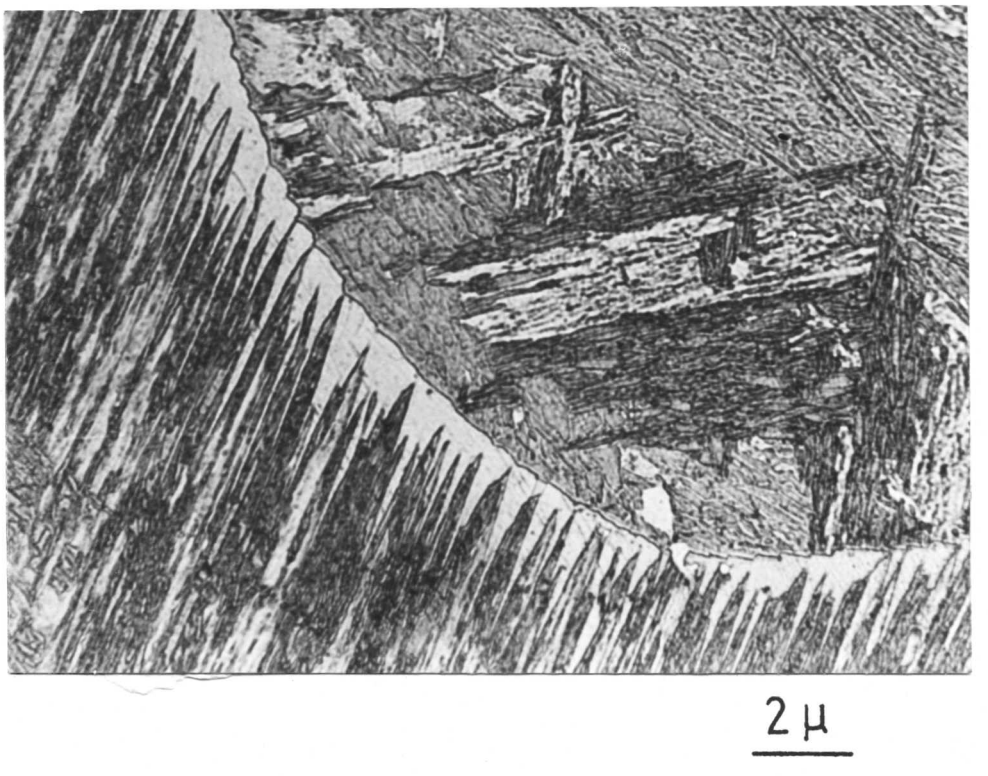

Figure 8.26: Formation of Widmanstätten ferrite along highly curved grain-boundaries. (650°C/50 sec).

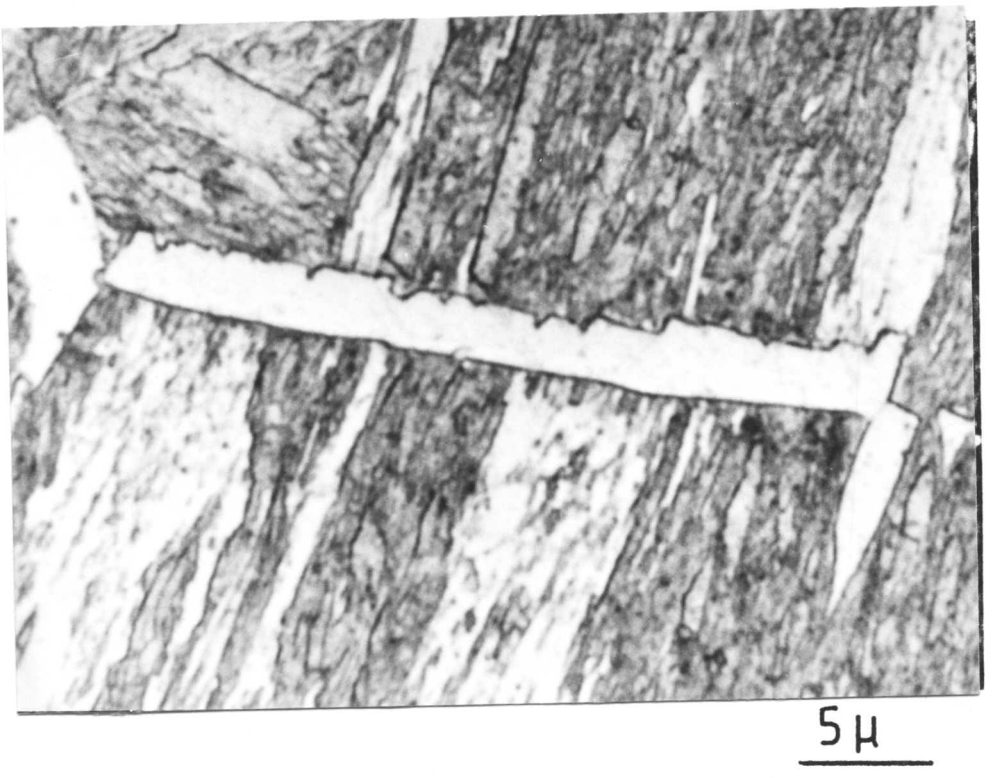

Figure 8.27: Showing evidence of interface pinning (610°C/50 sec).

Figure 8.28: Showing evidence of interface pinning. (610°C/20 min).

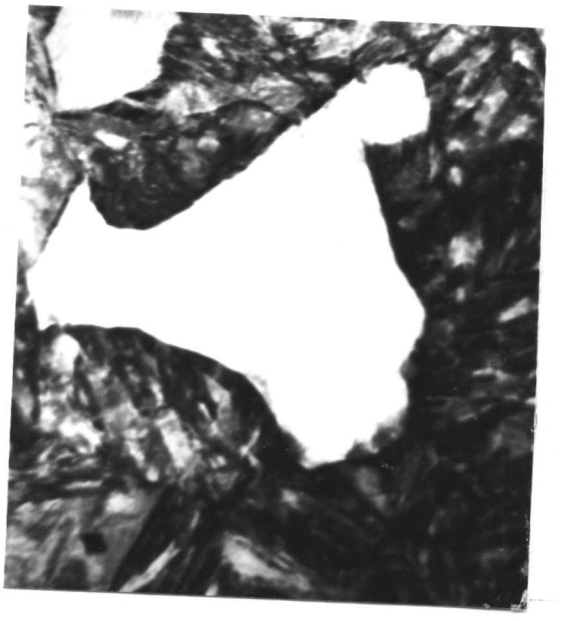

Figure 8.29: Carbide free ferrite formed during the early stages of transformation (610°C/15 sec).

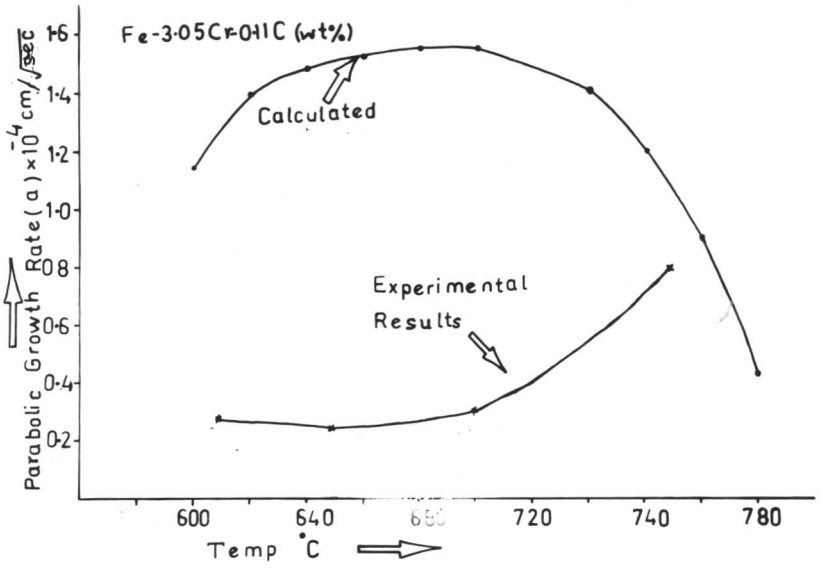

Figure 8.30: Plot of parabolic rate constant vrs temperature.

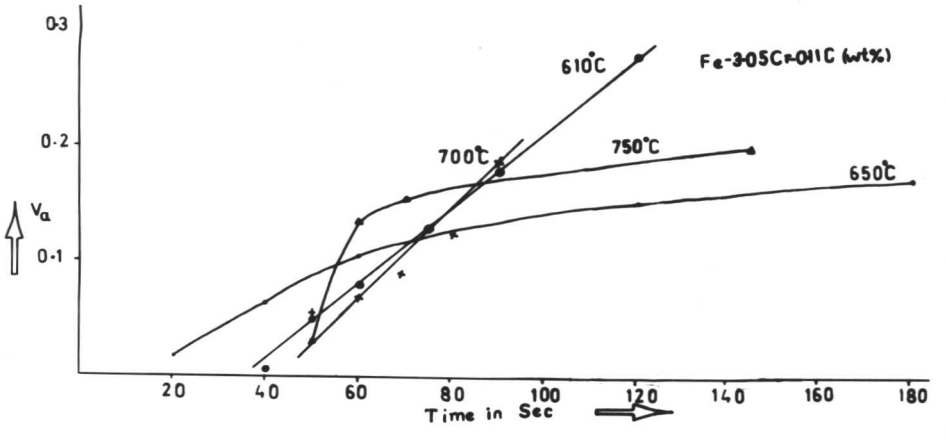

Figure 8.31: Plot of volume fraction vs temperature.

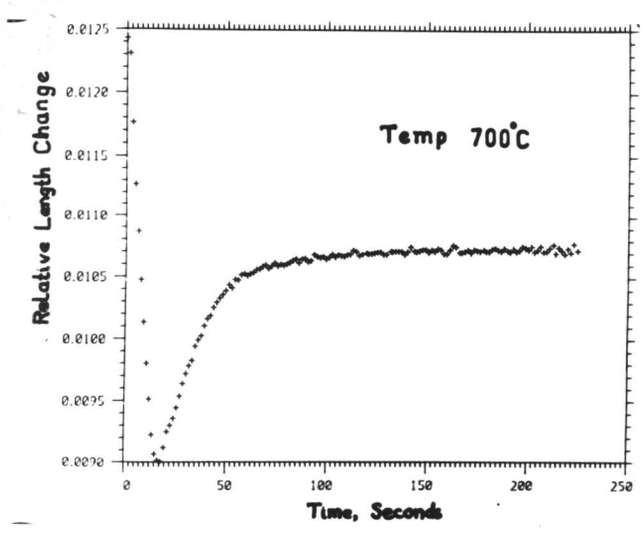

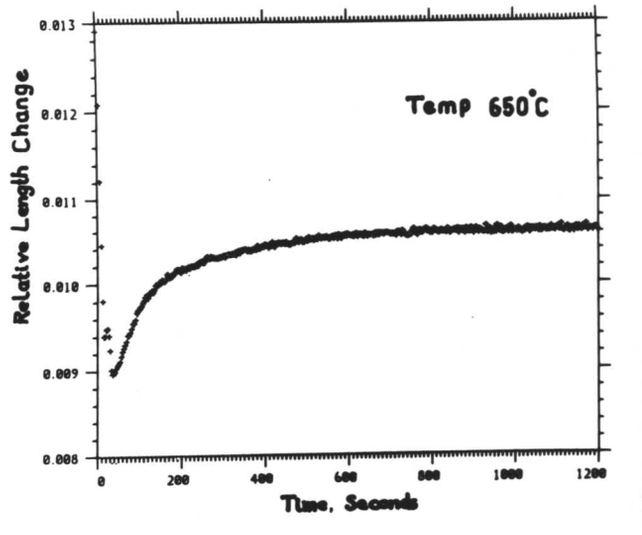

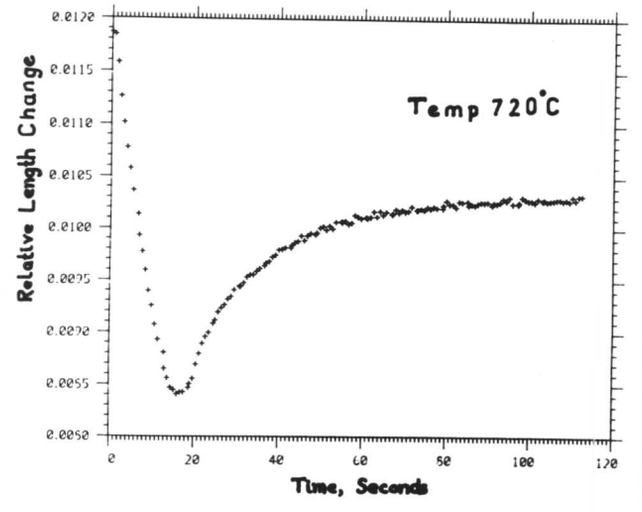

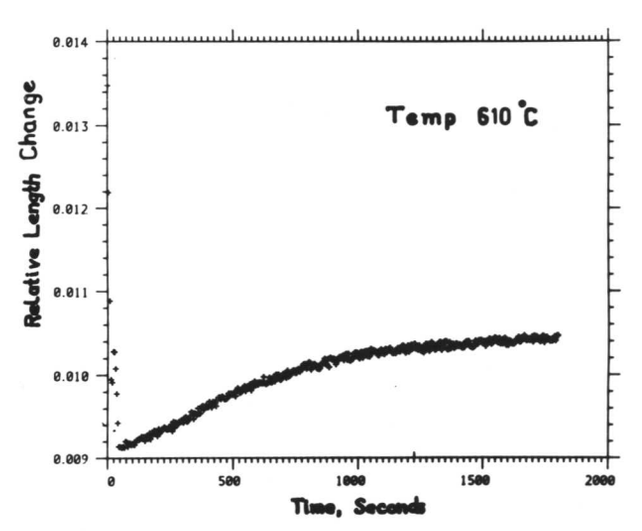

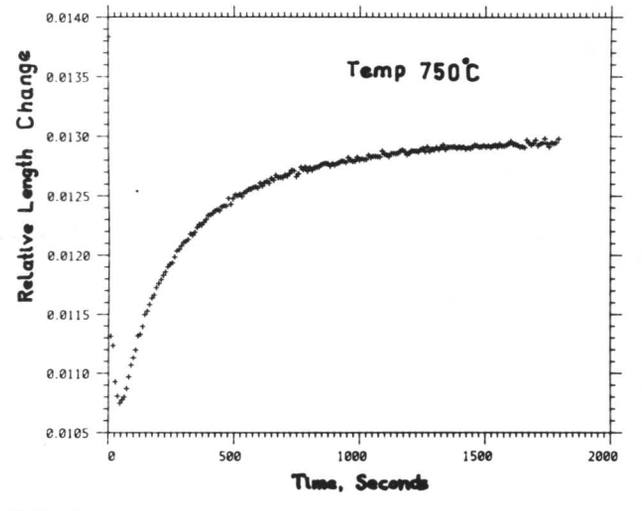

Figure 8.32: Plot of relative length change ($\frac{\Delta L}{L}$) vrs time at different isothermal temperature.

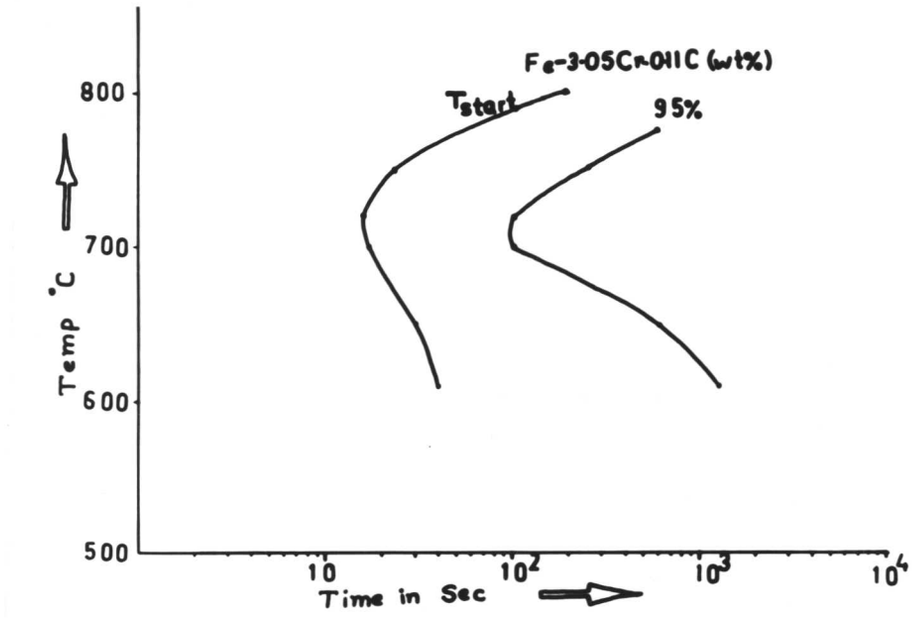

Figure 8.33: Experimentally determined TTT diagram.

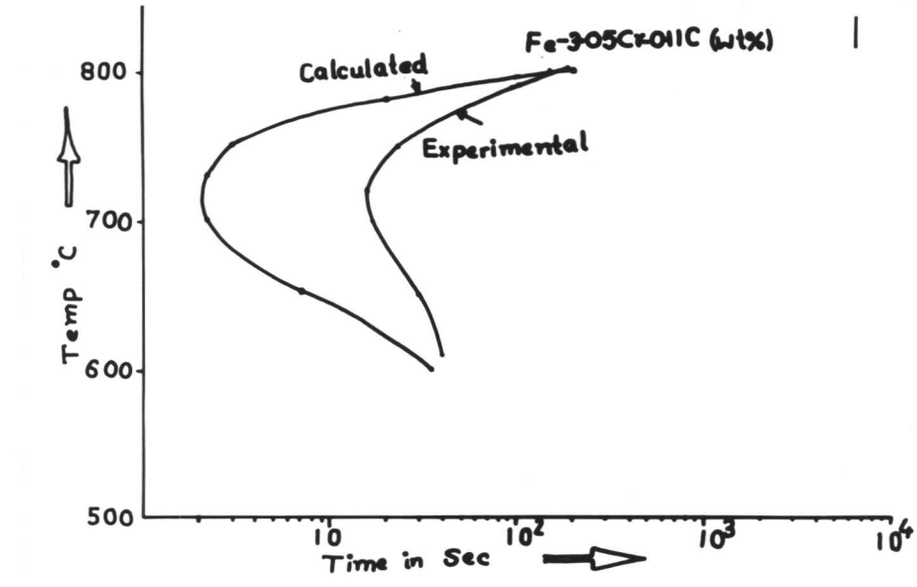

Figure 8.34: Showing comparison between calculated TTT and experimentally TTT diagram.

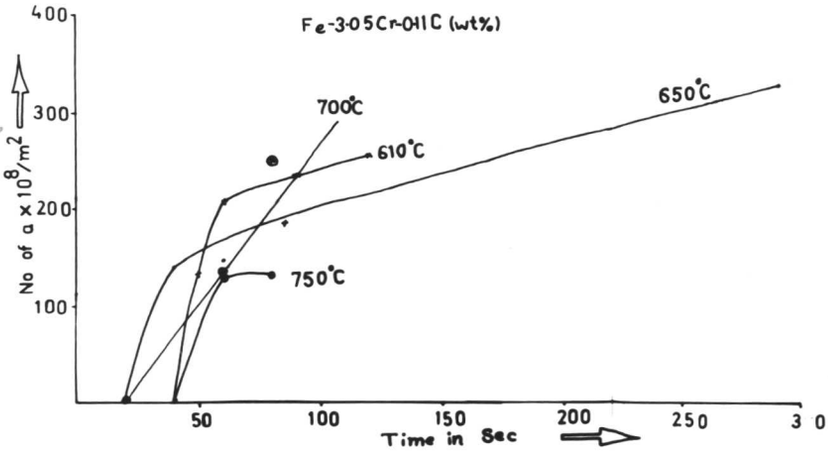

Figure 8.35: Plot of N_{α} vrs time.

CHAPTER IX

THE STUDY OF GROWTH KINETICS IN Fe-3.28Ni-0.11C (wt %) ALLOY

9.1 Introduction: This chapter is concerned with the growth kinetics of ferrite in a Fe-3.28Ni 0.11C(wt %) alloy. The choice of nickel as an alloying element appears to be ideal since it does not form any carbides. So the effect of carbide precipitation on the mobility of the γ/α interface can be minimized. It is thus expected that the $\gamma \rightarrow \alpha$ transformation will begin with the formation of virtually carbide-free proeutectoid ferrite. Parabolic growth rate constants determined from this allotriomorphic ferrite, as a function of isothermal transformation temperature, should provide a test for the various theoretical models (i.e. NPLE and PE) of diffusion-controlled growth.

9.2 Experimental Results: The exact composition of the alloy used was Fe-3.28Ni-0.11C (wt %). The details of the initial-heat-treatment given to this alloy have been already discussed in the Chapter II.

The alloy after austenitizing was subjected to isothermal transformation in the temperature range of 600°C to 700°C.

The TTT diagram for the beginning of austenite decomposition in this alloy was constructed on the basis of the model developed by Bhadeshia[1]. The calculated TTT curve for start of transformation is shown in Fig. 9.1a. This TTT curve was used to design the experiments and select the range of isothermal transformation.

Isothermal transformation at 700°C was carried out for different lengths of time. Optical microscopy showed that the observable nucleation of ferrite was recorded after 90 seconds at this temperature. (Fig. 9.2.) This incubation period is in close agreement with the one obtained from the calculated TTT curve which shows an incubation period of around 70 seconds. The nucleation of allotriomorphic ferrite occurred preferentially along prior austenite grain-boundaries. Growth followed rapidly along the grain-boundaries (i.e. lengthening). Its growth perpendicular to the grain-boundary occurred at a relatively low rate (i.e. thickening). With increasing time at the transformation temperature the ferrite grew rapidly along the grain boundaries to form a network (Fig. 9.3). These allotriomorphs of ferrite appeared to be "clean" with no evidence of interface pinning. The α/γ interface either appeared

planar or curved. No perturbations of the α/γ interface were observed. TEM observation could not detect any carbide precipitation during the early stages of transformation. However after prolonged transformation, extensive evidence of cementite was noticed. Two distinct modes of precipitation were observed. Fig. 9.4 shows precipitation of cementite on dislocations as well as in the matrix whereas Fig. 9.5 shows evidence of interphase precipitation. The plot of maximum half-thickness vrs square root of time is shown in Fig. 9.6. The slope of this curve for 700°C gives the value of parabolic rate constant as 0.43 $\mu m/\sqrt{sec}$. Fig. 9.6 also shows that the maximum half thickness of the ferrite is proportional to the square root of time indicating diffusion-controlled growth.

Isothermal transformation at 680°C led to the development of allotriomorphic ferrite at prior austenite grain-boundaries. The observable nucleation of ferrite was optically recorded after 30 seconds of incubation period. However the incubation period determined from the (Fig. 9.1) TTT curve is approximately 18-20 seconds which is slightly less than the optically recorded incubation period. The allotriomorphic ferrite formed a network along the prior austenite grain-boundaries with increasing isothermal time. (Fig. 9.7.) The parabolic growth rate constant was determined from Fig. 9.6 for 680°C as 1.02 $\mu m/\sqrt{sec}$. During the later stages of transformation precipitation of cementite on dislocations was observed using TEM. (Fig. 9.8.) A pearlitic structure was also observed in some areas as shown in Fig. 9.9. However, the allotriomorphic ferrite formed during the early stages of transformation (i.e. before 50 sec) remained free from cementite so that the measured parabolic growth rate constant should be reliable. Practically no evidence of interphase pinning was noticed. In some cases Widmanstätten ferrite was also observed. This is in close agreement with the theoretical calculation[17] which shows that Widmanstätten ferrite should begin to form in this range of 700°C - 660°C.

A slight increase in the parabolic growth rate constant to 1.2 $\mu m/\sqrt{sec}$ was observed at the isothermal temperature of 650°C (Fig. 9,6). Carbides were detected using TEM during the early stages of transformation at 650°C. These carbides, which are basically cementite, formed by three different mechanisms, Fig. 9.10 shows precipitation of cementite by the interphase mechanism. Occasionally precipitation on dislocations was also recorded as shown in Fig. 9.11. Formation of fibrous cementite appeared to be dominant at this temperature (i.e. 650°C Fig. 9.12) during the later stage of transformation. The calculated TTT curve shows an incubation period of 10 seconds whereas the optically determined value is 50 seconds. Transformation at 600°C followed the same general behaviour and the parabolic rate constant was found to be

1.2 μm/√sec. The data have been presented in Fig. 9.6. The observable (optically) nucleation of allortiomorphic ferrite started around 6 seconds, which is much faster than indicated in the calculated TTT curve.

The calculated TTT curve (for beginning of transformation) and the optically determined TTT curve (for observable nucleation of ferrite) were plotted in Fig. 9.1b. The TTT curves clearly show reasonable agreement at high temperatures (i.e. 700°C and 680°C) but they diverge at lower temperatures (i.e. 650°C and 600°C).

The calculated parabolic rate constants are plotted against temperature and compared with the experimentally determined values as shown in Fig. 9.13. There is good agreement in the temperature range 600°C to 680°C. But at a temperature of 700°C (close to the Ae_3 temperature), rather poor agreement is apparent.

Using the Quantimet 720, the volume fraction (V_α) was measured at successive intervals of time at each temperature and plotted against time. Figure 9.14 (a and b) shows a plot between V_α and time for temperatures, 600, 650, 680°C and 700°C. At least 10 fields were taken from each specimen to minimize the statistical error.

A curve was also plotted between log log $\frac{1}{1-V_\alpha}$ vrs log t, as shown in Fig. 9.15. From the slope of the this the value of n was determined. The values of 'n'are given (see Table 9.1).

9.3 Discussion

The experimental results indicate that the thickening of ferrite allotriomorphs occurs as a parabolic function of time (Fig. 9.6). This indicates that the interface moves under diffusion-control and does not seem to be limited by interface processes for the temperature range of 600°C to 700°C.[2]

The parabolic rate constants thus determined were plotted as a function of temperature and compared with the theoretically calculated values based on the paraequilibrium model (Fig. 9.13). Good agreement was observed in the temperature range 600°C to 680°C. Unlike Cr, nickel does not form any carbides, so that any "solute-drag-like" effect should be absent. This is consistent with experimental observations where not protuberances were detected on the γ/α interfaces. Secondly, nickel is believed to cause a high proportion of incoherent γ/α interface[3] thereby minimizing the effect of facetting on the mobility of γ/α interfaces. Except at 650°C, no carbide was detected during the early stages of transformation where most of the thickness measurements were done. Even at 650°C, not all the allotriomorphic ferrite exhibited cementite precipitation. This may be the reason why better agreement with calculated

parabolic rate constants is obtained for this alloy in the range of 700°C to 600°C. Fig. 9.15 shows a plot of log log $\frac{1}{1-V_\alpha}$ vrs log t. This was plotted to obtain the value of 'n' in Avrami's equation $V_\alpha = 1-\exp(-kt^n)$ where 'k' and 'n' are constants. Since the value of 'n' lies between 1.5 to 2.5, it was concluded that growth of allotriomorphic ferrite is consistent with diffusion controlled growth with decreasing nucleation rate.[4]

Microstructures: Carbide-free ferrite was detected at all temperatures (except at 650°C) during the early stage of transformation. The morphology of the ferrite obtained was consistent with Dubé's morphological classification.

Unlike the Cr-steel (where extensive evidence of interface pinning was noticed), this Fe-Ni-C alloy showed no evidence of serrated interfaces. All the interfaces were either planar or smoothly curved.

During the later stage of transformation four distinct modes of carbide precipitation were noticed:

1. Precipitation on dislocations, (Fig. 9.4).
2. Interface precipitation, (Fig. 9.5).
3. Fibrous precipitation, (Fig. 9.12.)
4. Pearlite , (Fig. 9.9).

1. Precipitation on dislocations: It has long been known that dislocations can act as sites for the nucleation of new phases. Cahn[5] has developed a model to estimate the effectiveness of a dislocation as a catalyst for such nucleation. In his model, he assumes that the nucleus of the precipitate lies along the dislocation core and is incoherent with the matrix. The lack of coherency between the two phases allows the relaxation of the stresses caused by the dislocation within the volume of the precipitation. This relaxation is the driving force for the precipitation on the dislocation. Formation of coherent precipitates on dislocations has also been reported[6]. In the present investigation, the carbides that formed on the dislocations were probably incoherent , since they did not give any strain-contrast[7].

2. Interphase-precipitation: In the absence of carbide forming elements like V, Ti, Cr, etc., it is possible for cementite to precipitate by an interphase-precipitation mechanism. Interphase-precipitation of cementite in Fe-C alloys has been previously reported[8, 9]. However in presence of carbide forming element, its precipitation at the advancing γ/α interface is replaced by alloy carbides. That is why in the case of steels containing carbide forming

elements, cementite is never reported to form at the advancing γ/α interface. The mechanism of interphase precipitation is discussed in the Chapter II.

3. Fibrous precipitation of cementite:- Fibrous precipitation of cementite in steel has never been reported earlier. Fibrous precipitation is similar to interphase precipitation in so far as it nucleates at the γ/α interface, but continues to grow in the direction of growth of the interface.

Whereas the interfaces for interphase-precipitation have a low interfaceal energy, the interfaces at which fibrous growth occurs are usually curved and of high energy. While the planar interfaces move by the ledge mechanism, the high energy curved interfaces move by unco-ordinated jumps of atoms across the interface. It is reported that the alloying elements which slow down the $\gamma \rightarrow \alpha$ transformation, increase the proportion of fibrous carbides. For example Mn & Ni addition lead to a higher volume fraction of fibrous type carbides.[10, 11] This result indirectly suggests that additions of Mn or Ni increase the proportion of incoherent interfaces which in turn favours the nucleation of fibrous carbides particularly at lower temperatures where the transformation is slowed down. This is consistent with the results obtained on isothermal transformation at 650°C.

Although in the present case, detailed crystallographic analysis has not been done due to lack of ability to retain the austenite at room temperature, the earlier workers[12, 13] have shown that the ferrite associated with fibrous carbide did not have a rational-orientation-relationship with adjacent austenite. But in the case of interphase precipitation the carbides are related to the ferrite either by K-S relationship[14] or Baker - Nutting relationships[15]. These carbides are also found to have a cube-cube relationship with the austenite.

4. Formation of pearlite: In addition to precipitation on dislocations, interphase and fibrous carbide precipitation, the formation of pearlite was also noticed. (Fig. 9.9). A full description of the mechanism of nucleation and growth of pearlite is beyond the scope of present investigation. However, it was generally noticed that the nucleation of pearlite nodules occurred at the prior austenite grain-boundaries. Pearlite is also found to nucleate on pro-eutectoid ferrite or cementite.

TTT Curve: Figure 9.1 shows the calculated TTT curve along with the experimentally (optically) determined TTT curve. Reasonable agreement was achieved at low undercoolings (i.e. at 700°C and 680°C) but at lower temperatures, (i.e. at 650°C & 600°C) the disagreement was significant. At

650°C, a bay in the TTT diagram was recorded, but the theoretically calculated TTT curve shows a bay at around 600°C. Such a bay in the TTT diagram is sometimes attributed to the solute-drag effect. However, the bay in the TTT diagram has been reported to occur due to two separate mechanisms.[1] The upper 'C' curve represents the diffusional transformation while the lower one represents the diffusionless transformation. Figure 9.1b also shows the TTT curve obtained by Shiflet et al.[16] Their TTT curve did not show any bay. Probably they might have missed the temperature at which the bay occurs. The reason for the lack of detailed agreement between experimental and calculated values can be understood on the basis of microstructural evidence. The ferrite which formed at higher temperatures was free of cementite, but not always at lower temperatures.

The calculations used for constructing TTT curves do not allow for effect of carbide formation on driving force. This may be the reason for discrepancies in the results where carbide precipitation was observed. The details of TTT calculation are discussed in the Appendix 1.

9.4 Conclusions

1. Good agreement was achieved between the experimentally determined parabolic growth-rate constants and theoretically calculated values based on the paraequilibrium model for diffusion-controlled growth for the temperature range of 700°C to 600°C (Fig. 9.13).

2. The $\gamma \rightarrow \alpha$ transformation always started at austenite grain-boundaries. The heterogeneous nucleation of the allotriomorphic ferrite at these boundaries is preferred because the nucleation of α at these heterogeneous sites results in significant decrease in the activation energy barrier required for nucleation. It also leads to an overall decrease in the surface energy by eliminating part of the grain boundary surface area.

3. Except at 650°C, the $\gamma \rightarrow \alpha$ transformation started with the formation of clean ferrite. However, during the later stages of transformation four distinct modes of carbide precipitation were noticed. These include precipitation on dislocations, interphase-precipitation, fibrous carbide precipitation and pearlite.

4. The theoretically calculated TTT curves matched well with the experimentally experimentally determined TTT curve at low undercoolings (i.e. at 700°C and 680°C). However, at lower temperatures (i.e. 650°C and 600°C) the agreement was poor. The reasons for disagreement have been discussed on the basis of available microstructural observations. It is believed that the formation of carbide

along with the ferrite alters the thermodynamic conditions and hence affects the result adversely.

TABLE 9.1

$$V\alpha = 1-e^{-kt^n}$$

Temp °C	n
600°C	1.66
650°C	2.00
680°C	2.12
700°C	2.4

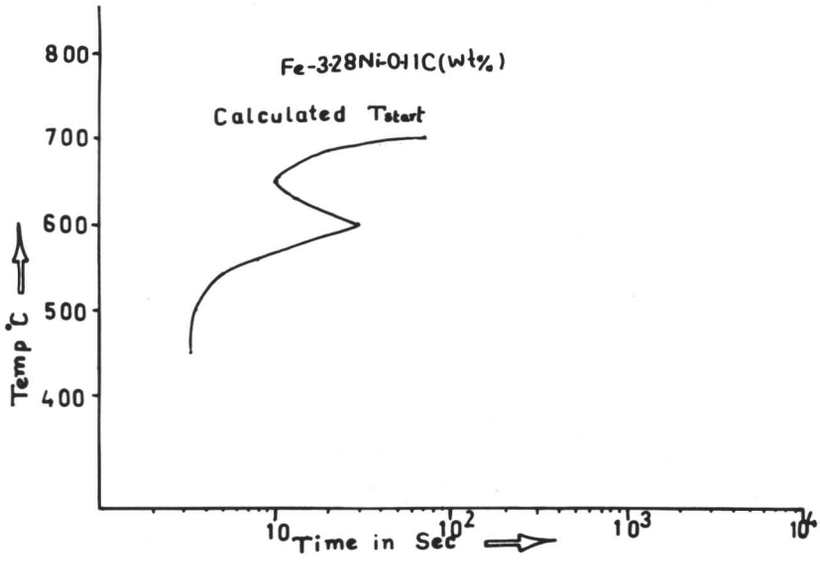

Figure 9.1a: Calculated TTT curve for start of transformation in Fe-3.28Ni-0.11C (wt%) alloy.

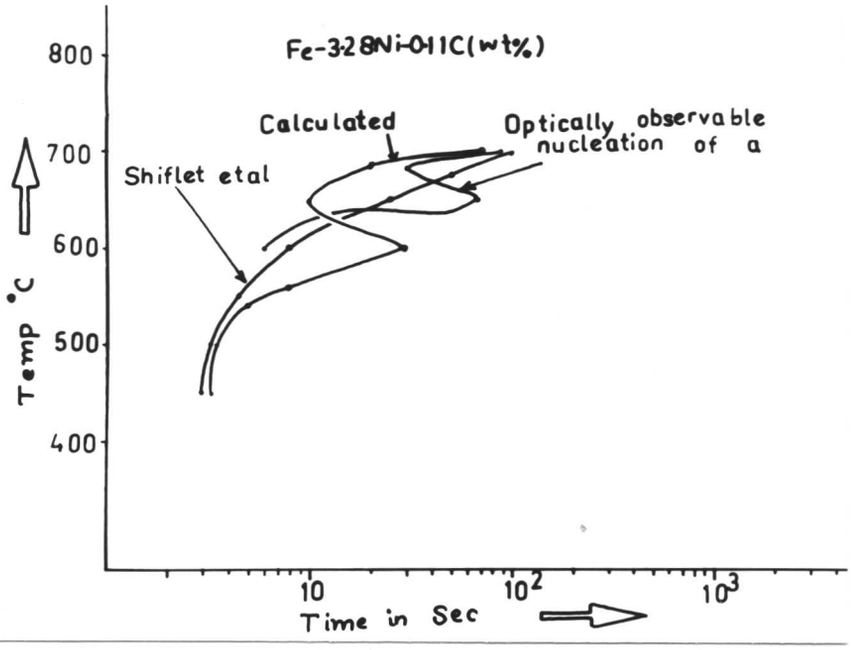

Figure 9.1b: Calculated TTT curve compared with experimentally determined TTT curve.

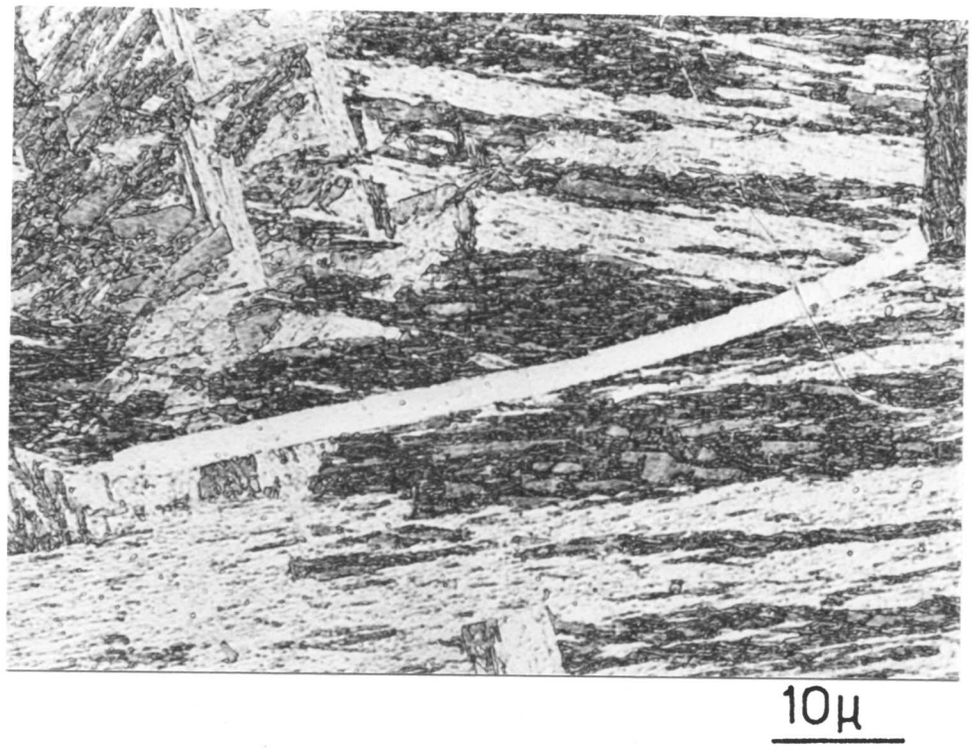

Figure 9.2: Grain-boundary allotriomorphic ferrite showing high aspect ratio. It is also virtually free of carbides (700°C/90 sec).

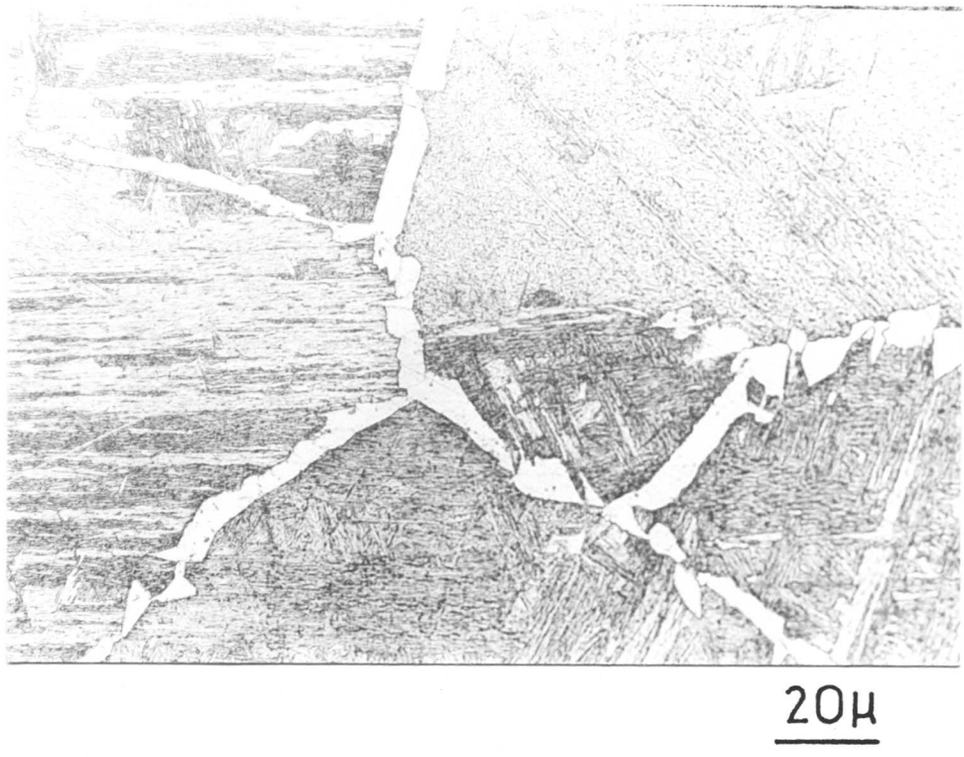

Figure 9.3: Network of allotriomorphic ferrite along the prior austenite grain-boundaries. (700°C/4 min).

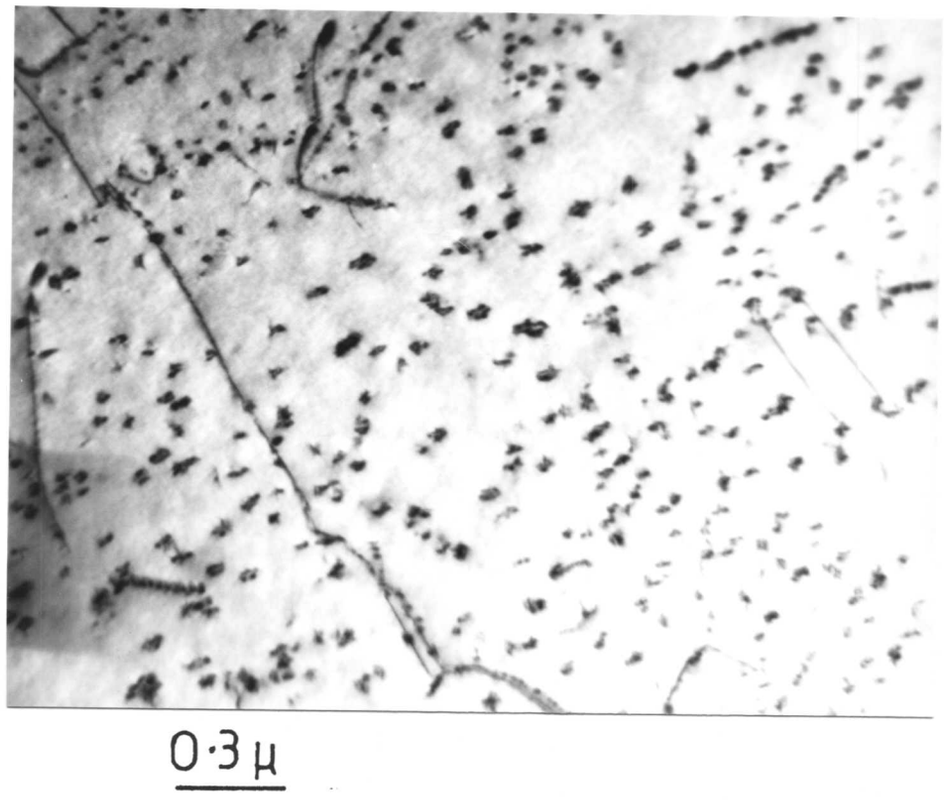

Figure 9.4: Precipitation of cementite on dislocations. (700°C/2 hrs).

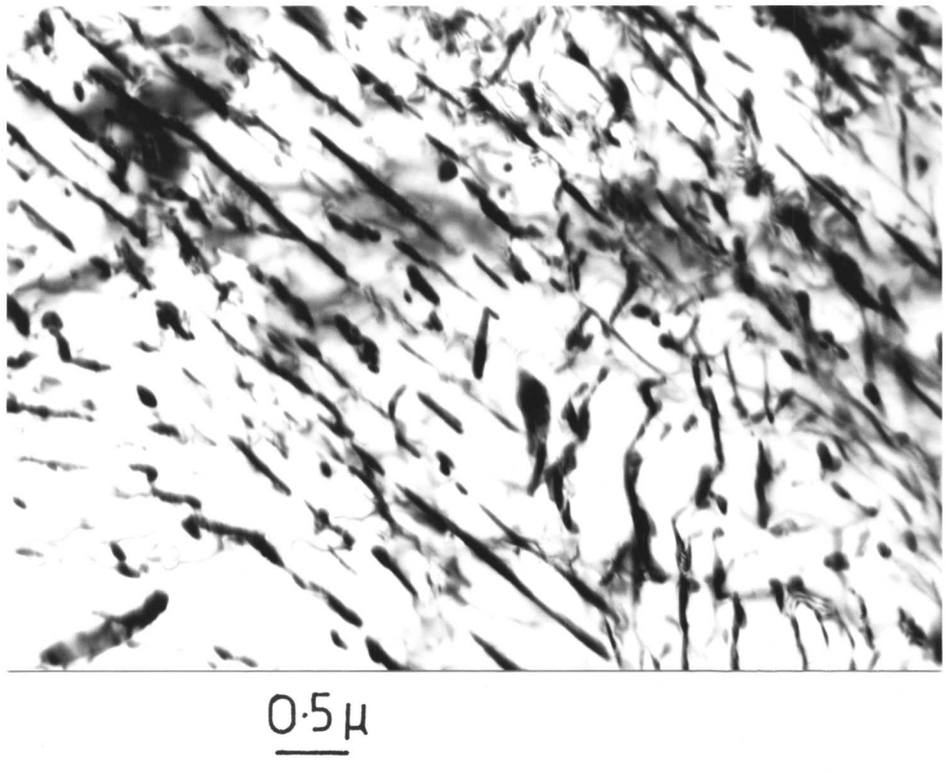

Figure 9.5: Cementite possibly formed by interphase-mechanism. (700°C/2 hrs).

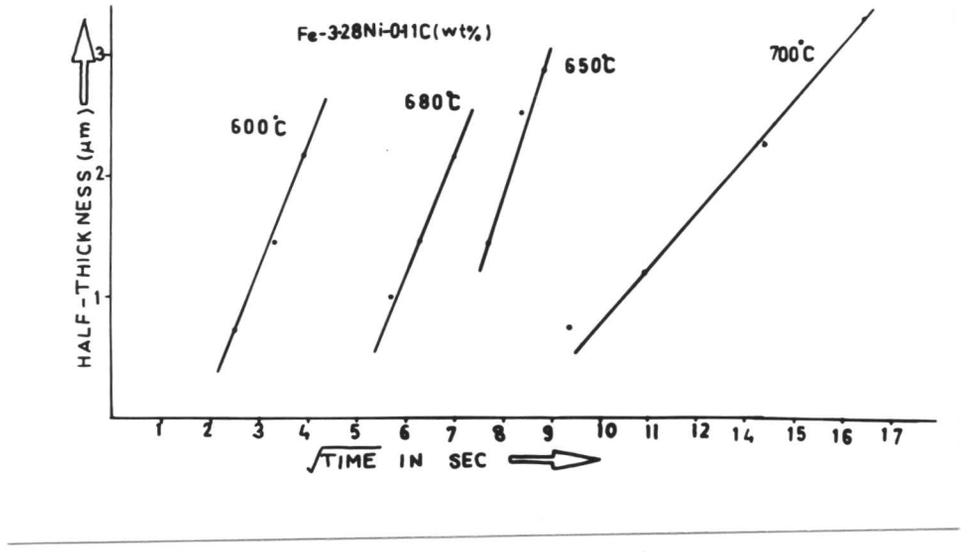

Figure 9.6: Plot of half thickness of ferrite vrs square root of time.

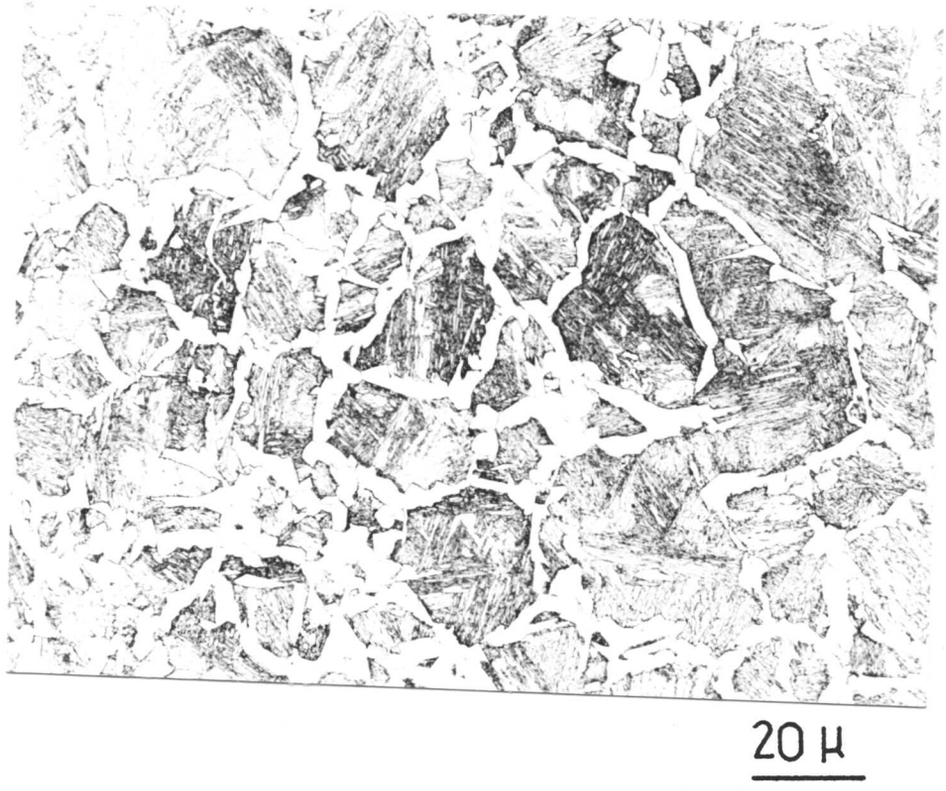

Figure 9.7: Net-work of allotriomorphic ferrite along prior austenite grain-boundaries (680°C/50 sec).

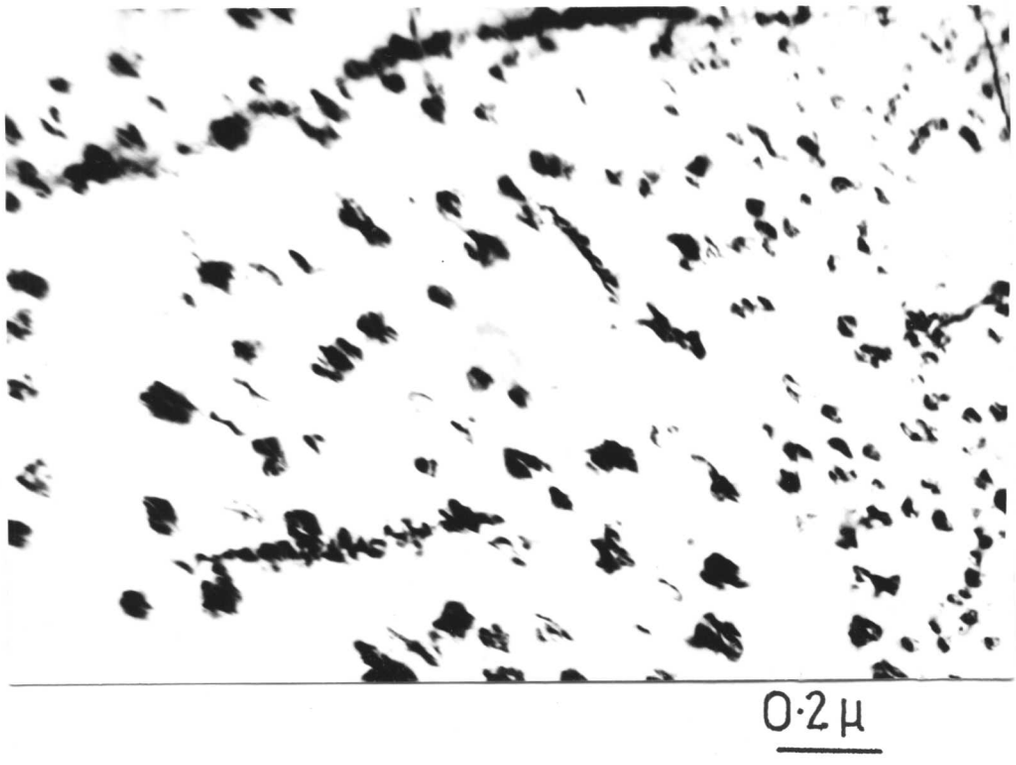

Figure 9.8: Precipitation of cementite on dislocations within the ferrite.

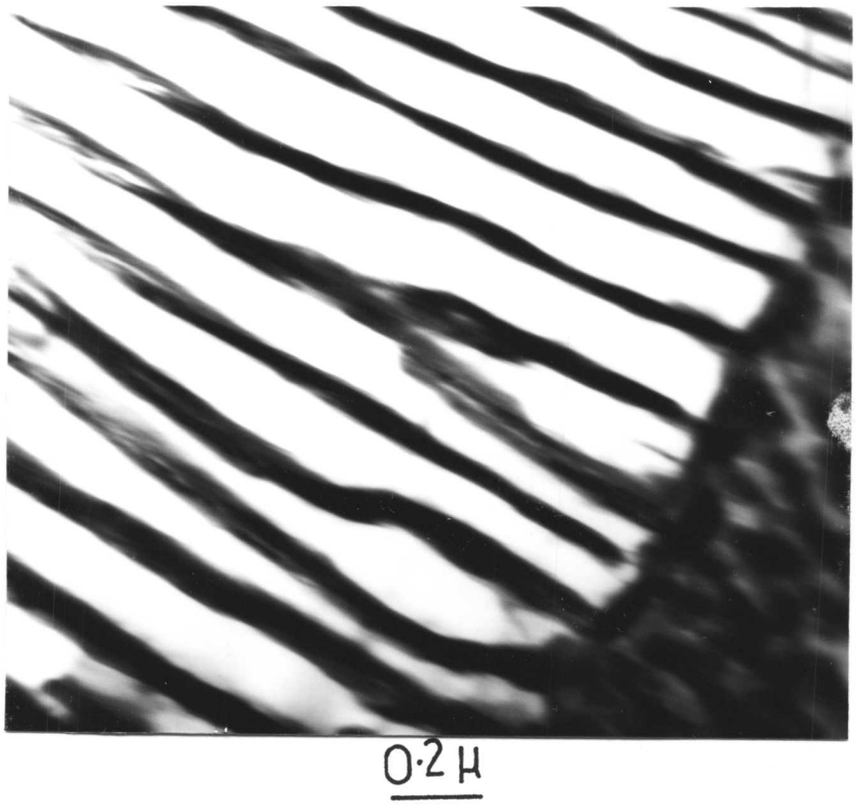

Figure 9.9: Pearlitic structure

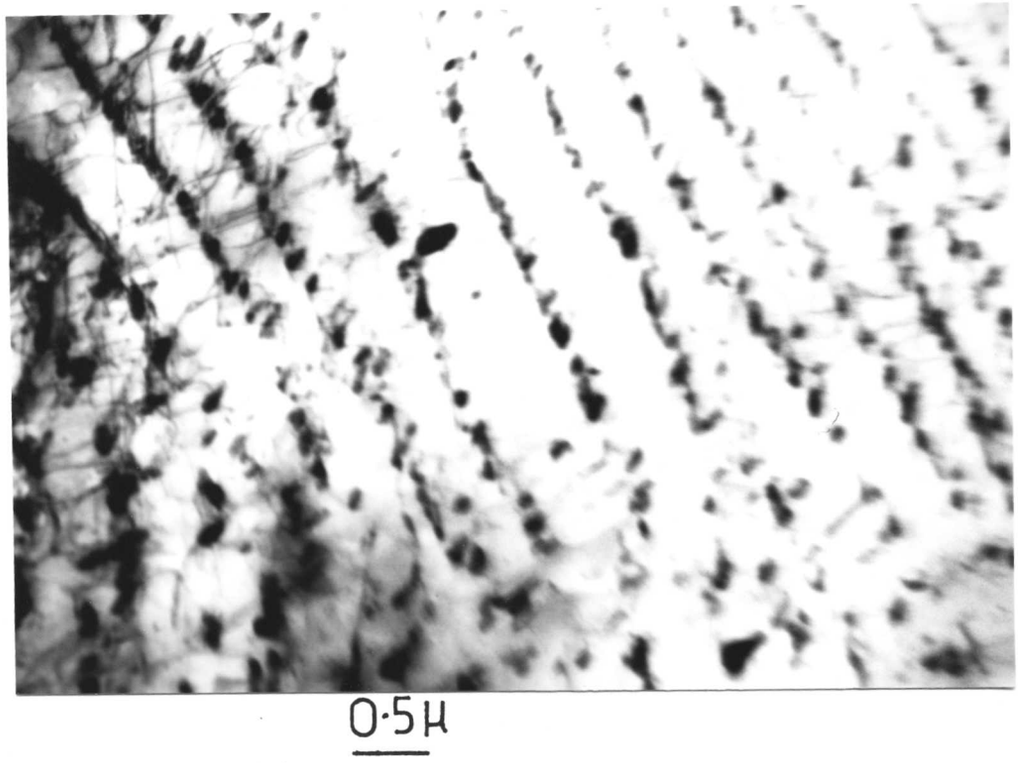

Figure 9.10: Precipitation of cementite by interphase mechanism.

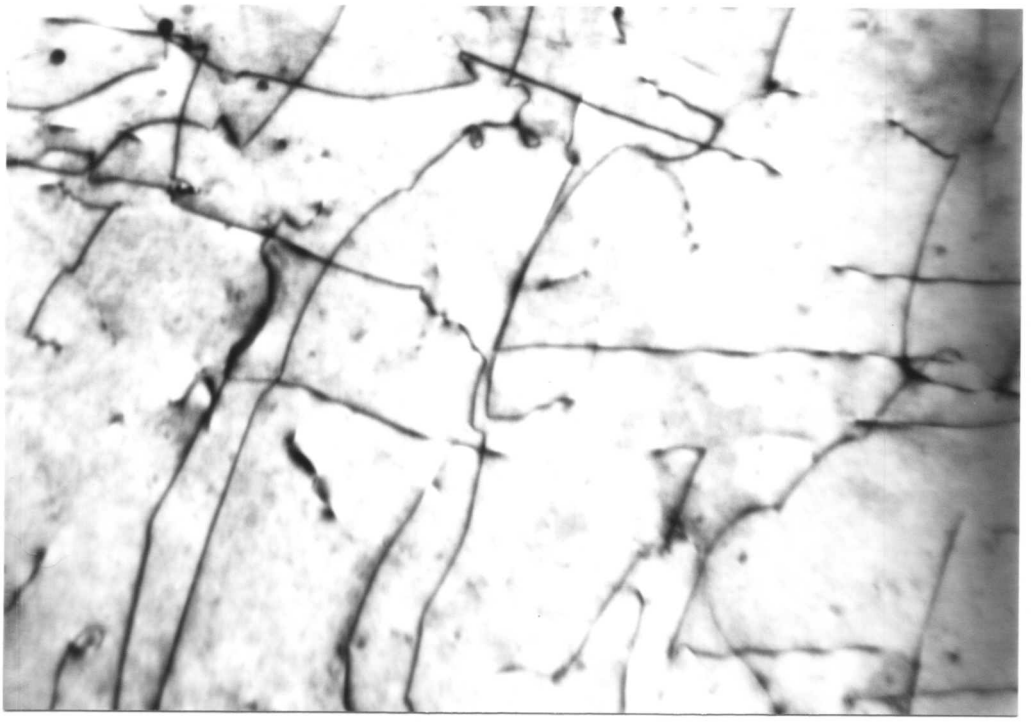

Figure 9.11: Precipitation of cementite on dislocations.

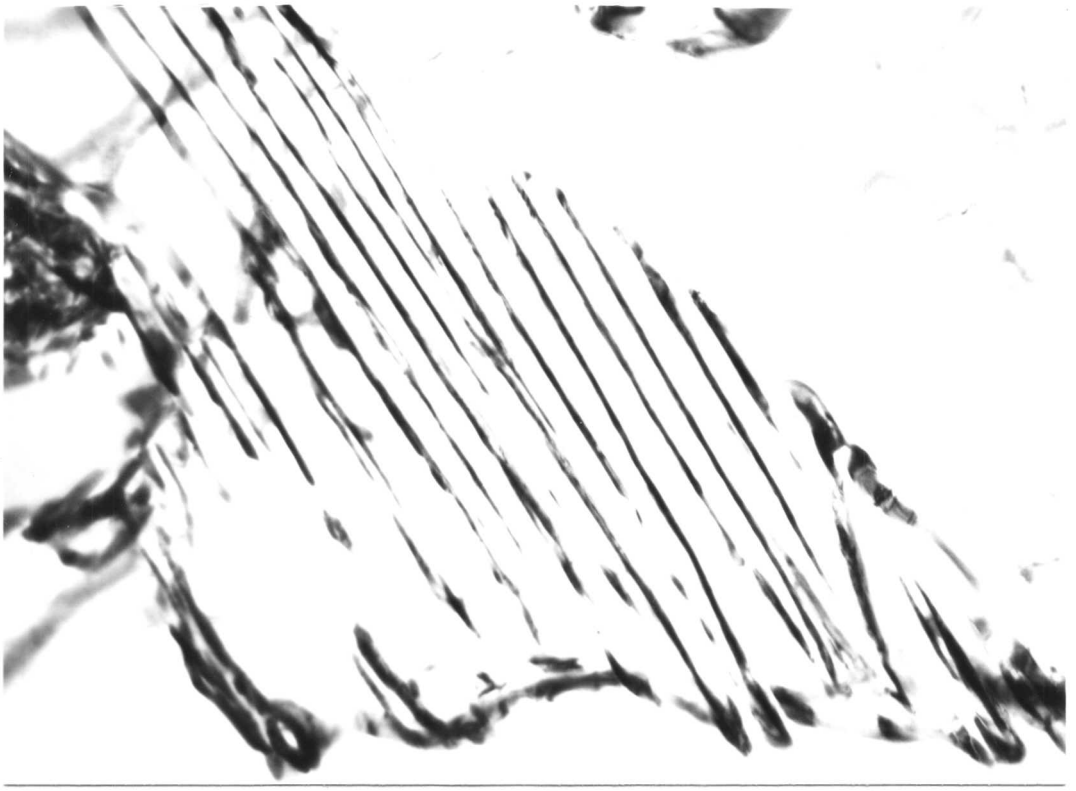

Figure 9.12: Precipititation of cementite in fibrous mode.

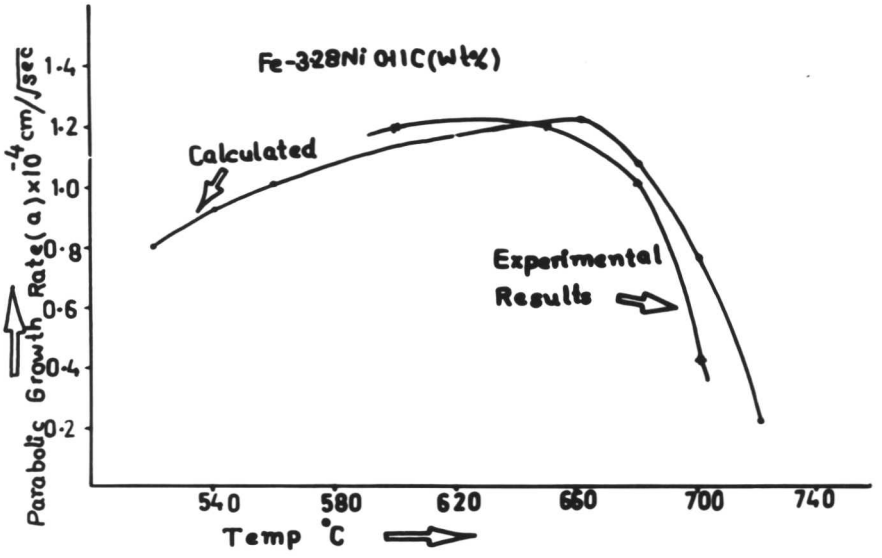

Figure 9.13: Plot of parabolic growth rate constant vrs temperature.

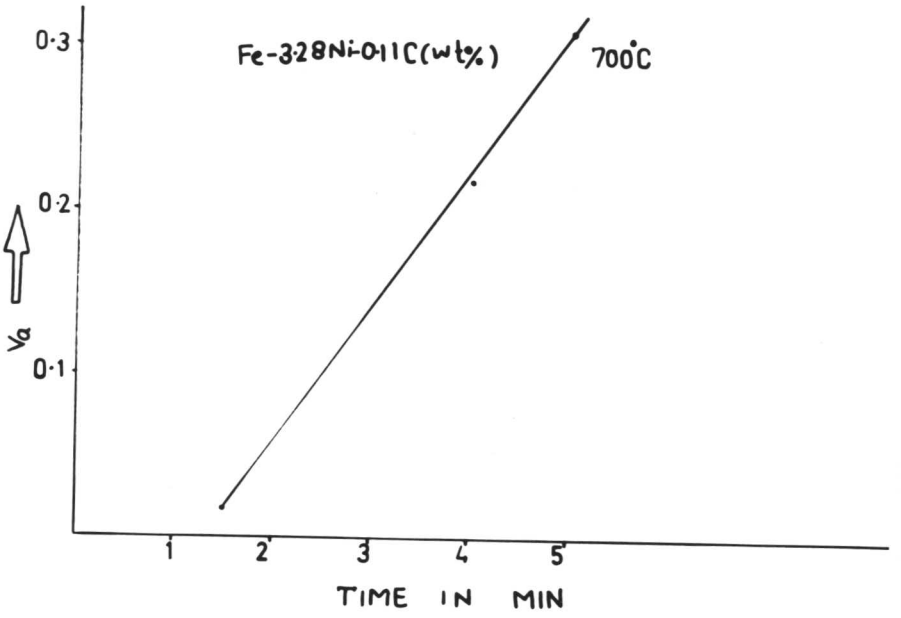

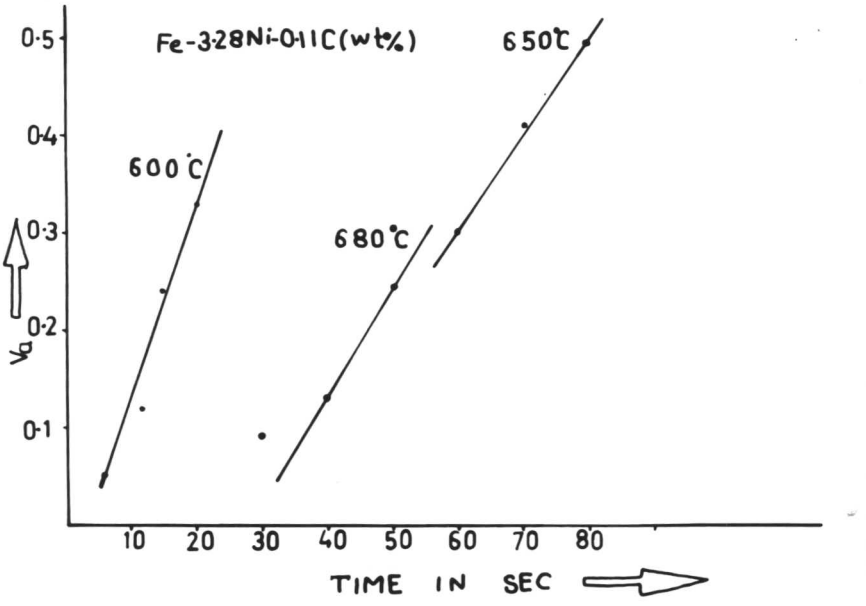

Figure 9.14a and b: Volume fraction of ferrite against time is plotted.

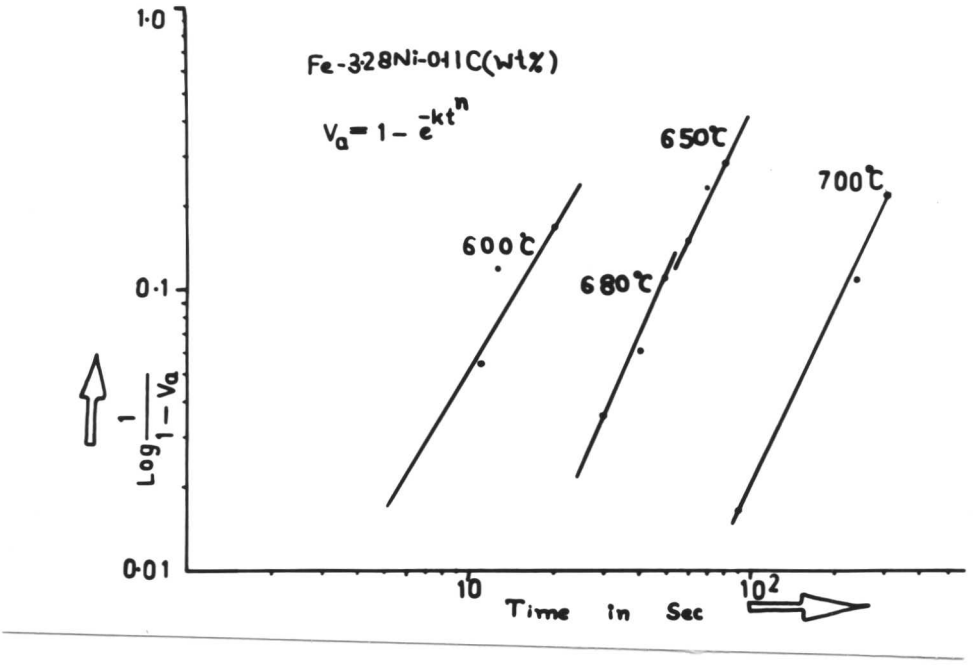

Figure 9.15: Plot of log log $\frac{1}{1-V\alpha}$ vrs log t, this is also known as Avrami's plot.

CHAPTER X

CONCLUSIONS AND SUGGESTIONS FOR FUTURE WORK:

10.1 Conclusions:

1. Silicon has a pronounced effect on enhancing interphase precipitation at high transformation temperatures. It expands the α-phase field and lowers the solid solubility of the carbides in ferrite. In addition, it has a strong tendency towards developing a high proportion of γ/α semi-coherent interfaces which move by a ledge mechanism. It can be anticipated that these factors may combine to enhance interphase precipitation in Fe-5.5W-2.03Si-0.37C (wt%) alloy. Silicon also accelerates the kinetics of the γ → α transformation.

2. Interphase precipitation is not only limited to the less mobile semi-coherent γ/α interfaces but it can also occur on more mobile ledges. This directly contradicts the hypothesis proposed by Honeycombe. According to his hypothesis, the high mobility of the ledges provides least opportunity for nucleation to occur there. Consequently nucleation takes place on less mobile semi-coherent interfaces.

3. Ledges may vary in height even at the same temperature and this variation may be an order of magnitude. The variation in ledge height occurs as a result of ledge multiplication during the transformation. However, some workers have reported that the ledge height depends upon the temperature and alloy composition. And it increases with increasing temperature.

4. Frequent evidence of cusps on semi-coherent low energy interfaces was noticed at the highest transformation temperatures. These cusps are developed as these interfaces move across the carbides during the transformation. Presence of cusps on low energy facets led to the view that these interfaces have moved normal to it in a way similar to that of incoherent interfaces. This contradicts the classical view the magnitude of the critical driving force required to move low energy facets is so high that it is never achieved in practice.

5. The alloy with the same chemical composition but without silicon showed a tendency to contract the α-phase field. Random dispersion of tungsten carbide was frequently observed in this alloy. The volume fraction of these carbides was found to increase with decreasing temperature. These carbides has formed from super-saturated ferrite or interphase precipitation at the incoherent γ/α interface.

6. Pinning of the incoherent as well as semi-coherent interface was recorded at all temperatures of transformation in Fe-5.8W-0.4C (wt%) alloy. The morphology of the γ/α interface appeared serrated as well as ragged. Serrated interface indicates that the pinning has occurred due to interphase carbide precipitation at the incoherent γ/α interface. Protuberances on the interface developed as the γ/α moved across the carbide particles present in the austenite. Interphase precipitation was less pronounced in this alloy.

7. When the carbon content is reduced from 0.4 to 0.23C wt% keeping the tungsten content the same, the α-phase field is expanded (Chapter V). The kinetics of the $\gamma \rightarrow \alpha$ transformation are accelerated by reducing the carbon level of the alloy. The ferrite formed during the early stage of transformation was found to be virtually free from carbides. No evidence of interphase precipitation was noticed in this alloy during the early stage of transformation. However, during the later stage of transformation at 850°C, the carbide precipitation started at the α/γ interface but appeared to grow in austenite. The sequence of the reaction that occurred at 850°C can be represented by

$$\gamma \rightarrow \alpha + \gamma_1 \rightarrow \alpha + M_6C + \gamma_2 \rightarrow \alpha + M_6C$$

A small addition of titanium (0.14 wt%) (i.e. Fe5.9W-0.14Ti-0.21C (wt%)) showed a dramatic effect on suppressing the kinetics of transformation in Fe-W-C alloys in the temperature range of 700°C-900°C.

8. The transformation characteristics of Fe-5W-2.3Si-0.15C wt% alloy is compared with that of Fe-5W-0.23C wt% alloy (Chapter V and VI). The alloy containing silicon again shows the tendency towards accelerating the interphase precipitation at the highest transformation temperature (850°C). But at lower transformation temperature (700°C), fine dispersion of alloy carbides is noticed within the α-ferrite. These fine dispersions of alloy carbides are formed from supersaturated ferrite and not by interphase mechanism. These carbides are surrounded by a PFZ within the ferrite grain.

It is also noticed that a grey rim appeared at the γ/α interface but grew in the austenite. With increasing time, the grey rim grew in size to consume the whole austenite grain. Occasionally a dark etched region appeared ahead of the growing rim. Optically no information could be obtained concerning the microstructural constituents of the growing grey area. But transmission electron microscopy revealed that it contains fine particles of carbides along with some coarse carbides. Microstructural features of this rim are similar to those observed in many discontinuous reactions. It is interesting to note that the reaction has occurred during the later stages of transformation. No such observations are recorded in the case of alloys containing no silicon. The rate of transformation at all temperatures (850°C - 700°C) is enhanced by the addition of silicon. The α-phase field is expanded and the solubility of carbides in the α-ferrite is greatly reduced by the addition of silicon. A high proportion of facetted low energy interface is also noticed at all transformation temperatures.

8. Rare evidence of Widmanstätten ferrite was noticed for transformations in the temperature range of 850°C - 700°C. During the early stages of transformation, ledges appeared frequently in all the alloys, but this frequency of ledges appeared more in alloys containing silicon.

9. The $\gamma \rightarrow \alpha$ transformation started at the austenite grain-boundary and grew along it to form allotriomorphs. The aspect ratio of these allotriomorphs increased with decreasing transformation temperature. These phenomena were observed in all the alloys investigated.

10. Formation of tungsten carbide (WC/M_6C) along the prior austenite grain-boundaries by pre-precipitation led to drastic drop in nucleation rate at low undercoolings (i.e. 800°C). Pre-precipitation induces the formation of copious precipitates of tungsten carbides along the austenite grain-boundaries. Presence of these carbides on active nucleation site are held responsible for dramatic drop in nucleation rate of α (Fig. 7.4 Chapter V).

11. The growth kinetics were studied in Fe-C-X alloys (Chapter VIII & Chapter IX). The nickel steel (i.e. Fe-3.28Ni-0.11C (wt%)) showed a good agreement between the experimentally determined growth rate and theoretically calculated value based on para-equilibrium model for diffusion controlled growth in the temperature range of 700°C to 600°C (Fig. 9.13). But in case of chromium steel, the agreement was rather poor. The discrepancies in our results have been attributed to the presence of facetting, solute-drag-like

effect, pinning of the γ/α interface by carbide; interaction of clusters with interfaces and stereological error.

10.2 Suggestions for Further Work

1. It is essential to examine the precise role played by silicon during the transformations at various transformation temperatures in Fe-C-X alloys.

2. A theoretical analysis concerning the effect of silicon on solid-solubility product will be helpful in understanding the complex nature of carbide precipitation.

3. To develop a model to calculate the critical driving force required to move the semi-coherent interface as a function of alloy composition.

4. Mechanisms of ledge nucleation as a function of temperature and alloy composition are needed to understand the mobility of the semi-coherent γ/α interface.

5. A model like Orowan bowing mechanism, is required to study the effects of pinning on the mobility of the γ/α interface. Such a model will be helpful in understanding the growth kinetics in steels contianing carbide forming elements like (Ti, Cr, Nb, W, Mo, etc).

6. To develop an expression to calculate the activation energy of nucleation at the γ/γ grain-boundary and at the carbide/austenite boundary as a function of temperature.

7. High resolution microanalysis in Fe-C-X alloys is need to establish the exact mode of growth (i.e. PE or NPLE) over a range of isothermal temperature.

8. It is essential to study the effect of alloying element on the morphology of the allotriomorphic ferrite as a function of temperature.

APPENDIX I

CALCULATIONS USED FOR CONSTRUCTING TTT DIAGRAMS:

Bhadeshia[1] developed a thermodynamic model to predict the isothermal transformation diagrams simply from a knowledge of the chemical composition of the steel. This model utilizes Russell's theory[2, 3] for calculating the incubation periods normally associated with TTT diagrams (i.e. the time period before the onset of a detectable amount of isothermal transformation, t_s). The incubation period (t_s), for nucleation at grain boundaries can be expressed[2, 3] as

$$t_s = \frac{T}{(\Delta F_m^v)^p D} \qquad \text{(A.1.1)}$$

where T = Absolute temperature.

D = An effective diffusion coefficient related to boundary or volume diffusion, depending on the coherency state of the nucleus concerned.

ΔF_m^v = the maximum volume free energy change accompanying the formation of a nucleus in a large amount of matrix phase.

p = An exponent whose magnitude is a function of the nature of the nucleus. Russell obtained p = 2 for coherent nucleus and p = 3 for an incoherent one.

The effective diffusion coefficient (D) is expressed in terms of entropy (s) and enthalpy (Q) for diffusion[4] as follows:

$$D \propto \exp(S/R) \exp(-Q/RT) \qquad \text{(A.1.2)}$$

Substituting this value of D in equation A.1.1, and multiplying ΔFm^v by the molar volume of ferrite, we get

$$\text{In} \left[(\Delta F_m^v)^p \, t_s/T \right] = Q/(RT) + C_1 \qquad \text{(A.1.3)}$$

where C_1 is a constant.

The numerical value of the chemical free energy change (ΔFm) accompanying the formation of 1 mole of nucleating phase in a large amount of matrix phase can be estimated as follows using the principle of parallel tangent construction[5] (Fig. A.1.1)

$$\Delta F_{Fe}^{\gamma \rightarrow \alpha} + RT \ln \frac{a_{Fe}^{\alpha}(1-C)}{a_{Fe}^{\gamma}(1-\bar{C})} - RT \ln \frac{a_{C}^{\alpha}(C)}{a_{C}^{\gamma}(\bar{C})} = 0 \quad \text{(A.1.4)}$$

$$\Delta F_{m} = RT \ln \left[\frac{a_{C}^{\alpha}(C_{m})}{a_{C}^{\gamma}(\bar{C})} \right] \quad \text{(A.1.5)}$$

where $a_{Fe}^{\alpha}(1-C)$ refers to the activity of iron in ferrite evaluated at the concentration $(1-C)$ and a similar rationale applies to the other activity terms. The term $\Delta F_{Fe}^{\gamma \rightarrow \alpha}$ refers to the free energy change accompanying the austenite - ferrite transformation in pure iron and R is the gas constant. The term $\bar{C}$ is the average carbon concentration of the steel concerned and C_m represents the composition of ferrite which satisfies equation (A.1.4).

The ideal nucleus composition is obtained by iteratively solving equation (A.1.4). The value of ΔF_{m}^{v} is obtained by substituting the nucleus composition in equation (A.1.5).

For alloy steels, the first term of the equation (A.1.4) is replaced by

$$\Delta F_{Fe}^{\gamma \rightarrow \alpha}\left\{ T - 100 \sum_{i} Y_i \Delta T_{magi} \right\} + 141 \sum_{i} Y_i (\Delta T_{magi} - \Delta T_{nmi})$$

where the terms in the curly brackets are to be interpreted as the arguments of the function $\Delta F_{Fe}^{\gamma \rightarrow \alpha}$. Y_i is the mole fraction of the ith substitutional alloying element and ΔT_{magi} and ΔT_{nmi} are the displacements in the temperature at which the free energy change accompanying the austenite - ferrite in pure iron is calculated, in order to account for the changes in the magnetic and non-magnetic components of $\Delta F_{Fe}^{\gamma \rightarrow \alpha}$ respectively.

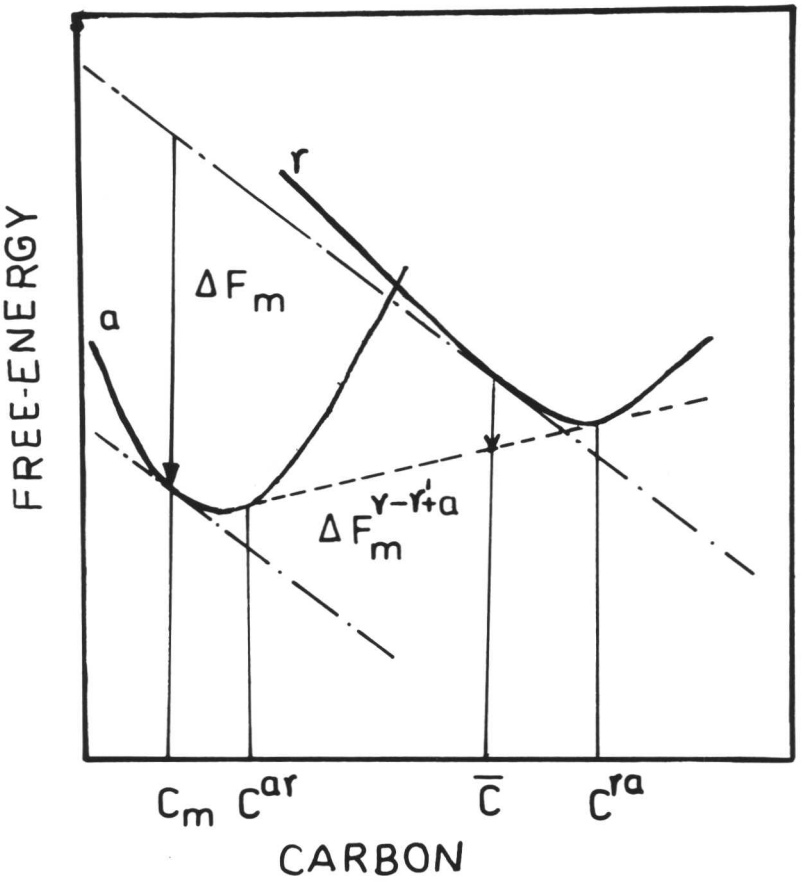

Figure A1.1: Schematic diagram showing free energy change during the $\alpha \rightarrow \gamma$ transformation.

APPENDIX II

A REVIEW ON THERMODYNAMICS OF DIFFUSIONAL DECOMPOSITION OF AUSTENITE:

In the present section, it has been tried to review in brief the thermodynamic analysis of diffusional decomposition of austenite. Such analysis are often vital importance to the metallurgist. Not only it provides with a better understanding of the factors influencing the transformation characteristics but also leads to precise assessment of the data needed in such studies. Within the past decade noteworthy progress has been achieved in developing more refined thermodynamic analysis.

Zener[1] using the thermodynamics of interstitial solid solution developed relationships for thermodynamic quantities of interest in the austenite → ferrite transformation. He assumed an ideal value of the positional entropy of carbon in austenite as well as ferrite. Although this method is less accurate than those developed later on, it turns out to be the only one presently feasible for a study of the influence of alloying elements upon the thermodynamics of the proeutectoid ferrite reaction. Subsequently Zener[2] realised the contribution of magnetic and non-magnetic component of pure iron towards change in free energy during $\gamma \rightarrow \alpha$ transformation. He also assumed that these components are affected by the alloying elements separately. For pure iron, the change in chemical free energy can be expressed as

$$\Delta F_{Fe}^{\gamma\rightarrow\alpha} = \Delta F_{FeNM}^{\gamma\rightarrow\alpha} + \Delta F_{FeMag}^{\gamma\rightarrow\alpha} \quad .. \quad .. \quad .. \quad .. \quad .. \quad .. \quad .. \quad .. \quad .. \quad \text{(A2.1)}$$

where $\Delta F_{FeNM}^{\gamma\rightarrow\alpha}$ and $\Delta F_{FeMag}^{\gamma\rightarrow\alpha}$ are the non-magnetic and magnetic components respectively of this free energy change. The non-magnetic component is free-dominant at temperatures below 600°C where $\Delta F_{FeMag}^{\gamma\rightarrow\alpha}$ is assumed to be negligible.

For Fe-X alloys, the equation developed[3] may be written as

$$\Delta F_{FeNM}^{\gamma\rightarrow\alpha} = 1.41\ (T - Y.\Delta_{NM}^{T} - 1013) \quad .. \quad .. \quad .. \quad .. \quad .. \quad .. \quad .. \quad .. \quad \text{(A2.2)}$$

where Y = atom per cent of X in either phase

ΔT = displacement in the temperature per atom per cent

The total free energy change for transformation of austenite to ferrite of the same composition in Fe-X alloys at temperature T is written as

$$\Delta F^{\gamma\to\alpha}{}^{1} = \Delta F^{\gamma\to\alpha}_{FeNM}\left[\ T-Y.\Delta T_{NM}\ \right] + \Delta F^{\gamma\to\alpha}_{FeMag}\left[\ T-Y.\Delta T_{Mag}\right] \quad .. \quad .. \quad .. \quad .. \quad (A2.3)$$

$\Delta T_{Mag} > \Delta T_{NM}$ for austenite stablizing elements and $\Delta T_{Mag} < \Delta T_{NM}$ for ferrite stablizing elements. For Fe-C-X alloys the total change in free energy without partioning of alloying elements or carbon may be written[3] as

$$\Delta F^{\gamma\to\alpha}{}^{1} = (1 - x_\gamma)\ \Big[\ 141y_\gamma\ (\Delta T_{Mag} - \Delta T_{NM}) + \Delta F^{\gamma\to\alpha}_{Fe}\ \Big(\ T - 100y_\gamma\ \Delta T_{Mag}\Big) +$$

$$x_\gamma\ (K-RT\ \ln\ 3)\Big] \quad .. \quad .. \quad .. \quad .. \quad .. \quad .. \quad .. \quad .. \quad .. \quad .. \quad .. \quad (A2.4)$$

where K = Free energy to transfer 1 mole of carbon from asutenite to ferrite = 9373 cal per mole[4].

y_γ = Mole fraction of X in austenite.

x_γ = Mole fraction of carbon in austenite.

The temperature at which austenite and ferrite of the same composition are in metastable equilibrium is commonly termed as T_o. It is obtained by employing the condition $\Delta F^{\gamma\to\alpha} = 0$ and solving for x_γ as a function of temperature by trial and error.

So far it has been possible to evaluate $\Delta F^{\gamma\to\alpha}$ and To for pure iron, Fe-X and Fe-X-C alloys using the original concept of Zener. However, there are other alternate approachs based on the standard chemical thermodynamic expression for evaluation of $\Delta F^{\gamma\to\alpha}$ and T_o These models differ from each other in the way the emperical relationship for a_γ and a_{Fe_γ} are substituted in the following expression:

$$\Delta F^{\gamma\to\alpha} = RT\ \left[\ x_\gamma\ \ln\ \frac{a^{\gamma\alpha}_\gamma}{a_\gamma} + (1-x_\gamma)\ \ln\ \frac{a^{\gamma\alpha}_{Fe_\gamma}}{a_{Fe_\gamma}}\ \right] \quad .. \quad .. \quad .. \quad .. \quad .. \quad (A2.5)$$

Bhadeshia et al[5, 6] recently developed an expression to evaluate 'T_o'. He assumed that the carbon content of ferrite equals that of the austenite at T_o. He also consider the Zener ordering[7] while developing expresssion for 'T_o'. These assumptions yield :

$$\Delta F^{\gamma\to\alpha} = 2xRT \ln x + x(\Delta\bar{H}_\alpha - \Delta\bar{H}_\gamma - (\Delta S_\alpha - \Delta S_\gamma)T + 4w_\alpha - 6w_\gamma)$$

$$- 4RT(1 - x)\ln(1 - x) + 5RT(1 - 2x)\ln(1 - 2x)$$

$$- 6RTx \ln \frac{\delta_\gamma - 1 + 3x}{\delta_\gamma + 1 - 3x} - 6RT(1 - x)\ln \frac{1 - 2\tau_\gamma + (4\tau_\gamma - 1)x - \delta}{2\tau_\gamma(2x - 1)}$$

$$+ 3RTx \ln(3 - 4x) + 4RTx \ln \frac{\delta_\alpha - 3 + 5x}{\delta_\alpha + 3 - 5x}$$

$$+ (1 - x)\left[141\sum_i Yi\Delta T_{Mag} - \Delta T_{NM}) + \Delta F^{\gamma\to\alpha}\left(T - 100\sum_i Yi\Delta T_{Mag}\right)\right] \div \Delta f^* \quad .. \quad (A2.6)$$

where $\delta_\alpha = \left[9 - 6x(2\tau_\alpha + 3) + (9 + 16\tau_\alpha)x^2\right]^{\frac{1}{2}}$

$\delta_\gamma = \left[1 - 2(1 + 2\tau_\alpha)x + (1 + 8\tau_\gamma)x^2\right]^{\frac{1}{2}}$

$\tau_\alpha = 1 - \exp(-w_\alpha/RT)$

$\tau_\gamma = 1 - \exp(-w_\gamma/RT)$

$\Delta\bar{H}_\alpha = 112212 \text{ J mole}^{-1}$

$\Delta S_\alpha = 51.5 \text{ J mole}^{-1} \text{ K}^{-1}$

$\Delta\bar{H}_\gamma = 38575 \text{ J mole}^{-1}$

$\Delta S_\gamma = 13.48 \text{ J mole}^{-1} \text{ K}^{-1}$

Based on this method, T_o temperature has been calculated for the Fe-C-X alloy used for study of growth kinetics of ferrite. The T_o - x curve is ploted for each alloy and represented in Fig A.2.1. In solving the equation (A2.6), Δf^* = Energy term due to Zener order is evaluated as in Ref[7], w_γ is calculated using ref[8, 9], w_α from ref[10, 11]. The value of $\Delta\bar{H}_\alpha$, ΔS_α, $\Delta\bar{H}_\gamma$ and ΔS_γ are obtained from ref 11 and ref 8 respectively.

Similarly the equation for Ae'_3 (transformation without partioning) is given[8] by

$$141\sum_i Yi(\Delta T_{Mag} - \Delta T_{NM}) + \Delta F^{\gamma\rightarrow\alpha}\left(T - 100\sum_i Yi\Delta T_{Mag}\right)$$

$$= 5RT\ \ln\left(\frac{1-x}{1-2x}\right) + 6RT\left[\ln\frac{1-2\tau_\gamma+(4\tau_\gamma-1)x - \sqrt{1-2(1+2\tau_\gamma)x+(1+8\tau_\gamma)x^2}}{2\tau_\gamma(2x-1)}\right] \quad \text{(A2.7)}$$

In evaluating equations (A2.6) and (A2.7), the values of $\Delta F^{\gamma\rightarrow\alpha}$ are obtained from ref 17. Both T_o and Ae'_3 are plotted vrs x and represented in Fig. A2.1.

Various nomenclature used in above equations are listed in table A2.1

TABLE A2.1

Nomenclature

a_{γ} = Activity of carbon in austenite

$a_{\gamma}^{\gamma\alpha}$ = Activity of carbon at $\gamma/(\alpha+\gamma)$ phase boundary.

$a_{Fe_{\gamma}}$ = Activity of iron in austenite.

$a_{Fe_{\gamma}}^{\gamma\alpha}$ = Activity of iron at $\gamma/(\alpha+\gamma)$ phase-boundary.

R = Gas constant.

T = Absolute Temperature.

$\Delta\bar{H}_{\alpha,\gamma}$ = Partial molar heat of solution of carbon in austenite.

$\Delta S\alpha,\gamma$ = Partial molar non-configurational entropy of solution in ferrite, austenite.

$w_{\alpha,\gamma}$ = Pairwise interaction energy between adjacent carbon atoms in ferrite, austenite.

Y_i = Mole fraction of substitutional alloying element in austenite or ferrite, disregarding the presence of carbon.

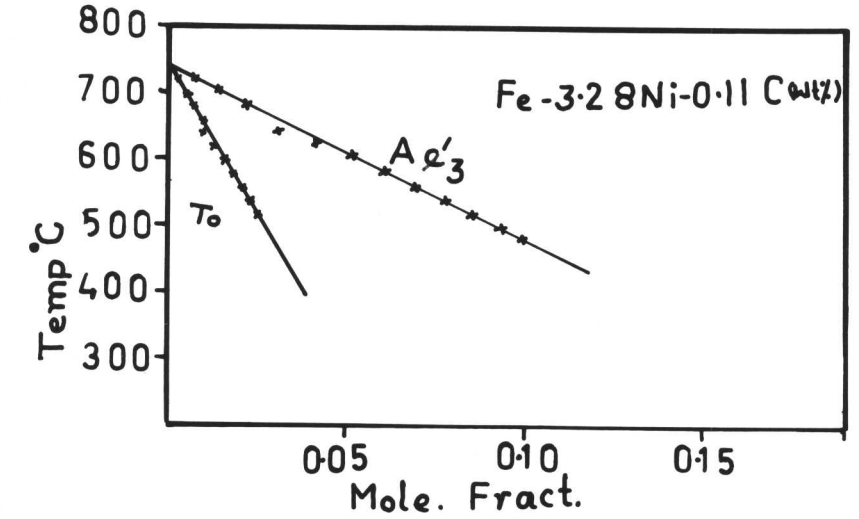

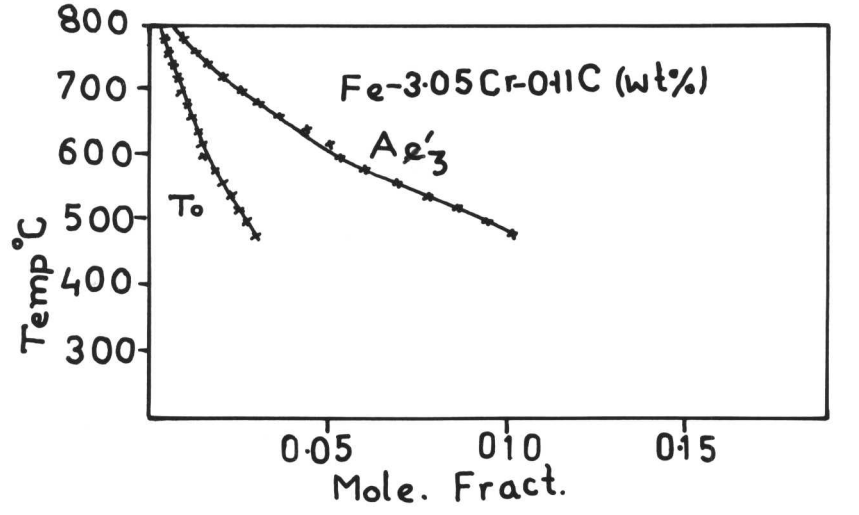

Figure A2.1: Plot of temperature vs carbon content in austenite.
(a) Fe-3.05Cr-0.11C (wt%).
(b) Fig-3.28Ni-0.11 (wt%).

APPENDIX III

NUCLEUS COMPOSITION

Study of the diffusion transformation requires a knowledge of nucleus composition. It is generally accepted that the composition of the nucleus can often be determined with the help of free energy vs composition diagram which may not necessarily represent the true composition of the nucleus during its early stage of development[1]. Gerlach[2] while working on Au-Ni alloy has found the precipitate containing higher Au-content at the beginning of precipitation than later. In order to explain why the nucleus will form with higher composition than the equilibrium, it is necessary to use the free energy diagram (Fig. A.3.1). Figure A.3.1 shows Gibbs free energy per mole for two phases (ferrite and austenite) in a Fe-C binary system. Suppose $\bar{x}$ represents the composition (i.e. carbon content) of the austenite phase (γ). Its free energy per mole is represented by the point O. The tangent at O gives the values of chemical potentials μ°_{Fe} and μ°_{C} for this composition. The chemical potential is defined by $\mu_{Fe} = dF/dn_{Fe}$ where F represents the Gibbs free energy of the specimen and n_{Fe} is the number moles Fe. Absolute chemical activity a_{Fe} can be obtained by the definition $\mu_{Fe} = RT \ln a_{Fe}$ .. ..(A3.1)

The free energy of the system can be decreased up to the point P provided it breaks up into one part of composition $x_{\gamma}^{\gamma\alpha}$ and another part of composition $x_{\alpha}^{\alpha\gamma}$. Thermodynamically the latter situation is more demanding and the nucleation of α is expected to occur with equilibrium composition $x_{\alpha}^{\alpha\gamma}$. Unfortunately formation of nucleus with equilibrium composition $x_{\alpha}^{\alpha\gamma}$ is highly unlikely[3] in presence of the surface tension as well as the strain energy involved in the nucleation of α. An additional change in free energy is required to counteract the effect arising from above two factors. This additional change in free energy can be achieved if the nucleus form with composition x_m. It is quite apparent from the Fig. A3.1 that $\Delta Fm > \Delta F$. This thermodynamically most favourable composition of the nucleus can be obtained by drawing a tangent to the curve α parallel with the tangent through the point O, representing the parent phase. The change in chemical potential referring to the nucleus composition x_m can be expressed as

$$\mu^{\circ}_{Fe} - \mu^{m}_{Fe} = \mu^{\circ}_{C} - \mu^{m}_{C} \quad .. \quad .. \quad .. \quad .. \quad .. \quad .. \quad .. \quad .. \quad .. \quad .. \quad (A3.2)$$

$$\frac{a^{\circ}_{Fe}}{a^{m}_{Fe}} = \frac{a^{\circ}_{C}}{a^{m}_{C}} \quad .. \quad .. \quad .. \quad .. \quad .. \quad .. \quad .. \quad .. \quad .. \quad .. \quad .. \quad .. \quad (A3.3)$$

It is now justified that the favourable composition (C_m) for nucleation of α involves a larger change in composition (i.e. C) from the parent phase (γ) than the equilibrium value $x^{\alpha\gamma}_{\alpha}$. It is also clear from the construction of parallel tangent that with increasing supersaturation, the nucleus composition will be, pushed further away from $x^{\alpha\gamma}_{\alpha}$. Once it has been established that the composition of the nucleus x_m is thermodynamically more favourable, it is a matter of simple calculation to determine its numerical value. The numerical value of C_m can be obtained[4] by the use of following equation:

$$\Delta F^{\gamma\to\alpha}_{Fe} + RT \ln \frac{a^{\alpha}_{Fe}\,(1 - x)}{a^{\gamma}_{Fe}\,(1 - \bar{x})} - RT \ln \frac{a^{\alpha}_{C}\,(x)}{a^{\gamma}_{C}\,(\bar{x})} = 0 \quad .. \quad .. \quad .. \quad .. \quad .. \quad (A3.4)$$

$$\Delta F_m = RT \ln \frac{a^{\alpha}_{C}\,(x_m)}{a^{\gamma}_{C}\,(\bar{x})} \quad .. \quad .. \quad .. \quad .. \quad .. \quad .. \quad .. \quad .. \quad .. \quad .. \quad (A3.5)$$

For alloy steel, the first term of equation (A3.4), is replaced by[7]

$$\Delta F^{\gamma\to\alpha}_{Fe}\left\{T - 100\sum_i Y_i \Delta T_{magi}\right\} + 141\sum_i Y_i\,(\Delta T_{magi} - \Delta T_{nmi})$$

where a^{α}_{Fe} (1 - C) refers to the activity of iron in ferrite evaluated at the concentration (1 - C), and other activity terms are defined in the same way. $\Delta F^{\gamma\to\alpha}_{Fe}$ is the change in free energy accompanying the austenite-ferrite transformation of pure iron and R is the gass constant. $\bar{x}$ refers to average carbon concentration of steel and x_m represents the composition of ferrite which satisfies equation (A3.4). Y_i refers to mole fraction of ith substitutional alloying element, disregarding the presence of carbon and ΔT_{magi} and ΔT_{nmi} shift is the temperature for pure iron due to magnetic and non-magnetic components of $\Delta F^{\gamma\to\alpha}_{Fe}$ respectively. This equation can be solved iteratively or with the use of Newton-Raphson method to obtain the value of x_m in equation (A3.5), we get ΔF_m. The results of such a calculation for different alloy steels are shown in Fig. A.3.2. Experimental evidence in support of such a calculation is extremely difficult to obtain, as the critical size of the nucleus hardly exceeds the limit (= 20A°) required for resolving under TEM[5].

The most favourable composition x_m not only provides the additional driving force to counteract the effect of surface tension and strain energy but it also helps the nucleus to grow beyond the size of critical nucleus. Figure A.3.1 shows that in the equilibrium state $\mu_{Fe}^{k.1}$ has lower potential than the original specimen μ_{Fe} for Fe but for carbon, it has higher chemical potential $\mu_C^{k.1}$ than the original specimen μ_C. So it is extremely difficult for α to receive even the negligible amount of carbon during its growth for survival under equilibrium conditions. But if the nucleus forms with composition x_m, it can easily grow by receiving both kinds of atoms (i.e. Fe and C) since its chemical potential for both the components are lower than the parent phase (γ). Gradually the carbon content of the austenite becomes appreciable and pushed toward equilibrium value $x_\alpha^{\alpha\gamma}$. This gradual change in carbon content takes place in such a way that all the time both potentials are lower in α than austenite (γ).

Under special circumstances, the nuclei with a different composition may form if kinetic parameters militate in their favour. In ternary Fe-C-X system, nuclei may form with or without partitioning of a sluggish diffusing species X.[6,7] At large supersaturations, the possibility exists that unpartitioned nuclei may form, because of greater time required for alloying element redistribution. Moreover, since the no-partition nuclei have a higher free energy than the true critical nucleus, it may pass over the barrier at much greater rate and dominate the nucleation process.[5]

From the above discussion it is clear that the precipitation of alloy carbide is more favourable than the precipitation of Fe_3C since the former involves relatively large charge in free energy.[9,10] So thermodynamically precipitation of alloy carbide by interphase precipitation is more likely to occur than the cementite.

The theoretical work by Cahn and Hilliard[8] showed that the nucleus composition need not be uniform throughout. The composition fluctuation within the nucleus may be represented by

$$2K\nabla^2 C + \left(\frac{dK}{dC}\right)(\nabla C)^2 = \frac{d\Delta F}{dC}$$

where $K(\nabla C)^2$ = Gradient energy coefficient.

ΔF = Change in free energy accompanying the formation of critical nucleus.

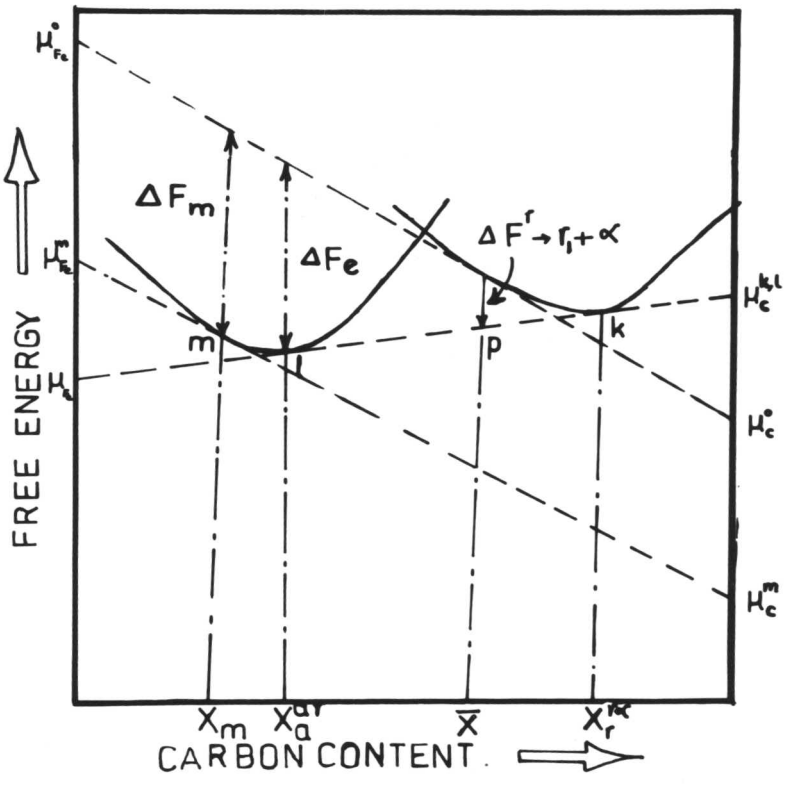
FREE ENERGY
CARBON CONTENT
ΔFm
ΔFe
m
p
k

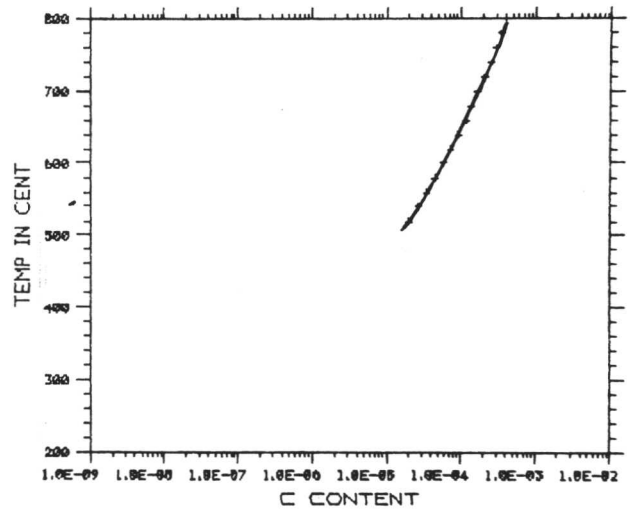

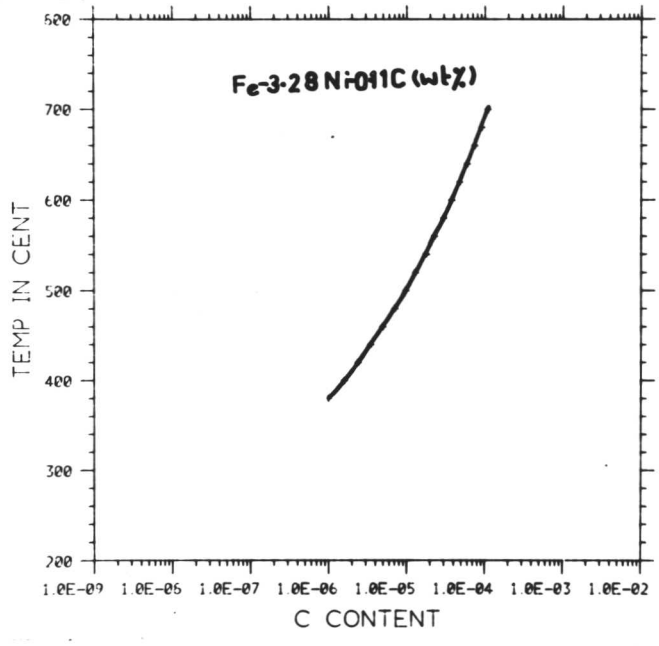

Figure A3.2: Carbon content of the nucleus vs temperature.
(a) Fe-3.05Cr-0.11C (wt%).
(b) Fe-3.28Ni-0.11C (wt%).

REFERENCES

CHAPTER II

1. Dubé, C. A., Ph.D. thesis, Carnegie Inst. of Technology, 1948.

2. Dubé, C. A., Aaronson, H. I. and Mehl, R. F., Rev. Met., 55, 201, 1958.

3. Aaronson, H. I., Decomposition of Austenite by Diffusional Processes, p. 387 ff: Interscience Publishers, New York, 1962.

4. Toney, S. and Aaronson, H. I., Trans. AIME, 221, p. 909, 1961.

5. Aaronson, H. I., Triplett, W. B. and Andes, G. M., Trans. AIME, 218, 331, 1960.

6. Hawbolt, B. and Brown, L. C., Trans. AIME, 239, p. 1916, 1967.

7. Clark, J. B., High Temperature, High-Resolution Metallography, p. 347, Gordon and Breach, New York, 1967.

8. Aaron, H. B. and Aaronson, H. I., Symposium on Altering the Time Cycle of Heat Treatment, Met. Soc. AIME, 1969.

9. Kelly, A. and Nicholson, R. B., Precipitation Hardening, Progress in Materials Science, 10, No. 3, 1963.

10. Townsend, R. D. and Kirkaldy, J. S., Trans. A.S.M., 61, p. 605, 1968,

11. Kurdjumov, G. and Sachs, G., Z. Physik, 64, p. 325, 1930.

12. Aaronson, H. I., Symposium on the Mechanism of Phase Transformations in Metals, Institute of Metals, London, p. 47, 1955.

13. Mehl, R. F., Barrett, C. S. and Smith, D. W., Trans. AIME, Vol. 105, p. 215, 1955.

14. Nabarro, F. R. N., Proc. Phys. Soc. (London), 52, 90 (1940).

15. Nabarro, F. R. N., Proc. Roy. Soc. (London), 175, 519 (1940).

16. Molt, N. F. and Nabarro, F. R. N., Proc. Phys. Soc. (London), 52, 86, 1940.

17. Smith, C. S., Trans. A.S.M., 45, 533, 1953.

18. Liu, Y. C., Aaronson, H. I., Kinsman, K. R. and Hall, M. G., Met. Trans., Vol. 3, p. 1319, 1972.

19. Hillert, M., Decomposition of Austenite by Diffusional Processes, p. 197, ff: Interscience Publishers, New York, 1962.

20. Morrison, W. B., J.I.S.I., 317, 1963.

21. Leslie, W. C. , National Physical Laboratory Symposium No. 15, "The Relationship between the Structure and Mechanical Properties of Metals", p. 333., 1963.

22. Mannerkoski, M., Acta Polytech. Scand., Ch. 26, p. 7, 1964.

23. Relander, K., Acta Polytech. Scand., Ch. 34, p. 7, 1964.

24. Tonino, M., Nishida, T., Ooka, T. and Yoshikawa, K., Proceedings of the Symposium on Micrometallurgy, Jamshedpur. 1965

25. Suzuki, H. G. and Tonino, M., Trans. I.S.I.J., 12, 217, 1972.

26. Suzuki, H,. G. and Tonino, M., Trans. I.S.I.J., 13, 80, 1973.

27. Gray, J. M. and Yeo, R. B. G., Trans. A.S.M., 61 , 255, 1968.

28. Davenport, A. T. D., Berry, F. G. and Honeycombe, R. W. K., Met. Sci. J., 2, 104, 104, 1968.

29. Baker, R. G. and Nutting, J., I.S.I., Sp. Report No. 64, 1, 1959.

30. Freeman, S., I.S.I., Report No. 45, 152, 1971.

31. Berry, F. G. and Honeycombe, R. W. K., Met. Trans. Trans., 1, 3279, 1970.

32. Davenport, A. T. D. and Honeycombe, R. W. K., Proc. Royal Soc., London, A322, 191. 1971.

33. Campbell, K., Ph.D. Thesis, March 1971.

34. Ricks, R. A., Howell, P. R. and Honeycombe, R. W. K., Met. Trans., 10A p. 1049, 1979.

35. Ricks, R. A., J. Mat. Sci., J. Mat. Sci., 16, p. 3006, 1981.

36. Campbell, K. and Honeycombe, R. W. K., Met. Sci., 8, 197, 1974.

37. Mannerkoski, M., Met. Sci. J., 3, 54, 1969.

38. Heikkinen, V. K., Acta Met., 21, 709, 1973.

39. Heikkinen, V. K., Scand. J. Met., 109, 112, 1973a.

40. Ricks, R. A. and Howell, P. R., Metal Science, 317, June 1982.

41. Ricks, R. A. and Howell, P. R., Acta Met., Vol. 31, No. 6, p. 853, 1983.

CHAPTER III

References

1. Davenport, A.T.: M. Tech. Thesis; University of Sheffield, May 1964.

2. Hilliard, J.E., and Cahn, J.W.: Trans. AIME 1961, 221, 244.

3. Yand, J.R. and Bhadeshia, H.K.D.H.: Unpublished work; University of Cambridge.

CHAPTER IV

References

1. Honeycombe, R.W.K., Met. Trans., p. 915, July 1976.

2. Aaronson, H.I., Plichta, M.R., Franti, G.W., Russell, K.C., Met. Trans. A., Vol. 9A, p. 363, 1970.

3. Ricks, R.A. and Howell, P.R., J. of Metal Sci., 18, 3393, 1983.

4. Ricks, R.A. and Howell, P.R., Metal Sci., Vol. 16, 317, 1982.

5. Ricks, R.A. and Howell, P.R., Acta Met., Vol. 31, No. 6, p. 853, 1983.

6. Kuo, K., J.I.S.I., April 1953.

7. Lupton, J.B. et al, Met. Trans., Vol. 3, 2923, 1972.

8. Davenport, A.T. and Honeycombe, R.W.K., Proc. Roy. Soc., Lond., A322, 191, 1971.

9. Bjorn Uhrenius, Hardenability Concepts with Applications to Steels, Edts. D.V. Doane and J.S. Kirkaldy, p. 20, Feb. 1978.

10. Goldschmidth, H.J., Interstitial Alloys, Butterworth and Co. (Publishers) Ltd., 1967.

11. Wilyman, P.R. and Honeycombe, R.W.K., Metal Sci., Vol. 16, p. 295, June 1982.

12. Kinsman, K.R., Eichen, E. and Aaronson, H.I., Met. Trans., Vol. 6A, Feb. 303, 2975.

13. Jones, G.J. and Trivedi, R., J. App. Phys., 42, 4299, 1971.

14. Jones, G.J. and Trivedi, R., J. Cryst. Growth, 29, 155, 1971.

15. Bhadeshia, H.K.D.H., Phys. State Solid (a), 69, 745, 1982.

16. Cahn, R.W. and Hassen, P., Physical Metallurgy, 3rd edition, 1983.

17. Johnson, W.C. et al, Met-Trans. A, 6A, 911, 1975.

18. Cahn, R.W., Acta Met., 4, 449, 1956.

19. Smith, C.S., Trans. A.S.M., Vol. 45, p. 533, 1953.

20. Howell, P.R. and Honeycombe, R.W.K., Proceedings of an Int. Conf. on Solid-Solid Phase Transformations, edited by Aaronson, H.I. et al, Aug. 1981, p. 399.

21. Ryder, P.L., Pitch, W. and Mehl, R.F., Acta Met. 15, 1431, 1967.

22. King, A.D. and Bell, T., Met. Sci. J., 8, 253, 1974.

23. King, A.D. and Bell, T., Met. Trans. A, 6A, 1419, 1975.

24. King, A.D. and Bell, T., Metall., 9, 397, 1976.

25. Aaronson, H.I., Decomposition of Austenite by Diffusional Processes, p387, ff, Interscience Publishers, New York, 1962.

REFERENCES

CHAPTER V

1. Kinsman, K.R. and Aaronson, H.I., "Transformation and Hardenability in Steels", Climax Molybdenum Co., Ann Arbor, Mich., p.39, 1967.

2. Hillert, M., Jernkontorets Ann., 141, 757, 1957.

3. K.R. Kinsman and H.I. Aaronson. Metall. Trans., Vol. 4, P.959, 1973.

4. C. Atkinson, H.B. Aaron, K.R. Kinsman and H.I. Aaronson, Metall. Trans., Vol. 4, P.783, 1973a.

5. Aaronson, H.I., Laird, C. and Kinsman, K.K., Phase Transformation, A.S.M., Metals Park, Ohio, 1970.

6. Honeycombe, R.W.K., Met. Trans., Vol. 7A, 915, 1976.

7. Berry, F.G. and Honeycombe R.W.K., Met. Trans., 1, 3279, 1970.

8. Balliger, N.K. and Honeycombe, R.W.K., Met. Trans., 11A, 421, 1980.

9. Sakuma, T. and Honeycombe, R.W.K. Unpublished work.

10. Kuo, K., J.I.S.I., p. 363, April 1953.

11. Lupton, J.B., Murphy, S. and Wookhead, J.H., Met. Trans., Vol. 3, 2923, 1972.

12. Davenport, A.T. and Honeycombe, R.W.K., Proc. Roy. Soc., Lond., A, 322, 191 - 205, 1971.

13. Goldschmidt, H.J., Interstitial Alloys, Butterworth and Co. (Publishers) Ltd., 1967.

14. Storms, E.K. "The refactory carbides". P6; 1967. Academic Press, New York.

15. Pickering, F.B. and Gladman, T. ISI Spec. Rep. 81, P10, 1963.

16. Smith, C.S., Trans. A.S.M., Vol. 45, P533, 1953.

17. Hillèrt, M., "The Decomposition of Austenite by Diffusional Processes", Interscience, New York, P197, 1962.

18. Ryder, P.L., Pitsch, W. and Mehl, R.F., Acta Met., 15, 1431, 1967.

19. King, A.D. and Bell, T., Met. Sci. J., 8, 253, 1974.

20. King, A.D. and Bell, T., Met. Trans. A, 6A, 1419, 1975.

21. Howell, P.R. and Honeycombe, R.W.K., "Solid-Solid Phase Transformation", edited by Aaronson, P399, 1983.

22. Aaronson, H.I., "Decomposition of Austenite by Diffusional Processes", P387 ff, Interscience Publishers, New York, 1962.

23. Aaronson, H.I., Plichta, M.R., Franti, G.W. and Russell, K.C., Met. Trans., 9A, 363, 1978.

24. Coates, D.E., Met. Trans., Vol. 4, 2313, October 1973.

25. Teizchi, A. and George, K., Met. Trans. A., Vol. 14A, 261, 1983.

26. Gilmour, J.B., Purdy, G.R. and Kirkaldy, J.S., Met. Trans., Vol. 3, P3213, 1972.

27. Aaronson, H.I. and Domain, H.A., Trans. TMS-AIME, Vol. 236, P761, 1966.

CHAPTER VI

References

1. Honeycombe, R.W.K.: Effect of Second Phase Particles on the Mechanical Properties of Steel, ISI, p. 136, 1971.

2. Batte, A.D. and Honeycombe, R.W.K.: JISI, Vol. 221, p. 187, 1973.

3. Irvine, K.J.: 'Strong, Tough Structural Steels', Special Publ., Vol. 104, p. 1, 1967, London (Iron Steel Inst.).

4. Honeycombe, R.W.K.: Met. Trans., Vol. 7A, No. 7, p. 915, 1976.

5. Batte, A.D. and Honeycombe, R.W.K.: JISI, Vol. 211, p. 284, 1973.

6. Berry, F.G. and Honeycombe, R.W.K.: Met. Trans., Vol. 1, p. 3279, 1970.

7. Berry, F.G.: Ph.D. Dissertation, University of Sheffield, 1968.

8. Davenport, A.: Ph.D. Dissertation, University of Sheffield, 1968.

9. Ohmori, Y.: Ph.D. Dissertation, University of Cambridge, 1969.

10. Freeman, S.: Ph.D. Dissertation, University of Cambridge, 1971.

11. Campbell, K.: Ph.D. Dissertation, University of Cambridge, 1971.

12. Law, N.C.: Ph.D. Dissertation, University of Cambridge, 1977.

13. Balliger, N.K.: Ph.D. Dissertation, University of Cambridge, 1977.

14. Southwick, P.D.: Ph.D. Dissertation, University of Cambridge, 1978.

15. Ricks, R.A.: Ph.D. Dissertation, University of Cambride, 1979.

16. Parsons, S.A.: Ph.D. Dissertation, University of Cambridge, 1981.

17. Howell, P.R. and Honeycombe, R.W.K.: Int. Conf. on Solid-Solid-Phase Transformations, ed. H.I. Aaronson et al., AIME publications, p. 399. 1982.

18. Predel, B. and Gust, W.: Mat. Sci., Engg., Vol. 17, p. 41, 1975.

19. Liu, Y.C. and Aaronson, H.I.: Acta Met. Vol. 16, p. 1343, 1968.

20. Gust, W., Predel, B. and Nguyen, Tal L.: Z. Metallkde, Vol. 67, p. 110, 1976.

21. Tu, K.N. and Turnbull, D.: Acta Met., Vol. 15, p. 369, 1967.

22. Fournelle, R.A. and Clark, J.B.: Met. Trans., Vol. 3, p. 2757, 1972.

23. Fournelle, R.A.: Acta Met. p. 1135, 1979.

24. Geisler, A.H.: Phase Transformations in Solids, p. 387, Wiley, 1951.

25. Rosenbaum, H.S. and Turnbull, D.: Acta Met., Vol. 7, p. 664, 1959.

26. Thomas, G. and Nutting, J.: Inst. of Metals, Vol. 88, p. 81, 1959-60.

CHAPTER VII

References

1. Morrison, W.B.: J. Iron Steel Inst., London 201, 317 (1963).

2. Fisher, G.L. and Geils, R.H.: Trans. Metall. Soc. AIME 245, 2405 (1969).

3. Serin, B., Desalas, Y., Maitrepierre, Ph. and Rofes-Vernis, J.: Mem. Sci. Rev. Metall., 75, 355 (1978).

4. Thomas, M.H. and Michal, G.M.: Proce. of Int. Conf. on Solid-Solid Phase Transformations; edited by H.I. Aaronson, D.E. Laughlin, R.F. Sekeyka and C.M. Wayman, Aug. 10-14, 1981, JMS-AIME, Warrendale, Pennsylvania, p. 399, 1981.

5. Maitrepierre, Ph., Thivellier, D., Rofes-Vernis, J., Rosseare, D. and Tricot, R.: Hardenability concepts with applications to steel. The Metallurgical Society of AIME, 421 (1978).

6. Ohmori, Y.: Trans. Iron Steel Inst., Japan 11, 339 (1971).

CHAPTER VIII

References

1. Ham, F.S.: Jnl. App. Phy. 20, p. 950. 1959.

2. Aaronson, H.I.: Phase-Transformations, York Conference, Insitute of Metallurgists, London, p. 11-1, 1979.

3. Coates, D.E.: Met. Trans., Vol. 4, p. 2313, 1973.

4. Coates, D.E.: Met. Trans., Vol. 3, p. 1203, 1972.

5 . Trivedi, R. and Pound, G.M.: J. Appl. Phys., Vol. 38, p. 3569, 1967.

6. Brown, L.C.: J. Appl. Phys., Vol. 43, p. 4443, 1972.

7. Bolze, G., Coates, D.E. and Kirkaldy, J.S.: Met. Trans., Vol. 62, p. 959, 1969.

8. Hillert, M.: Internal Report, Swedish Institute of Metals Research, 1953.

9. Kirkaldy, J.S.: Canda. J. Physics, 36, 907, 1958.

10. Purdy, G.R., Weichert, D.H. and Kirkaldy, J.S.: Trans. TMS-AIME, Vol. 230, p. 1025, 1964.

11. Hultgren, A.: Trans. ASM, Vol. 39, p. 915, 1947.

12. Hillert, M.: Jernkont. Ann; Vol. 136, p. 25, 1952.

13. Rudberg, E.: Jernkont. Ann; Vol. 136, p. 91, 1952.

14. Aaronson, H.I., Domain, H.A. and Pound, G.M.: Trans. TMS-AIME; Vol. 236, p. 768, 1966.

15. Gilmour, J.B., Purdy, G.R. and Kirkaldy, J.S.: Met. Trans., Vol. 3, p. 1455, 1972.

16. Bhadeshia, H.K.D.H.: Diffusional Formation of Ferrite in Iron and its Alloys, Prog. Mat. Sci., Vol. 29, pp. 328-386, 1985.

17. Wagner, C.: Thermodynamics of Alloys, p. 51, Addison-Wesley, Reading, Mass., 1952.

18. Purdy, G.R. and Kirkaldy, J.S.: TMS-AIME, Vol. 227, p. 1255.

19. Purdy, G.R., Weichert, D.H. and Kirkaldy, J.S.: TMS-AIME, Vol. 230, p. 1025, 1964.

20. Kinsman, K.R. and Aaronson, H.I.: 'Transformation and Hardenability in Steels', Climax Moly. Co., Ann Arbor, Mich., p. 39, 1969.

21. Kinsman, K.R. and Aaronson, H.I.: Metall. Trans., Vol. 4, p. 959, 1973.

22. Bradley, J.R. and Aaronson, H.I.: Metall. Trans. A., Vol. 8A, p. 317, 1977.

23. Bradley, J.R. and Aaronson, H.I.: Metall. Trans. A., Vol. 12A, p. 1729, 1981.

24. Hillert, M.: The Mechanism of Phase-Transformation in Crystalline Solids, edited by Inst. of Metals, London, p. 231, 1969.

25. Aaronson, H.I. and Domain, H.A.: TMS-AIME, Vol. 236, p. 781, 1966.

26. Zener, C.: J. Appl. Phys., Vol. 20, p. 950, 1949.

27. Christian, J.W.: Theory of Phase-Transformation in Metals and Alloys, 2nd edition, Part I, p. 482, Pergamon Press, Oxford, 1975.

28. Bhadeshia, H.K.D.H.: Metal-Science, 15, p. 175, 1981.

29. Bhadeshia, H.K.D.H.: Metal-Science, 15, p. 178, 1981.

30. Bhadeshia, H.K.D.H. and Edmonds, D.V.: Acta-Metall., Vol. 28, p. 1265, 1980.

31. Bhadeshia, H.K.D.H.: Metal-Science, Vol. 15, p. 477, 1981.

32. Bhadeshia, H.K.D.H.: Unpublished work, University of Cambridge.

33. Kinsman, K.R. and Aaronson, H.I.: Transformation and Hardenability in Steels, p. 39, Climax Molybdenum Co., Ann Arbor, Michigan, 1967.

34. Kinsman, K.R. and Aaronson, H.I.: Metall. Trans., Vol. 4, p. 959, 1973.

35. Atkinson, C., Aaron, H.B., Kinsman, K.R. and Aaronson, H.I.: Met. Trans., Vol. 4, p. 783, 1973.

36. Bradley, J.R., Rigsbee, J.M. and Aaronson, H.I.: Metall. Trans. A, Vol. 8A, p. 323, 1977.

37. Hillert, M.: Decomposition of Austenite by Diffusional Processes, eds. Zackay and Aaronson, p. 387, Interscience, 1962.

38. Ryder, P.L., Pitsch, W. and Mehl, R.F.: Acta Met., Vol. 15, p. 1431, 1967.

39. King, A.D. and Bell, T.: Met. Sci. J., Vol. 8, p. 253, 1974.

40. King, A.D. and Bell, T.: Met. Trans. A, Vol. 6A, p. 1419.

41. Aaronson, H.I.: Decomposition of Austenite by Diffusional Processes, p. 287, Interscience, eds. Zackay and Aaronson, 1962.

42. Aaronson, H.I., Laird, C. and Kinsman, K.R.: Phase Transformations, p. 313, ASM, Metal Park, Ohio, 1970.

43. Honeycombe, R.W.K.: Met. Trans. A, Vol. 7A, p. 915, 1976.

44. Honeycombe, R.W.K.: Met. Trans. A, Vol. 7A, p. 915, 1976.

45. Purdy, G.R.: Acta Metall., Vol. 26, p. 477, 1978.

46. Middleton, C.J. and Edmonds, D.V.: Metallography, Vol. 10, p. 55, 1977.

47. Bradley, J.R. and Aaronson, H.I.: Met. Trans., A, Vol. 12A, p. 1729, Oct. 1981.

48. Uhrenius, B.: Hardenability Concepts with Applications to Steels, eds. D.D. Doane and J.S. Kirkaldy, AIME publications, p. 28, 1978.

49. Gilmour, J.B., Purdy, G.R. and Kirkaldy, J.S.: Metall. Trans., Vol. 3, p. 3213, 1972.

50. Hillert, M.: Acta Met., Vol. 3, p. 34, 1955.

51. Hillert, M.: Mech. of Phase Transformations in Cryst. Solids, Institute of Metals (London), Monograph 13, p. 231, 1969.

52. Shiflet, G.J., Aaronson, H.I. and Bradley, J.R.: Met. Trans. A, Vol. 12A, p. 1743, 1981.

53. Cahn, J.W.: Acta Met., Vol. 10, p. 789, 1962b.

54. Sharma, R.C. and Purdy, G.R.: Metall. Trans., Vol. 4, p. 2303, 1973.

55. Kirkaldy, J.S. and Baganis, E.A.: Metall. Trans. A, Vol. 9A, p. 495, 1978.

56. Boswell, P., Kinsman, K.R. and Aaronson, H.I.: Unpublished work, Ford Motor Co., Dearborn, Michigan, 1968.

57. Aaronson, H.I. and Domain, H.A.: TMS-AIME, Vol. 236, p. 768, 1966.

58. Clemm, P.J. and Fisher, J.C.: Acta Met., Vol. 3, 70, 1955.

59. Gronsky, R. and Furrer, P.: Met. Trans. A, Vol. 12A, p. 121, 1981.

60. Dubé, C.A.: Ph.D. Thesis, Carnegie Institute of Technology, 1948.

61. Howell, P.R. and Honeycombe, R.W.K.: Proc. Int. Conf. on Solid-Solid Phase Transformation: TMS-AIME, Warrendale, Pennsylvania, p. 399, 1981.

62. Cahn, J.W.: Acta Met., Vol. 8, p. 554, 1960.

63. Bhadeshia, H.K.D.H.: Acta Met., Vol. 29, p. 1117, 1981.

64. Kinsman, K.R., Eichen, E. and Aaronson, H.I., Met. Trans., Vol. 6A, p. 303, 1975.

65. Aaronson, H.I.: Decomposition of Austenite by Diffusional Processes, p. 387, ff, Interscience Publishers, New York, 1962.

66. Russell, K.C.: Phase Transformations, p. 219, ASM, Metal Park, Ohio, 1970.

67. Avrami, M.: J. Chem. Phys., Vol. 7, 1103, 1939, 1 bid: 8.212, 1940, 1 bid. 9, 177, 1941.

68. Mazanec, K. and Cadek, J., Rev. Met., Vol. 212, p. 501, 1958.

69. Christian, J.W.: 'The Theory of Phase Transformations in Metals and Alloys', Pergamon Press, London, 1965.

CHAPTER IX

References

1. Bhadeshia, H.K.D.H.: Metal Science, Vol. 16, p. 159, March 1982.

2. Christian, J.W.: 'Theory of Transformations in Metals and Alloys', 2nd edition, Pt. 1, Pergamon Press, Oxford (1975).

3. Honeycombe, R.W.K.: Carbide Precipitation in Ferrite, Proc. of an Inter. Conf. on Phase Transformation in Ferrous Alloy (1983), AIME, ed. by A.R. Marder and J.I. Goldstein.

4. Christian, J.W.: 'Theory of Transformations in Metals and Alloys', Pergamon Press, Oxford, (1965).

5. Cahn, J.W.: Acta Met., Vol. 5, p. 169, March 1957.

6. Dollins, C.C.: Acta Met., Vol. 18, p. 1209, November 1970.

7. Ashby, M.F. and Brown, L. M.: Phil. Mag., Vol. 8, p. 1083, 1963.

8. Ohmori, Y.: Ph.D. Dissertation, University of Cambridge, 1969.

9. Davenport, A.T. and Becker, P.C.: Met. Trans., Vol. 2, p. 2962, 1971.

10. Batte, A.D. and Honeycombe, R.W.K.: J. Iron and Steel Inst., Vol. 211, p. 284, 1973.

11. Law, N.C.: Ph.D. Dissertation, University of Sheffield, 1968.

12. Campbell, K. and Honeycombe, R.W.K.: Met. Sci., Vol. 8, p. 197, 1974.

13. Berry, R.G. and Honeycombe, R.W.K.: J. Iron and Steel Instit., Vol. 211, p. 284, 1973.

14. Howell, P.R. et al.: Phil. Mag., Vol. 41 (2), p. 165, 1980.

15. Davenport, A.T. and Honeycombe, R.W.K.: Proc. Roy. Soc., Vol. A332, p. 191, 1971.

16. Shiflet, G.J., Aaronson, H.I. and Bradley, J.R.: Met. Trans. A, Vol. 12A, p. 1743, 1981.

APPENDIX I

References

1. Bhadeshia, H.K.D.H.: Metal Science, Vol. 16, p. 159, March 1982.

2. Russell, K.C.: Acta Metall., Vol. 16, p. 761, 1968.

3. Russell, K.C.: Acta Metall., Vol. 17, p. 1123, 1969.

4. Kirkaldy, J.S. et al.: Hardenability concepts with applications to steels, p. 82, 1978, Metals Park, Ohio, U.S.A., ASM.

5. Hillert, M.: Acta Metall., Vol. 1, p. 764, 1953.

6. Aaronson, H.I. et al.: Trans. Met. Soc., AIME, Vol. 236, p. 768, 1966.

APPENDIX II

References

1. Zener, C.: AIME Trans., Vol. 167, p. 513, 1946.

2. Zener, C.: AIME Trans., Vol. 203, p. 619, 1955.

3. Aaronson, H.I., Domain, H.A. and Pound, G.M.: Trans. Met. Soc., AIME, vOL. 236, p. 768, 1966.

4. Aaronson, H.I., Domain, H.A. and Pound, G.M.: Trans. Met. Soc., AIME, Vol. 236, p. 753, 1966.

5. Bhadeshia, H.K.D.H. and Edmonds, D.V.: Acta Met., Vol. 28, p. 1265, 1980.

6. Bhadeshia, H.K.D.H.: Unpublished work.

7. Fisher, J.C.: Met. Trans. Vol. 185, p. 688, 1949.

8. Shiflet, G.J., Bradley, J.R. and Aaronson, H.I.: Metall. Trans. A, Vol. 9, p.999, 1978.

9. Oblak, J.M. and Hehemann, R.F.: Transformations and Hardenability in Steels, p. 15, Climax Moly, Ann Arbor, 1967.

10. Bhadeshia, H.K.D.H.: Metal Sci. J. (1980).

11. Lobo, J.A. and Geiger, G.H.: Metall. Trans. A, Vol. 7, p. 1347, 1976.

12. Kaufman, L., Clougherty, E.V. and Weiss, R.J.: Acta Metall., Vol. 11, p. 323, 1963.

APPENDIX III

References

1. Hillert, M.: Acta Metall., Vol. 1, p. 764, 1953.

2. Gerlach, W.: Z. Metalk., Vol. 40, p. 281, 1949.

3. Hillert, M.: Lectures on the Theroy of Phase Transformations, Ed. Aaronson, H.I., AIME, May 20, 1974, pp. 1-44.

4. Bhadeshia, H.K.D.H.: Metal Science, Vol. 16, p. 159, March 1982,

5. Russell, K.C.: Phase Transformations, p. 219, ASM, Metal Park, Ohio, 1969.

6. Aaronson, H.I., Domain, H.A. and Pound, G.M.: Trans. TMS-AIME, Vol. 236, p. 768, 1966.

7. Aaronson, H.I., Domain, H.A.: Trans. TMS-AIME, Vol. 236, p. 781, 1966.

8. Cahn, J.W. and Hilliard, J.E.: Journal of Chemical Physics, Vol. 31, No. 3, p. 688, 1959.

9. Entin, R.I.: Decomposition of Austenite by Diffusional Process, p. 295, Interscience Publishers, New York, 1962.

10. Colters, R.G.: Materials Science and Engineering, Vol. 76, p. 10, 1985.